Etude des propriétés adsorbantes de biomasses fongiques : application au traitement d'effluents métallifères

Lenka Svecova

N° d'ordre : 438 SGE

THESE
présentée par

Lenka Švecová

Pour obtenir le grade de Docteur
de l'Ecole Nationale Supérieure des Mines de Saint-Etienne

Spécialité : Sciences et Génie de l'Environnement

Etude des propriétés adsorbantes de biomasses fongiques – Application au traitement d'effluents métallifères

Soutenue à Alès le 1er février 2007

Membres du jury

Rapporteurs :
František Kaštánek   Professeur, Academy of Sciences of the Czech Republic, Prague
Rémy Gourdon   Professeur, INSA Lyon

Examinateurs :
Jacques Bourgois   Professeur, ENSM Saint Etienne
Mečislav Kuraš   Professeur, Institute of Chemical Technology, Prague

Directeurs de thèse :
Jean Roussy   Chargé de mission, Ecole des Mines d'Alès
Martin Kubal   HDR, Institute of Chemical Technology, Prague

Invité :
Eric Guibal   Chargé de recherche, Ecole des Mines d'Alès

● **Spécialités doctorales :**   **Responsables :**

SCIENCES ET GENIE DES MATERIAUX   **J. DRIVER** Directeur de recherche – Centre SMS
MECANIQUE ET INGENIERIE   **A. VAUTRIN** Professeur – Centre SMS
GENIE DES PROCEDES   **G. THOMAS** Professeur – Centre SPIN
SCIENCES DE LA TERRE   **B. GUY** Maitre de recherche
SCIENCES ET GENIE DE L'ENVIRONNEMENT   **J. BOURGOIS** Professeur – Centre SITE
MATHEMATIQUES APPLIQUEES   **E. TOUBOUL** Ingénieur
INFORMATIQUE   **O. BOISSIER** Professeur – Centre G2I
IMAGE, VISION, SIGNAL   **JC. PINOLI** Professeur – Centre CIS
GENIE INDUSTRIEL   **P. BURLAT** Professeur – Centre G2I
MICROELECTRONIQUE   **Ph. COLLOT** Professeur – Centre CMP

● **Enseignants-chercheurs et chercheurs autorisés à diriger des thèses de doctorat** (titulaires d'un doctorat d'Etat ou d'une HDR)

BENABEN	Patrick	PR 2	Sciences & Génie des Matériaux	SMS
BERNACHE-ASSOLANT	Didier	PR 1	Génie des Procédés	CIS
BIGOT	Jean-Pierre	MR	Génie des Procédés	SPIN
BILAL	Essaïd	MR	Sciences de la Terre	SPIN
BOISSIER	Olivier	PR 2	Informatique	G2I
BOUDAREL	Marie-Reine	MA	Sciences de l'inform. & com.	DF
BOURGOIS	Jacques	PR 1	Sciences & Génie de l'Environnement	SITE
BRODHAG	Christian	MR	Sciences & Génie de l'Environnement	SITE
BURLAT	Patrick	PR 2	Génie industriel	G2I
COLLOT	Philippe	PR 1	Microélectronique	CMP
COURNIL	Michel	PR 1	Génie des Procédés	SPIN
DAUZERE-PERES	Stéphane	PR 1	Génie industriel	CMP
DARRIEULAT	Michel	ICM	Sciences & Génie des Matériaux	SMS
DECHOMETS	Roland	PR 2	Sciences & Génie de l'Environnement	SITE
DELAFOSSE	David	PR 2	Sciences & Génie des Matériaux	SMS
DOLGUI	Alexandre	PR 1	Informatique	G2I
DRAPIER	Sylvain	PR 2	Mécanique & Ingénierie	CIS
DRIVER	Julian	DR	Sciences & Génie des Matériaux	SMS
FOREST	Bernard	PR 1	Sciences & Génie des Matériaux	SMS
FORMISYN	Pascal	PR 1	Sciences & Génie de l'Environnement	SITE
FORTUNIER	Roland	PR 1	Sciences & Génie des Matériaux	CMP
FRACZKIEWICZ	Anna	MR	Sciences & Génie des Matériaux	SMS
GARCIA	Daniel	CR	Génie des Procédés	SPIN
GIRARDOT	Jean-Jacques	MR	Informatique	G2I
GOEURIOT	Dominique	MR	Sciences & Génie des Matériaux	SMS
GOEURIOT	Patrice	MR	Sciences & Génie des Matériaux	SMS
GRAILLOT	Didier	DR	Sciences & Génie de l'Environnement	SITE
GROSSEAU	Philippe	MR	Génie des Procédés	SPIN
GRUY	Frédéric	MR	Génie des Procédés	SPIN
GUILHOT	Bernard	DR	Génie des Procédés	CIS
GUY	Bernard	MR	Sciences de la Terre	SPIN
GUYONNET	René	DR	Génie des Procédés	SPIN
HERRI	Jean-Michel	PR 2	Génie des Procédés	SPIN
JOYE	Marc	Ing. (Gemplus)	Microélectronique	CMP
KLÖCKER	Helmut	CR	Sciences & Génie des Matériaux	SMS
LAFOREST	Valérie	CR	Sciences & Génie de l'Environnement	SITE
LE COZE	Jean	PR 1	Sciences & Génie des Matériaux	SMS
LI	Jean-Michel	EC (CCI MP)	Microélectronique	CMP
LONDICHE	Henry	MR	Sciences & Génie de l'Environnement	SITE
MOLIMARD	Jérôme	MA	Sciences & Génie des Matériaux	SMS
MONTHEILLET	Frank	DR 1 CNRS	Sciences & Génie des Matériaux	SMS
PERIER-CAMBY	Laurent	MA1	Génie des Procédés	SPIN
PIJOLAT	Christophe	PR 1	Génie des Procédés	SPIN
PIJOLAT	Michèle	PR 1	Génie des Procédés	SPIN
PINOLI	Jean-Charles	PR 1	Image, Vision, Signal	CIS
SOUSTELLE	Michel	PR 1	Génie des Procédés	SPIN
STOLARZ	Jacques	CR	Sciences & Génie des Matériaux	SMS
THOMAS	Gérard	PR 1	Génie des Procédés	SPIN
TRAN MINH	Cahn	MR	Génie des Procédés	SPIN
VALDIVIESO	Françoise	CR	Génie des Procédés	SPIN
VAUTRIN	Alain	PR 1	Mécanique & Ingénierie	SMS
VIRICELLE	Jean-Paul	CR	Génie des Procédés	SPIN
WOLSKI	Krzysztof	CR	Sciences & Génie des Matériaux	SMS
XIE	Xiaolan	PR 1	Génie industriel	CIS

Glossaire :   ## Centres :

PR 1	Professeur 1ère catégorie	SMS	Sciences des Matériaux et des Structures
PR 2	Professeur 2ème catégorie	SPIN	Sciences des Processus Industriels et Naturels
MA(MDC)	Maître assistant	SITE	Sciences Information et Technologies pour l'Environnement
DR 1	Directeur de recherche	G2I	Génie Industriel et Informatique
Ing.	Ingénieur	CMP	Centre de Microélectronique de Provence
MR(DR2)	Maître de recherche	CIS	Centre Ingénierie et Santé
CR	Chargé de recherche		
EC	Enseignant-chercheur		
ICM	Ingénieur en chef des mines		

Acknowledgements

This work has been performed within the frame of the co-tutelary fellowship programme of the French Embassy in Prague. The research work has been performed in parallel at the Department of Environmental Technology (Institute of Chemical Technology, Prague, Czech Republic) and Laboratoire Génie de l'Evironnement Industriel (Ecole des Mines d'Alès, France), while every year of my Ph.D. studies has been divided into 6 months spent in Alès and 6 months spent in Prague.

I would like to express my deepest acknowledgements to Jean Roussy and Martin Kubal, directors of my thesis, for their understanding, their help with organization of my work and their useful and helpful assistance.

I am very grateful to Eric Guibal for supervising my research work. I would like to convey him my special thanks for his guidance, assistance and encouragement. During long months he had been patiently revising my manuscript, which would never be the same without his precious comments, helpful criticism and suggestions.

I would like to express my sincere appreciation to František Kaštánek, professor at the Academy of Sciences of the Czech Republic, for accepting to review my manuscrit. I am also very grateful to Rémy Gourdon, professor at INSA Lyon, for becoming the reviewer of my thesis.

I would like to express my acknowledgement to Mečislav Kuraš, professor at the Institute of Chemical Technology Prague, and to Jacques Bourgois, professor at Ecole Nationale Supérieure des Mines de Saint Etienne, for their participation in the jury.

I would like to take this opportunity to thank Markéta Španělová for encouraging me to do my Ph.D. thesis and for her precious help in its beginnings.

I am very grateful to Lenka Česáková, who prepared her final engineering project under my responsibility, for her enthusiasm, her motivation and her good mood and also for the patience and the accuracy that she proved throughout the experiments.

Contents

1 Introduction

Human activity affects significantly the environment. The industrial activities have created contamination of huge impact. The contaminants could be both of organic or inorganic origin, while the inorganic contaminants and more specifically toxic metals were in the centre of our attention.

Natural cycles of metals have been significantly altered by human activities. People have introduced in the environment significant amounts of toxic metals via different activities (burning of fossil fuels, use of pesticides and fertilizers and direct discharge of metallic effluents into rivers, lakes and seas without any adequate pretreatment).

During last century various treatment methods have been developed to treat the industrial effluents (precipitation, ion exchange etc.). The drastically increasing legislative requirements regarding metal discharge to the environment, the technical limits of these methods and their costs have directed the attention of research community to biosorption.

Biosorption is a physico-chemical process dealing with the interaction of a material of biological origin and a contaminant. The sorption process occurs on the constituents of this material, making profit of the presence of various functionnal groups. The main advantage of this process is its cost efficiency since using very cheap sorption materials to treat environmental pollution. A number of materials has been tested for biosorption purposes (including bacteriae, yeasts, fungi or algae). Some of them are very abundant in nature where they colonize lakes and coastal areas and may cause their eutrophisation. Their removal may thus be required for environmental reasons. This is the case of some algae (*Sargassum*, *Ascophyllum*). However, many of the tested organisms (especially fungi) are also frequently used for fermentation processes in agro-industries where, after enzyme extraction and biochemical transformations, their biomass cannot be re-used and constitutes waste material that is, in general, poorly valorized.

These biomasses may be used for the uptake of metal ions, while their low cost generally do not require a recycling and the biomass can be burnt after saturation concentrating the metal in ashes with high metal content. This concentration effect can be used for metal recycling or for reducing the volume of toxic wastes, minimizing the cost of their stabilization for final storage.

The objective of the present work was to study the biosorption of four metals among the most toxic ones – mercury, cadmium, lead and hexavalent chromium – by waste materials originated from Czech fermentation industry. These metals were selected for their particular toxicity and their intensive use in many industrial branches.

Two kinds of waste biomass *(Penicillium oxalicum* var. Armenica, *Tolypocladium* sp.) used in fermentation industry were submitted to different treatments and were tested as biosorbents of mentioned metals. At first, the sorption properties of these materials have been checked for the recovery of selected heavy metals from pure synthetic solutions. The influence of pH has been investigated in the first step, before the sorption isotherms and the uptake kinetics were carried out at optimum pH. The instrumental analyses were employed for the characterization of these materials and to investigate the sorption mechanism. The sorption from synthetic bimetallic solutions was tested further. Finally, the dynamic sorption using fixed bed column system was studied.

2 Literature survey

2.1 Toxic metals

The terms *trace metals*, *heavy metals*, and *toxic metals* are different terms traditionally associated with metals. *Toxic metals* are all those metals whose concentrations in the environment or human body are considered to be harmful. The term *trace metals* refers to metals that are present either in the environment or in the human body in very low concentrations, such as copper, iron or zinc. *Heavy metals* are those trace metals whose densities are at least five times greater than water, such as lead and mercury.

Metals have many properties that make them both interesting to study and important to human health. For example, some metals are essential for good health, and their deficiency can lead to a disease. Iron insufficiency, for example, causes anaemia. At the same time, metals that are necessary for good health in small amounts can become toxic if ingested in large doses. Molybdenum is required for certain enzymes to function properly, but a higher dose can lead to gout. Finally, some metals, such as lead, have no known functions in the body and any internal exposure may be harmful.[1]

Another important property of metals is that they never degrade. Unlike many organic pollutants that break down with exposure to sunlight or heat, metals persist. They can be buried in landfills or washed into sediments, but they never disappear entirely and always remain a threat for the future.

Human activities have significantly altered the natural cycle of metals. Metals belong to the natural contaminants of coal and oil, whereas burning coal and oil have become the main artificial source of metal contamination. In the past lead was added to petrol to prevent engine knocks, and cars became the greatest source of lead to the environment. Ore refining, trash burning and cement production are other important sources of air-borne metals. Landfills containing metals often leak these metals into underground water supplies.

Other ways of adding metals to the environment are via the use of fertilizers and pesticides and via acid rain. Arsenic has long time been a component of pesticides, and though its use is now declining, permanent contamination of many orchards and cropland has occurred.[2] Cadmium is a trace contaminant of phosphate fertilizers and is slowly but steadily

building up in agricultural soils.[3] Acid rains, caused largely by the burning of fuels, dissolves aluminium from surface rocks and soil and washes it into lakes and streams.[4]

Once mobile in the environment, metals find countless ways into the body through drinking of water, food and air.

2.1.1 Mercury

Mercury is a silvery-white liquid metal. It is used in thermometers and in the manufacturing of electrical equipment, including small batteries, mercury lamps and switches. It is also used in the production of chlorine and caustic soda, as an anti-mildew agent in paints and in industrial and control instruments.

The toxic effects of mercury depend mainly on its chemical form. Mercury is the only metal liquid at room temperature. Its vapour is more hazardous than the liquid form because it can be inhaled and is easily absorbed into the bloodstream. It is a potent neurotoxin capable of causing severe brain damage.[1]

Inorganic compounds of mercury are not highly toxic because they are not well absorbed and do not easily penetrate the blood-brain or placental barriers. Nevertheless, they are easily converted by bacteria to the far more hazardous organic forms, whereas methyl mercury is the best known and most important example. It has dramatic effects on the nervous system, particularly in the developing foetus and in small children because the brain is developing rapidly at these times.

Two major incidents of methyl mercury poisoning occurred in Japan in the areas of Minamata Bay and the Niigata River, and one occurred in rural Iraq. In Japan industrial effluents contaminated fish, a main component of the local diet.[5,6] In Iraq, methyl mercury treated seed grain was used to make bread that was subsequently eaten.[7]

Methyl mercury represents equally an important environmental threat, because it is bioacculmulative and can biomagnify in the food chain. Dusek et al.[8] reported bioaccumulation of mercury in muscle tissues of fish in the Elbe River (Czech republic) and found that the amount of mercury in the analyzed tissues depended largely on the position of given species in the throphic chain.

The contamination of fish tissues in freshwater reservoirs or lakes is inversely correlated to the pH of water, which relates the problematic to another great environmental problem – acid rains and the increasing acidification of surface waters that it causes. The

more acidic conditions shift the organic mercury to forms that are more readily absorbed by fish (dimethylmercury to monomethylmercury), thus raising the levels in fish to which humans are exposed. Hrabik a Watras[9] confirmed that the decrease in SO_2 and Hg emissions had apparently an immediate positive impact on de-acidification and on reduced mercury levels in Little Rock Lake (USA).

Besides mercury contaminated waste waters, atmospheric deposition plays also an important role in mercury pollution. Wong et al.[10] reported three main sources of atmospheric mercury emissions in Asia, namely coal combustion, steel production and gold mining.

2.1.2 Chromium

Chromium is a metal widely used in chrome plated steel and stainless steel. It has the unique property of being required for human health in one form (Cr(III)), while being among the strongest known causes of lung cancer in another form (Cr(VI))[11].

Chromium occurs in three stable forms: chromium metal, chromium (III), and chromium (VI). Chromium metal is extremely resistant to chemical attack (corrosion and oxidation), which accounts for its use in stainless steel and chrome plating.

Chromium (VI) is used in metal finishing (chrome plating), chromium chemicals production, chromium pigments for paint and textiles, leather tanning, and some wood preservatives. It is also used in electrical power plant cooling towers to prevent corrosion in the cooling loops.

Chromium metal appears to be biologically inert and no harmful effects have been reported. Chromium (III) (or trivalent chromium) is required for human health, participating along with insulin, in maintaining proper blood sugar levels. All ordinary exposures are considered to be safe.[1] It is the more stable of the two forms.

Hexavalent chromium (Cr(VI)) can produce liver and kidney damage, internal haemorrhage, dermatitis and respiratory damage. A common response is also an allergic skin reaction after exposure to chromium in such diverse products as leather, cement, wood preservatives and paint pigments.[1]

In the environment hexavalent chromium is rapidly transformed into trivalent chromium, thus the hazard exists mainly in the vicinity of direct discharges and significant quantities of chromium (VI) are almost always the result of human releases. It was proved that microbial activity decreases the toxicity and the mobility of chromium(VI). Desjardin et al.[12] reported that the metabolic activity of indigenous microoganisms isolated from a

hexavalent chromium contaminated soil modified the speciation of Cr(VI). The isolated microoganisms were found to reduce Cr(VI) to Cr(III), when a source of carbon and nutrients were provided. In another study, Fulladosa et al.[13] showed that *Vibrio fischeri* bacterium (used in acute and chronic toxicity tests) is resistant to the toxicity of Cr(VI), which may be partially explained by its capacity to reduce hexavalent chromium to its trivalent form.

Steel production, coal and oil combustion and chromium chemicals production are responsible for air-borne chromium release. Electroplating operations, leather tanneries, and textile manufacturing are the largest sources of water releases. Chromium chemical plants and chromite ore refineries are the largest sources of chromium-containing solid wastes. Important quantities of hexavalent chromium are also released when municipal waste is incinerated[14,15] and when sewage sludge and waste from electroplating and chromite refinery operations are disposed.[16] Solid waste containing hexavalent chromium can become a hazard when disposed of in landfills, because their form of chromium is very mobile in groundwater, whereas chromium (III) is not.[17]

2.1.3 Cadmium

Cadmium is an element mined in association with zinc and has also similar chemical behaviour. Discovered in 1817, it was rarely used until about 50 years ago. But today, cadmium is widely used in a myriad of products and industrial processes. It is used to galvanize metal parts, as a pigment in paints and plastics, in rechargeable nickel-cadmium batteries, and as a catalyst and preservative in the plastics industry. Many special-purpose alloys and solders are formulated on cadmium basis. Ceramic glazes and oil paints often contain cadmium-based pigments.

Cadmium is not known to be an essential human nutrient. Inhaled cadmium is associated with lung cancer in people.[18] Chronic exposure to low levels of cadmium may also result in progressive lung diseases and is also associated with a wide range of other diseases, including heart disease, anaemia, skeletal weakening, depressed immune system response, and kidney and liver disease.[1]

High levels of cadmium in the body are also associated with brittle bones. The cadmium-caused combination of brittle bones and kidney damage is called the Itai-Itai disease. In Japan, widespread contamination of rice with cadmium from zinc mines

contributed to numerous cases of this disease.[19] In the population, women were particularly affected.[20]

Smoking is another significant source of exposure. On the basis of a large scaled survey on the population of the Czech Republic Batariova et al.[21] reported three times higher levels of cadmium in blood of smokers than non smokers. In contrast to lead and mercury, the placenta acts as barrier for cadmium.[22]

The most important sources of atmospheric cadmium contamination are the burning of fossil fuels (especially coal), municipal and medical waste and sewage sludge. Cadmium tends to stick to fly ash, dust, soil particles and sediments.[23] Cadmium and zinc mining and application of phosphate fertilizers are other sources of cadmium in soil, water, and sediments. Many plants readily take up cadmium from the soil.[3] Thus, fruits, vegetables, grains and tobacco grown in cadmium-laden soil will contain significant concentrations of the metal.[24] Cadmium is strongly accumulated by organisms at all levels. It is not metabolized and passes unchanged along the food chain.[1] Food and drink contamination may also arise as a result of using water from pipes soldered with cadmium-containing materials or from dissolution of cadmium from pottery painted with cadmium containing pigments.[25]

2.1.4 Lead

The major uses of lead are in storage batteries, gasoline additives and other chemicals. It is also used in production of ammunition (shots and bullets) and solders. Lead is a common industrial metal that has become widespread in air, water, soil, and food. Leaded pipe and solder in pipe joints in water distribution systems and home plumbing can release lead too.

Lead affects the human nervous system, the production of blood cells, kidneys, reproductive system and human behaviour.[1] Lead poisoning is also known as saturnism. It behaves like calcium in the body and accumulates in bones. At times of calcium requirements, such as during pregnancy, lead can be mobilized from bones and enter the blood stream, where it creates elevated levels. Pregnant women are at high risk because lead can cross placenta and damage developing foetal nervous system; it can also induce miscarriage. There are no known physiological requirements for lead.

Lead is released into the environment primarily through the air by the burning of petrol and solid wastes.[23] From the atmosphere it is deposited onto soils, plants and water. Fortunately, emissions of lead into the air have declined dramatically in recent years because

of progressive restrictions on the lead content in petrol and the increasing use of unleaded fuels.[26] Even though, the use of lead as an antiknock additive in the recent past has created a contamination problem of global proportions. Additionally, in many countries deteriorating of lead paint used for indoor and outdoor household decorations and lead-glazed ceramics used for storage and preparation of food have remained important sources of contamination.[27]

There are no doubts about the toxicity of above mentioned metals. Therefore very severe standards for both drinking and waste waters are applied throughout the world. As an illustration the limits applied in the Czech Republic are cited in Table 1.

Metal	Drinking water standards [$\mu g\ L^{-1}$]
Hg	1.0
Cr_{total}	50
Cd	5
Pb	50

Table 1 Drinking water standards in the Czech Republic[28]

2.1.5 Conventional treatments of metal contaminated industrial effluents

Conventional treatment methods for metal contaminated effluents include chemical precipitation and sludge separation, chemical or biological oxidation/reduction, ion exchange, reverse osmosis, electrochemical treatment and evaporation. Their advantages and disadvantages are summarized in Table 2.

Method	Disadvantages	Advantages
Chemical precipitation and filtration	Suitable for high concentrations, difficult sludge separation, sludge disposal	Simple & cheap
Chemical or biological oxidation/reduction	Chemicals required (chemical process), climate sensitive - slow rates (biological process)	Mineralization
Electrochemical treatment	Suitable for higher concentration, expensive	Mineralization
Reverse osmosis	High pressures, membrane scaling, expensive	Metal recovery
Ion exchange	Sensitive to particles, expensive resins	Effective, pure effluent, possible metal recovery
Adsorption	Used in large scale for organic contaminants	Conventional sorbents (activated carbon)
Evaporation	Energy intensive, expensive, sludge creation	Pure effluent (for recycle)

Table 2 Conventional metal removal technologies[29]

Traditionally, metal-finishing waste waters have been treated via hydroxide precipitation. It was and still remains the most dominant method of waste solids precipitation. Since most heavy metals have low solubilities as hydroxides, the addition of an alkali to adjust the pH to a common pH range of 9 to 10 standard units provides adequate metal precipitation to meet discharge limits.

Carbonates and sulphides precipitations offer an alternative to the use of hydroxides. Gonzales-Munoz et al.[30] demonstrated the feasibility of cadmium and lead precipitation from metal industry waste waters in form of sulphides. The possibility of coupling the precipitation process with nanofiltration was also proposed. Lead removal from battery manufacturing waste waters based on carbonate precipitation was presented by Macchi et al.[31]

The use of alternative commercial precipitation products has been proposed recently. One of them is dithiocarbamate (DTC), commonly used in the form of sodium dimethyldithiocarbamate and diethyldithiocarbamate. DTC is usually dosed in stoichiometric ratio with dissolved heavy metals to form insoluble metal-dithio salts.[32] Another product is commercialized by Degussa Corp. under the name TMT-15. It is a 15% aqueous solution of trimercaptotriazine. Henke et al.[33] reported the use of TMT as a precipitation agent for mercury-bearing waste waters, but the precipitates revealed to be unstable under various

aqueous or atmospheric conditions. TMT may also be used to precipitate cadmium, lead and zinc, but Matlock et al.[34] reported that their precipitates were more soluble in water than corresponding sulphides and some hydroxides. In another study, Matlock et al.[35] compared three commercial reagents (TMT, Thio-Red$^®$ - potassium/sodium thiocarbonate and HMP-2000 sodium dimethyldithiocarbamate) and found that the compounds were unable to sufficiently reduce the concentrations of single metal solutions (containing 50 ppm of divalent cadmium, copper, iron, lead or mercury, respectively) to meet the EPA standards. Additionally, the compounds displayed high leaching rates and in some cases decomposed to produce toxic substances. On the other hand, Tassel et al.[36] reported high efficiency in mercury removal from mercury cyanide complexes (originated from the processing streams of gold cyanidation circuits), where selective aggregation of mercury was carried out after precipitation of the complexes with sodium dimethyldithiocarbamate (NaDTC), coagulation with colloidal hydroxides, flocculation with polymer and final aggregates removal by flotation.

A combined method of reduction/precipitation has traditionally been used for hexavalent chromium contaminated waste waters. The conventional treatment consists of four steps, including the reduction of the hexavalent to the trivalent form at acidic pH, the precipitation of Cr(III) as Cr(OH)$_3$ at high pH, the settling of the insoluble metal hydroxide and finally the disposal of the dewatered sludge. Waste waters containing relatively low concentrations of Cr(VI) can be treated with ion-exchange resins which offer the advantage of the recovery of chromic acid but at a high cost brought by the high cost of the resins.[37]

Sakalis et al.[38] proposed an electrochemical method (based on electrolysis) for treatment of textile industry waste waters and high efficiency (90%) in colour removal was reported. The application of electrochemical technique on plating industrial effluent (containing Cu^{2+}, Cr(VI), Ni^{2+}) was tested by Humson et al.[39], whereas high efficiency in metal reduction and low effluent concentrations were achieved.

Another treatment method listed in Table 2 is reverse osmosis. It is a process, where solvent is transported from a region of high solute concentration to a region of low solute concentration through a membrane by applying a pressure in excess of the osmotic pressure. Semipermeable membranes allowing the passage of solvent but not of solute are used. This process is known for its use in desalination. For example, potable municipal water in

Askhelon (Israel) is produced by desalination of seawater by reverse osmosis.[40] The application of reverse osmosis on arsenic removal from drinking water was studied by Gholami et al.[41] In industrial scale, reverse osmosis is also used for removing minerals from boiler water at power plants.[42] Reverse osmosis can equally be used for the production of deionised water.

Ion exchange is a method traditionally used in water treatment, such as water softening or manufacturing of ultra-pure water used in semiconductor processes. Eom et al.[43] proposed ion exchange as a treatment and recovery method for plating waste waters containing nickel. The use of natural and modified zeolites as lead and cadmium exchangers were proposed by Curkovic et al.[44] The use of weak acid cation exchangers and modified strong acid cation exchangers for the treatment and recovery of copper from electroplating rinse waste waters was studied by Dobrevsky et al.[45].

Adsorption technique was applied at industrial scale for waste waters contaminated by organics.[46] Activated carbon has traditionally been used as adsorbent. Moreover, adsorption was also applied for the removal of dyes from waste waters from textile industry. Metal adsorption is not as widespread as organic pollutant adsorption and was mostly studied at laboratory scale.

Evaporation is usually employed as a treatment technology, when the main objective is the waste minimization and the water reuse. Evaporation technique separates waste water in condensate, which is reused as rinsing water, and concentrate, which is either reused in the plating process or disposed depending on the waste management of the plating company.[47] Salzman studied the efficiencies of evaporation ponds as a disposal technique for aluminium smelter waste waters (Australia), whereby sunlight was used as the source of energy.[48]

2.2 Materials of biological origin in water treatment (biosorption, bioaccumulation, bioprecipitation)

Biosorption is an alternative process to conventional treatments mentioned in section 2.1.5. It deals with the uptake of contaminants from aqueous solutions by biological materials, but it refers to different modes of non-active metal uptake by microbial biomass. In a

biosorption process, metals are sequestered by cells via ion exchange, coordination, complexation etc. The major advantages of biosorption technology are: its effectiveness in reducing the concentrations of heavy metal ions to very low levels and the use of inexpensive biosorbent materials.

Nevertheless living microorganism can also be used in metal contamination treatment since they play an important role in metal cycles in the environment. Johnson[49] described several microbiologically – mediated mechanisms of environmental transformation of metals. These are namely: assimilation/adsorption and mineralization, precipitation and dissolution, oxidation and reduction and methylation and dealkylation reactions. In some cases, these transformations involve phase changes (e.g. from a soluble to a volatile state) and/or changes in oxidation states.

Assimilation of metals (both essential and non-essential) by microorganisms results in their accumulation in living biomass by the way of intracellular accumulation, cell surface interactions or adsorption onto extracellular polymeric materials. Accumulation of metals inside microbial cells usually involves an energy-dependent transport system, whereby they first bind to the extracellular cell surface and then are actively transported inside the cell membrane.

Microorganisms may also promote the mobilisation or immobilisation of metals in ecosystems by causing their dissolution or precipitation. Some microbial processes, such as fermentation, nitrification and sulphur-oxidation, generate acidity while others, such as ammonification, denitrification, sulphate-reduction and methanogenesis, generate alkalinity. Organic acids may also be formed as fermentation products and are also excreted by some aerobic microorganisms (mainly fungi). Besides their effects on pH, some of them (e.g. oxalic and citric acids) are able to chelate metals and form highly soluble metal complexes.

Microbially mediated precipitation of metals can result from the formation of insoluble extracellular hydroxides, phosphates, carbonates and sulphides. [50] Precipitation of metal sulphides is particularly important in mine-impacted environments (spoils, tailings and acid mine drainages).

Microorganisms are also capable of metal oxidation/reduction. These redox transformations mostly involve active metabolism, while they have been demonstrated for iron, manganese, chromium, copper, uranium etc. In some cases, redox transformations of metals are involved in energy conservation, i.e. metals act as direct or indirect electron donors or acceptors in microbial metabolism. In the case of iron, oxidation of ferrous to ferric form results (when pH>2.5) in the transformation of a soluble metal to an insoluble form. In other

cases, such as oxidation of uranium(IV) to uranium(VI), and of chromium(III) to chromium(VI), oxidation transforms a more insoluble species to the more soluble (and bioavailable) form.

Meanwhile, transformations of metals by methylation and dealkylation reactions are carried out apparently as a defence mechanism. In contrast to other forms of metal transformations, methylamine usually results in the production of volatile complexes. The most well studied metal methylamine reaction concerns mercury.

Although all of the mentioned mechanisms are interesting and worth to study, the process of biosorption was in the centre of our attention and will be studied in detail in the following chapters.

2.2.1 Biosorbents

A wide range of biological materials have been tested for biosorption purposes. Fungi, bacteria, yeast and algae were all employed in metal biosorption. Both cationic and anionic metal uptakes were studied, whereas more attention was given to the biosorption of cations. However, biosorption of organic pollutants was also investigated.

Many materials exhibit sorption properties, but only those with significantly high metal binding capacities and performing certain selectivity can be considered for future valorisation in a full scale biosorption process. An overview of the principle materials used in biosorption studies is introduced in following paragraphs.

2.2.1.1 Fungal biosorbents

Biosorbents are traditionally divided into three groups according to their origin (e.g. fungal, algal and bacterial biosorbents). The first group constitutes of biomass of fungi and yeast. It was proved that the main site of metal deposition in fungi is its cell wall, which is in general seen as a two-phase system. The inner micro-fibrillar layer of the wall usually consists of chitin (Figure 2), but cellulose (Figure 1) or non-cellulosic β-glucan can also occur, depending on the taxonomic group. The outer more amorphous layer constitutes mostly of glucans, but can also contain mannans, galactans, chitosan or glycogen. Phosphated polysaccharides may also be found.[51]
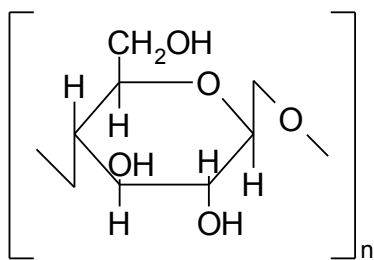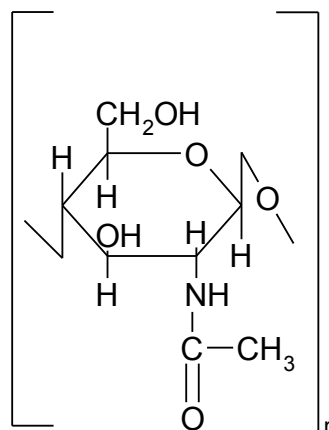
Figure 1 cellulose monomer unit   **Figure 2 chitin monomer unit**

Phosphate and carboxyl groups are thought to be responsible for negative charge in the fungal wall, while amine groups create a positive charge (in acidic solutions). Apart from electrostatic attraction to these charged groups, complexation with N or O donors (e.g. of chitin or chitosan) may occur. Since the protein content is low (in general), the importance of amine acid functional groups in metal uptake is small. Released metabolites can lead to micro-precipitation (oxalates due to oxalic acid, sulphides due to H_2S) or chelation (citric acid).

Several possible metal binding sites were identified in *Absidia orchidis*[52] used in steroid transformation. Besides glucan and chitin, phosphate, hydroxyl and –SH functional groups were identified in its cell walls, all of them capable of forming chelate complexes with metals. Additionally, metals could also be entrapped in the inter-fibrillar capillaries in both glucan and chitin.

Many studies demonstrated that, particularly, the biomass of the order of Mucorales (R*hizopus arrhizus, Rhizopus nigricans*) represented a good biosorbent material for a wide range of heavy metals.[52, 53] Chitin and chitosan contents were confirmed in both *Rhizopus arrhizus* and *Rhizopus nigricans* cell walls. While these compounds may be active, they may not necessarily be the key components in biosorption.

Fungal biosorbents were abundantly used in metal biosorption. For example, *Rhizopus arrhizus*[54], *Rhizopus nigricans*[55], *Aspergillus niger*[56,57] and *Lentinus sajor-caju*[58] were used for hexavalent chromium biosorption. *Mucor rouxii*[59], *Rhizopus arrhizus*, *Mucor miehei* and *Penicillium chrysogenum*[60] were tested for cadmium biosorption. *Phanerochaete chrysosporium* was used for mercury sorption.[61,62] *Aspergillus niger*[63]and *Penicillium chrysogenum*[64] were tested for the biosorption of lead. Huang and Huang[65] successfully used

biomass of *Aspergillus oryzae* and *Rhizopus oryzae* for copper uptake. McAffee et al.[66] sequestered zinc, chromium, arsenic and copper on *Rhizopus oryzae* biomass too. Waste fermentation biomass of *Streptoverticillium cinnamoneum* was used to sequester lead and zinc by Puranik and Paknikar.[67]

The fungal biomass was also successfully tested for the biosorption of non-metallic species, for example dye uptake by *Rhizopus arrhizus* [68] and by *Aspergillus niger*[69] or phenol binding[70]. The biosorption of radionuclides was not left out of consideration. Uranium uptake was performed by *Aspergillus niger*[71], *Mucor miehei*[72] and *Rhizopus arrhizus*[73]. Particularly interesting results were obtained by Guibal et al.[72] using *Mucor Miehei* biomass (by-product of the enzyme industry). Sorption capacities as high as 240 mg U g^{-1} were obtained at pH 6, while the maximum uptake decreased with decreasing pH. This fact was connected to complicated uranyl chemistry (hydrolysis phenomenon).

2.2.1.2 Algal biosorbents

The second important group of biosorbents comprises biomass of both marine and freshwater algae. Biosorption in algae has also been attributed to the cell wall, while the typical algal cell wall of red, green and brown algae consists of a fibrillar skeleton and an amorphous embedding matrix. The most common fibrillar material in algal cell walls is cellulose (Figure 1) which shows unfortunately negligible metal biosorption. In brown algal matrix, the alginic acid or alginate, composed of mannuronic and guluronic acid units (Figure 3), are the dominant constituents with a smaller amount of sulphated polysaccharide (fucoidan). A number of carboxylic groups is thus present on the biomass surface and these groups are believed to be responsible for metal binding, whereas sulphate groups contribute to this binding only to a lesser extent. Both mentioned groups are acidic and bear a negative charge when deprotonated.[74]
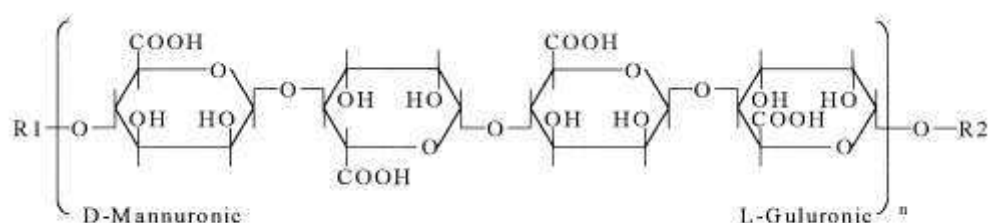

Figure 3 Chemical structure of alginic acid[75]

The material that was traditionally and widely used for biosorption purposes is the brown seaweed *Sargassum* sp., which was successfully tested for lead[76], chromium[37], uranium[77] and copper[78] biosorption. Other brown marine algae were tested too, for example *Laminaria japonica* for lead biosorption.[79] Yu et al.[80] tested a variety of marine algae (*Ascophyllum nodosum, Lessonia flavicans, Ecklonia radiata, Durvillaea potatorum*) as cadmium, lead and copper biosorbents. Brown algae have in general exhibited higher sorption capacities than red and green algae as confirmed by Hashim et al.[81] for cadmium biosorption. The fungal and algal biosorptions were compared in some studies. For illustration, Nourbakhsh et al.[82] reported that binding capacities for hexavalent chromium decreased in order algae > fungi > yeast > activated sludge bacterium.

2.2.1.3 Bacterial biosorption

Bacterial biomass (*Bacillus, Streptomyces, and Citrobacter*) was more often used in bioaccumulation and bio-precipitation (also called microprecipitation). Nevertheless, the complexation by N and O ligands in the cell wall as well as electrostatic attraction to charged groups in the cell wall may also occur. For example, microprecipitation is often preceded by binding to specific sites which provides nucleation points.[83]

The higher metal binding capacity of gram positive, over gram negative bacteria was observed and this fact was ascribed to thicker peptidoglycan layer in which teichoic and teichuronic acids are embedded. The most tested biomass was *Bacillus subtilis* and for this material the major importance of carboxyl groups of peptidoglycan layer as well as a minor contribution of phosphate groups was demonstrated, while amine groups did not appear to be relevant.[83] A lot of application-orientated work was done on metal biosorption by waste bacterial biomass of *Bacillus subtilis*[84,85], but a large industrial success of this method was not achieved.

Gram negative bacteria are characterized by an outer membrane containing lipopolysaccharides and phospholipids. Their phosphonate groups create a negative surface charge and were confirmed to be the primary metal binding site in *E. coli*.[83]

2.2.1.4 Other biosorbent materials

A number of studies focused on metal binding using aminopolysaccharides such as chitin and chitosan. Chitin is one of the most abundant biopolysaccharides in nature. Chitosan is the deacetylated form of chitin (Figure 4). Chitin can be obtained from fungi, insects, lobster, shrimp and krill, but the most important commercial sources are the exoskeletons of crabs obtained as waste from seafood industrial processing. Chitin and mainly chitosan have demonstrated a promising potential for metal removal. This material was widely studied in the frame of LGEI laboratory and numerous papers have been published. Just for illustration, chitosan and its derivates were successfully used for vanadium and uranium[86], cadmium[87], platinum and palladium[88], copper[89], gold[90], arsenic[91] and Reactive Black 5 dye[92] sorption.
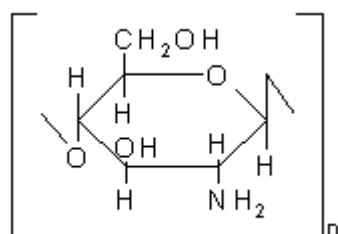

Figure 4 Chitosan monomer unit

A number of other materials was tested among them plant materials, agricultural products and by-products, wooden materials etc. Uptake of chromium cations and anions by milled peat (complex material containing lignin and cellulose as its major constituents[93]) was studied by Dean and Tobin.[94] The seed bearing cone biomass of coniferous tree *Pinus sylvestris* was used by Ucun et al. to sequester chromium(VI)[95] and lead(II)[96] from its solutions. Dakiky et al.[97] published an extensive study dealing with the use of wool, olive cake, saw dust, pine needles, almond shells, cactus leaves and charcoal, all abundant low-cost locally available adsorbents, to remove chromium (III and VI).

Lister and Line[98] examined sewage sludge, paper mill waste (cellulosic material) and composted paper mill waste for potential utilisation as cadmium, copper, zinc and lead biosorbents. Villanueva-Espinosa et al. [99] used heat treated scales of fish *Oreachromis niloticus* to study the adsorptive properties for the removal of Cu^{2+}, Pb^{2+}, Co^{2+} and Ni^{2+}. Conrad and Bruun Hansen[100] tested the ungrounded and unmodified coir (fibres from *Coco nucifera*), a waste product from the copra industry, for sorption of zinc and lead. Niol et al. [101]

investigated the sorption properties of olive stone waste (olive oil production waste product) for the biosorption of cadmium, lead, nickel and copper.

2.2.1.5 Biosorption applications, advantages and disadvantages

Two possible applications of biosorption process could be intended. The first application concerns waste water treatment as the severe water standards may be reached by the existing biosorption technology. Additionally, broad range of service conditions can be employed and low cost sorbents are used.

Biosorption can equally be used to recover precious metals from processing solutions. The saturated biosorbents may concentrate metals from the liquid phase, while the metals may be desorbed afterwards. Several studies have shown that elution of the biomass by acid solutions could be highly effective.[102, 37, 59] In general, the elution process does not significantly reduce the binding capacities of the biomass and several cycles may be employed.[62] With a high concentration factor, it should be possible to reduce the volume of waste that is produced by applying an iterative metal sorption - desorption process such that only a small volume of solid waste is generated. According to this scenario, the biosorbent is regenerated and a highly concentrated metal solution is obtained. This concentrate may then be treated by either co-precipitation, flocculation or electro-winning. The selection of the process depends on metal concentration, composition of the solution and the value of the metal.

There is no doubt that the major advantage of biosorption process is the low cost of biosorbents. It offers a possibility of industrial waste by-products valorisation. For example, fungi and yeast are employed in a variety of industrial productions. The growth of the biomass is connected with the production process. Once the production process is achieved, the biomass cannot be reused and significant amounts of biological wastes are produced. Fungi and yeast are so readily available and can easily become an important source of biosorbents. The idea of biomass valorisation is summarized in Figure 5. As an illustration, *Aspergillus niger* is used in the production of citric acid and glucamylase enzyme. *Saccharomyces cervisiae* is employed in food and beverage industry. *Rhizopus arrhizus* produces lipase enzyme.[103] Bacterial biomass can be also obtained as a waste product from fermentation industries which make it a cheap raw material.
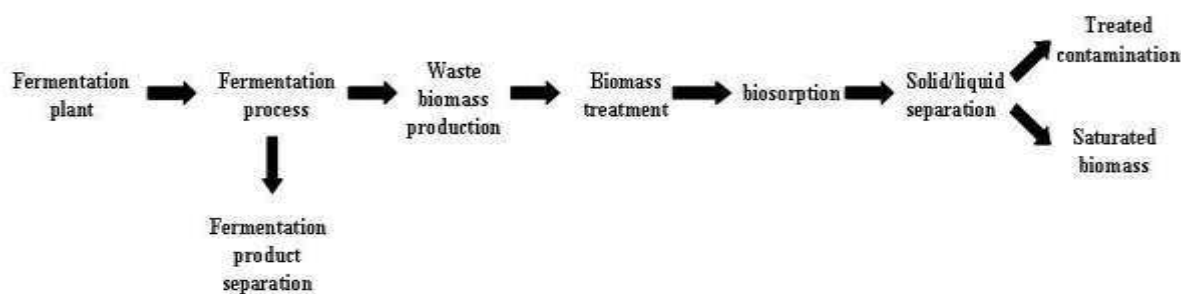
Figure 5 Biomass valorisation for biosorption purposes

However, some disadvantages exist too. Two major drawbacks are often mentioned. Firstly, fermentation biomass waste may contain fermentation broth residues and it may also be contaminated by fermentation metabolites, which may lead to metal precipitation (in form of oxalates due to oxalic acid as observed by Spanelova et al.[104]) or chelation (citric acid). Both of these processes would interfere biosorption process.

Secondly, the composition (and sorption capacities) of biomass may vary with changes in fermentation conditions (broth composition, pH, temperature) as shown by Dostalek et al.[105] Furthemore, biomass separation may sometimes pose problems. While some filamentous fungi such as *Aspergillus niger* grow in pellets and are easily separable, other types of fungi (growing in fibres) create problems of solid/liquid separation. Additionally, immobilization process is often required before the use in a biosorption column, which would increase the costs. The same precautions are valid for bacterial biomass.

On the other hand, algal biomass is a very abundant material, especially marine algae. Seaweed biomass is also better defined than microbial industrial biomass because the conditions in the sea water are less variable than those in fermentation media. Finally, seaweeds are large and often sturdy, so that they do not require granulation and immobilization pretreatments. Nevertheless partial solubilization of algal biomass was described by some authors.[112]

While the ocean-based seaweed materials are not readily available in landlocked regions, waste mycelia from industrial fermentation appear as a good ecological and economical solution.

Unfortunately, only little application oriented work has been done so far. Two commercialized biosorbents are worth to mention. One of them, AlgaSORB™ consists of dead algal cells (*Chlorella vulgaris*) immobilized in a silica gel polymer (developed by Bio-recovery Systems Inc., USA).[106,107] The other one, AMT-BIOCLAM™ (MRA) employed

Bacillus microorganism to manufacture granulated material for wastewater treatment and metal recovery.[84,85] Nevertheless, a considerable commercial success of these materials has not been reported so far.

2.2.1.6 Biosorption mechanisms

As already mentioned, biosorption process is defined as a passive sequestering of metal ions by metabolically inactivated biomass. The nature of metal binding can be either physical or chemical. Volesky[51] distinguished three principle biosorption mechanisms – namely: ion exchange, adsorption and micro-precipitation.

Ion exchange is a process in which ions are exchange between solution ion exchanger (usually a solid). Following principle of ion exchange process was proposed for alginic acid (ALG):

$$2\mathbf{NaALG} + \mathbf{Me}^{2+} \Leftrightarrow \mathbf{Me(ALG)_2} + 2\mathbf{Na}^+$$
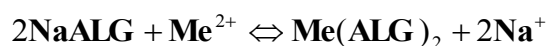
Recently it has been confirmed that ion exchange is predominantly involved in metal biosorption by algal polymer.[108]

The term adsorption implies a surface phenomenon and the actual sequestration may take place by either physical phenomenon (so-called physical adsorption) or via a variety of chemical binding procedures (chemisorption). Examples of chemisorption are metal complexation, coordination and chelation. Complexation is defined as formation of species by the association of two or more species (one of them usually being a metal ion). When the central atom of a complex is bound to its immediate neighbours by covalent bonds then the process is called coordination. On the other hand, some ligands are attached to a metal atom by more than one donor atom in such a manner as to form a heterocyclic ring. This type of ring is called a chelate ring and the molecule or ion from which it is formed is known as a chelating agent or chelator. The process of forming a chelate ring is called chelation.

The major binding sites playing role in a biosorption process were identified in chapters 2.2.1.1 - 2.2.1.3. The majority of them are acidic. Hydroxyl, carboxyl, sulfhydryl, sulfonate, phosphonate are neutral when protonated and negatively charged when deprotonated. When the pH of the solution exceeds their pKa these groups become mostly

available for attraction of cations. On the other hand, amine, imine, amid and imidazole groups are neutral when deprotonated and positively charged when protonated. Therefore, they attract anions if the pH is lowered such that the groups are protonated.[109]

Inorganic micro-precipitation appears when the solubility of the sorbate reaches its limits. This may happen even due to local conditions (on and/or inside the sorbent) and not necessarily in the bulk of the solution. On one hand, micro-precipitation could contribute to the overall metal removal efficiency. On the other hand, it interferes the proper biosorption process and makes difficult the interpretation of experimental results.

Knowledge of acid-base properties of tested materials and understanding the exact mechanism of the process could make the predictions easier. For example, knowing that the mechanism of biosorption is largely based on an ion exchange implies that changes in the ionic strength of the solution would affect metal uptake. Another example is that metal binding to acidic groups could be reversed by reducing the pH and thereby protonating these groups.

Unfortunately, it is not easy to discover the proper biosorption mechanism since simple and clearly defined chemical compounds are not involved in such a process. Biosorbents comprise different types of cells with a complex structure whose various building units consist of a range of different molecules which can display several binding sites. Moreover, even one binding site can participate in different mechanisms; for example, carboxyl groups can be engaged both in a complexation and an electrostatic attraction of metal cations.

The biosorption of target metals will be discussed in detail in following chapters with the regards to diversity of used materials, experimental conditions, obtained results and biosorption mechanisms.

2.2.1.7 Mercury biosorption

Surprisingly, very little information has been so far published on mercury biosorption. The main characteristics and general trends of data published on mercury sorption are

summarized in Table 3 and only certain of them will be discussed further if they revealed information relevant to biosorption mechanism.

Biomass type	Biomass class	Biomass treatment	Conditions			Other metals studied	References
			Optimum initial pH	Sorption capacity [mg g^{-1}]	[mmol g^{-1}]		
Bacillus sp.	Bacterium	Autoclaved, dried	4.4 – 6	8	0.04	-	Green-Ruiz (2005)[110]
Cystosteira baccata	Macroalga	Dried	6	330	1.6	-	Herrero et al. (2005)
Microcystis aeruginosa	Cyanobacterium	Lyophilised	No information	Column mode	-	Cd, Pb	Chen et al. (2005)[111]
Ulva lactuca	Alga	Protonated, dried	7	150	0.7	-	Zeroual et al. (2003)[102]
Phanerochaete chrysosporium	White-rot fungus		7	50	0.25	-	Saglam N. et al. (1999)
Phanerochete chrysosporium	White-rot fungus	Immobilized on carboxymethyl cellulose	6	80 (viable)	0.4	-	Saglam A. et al. (2001)
				100 (heat inactivated)	0.5		
				40 (carboxymethylcellulose)	0.2		

**Table 3 Mercury biosorption (literature screening)**

Saglam N. et al.[61] described the use of white-rot fungus *Phanerochaete chrysosporium* as a biosorbent for inorganic mercury and alkylmercury species. For both organic and inorganic mercury species, the maximum sorption was observed at around neutral pH. The biomass performed slightly higher biosorption capacities for the organic mercury species. The affinity of the sorbent (based on molar units) for the different mercury species was ranked according to: $CH_3HgCl > C_2H_5HgCl > HgCl_2$.

Phanerochaete chrysoporium immobilized on carboxymethylcellulose was also used by Saglam A. et al.[62] for the removal of mercury ions from aqueous solutions. Both viable and heat-inactivated cells were tested and compared to carboxymethylcellulose. High desorption efficiency and a reuse in three cycles was achieved.

Herrero et al.[112] published an extensive study on mercury biosorption by non-viable biomass of the brown marine macro alga *Cystosteira baccata*. Experiments were performed at constant pH and *C. baccata* showed a very high Hg(II) uptake capacity. A lot of attention was given to mercury speciation in the solution. While other metals are generally present in their free ionic form all along the pH range studied, non-ionic speciation of mercury was found. The majority of mercury existed in the form of $HgCl_2$ at pH 6 (optimum pH). This finding was considered crucial by Herrero et al.

The influence of solution salinity was also studied. An increase in concentration of nitrate salts (either sodium or potassium) caused greater mercury uptake, while a larger presence of NaCl salt led to a drop in the sorption. Authors resumed, that the presence of light metal ions did not affect the mercury uptake, while the major effect on the mercury biosorption capacity was caused by the salt anions. Such behaviour was explained by taking into account mercury speciation in the excess of chloride ions, which induced the formation of $HgCl_3^-$ and $HgCl_4^{2-}$ complexes with low sorption capacity, whereas nitrate salts did not tend to form strong mercury complexes of any kind.

Moreover, the addition of different divalent cations (Ca, Mg, Cd, Pb and Cu) at much higher concentration than mercury revealed a negligible effect on the uptake process. Only Cu(II) ions seemed to slightly decrease mercury sorption, whereas Pb(II) ions increased it. Such results were explained by authors in terms of the different chemical speciation of metal at the pH studied, which had a significant effect on the adsorption mechanism. Whereas mercury was largely present as neutral species, $HgCl_2$, the other metals appear as divalent ions, M^{2+}, which may interact with the algal cell walls mainly through an electrostatic mechanism, thus avoiding any competition with the sorption process of neutral species of mercury. In this way, its interaction with the functional groups of the algal wall (represented by A^-) was illustrated by a reaction of the type:

$$A^- + HgCl_2 = AHgCl_2^-$$
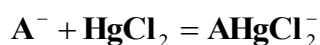
According to Herrero et al., such a mechanism did not lead to any change in the charge of the algal surface, which hence, could still bind any other metal cation present in solution. Such specific adsorption of the neutral species was also supported by the small changes in mercury adsorption when the effect of ionic strength was studied.

Due to the relatively "soft" character (Pearson's HSAB theory) of copper, Cu(II) tends to form covalent bonds more readily then hard cations such as Ca^{2+} or Mg^{2+}, which are mainly electrostatically bound. Since Hg(II) has a strong "soft" character (especially in the form of neutral species), it may therefore be expected that Cu(II) species will compete to some extent with mercury. On the contrary, Pb(II) seemed to reinforce mercury uptake, but no consistent explanation was found.

Furthermore, two simple isotherm models were proposed reflecting either 1:1 or 1:2 stoichiometry of interaction between algal sorption sites (ligands) and mercury/protons. However, the stoichiometry of mercury biosorption could not be clearly established. The 1:2 isotherm fitted very well the experimental data at low ratios of metal to algal acid sites, while

the maximum mercury loadings at a relatively high pH could only be explained by a 1:1 relationship. According to authors the actual binding mechanism would probably involve a combination of both mono and bidentate sites, or even some degree of interaction between mercury and non-ionized sites of the algal surface.

Due to the low number of studies dealing with mercury biosorption, it is difficult to make any conclusions. Nevertheless, the pH dependence of mercury biosorption was clearly demonstrated, while the optimum was found in the range 6 − 7. Non-ionic interaction of mercury species with sorption sites of biosorbent was also illustrated by Herrero et al.[112].

2.2.1.8 Chromium biosorption

Chromium occurs in waste waters typically in two oxidation states, as a trivalent Cr(III) form and a hexavalent Cr(VI) form. The hexavalent chromium appears as an anion and its exact speciation depends largely on the pH of the solution. These two oxidation states have different chemical, biological and environmental properties as described in chapter 2.1.2. Biosorption of both forms has been extensively studied over the last decade. As implied from literature, Cr(III) biosorption follows the trends common for other cationic species. Therefore Cr(III) and Cr(VI) biosorptions were often studied separately. Hence, the biosorption of the trivalent chromium form is not comprehended in this review.

The main characteristics and general trends of data published on hexavalent chromium biosorption are summarized in Table 4.

| Biomass type	Biomass class	Biomass treatment	Conditions			References
			Optimum initial pH	Sorption capacity		
				[mg g^{-1}]	[mmol g^{-1}]	
Rhizopus arrhizus strain NCL 977	Fungus	Autoclaved	2	Freudlich relationship used	-	Prakasham et al. (1999)[54]
Rhizopus nigricans	Fungus	Autoclaved, powered	2	47	0.9	Bai and Abraham (2001)
Natural wool from sheep			2	41	0.8	Dakiky et al. (2002)[97]
Sargassum sp.	Brown seaweed	Protonated, Ca-form	2	No information available	-	Kratochvil et al. (1998)
Ecklonia sp. (brown seaweed)	Brown seaweed	Non-viable, dried, protonated (1M H$_2$SO$_4$)		230	4.5	Park et al. (2004)

Table 4 Hexavalent chromium biosorption (literature screening)

Biomass type	Biomass class	Biomass treatment	Conditions			References
			Optimum initial pH	Sorption capacity		
				[mg g^{-1}]	[mmol g^{-1}]	
Peat	-	Dried	2	30	0.6	Dean and Tobin (1999)
Crosslinked sodium alginate and gelatine	Biopolymeric matrix	-	8.9	No information available	-	Bajpai et al. (2004) [113]
Spirogyra sp.	Filamentous algae	Dried	2	15	0.3	Gupta et al. (1999) [114]
Chlamydomonas reinhardtii	Microalgae	Native	2	18	0.4	Arica et al. (2005) [115]
		Heat treated		26	0.5	
		Acid treated		21	0.4	
Sargassum siliquosum	Brown seaweed	Sun-dried and protonated	2.1 – 2.8	66	1.3	Cabatingan et al. (2001)
Bacillus laterosporus,	Bacteriae	Autoclaved	2.5	62	1.2	Zouboulis et al. (2004) [116]
Bacillus licheniformis				73	1.4	
Aspergillus niger	Filamentous fungus	Grown on wheat bran; autoclaved	5 – 6	16	0.3	Chandra Sekhar et al. (1998)
Lentinus sajor-caju	White-rod fungus	Untreated	2	11	0.2	Bayramoglu et al. (2005) [58]
		Heat-treated		26	0.5	
		Acid-treated		16	0.3	
		Alkali-treated		21	0.4	
Cone biomass of *Pinus sylvestris*	Seed bearing cones of coniferous tree	Dried, sieved	1	200 (Freundlich)	3.9	Ucun et al. (2002)
Aspergillus niger	Filamentous fungus	Autoclaved	2	No information available	-	Park et al. (2005)
Chlorella vulgaris	Green algae	Dried	1-2	Freundlich	-	Nourbakhsh et al. (1994)
Clodophara crispata	Green algae					
Zoogloea ramigera	Activated sludge bactery					
Rhizopus arrhizus	Fungus					
Saccharomyces cerevisiae	Yeast					

Table 5 Hexavalent chromium biosorption (literature screening) - continued

As evident from the above table, in most cases authors observed, that the optimum pH of the biosorption process was in the vicinity of pH 2, independent of biomass type. At this pH, Cr(VI) exists mainly as $HCrO_4^-$. Dean and Tobin[94] emphasized the necessity to know the chemistry of hexavalent chromium in order to understand and interpret correctly the chromium biosorption phenomenon. It is equally important to note that chromate compounds are strong oxidizing agents, thus Cr(VI) has the tendency to be reduced to more stable Cr(III).

Most studies dealing with hexavalent chromium biosorption concluded that the Cr(VI) was removed from aqueous systems by anionic adsorption as Cr(VI) behaves as an oxyanion in aqueous medium[55,118,119,54]. Therefore, it cannot be bound at neutral pH due to respective charge repulsion by negatively charged functional groups on the biomass surface (carboxylate, phosphate and sulphate etc.). On the contrary at low pH, the amine groups of the major cell wall components of the fungal biomass are protonated and the negatively charged chromate ions become electrostatically attracted to the positively charged amine groups of the fungal cell wall according to following simplified reaction scheme:

$$biomass - NH_3^+ + HCrO_4^- \rightarrow biomass - NH_3^{+\,-}HCrO_4$$
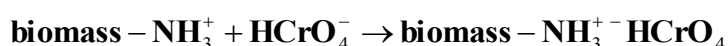
Nevertheless some researchers have reported that Cr(VI) was partially removed via a reduction mechanism, as well as an anionic adsorption, especially under acidic conditions. This possibility of partial/total reduction was highlighted by several authors[37,120,121]. Aoyama[117] pointed out the fact that, when Cr(VI) comes in contact with organic substances or reducing agents in an acidic medium, some portions of the originally added hexavalent chromium are reduced to the trivalent state. Therefore Aoyama recommended to check the total chromium as well as the hexavalent chromium concentration in the equilibrium solution.

Bai and Abraham[55] tested the ability of powdered autoclaved biomass of *Rhizopus nigricans* to remove hexavalent chromium. It was illustrated that a higher sorption capacity and a higher adsorption rate appeared at lower metal concentrations. The smaller was the particle size of the biosorbent, the higher efficiency of the process was observed. The adsorption capacity increased with increasing both temperature and agitation rate (optimum found at 45ºC and 120 rpm).

Chemical modifications of this biomass were performed to clarify the mechanism of the process in another study by Bai and Abraham[118]. The treatment with agents such as 0.01 N NaOH or ammonia solution, as well as formaldehyde deteriorated the biosorption efficiency, while the extraction by acids, alcohol and acetone improved the chromium uptake capacity. A treatment of amino-constituents of the cell walls with carboiimide decreased drastically biosorption potential. Whereas, blocking of carboxylic groups with the same agent resulted in a decrease too. Biomass modification performed by using Cetyl Trimethyl Ammonium Bromide (CTAB), polyethylenimine (PEI) and Amino Propyl Trimethoxy Silane (APTS)

improved the biosorption efficiency to high levels. The FT-IR spectroscopic analysis of the native, chromium saturated and chemically modified biomass samples indicated the involvement of amine groups present in the cell walls of the biomass in chromium binding.

Bai and Abraham[119] subsequently immobilized the biomass in several matrices. Adsorption and desorption experiments were performed in a stirred batch reactor. The biomass was entrapped in calcium alginate, polyvinyl alcohol, polyacrylamide, polyisoprene and polysulfone, respectively, or physically immobilized in polyurethane foam or coir fibres. The sorption capacities of all immobilized samples were lower than the native, powdered biomass. The physical immobilization revealed to be ineffective in comparison to chemical treatments. All five chemically immobilized samples were acid-resistant, but the polysulfone beads exhibited the best mechanical and chemical stability. The bound Cr(VI) was eluted successfully using 0.01 N NaOH, $NaHCO_3$ and Na_2CO_3. The successive sorption-desorption procedure was performed with polysulfone entrapped biomass. The beads were regenerated and reused in 25 cycles with high regeneration efficiency.

Kratochvil et al.[37] examined the sorption capabilities of protonated and Ca-form of a *Sargassum* seaweed biomass to bind both trivalent and hexavalent chromium. The objective of this study was to provide a unified approach to the removal of both Cr(III) and Cr(VI) forms. An ion-exchange model assuming that the only species taken up by the biomass was $Cr(OH)_2^+$ successfully fitted the experimental biosorption data for Cr(III) at pH >2.5.

The maximum uptake of Cr(VI) by protonated *Sargassum* biomass occurred at pH 2. A hypothesis of a simultaneous anion exchange and a Cr(VI) to Cr(III) reduction was postulated. Following combined ion exchange-redox reaction mechanism was proposed by authors:
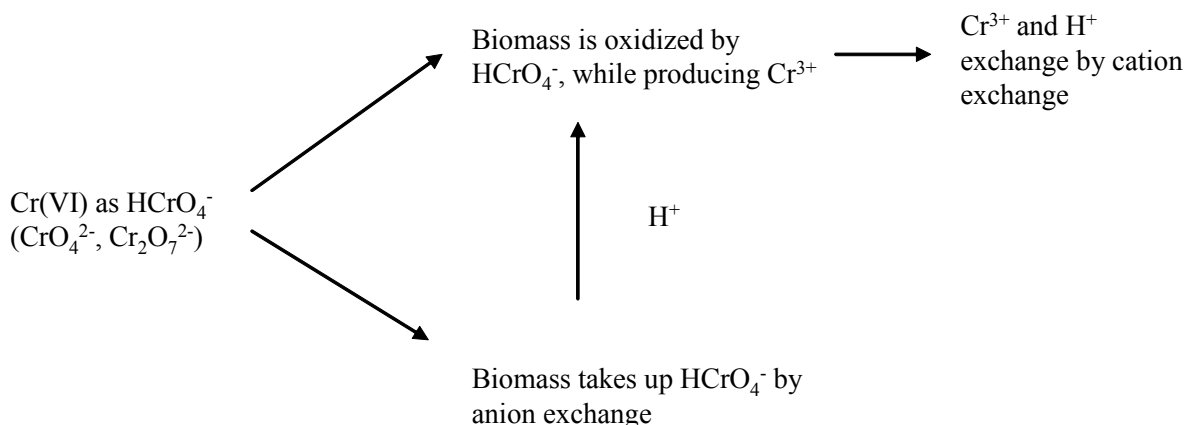
Figure 6 Combined ion exchange-redox mechanism of chromium biosorption on *Sargassum* biomass according to Kratochvil et al.[37]

The reaction scheme (Figure 6) suggests that $HCrO_4^-$ can simultaneously bind onto biomass by ion exchange and oxidize the biomass. Furthermore, the ion exchange and the redox reactions may proceed either sequentially or in parallel. As demonstrated in the above scheme, biomass could play the role of anion exchanger removing Cr(VI) from aqueous solutions by the so-called "acid adsorption" (mechanism described for weak anion-exchange resins). The most important feature of the process is that, in order for the uptake of chromium to occur, the liquid has to contain enough protons to push effectively the equilibrium of reaction towards the products. Consequently, the equilibrium uptake of hexavalent chromium is expected to decrease with increasing pH. From the thermodynamic point of view, the oxidation of biomass and the reduction of hexavalent chromium may occur only if the reduction potential of $HCrO_4^-$ ions is greater than the reduction potential of the biomass. Kratochvil et al. concluded that pH had a much stronger effect on the reduction potential of chromate than the ratio of hexavalent to trivalent chromium. A critical value of pH (pH_c) was defined, so that at pH equal to pH_c, the reduction potential of $HCrO_4^-$ ion and the biomass, respectively, were equal. At pH lower than pH_c, the reduction potential of chromate ions is greater than the reduction potential of biomass, so the chromate ions oxidize the biomass. While at pH greater than pH_c all chromium stays in its hexavalent form.

As soon as the equilibrium pH was lowered below the value of pH_c, chromate ions started oxidizing the biomass while producing Cr^{3+} ions. These Cr^{3+} ions then competed for the binding sites in the biomass with protons via cation exchange reaction. A further decrease of pH caused also desorption of Cr^{3+} ions from the biomass leading to low uptakes of total chromium.

Thereby, the uptake of chromium from solutions containing hexavalent chromium by biomass was maximized at a pH value which was low enough for the equilibrium of the anion-exchange reaction to be shifted to the right, but still high enough to be in the vicinity of pH_c so that the reduction of $HCrO_4^-$ to Cr^{3+} did not dominate the system.

The conclusion was made that at pH<2, the reduction of Cr(VI) to Cr(III) dominates the equilibrium behaviour of the batch systems. This effect was explained by the dependence of the reduction potential of $HCrO_4^-$ ions on the pH. At pH >2, the removal of Cr(VI) was linked to the depletion of protons in equilibrium batch systems via an anion-exchange reaction. The optimum pH for Cr(VI) removal by sorption lied in the region where the two mechanism overlapped, which was for *Sargassum* biomass in the vicinity of pH 2. The existence of the optimum pH for the removal of Cr(VI) may be explained by taking into account the desorption of Cr(III) from biomass at low pH and the effect of pH on the reduction potential of Cr(VI) in aqueous solutions. As a conclusion desorption experiments were performed. Cr(VI) bound to the seaweed at pH 2 was desorbed with 0.2 M H_2SO_4 via reduction in Cr(III) form.

Hexavalent chromium reduction by another seaweed - protonated biomass of *Ecklonia sp.* - was studied by Park et al.[120] Authors proved that the removal mechanism proceeded only via the reduction of Cr(VI) to Cr(III). The reduction efficiency was found to be always 100% in the pH range of this study (pH 1 – 5). The Cr(VI) reduction was independent of the Cr(III) concentration, suggesting that the reaction was irreversible process under the selected experimental conditions. Protons were consumed during the process and the rate of Cr(VI) reduction increased with decreasing pH. The electrons required for Cr(VI) reduction also caused oxidation of organic compounds in the biomass. Reduced trivalent chromium appeared partially in the solution and was partially bounded to the surface of biomass. Approximately 50% of hexavalent chromium was completely removed from the solution.

In the following study Parker et al.[121] investigated the above mentioned mechanism using various chemical treatments of the biomass to elucidate the mechanisms regulating the hexavalent chromium reduction. Among selected treatment agents, the acid treatment exhibited the best performance in regards of hexavalent chromium reduction, while the treatments with organic solvents significantly improved the total chromium removal efficiency. The methylation of the amine groups significantly decreased the removal rate, but on contrary amination of the carboxyl groups significantly increased the Cr(VI) removal rate. Meanwhile, esterification of the carboxyl groups and carboxylation of the amine groups

decreased the Cr(VI) removal rate, but the former showed more negative effect than the latter. It is evident that amine groups were involved in the process, whereas the role of carboxylic groups was only minor.

Two different mechanisms of the Cr(VI) removal process were proposed. Mechanism I was based on direct reduction of hexavalent chromium in the aqueous phase by contact with electron-donor groups of the biomass (i.e. groups having lower reduction potential values than that of Cr(VI)). Mechanism II (indirect reduction) consisted of three particular steps. The binding of anionic chromium ion species to the positively-charged groups present on the biomass surface was followed by reduction by adjacent electron-donor groups. Then the release of the Cr(III) into the aqueous phase due to electronic repulsion between the positively charged groups and the Cr(III) ions occurred, but a complexation of the Cr(III) with adjacent groups capable of chromium binding was not excluded. According to Park et al. amino and carboxyl groups would take part in the indirect reduction mechanism.

The hexavalent chromium uptake mechanism of non-viable biomass of *Aspergillus niger* was also investigated by Park et al.[55] It was again concluded that the governing mechanism was chromium reduction, prior to direct or indirect mechanisms. Hexavalent chromium completely disappeared from the solution, but only 25% of total chromium was removed. Since protons were required for the reduction, solution pH increased slightly during the process. Particularly very long contact times were used in this study (up to 600 hours). The photoelectron spectroscopy analysis (XPS) was employed to determine the valence state of the chromium bound on the biomass. The spectra indicated the presence of Cr(III), but the presence of Cr(VI) was not excluded due to the existence of serious noise peaks.

Cabatingan et al.[122] prepared a very interesting paper, whereby authors disagreed with the conclusion of number of previous studies claiming a good biosorption potential of tested materials based uniquely on high chromium uptake capacities, which were derived from a single metal batch arrangement. They pointed out the need to check the stability of sorbents against oxidation, as chromate ions are strong reducing agents. This reality was often left out of consideration by many authors. Furthermore elution of bound chromate, if possible without accidental Cr(VI) reduction, and the regenerability of chromate-loaded sorbent should be also involved in hexavalent chromium biosorption studies according to Cabatingan et al.

Equilibrium and kinetic data on chromate biosorption by the seaweed *Sargassum siliquosum* were presented. When batch experiments were performed, both trivalent and hexavalent chromium were found in equilibrium solutions, though only hexavalent chromium

was present in the initial solution (observed at pH 2 and pH 4, no discrepancy at pH 6). As the trivalent form could only come from the reduction of chromate, the electrochemical process according to Kratochvil and al.[37] was suggested. A lower pH appeared to favour the biosorption of chromium and pH 2.5 was an apparent optimum pH for maximum biosorption of Cr_{tot}. In most cases (Table 4) the optimum pH for Cr(VI) removal is found in the range pH 2 – 3 (regardless of the biosorbent). The question about the existence of such an optimum was further discussed in this article too.

The direct reduction of Cr(VI) suggested that some of the components in the biomass were oxidized, but it was proven that the reduction was not due to components that were leached out of the biomass.

In kinetics experiments simultaneous biosorption and reduction of chromate were monitored. The decrease in hexavalent chromium concentration was reported to be due both biosorption and reduction, while the change in the Cr_{tot} to sorption only. Authors observed that the biosorption and reduction were two parallel processes occurring at different rates. To validate this hypothesis a simplified model was tested. According to this model sorption and reduction were coupled in a parallel way, increasing the rate of one process would also increase the rate of the other. This means, that sorption was always accompanied by reduction and no change of experimental conditions would prevent the reduction process.

Desorption was performed using a 0.2M H_2SO_4. Increasing temperature increased recovery percentage. Only 10% of chromium was recovered in Cr(VI) form, but it was thus possible to recover chromium as Cr(III). The same was already reported by Kratochvil et al.[37] Relatively long contact times were necessary to obtain the maximum percentage recovery.

An applicability of biosorption in the chrome-plating industry was discussed. Especially chromate recovery from the contaminated rinse waters was found suitable. In this case, chromate concentrations are relatively dilute, while it is necessary to separate chromate ions from metal cations. Ideally, chromate should be the only ion taken up by the sorbent and then subsequently eluted. Recovering of chromate in the form of a concentrate, which could be reused in the bath, would be the principle objective of such a process. Given these requirements, two advantages readily stand out for biosorbents. Chrome-plating rinse waters are acidic, so it is an advantage that the maximum uptake for chromate by biosorbents is obtained in the pH 2 – 3 range. The biosorption high efficiency in recovering chromate in dilute rinse waters would also be an advantage.

The major drawback is the poor stability of the sorbent in acidic solution. The oxidation degrades the reactive sites and this may significantly reduce the number of re-use

cycles of the sorbent. The fact that the bound chromate cannot be easily recovered as chromate but only as Cr(III) is also unfavourable.

As obvious from the above paragraphs, a serious controversy on the hexavalent chromium biosorption mechanism exists. Several biosorption mechanisms were proposed, including electrostatic attraction, ion exchange mechanism, partial or total reduction or their combinations. Nevertheless, it was clearly demonstrated, that the optimum pH of the process is found in the vicinity of pH 2. It was also pointed out, that the content of both forms of chromium should be checked in equilibrium solutions. Moreover, the stability of biosorbent against oxidizing power of chromate ions should not be left out of consideration, regarding the acidic pH employed in experiments.

2.2.1.9 Cadmium biosorption

Contrary to mercury, a number of studies is available on cadmium biosorption. The main characteristics and general trends of published data are summarized in Table 6. Regarding the high number of studies published, only papers revealing particularly important findings will be discussed within this chapter.

Biomass type	Biomass class	Biomass treatment	Conditions			Other metals studied	References
			Optimum initial pH	Sorption capacity			
				[mg g^{-1}]	[mmol g^{-1}]		
Peat	-	Dried, ground, sieved	7	34	0.3	Cr(III), Cu	Wei Ma and Tobin (2004)[123]
Sargassum siliquosum	Brown seaweeds	Washed and dried	5	82	0.73	-	Hashim et al. (2004)[81]
Sargassum baccularia				83	0.74		
Padina tetrastomatica				-	-		
Chaetomorpha liunum	Green seaweed			-	-		
Gracilaria changii	Red seaweeds			-	-		
Gracilaria edulis				-	-		
Gracilaria salicornia				-	-		
Fontalis antipyretica	Aquatic moss	Rinsed and dried	5	28	0.3	Zn(II)	Martins and Boaventura (2004)[124]
Sargassum sp.	Brown seaweed	Dried and ground	5.5	120	1.1	-	Cruz et al. (2004)[125]

Table 6 Cadmium biosorption (literature screening)

Biomass type	Biomass class	Biomass treatment	Conditions			Other metals studied	References
			Optimum initial pH	Sorption capacity			
				[mg g^{-1}]	[mmol g^{-1}]		
Saccharomyces cerevisiae	waste baker's yeast	Untreated	6	-	-	Pb, Cu	Goksungur et al. (2004)[126]
		Ethanol treated		31.75	0.3		
		NaOH treated		-	-		
		heat treated		-	-		
Bacillus laterosporus, *Bacillus licheniformis*	Bacteriae	Autoclaved	7	140 / 160	1.3 / 1.4	Cr(VI)	Zouboulis et al. (2004)
Spirulina platensis TISTR 8217	Cyanobacteria	Immobilized in silica gel	7	70	0.6	-	Rangsayatorn et al. (2004)[127]
		Immobilized in alginate gel		37	0.3		
Saccharomyces cerevisiae)	Baker's yeast	Heat deactivated, acid treated and converted to Na-form	6.5	No information available	-	-	Vadsudevan et al. (2003)
Mucor rouxii	filamentous fungus	Living,	5	8	0.07	Pb, Zn, Ni	Yan et Viraraghavan (2003)
		Autoclaved		-	-		
		NaOH treated	6	20	0.2		
Saccharomyces cerevisiae (carlsbergensis)	Yeast	Freezed-dried	No information available	Reached about 20 mg/g for K-limited biomass, not described with commonly used models	-	Ag, Cu	Dostalek et al., (2004)[105]
Sewage sludge Paper mill waste Composted paper mill waste		Air dried	6	14	0.1	Cu, Pb, Zn	Lister and Line (2001)
Saccharomyces cervisae	Yeast	Immobilized in silica gel (sol-gel technique)	5.2	No information available	-	-	Marseaut et al. (2004)[128]
Rhizopus arrhizus *Mucor miehei,* *Penicillium chrysogenum*	Fungi	Washed and dried	7	44 / - / -	0.4 / - / -	Ni, Zn, Ag, Pb	Fourest et al. (1994)

Table 7 Cadmium biosorption (literature screening) - continued

Yan and Viraraghavan[59] tested the use of viable, autoclaved and alkali-treated cells of *Mucor rouxii* to sequester cadmium, together with lead, zinc and nickel both from single and multi-metal systems. An increase in final pH values of reaction mixtures was observed when alkali-treated samples were used. This observation could be attributed either to the adsorption of hydrogen ions from aqueous solutions or more probably to the neutralization of H$^+$ ions

with OH⁻ released from the alkali-treated biomass. The same behaviour was also observed by Rao et al.[70] and Kapoor et al.[63]. When two- or three - metal ion systems were studied compared to the single ion system, the biosorption capacities for individual metal ions were reduced in the presence of other metal ions, indicating the existence of competitive binding. However, in comparison with the single-ion system, total biosorption capacity increased, with higher values in three-metal ion systems than those in bi-metal ion systems. Several elution agents were tested. HNO_3 proved to be the most effective one. After desorption two regeneration agents were used; deionised water or NaOH solution, respectively. When the latter was used the biomass regained its initial metal removal capacity and the values in the cycles 2 – 5 were even higher than that obtained in cycle 1 using raw NaOH-pretreated biomass. This was explained by the authors by the fact that caustic regenerations decreased protonation and substituted sodium ions on functional groups so these ions can be readily displaced by heavy-metals ions.

Fourest et al.[60] used three samples of fungi (*Rhizopus arrhizus, Mucor miehei* and *Penicillium chrysogenum*), supplied as by-products of fermentation industry, for the uptake of cadmium, nickel, zinc, silver and lead in both batch and column systems. The objective of this study was particularly the characterization of the pH contribution to the sorption equilibrium reaction in order to clarify the sorption mechanism.

The maximum sorption capacities and the dissociation constants values were ranked according: Pb>>Cd>Ag>Zn>Ni at pH 6. Logarithms of dissociation constants (pKd – reciprocal value of b constant of the Langmuir isotherm equation) varied linearly with increasing pH. This correlation between pH and sorption binding strength demonstrated biosorption inhibition in presence of protons.

The uptake capacities of tested materials decreased in following order: *Rhizopus arrhizus > Mucor miehei > Penicillium chrysogenum*. An important pH decrease of observed in case of *M. miehei* and *P. chrysogenum* and according to Forest et al. this finding was related to lower sorption capacities of these samples. When experiments were performed at controlled pH, much closer sorption capacities were obtained for all three tested samples. Moreover, an experiment with calcium saturated biomass samples revealed a mol-to-mol exchange between studied metal and calcium cations for each sorbent. Furthermore the pH did not decrease as low as with Ca-free biomasses. Calcium ions seemed to play an important buffering function that could significantly increase the metal uptake performance in batch systems. The former observations were confirmed in continuous flow fixed-bed system with *Rhizopus* or *Penicillium* granules.

Cadmium biosorption process was found to be pH dependent and the optimum pH occurred in general in neutral area ranging between pH 5 and pH 7 (Table 6). The low biosorption capacity of biological materials at pH values below 4.0 was usually attributed to hydrogen ions that compete with metal ions of the sorption sites.[65,129] At lower pH, due to protonation of the binding sites resulting from a high concentration of protons, the negative charge density on the sites is reduced resulting in the reduction or inhibition of the binding of metal ions. Fourest et al.[53] demonstrated that ion exchange was involved in cadmium biosorption. Influence of background ions was found negligible for algal biomass[81]. An important competition between tested metals was observed in case of fungal biomass[59]. General influence of pre-treatement was neither found. Though ethanol pre-treatment gave the best results for yeast biomass[126] alkaline treatment seemed to be more appropriate for fungal biomass[63].

2.2.1.10 Lead biosorption

A lot of attention was given to lead biosorption and consequently a high number of studies dealing with this problem were published. This is certainly due to high toxicological danger of lead and due to large lead contamination caused in the recent past. Table 8 summarizes the studies focusing on lead biosorption.

| Biomass type | Biomass class | Biomass treatment | Conditions | | | Other metals studied | References |
| | | | Optimum initial pH | Sorption capacity | | | |
				[mg g^{-1}]	[mmol g^{-1}]		
Aspergillus niger	Fungus	NaOH treated	5	10	0.05	Cd, Cu, Ni	Kapoor and Viraraghavan (1999)
Scales of *Oreochromis Niloticus*	Fish	Heat treated	5.0 – 6.0	30	0.14	Cu, Ni, Co	Villanueva-Espinosa et al. (2001)
Penicillium Chrysogenum	Fungus	Dried	4.5	116	0.56	-	Niu et al. (1993)[64]
Phellinus badius	Macro fungus	Dried	5.0	170	0.82	-	Matheickal and Yu (1997)[130]
Coir	Fibres from *Coco nucifera*	No treatment	5.6	19	0.09	Zn	Conrad and Bruun Hansen (2006)
Streptomyces rimosus	Bacteria	0.1M NaOH		135	0.65	-	Selatnia et al. (2004)[131]
Cone biomass of *Pinus sylvestris*	Seed bearing cones of coniferous tree	Dried, sieved	4.0	Freundlich	-	-	Ucun et al. (2003)

Table 8 Lead biosorption (literature screening)

| Biomass type | Biomass class | Biomass treatment | Conditions | | | Other metals studied | References |
| | | | Optimum initial pH | Sorption capacity | | | |
				[mg g^{-1}]	[mmol g^{-1}]		
Durvillaea potatorum	Brown marine algae	Modified by CaCl$_2$ solution, dried	5	320	1.55	Cu	Matheickal and Yu (1999) [132]
Ecklonia radiata				260	1.26		
Aspergillus niger	Fungus	NaOH treated	4	33	0.14	Cu	Dursun (2006) [133]
Cystosteira baccata	Macroalga	Dried	4.5	190	0.9	Cd	Lodeiro et al. (2006)
Sargassum sp.	Brown algae	Dried	5	270	1.26	-	Martins et al. (2006) [76]
Laminaria japonica	Brown algae	Epichlor hydrin treated	5.4	350	1.7	-	Luo et al. (2006)
		KMnO$_4$ treated		320	1.5		
		dried		250	1.2		
Streptoverticillium cinnamoneum	Fungus	Boiled in water	4	58	0.28	Zn	Puranik and Paknikar (1997)
Olive stone waste	Waste (olive oil production)	Washed with boiling water, dried	5.5	15	0.07	Ni, Cu, Cd	Fiol et al.(2006)
Pseudomonas aeruginosa PU21	Fungus	Autoclaved	5.5	70	0.34	Cu,Cd	Chang et al. (1997) [134]
Rhizopus arrhizus	Fungus	Freezed-dried		190	0.9		Naja et al. (2006)
Absidia orchidis	Fungus	Dried	3.5	351		Cd, Ni,	Holan et al. (1995) [52]

Table 9 Lead biosorption (literature screening) - continued

Kapoor and Viraraghavan focused their interest on the possible utilization of *Aspergillus niger* as biosorbent. The effect of biomass pre-treatment on biosorption of lead, cadmium, copper and nickel was studied and biosorption results were compared to accumulation by viable biomass.[135] The pre-treatment of live biomass using sodium hydroxide, a commercial detergent, formaldehyde and dimethyl sulphoxide increased the biosorption of lead by three times in comparison with live biomass, while pre-treatment using acetic acid, ammonium persulphate, ether and ethanol increased it only slightly. On contrary, autoclaving and o-phosphoric acid pre-treatment marginally decreased lead biosorption. The hydrogen peroxide pre-treatment also reduced biosorption of lead in comparison with live cells.

The pre-treatment of biomass with boiling sodium hydroxide solution resulted in a significant improvement in lead, cadmium and copper removal in comparison with live biomass, with the exception of nickel, which was better removed by viable biomass.[63]

An increase in suspension pH was observed during the process. The final pH values of the reaction mixtures increased with an increase in the initial pH values. Little or no biosorption of metal ions was observed for pH less than 3.0, while the removal capacity increased very sharply with an increase in pH from 3.2 to 4.0. A sudden increase in sorption with a slight increase in pH was referred as an *adsorption edge*. Beyond pH 4.0, the metal ions removal increased with pH. The low metal biosorption at pH 3.0 has been attributed to the competition that metal ions face from hydrogen ions for the available biosorption sites. With an increase in pH, the negative charge density on the cell surface increases due to deprotonation of the metal binding sites and thus increases biosorption. The highest removals of lead, cadmium and copper were observed when they were present alone in aqueous solutions. Lead biosorption was more sensitive to the presence of copper than cadmium. When all the three metals were present, *A. niger* biomass biosorbed the heavy metals in the following order: lead>copper>cadmium.

The use of fungal biomass as a potential biosorbent depends not only on the biosorptive capacity, but also on how well the biomass can be reused. The biomass was used for five cycles of biosorption-elution-regeneration. Nitric acid was the most efficient elution agent. The biomass regenerated with deionised water and then contacted with a solution containing Ca^{2+}, Mg^{2+}, K^+ ions exhibited higher metal biosorption capacity than the one regenerated using deionised water only. The release of calcium, magnesium and potassium ions was observed during the biosorption of metal ions, indicating that ion-exchange played an important role in biosorption of metal ions.

The role played by various functional groups in the cell wall of *A. niger* in biosorption of lead, cadmium and copper was investigated. [136] The biomass was subjected to several chemical treatments to modify the functional groups (carboxyl, amino and phosphate). These modifications were examined by infrared spectroscopy. It was found that the esterification of carboxyl and methylation of amine groups present in the cell wall of the biomass significantly decreased biosorption of the heavy metals studied. Lead biosorption was observed to be more sensitive to modifications of the carboxyl group than of the amine group, while cadmium and copper biosorption was found to be more sensitive to modifications of the amino group than the carboxyl group. These findings suggested that carboxyl and amine groups were important in metal ion biosorption, while phosphate groups and the lipids fraction of the biomass did not play a significant role in the process. Biosorption of lead and cadmium displaced calcium, magnesium and potassium ions present on the biomass surface, indicating that biosorption took place as a result of ion exchange mechanism.

Finally, the biomass of *Aspergillus niger* was immobilized in polysulfone matrix and were tested in a column system by Kapoor and Viraraghavan.[137] Polysulfone is an amorphous, rigid, heat resistant and chemically stable thermoplastic material. The prepared beads contained approximately two thirds of biomass and one third of polysulfone by weight. The beads were successfully used in column arrangement with a down flow of the liquid. The adsorbed metals were easily eluted by nitric acid and the acid wash had no visible effects on the physical properties of the beads.

Lead biosorption by alga *C. baccata* was studied by Lodeiro et al.[138] High sorption capacities towards lead(II) and also cadmium(II) were observed (slightly higher for lead compared to cadmium). Carboxyl groups from mannuronic and guluronic acids of alginates were identified through the acid-base titration. Moreover, the presence and participation of these groups in metal uptake was confirmed by FTIR analysis. The speciation of metal ions were also investigated and it was stated that only free cadmium(II) and lead(II) ions were the predominant species formed in the pH interval studied. The presence of salts within the examined concentration range affected the metal uptake. Lead sorption was less affected by the presence and by the increase of sodium ion in the solution than cadmium. This observation was explained by more covalent character of lead (electrostatic factors played a secondary role in this case) and, as a consequence, its stronger binding capacity, which made the influence of this background ion less significant. On the other hand, the presence of divalent calcium exerted a stronger influence, which was reflected even at lower salt concentrations. This could be a consequence of its higher electrostatic accumulation and its greater affinity for the binding sites. As expected, the influence of calcium on lead adsorption was less important than in the case of cadmium uptake.

The waste material originated from the olive oil production - olive stone waste - was successfully tested for lead biosorption together with other metal cations (Cu, Ni, Cd) by Fiol et al.[101] The presence of sodium chloride and perchlorate salts significantly reduced metal removal. Moreover NaCl exerted slightly greater influence on metal removal. The existence of ion-exchange mechanism during the metal sorption was investigated by measuring the releases of calcium, magnesium and potassium ions from biosorbents during sorption. There was a significant release of mentioned ion, but nevertheless the ratio of sorbed metal to released cations was close to one only for nickel, but higher for other metals evidencing a

different sorption mechanism. Desorption experiments using HCl and EDTA solution were efficient only to lower extent.

The binding mechanisms of Pb and Zn to *Penicillium chrysogenum* cell walls was studied by Sarret et al.[139] EXAFS (extended X-ray absorption fine structure) technique was used to analyzed metal saturated samples as this method allows to determine formally the nature, number, and distance of atoms located near the selected atom. The biomass was submitted to a sorption experiment in the presence of a background electrolyte ($NaNO_3$). The metal saturated biomass was dried and stored for subsequent EXAFS measurements (drying removed hydration water, but not structural water possibly coordinated to Zn or Pb). Zn and Pb isotherms differed in shape at low equilibrium concentrations. The Zn isotherm was fitted with a Langmuir-based sorption model by assuming a single Zn site. A slightly better fit was obtained assuming the presence of low affinity sites of low concentration, amounting to 5% of total sites. The adsorption isotherm for Pb was clearly different from that for Zn and was divided into two regions separated by a plateau at low initial lead concentration. This line shape unequivocally indicated the presence of a strong binding site, which was saturated at low metal concentration. Pb was subsequently complexed by a weaker site, which was the predominant functional group of the cell wall. Consequently authors demonstrated that Zn was overwhelmingly complexed by phosphoryl groups in the tetrahedral coordination. Despite some intrinsic limitations, the presented data showed that Zn was predominantly complexed to phosphoryl groups from low to high concentration and additionally to carboxyl groups near the saturation of the reactive surface sites. EXAFS spectra for Pb-biomass complexes allowed concluding that lead was predominantly bound to carboxyls at a very low concentration and to phosphoryls at high concentrations.

Naja et al.[140] proposed to use an interactive metal-based potentiometric titration method using an ion selective electrode for studying the sorption of metal cations. This type of a titration method allowed to follow directly the sorption experiment in the real time. The accuracy of this technique was verified by studying the lead sorption mechanism of *Rhizopus arrhizus* fungal biomass and diatomite (a siliceous non-active compound). The classification of the time before the equilibrium was reached and indicated the existence of three types of chemically active sites. Lead was sorbed by strong binding sites that became completely saturated at low metal concentrations and by a weaker type of sites, apparently dominant throughout cell walls of the biomass examined. The lead uptake curves for *R. arrhizus*, as compared to those for diatomite, were characterized by the appearance of several steps

indicating most probably the presence of several types of sorption sites having particular reactivities, whereas the diatomite sorption curve appeared quite regular during the titration experiment. Lead sorption was also characterized by a quantity of released protons. Thus the pH curve indicated also the existence of several kinds of reacting sites. The weak pH variations during lead uptake onto diatomite confirmed the conclusions made from the sorption curve. The used biomass featured not only a chemical heterogeneity (various functional groups) but also a structural heterogeneity (different types and size of pores) and therefore, the developed metal-based potentiometric titration appeared to be a good tool to elucidate the chemical structure of the biomass and of its structural heterogeneity.

As in the previous cases, the dependence of the process on pH was again observed. The optimum pH lied close to pH 5, regardless of used biomass (Table 8). The existence of so-called *adsorption edge* was reported and it was related to competition between metal ions and protons. Strong indications were obtained about the involvement of carboxyl groups in lead binding for both fungal and algal materials. Ion-exchange seemed to be the major binding mechanism. This hypothesis was supported by the negative effect of increased ionic strength on sorption capacity in some cases. Nevertheless Sarret et al.[139] and Naja et al.[140] confirmed the presence of several binding sites (phosphoryl and carboxyl).

2.3 Evaluation of sorption performance

The first step in biosorption experiments is to quantify the uptake capacity of tested biomass. This is traditionally done by characterizing the equilibrium state of the system after the biomass has been allowed to react with an aqueous solution of the target metal in a batch mode. The equilibrium is reached when the amount of metal remaining in solution becomes time invariant.

2.3.1 Sorption equilibrium

In general, the experiments dealing with sorption equilibrium are performed in a batch mode. Open or closed reactors are usually used, whereas homogeneity of the system is assumed and thus perfect stirring is required. The experiments performed at sorption

equilibrium are used to determine sorption isotherms, to evaluate uptake selectivity and effect of competitor ions. The experiments should be performed at constant experimental conditions (temperature, agitation speed etc.).

2.3.1.1 The role of pH

As already illustrated in previous chapters, the most important single parameter influencing the sorption capacity of a biosorbent is the pH of adsorption medium. The initial pH is closely related to biosorption mechanisms and reflects the nature of physico-chemical interactions of sorbate with the sorptive sites of biosorbents. The influence of this parameter on both the metal speciation and ion state of the biomass (protonation/deprotonation of its functional groups) is of a great importance. Therefore the optimum pH for anion biosorption is opposite to that of cation biosorption as illustrated in the previous sections.

The lack of cations sorption at low pH is traditionally explained by competition for sorption sites between protons and metal cations for surface sites (high proton concentration, studied metals present as free cations). Such a competitive behaviour was confirmed by Fiol et al.[101] Olive mill stone material subjected to HCl solution rinsing prior to the biosorption process, released alkaline and alkaline earth metals into the solution as a consequence of the displacement of these cations by the protons of the solution.

2.3.1.2 Description of sorption equilibrium - Isotherms

The proper sorption process involves a solid phase (biosorbent) and a liquid phase (water) containing dissolved species (metal, organic molecules) to be sequestered. Due to the various mechanisms described in chapter 2.2.1.6 the sorbate is attracted to the sorbent and subsequently bound. This process is proceeding until the equilibrium is attained in the system. The sorption equilibrium is once established when the concentration of a sorbate in a bulk solution is in a dynamic balance with that of the sorbent interface. The degree of the sorbent affinity for the sorbate determines its distribution between the solid and the liquid phases. The quality of the sorbent material is evaluated according to how much sorbate it is able to attract and retain.

For this purpose the metal uptake (q) is determined from the mass balance as the amount of sorbate bound by the unit of the solid phase. The calculation is based on an assumption that the sorbate disappeared from the solution must be found in the solid phase, so the following equation can be written:

$$q = (C_f - C_i)\frac{V}{m}$$

Where:

C_i	is the initial metal concentration in solution [mg L^{-1}, mmol L^{-1}]
C_f	is the final (equilibrium) metal concentration in solution [mg L^{-1}, mmol L^{-1}]
m	is the mass of added biosorbent on the dry basis [g]
V	is the volume of the metal solution [L].

The sorption uptake q can be equally expressed in different units depending on the purpose of the operation:

a) In mg g^{-1}, for practical and engineering processes
b) In mmol g^{-1} (or meq g^{-1}), when working on the stoichiometry or determining mechanism of the process
c) Exceptionally in mg L^{-1}, if the reactor volume is considered (a packed-bed column), but the volume porosity may present a complication in a quantitative comparison.[144]

The analysis of equilibrium data is important for the development of mathematical models – sorption isotherms, which are used for the quantitative description of obtained results. The equation parameters and the underlying thermodynamic assumptions of these equilibria models should be capable to predict metal biosorption, to reflect the mechanism of the sorbate uptake and the influence of variables such as pH, ionic strength, presence of competing cations etc. However, in most cases, equilibria models are used only empirically as functional expressions capable to simulate favourable equilibria uptake curves.

In a graphic form, sorption isotherm expresses the relationship between sorption capacity (q) and residual concentration of the metal in the solution at equilibrium (C_{eq}, C_f).

This distribution of the adsorbate between the solid and the liquid phase is obtained by varying the symmetrical experimental parameters (initial metal concentration, volume of solution or sorbent mass).[141] Several isotherm relationships appeared in biosorption literature where they were applied to interpret equilibrium data and will be described in the following chapter.

2.3.1.2.1 Langmuir isotherm relationship

The Langmuir isotherm relationship was originally developed to describe the gas-solid phase adsorption on activated carbon.[142] Langmuir assumed that the forces that are exerted by unsaturated surface atoms (total number of binding sites) do not extend further than the diameter of one sorbed molecule and therefore sorption is restricted to a monolayer. It was further assumed that:

- There exists a fixed number of well defined adsorption sites on the adsorbent surface.
- All sorption sites are energetically equivalent (i.e. constant heat of adsorption).
- Each site can hold only one sorbate (one sorbate molecule reacts with one active site).
- There are no interactions between species sorbed on neighbouring sites.

As long as its restrictions and limitations are clearly recognized, the Langmuir equation can be used for describing equilibrium conditions for sorption behaviour in different sorbate-sorbent system. Therefore its use was later extended to describe empirically equilibrium relationships between a bulk liquid phase and a solid phase.

Langmuir isotherm equation, is today one of the most commonly used equations for modelling biosorption equilibrium data. It has a hyperbolic form and is usually expressed as follows:

$$q = \frac{b q_{max} C_f}{1 + b C_f} \qquad \textbf{Eq. 2}$$

Where:

q	is the amount of adsorbed metal per unit weight of biosorbent, [mg g^{-1}, mmol g^{-1}]
q_{max}	is the maximum sorbate uptake under the given experimental conditions, [mg g^{-1}, mmol g^{-1}]
C_f	is the remaining (or equilibrium - C_{eq}) metal ion concentration in solution, [mg L^{-1}, mmol L^{-1}]
b	is the coefficient related to the affinity between the sorbent and sorbate, [L mg^{-1}, L mmol^{-1}].

The Langmuir relationship can be linearized by plotting either ($1/q$) versus ($1/C_f$) or (C_f/q) versus C_f. Alternatively, non-linear regression facilities of mathematical packages can be used to determine the parameters of the model. It has traditionally been used to quantify and contrast the performance of different biosorbents.

The Langmuir constant is related to the energy of adsorption ($b=1/K$) through the Arrhenius equation. The magnitude of the coefficient b reflects the slope of the adsorption isotherm which is a measure of whether adsorption is favourable or unfavourable. The higher is b and the smaller is K, the higher is the affinity of the sorbent for the sorbate.[143] q_{max} can also be interpreted as a sorption capacity corresponding to the total number of binding sites that are available for biosorption and q as a sorption capacity corresponding to the number of binding sites that are in fact occupied by the sorbate at the concentration C_f.

Since the Langmuir model was derived from the theory of condensation/evaporation, it does not indicate the mechanistic aspects of sorption. However, it provides information on uptake capacities and is capable of reflecting the usual equilibrium sorption process behaviour.

Concerning the application of this relationship to the description of biosorption equilibrium, it is worth to note, that at least one of the Langmuir assumptions is implicitly not

met in the case of biosorption. It has been clearly illustrated in previous sections that more than one type of functional groups contributes to the biosorption process, each of them having a different affinity for sorbing metal. Furthermore, the one-to-one stoichiometry is also not complied with in the case the ion exchange is the governing mechanism, as approximately two protons are released upon the binding of one divalent heavy metal ion.

In this context, b is not truly the Langmuir adsorption constant, but rather a simple fitting parameter because, as indicated above, the system does not comply with the assumptions of the model and cannot be related to the Gibbs free energy of a specific reaction. The parameter is nonetheless quite useful as a measure of the biosorption affinity or efficiency of different types of biomass.

Despite this fact, the Langmuir equation is frequently used to fit experimental data, as it incorporates two easily interpretable constants: q_{max}, which corresponds to the highest possible sorbate uptake (the complete saturation isotherm-curve plateau); and coefficient b, which is related to the affinity between the sorbent and the sorbate. High values of b are reflected in the steep initial slope of a sorption isotherm, indicating a desirable high affinity. Thus, for a good sorbent in general, a high q_{max} and a steep initial sorption isotherm slope are desirable.[144]

2.3.1.2.2 Freundlich isotherm relationship

The Freundlich isotherm relationship has also been employed to quantify equilibria in biosorption systems.[145] Like the Langmuir isotherm, the extent of adsorption/sorption is determined as a function of the equilibrium concentration of the metal in solution, without reference to pH or other ions in the same aqueous system. The Freundlich isotherm relationship is exponential.

It is originally of an empirical nature, but was later interpreted as a sorption to heterogeneous surfaces or surfaces supporting sites of varied affinities. It is assumed that the stronger binding sites are occupied first and that the binding strength decreases with increasing degree of site occupation. Specifically, the Freundlich isotherm is obtained when a log-normal affinity distribution is assumed. Freundlich isotherm is defined by the following expression:

$$q = k\left[C_f\right]^{1/n} \qquad\qquad \textbf{Eq. 3}$$

Where:

k is an empirically determined constant being related to the maximum binding capacity[L g^{-1}, L mol^{-1}]

n is an empirically determined constant related to the affinity or binding strength, [dimensionless].

In the case of the Freundlich isotherm equation it is commonly accepted that the greater is the coefficient n the greater is the affinity of the sorbent for the metal. It does not indicate a finite uptake capacity of the sorbent and can thus be reasonably applied in the low to the intermediate concentration ranges (C_f). However, it is easy to handle mathematically as it can be easily linearized by plotting in a log-log format, but evidently non-linear regression can be equally use to direct determination of model parameters.

2.3.1.2.3 Other sorption isotherm relationships

Other sorption isotherm relationships appeared in the biosorption literature and they are summarized in Table 10. It is necessary to realize that these relationships basically do not reflect the underlying physico-chemical principles of the sorption process. For all practical biosorption purposes they are just mathematical models of the phenomenon capable of describing the q versus C_f relationship as experimentally observed. Neither of these models can contribute to clarify the sorption mechanism, nor to be sensitive to external process variables (e.g. pH, ionic strength etc.)

While the Langmuir adsorption model is valid for a single-layer adsorption, the BET model represents sorption isotherms reflecting an apparent multi-layer adsorption. Both equations are limited by the assumption of uniform energies of adsorption on the surface. The BET isotherm reduces to the Langmuir model when the limit of adsorption is a mono-layer. The BET model assumes that the Langmuir equation applies to each layer. The Redlich-Peterson equation only differs from the Langmuir-Freundlich equation by the absence of an exponent of C_{eq} at the numerator part of the equation.

Brunauer-Emmet-Teller (BET)[146]	$$q = \frac{BQC_f}{(C_s - C_f)[1 + (B-1)(C_f / C_s)]}$$	C_s is the saturation constant of the solute	**Eq. 4**
		B is the constant relating to the energy of interaction with the surface	
		Q is the number of moles of solute adsorbed per unit weight of adsorbent in forming a complete monolayer on the surface	
Dubinin-Radushkevich[147]	$$\ln q = \ln q_m - BE^2 q$$	B is a constant related to the sorption energy	**Eq. 5**
		E is Polanyi potential	
Radke-Prausnitz[148]	$$\frac{1}{q} = \frac{1}{aC_f} + \frac{1}{bC_f{}^{\beta}}$$		**Eq. 6**
Reddlich-Peterson[149]	$$q = \frac{aC_f}{1 + bC_f^n}$$	Where n lies between 0 and 1	**Eq. 7**
Langmuir-Freundlich[150]	$$q = \frac{bq_m C_f^{1/n}}{1 + bC_f^{1/n}}$$		**Eq. 8**

Table 10 Other sorption isotherms equations

Sag and Aktay[151] attempted to apply the Redlich-Peterson and the BET relationships together with Langmuir and Freundlich, but found that the BET equation did not satisfactorily correlate the experimental data. Lodeiro et al.[138] and Luo[79] used the combined Langmuir-Freundlich relationship. Pagnanelli et al.[177] reported that the use of Redlich-Peterson

relationship was not suitable due to the large standard error of the parameters and that its use was not necessary because Langmuir and Freundlich models, with a lower number of parameters, fitted well the experimental data.

The problem of biosorption is that very few information are available on the proper mechanism of the process, though the mentioned relationships become just mathematical fitting capable of following experimental data. The usual concept of the solid-phase sorbent with physical pores and surface area may not be so close to the real structure, appearance and behaviour of biosorbent materials. It is thus usually recommended to restrain the selection of isotherms relationships only to Eq. 2 and Eq. 3.

Several studies attempted to develop the appropriate biosorption isotherms. Even though they will not be applied in this study, the most important relationships are summarized in following paragraphs in order to complete the summary.

2.3.1.2.4 Competitive Langmuir isotherm model

A number of studies focused on the effect of pH on sorption isotherms were performed and were based on multi-component adsorption, the proton being one of these components. The so-called competitive (or extended) Langmuir model was developed[152]:

$$q = \frac{q_m b C_{eq}}{1 + b C_{eq} + b b_H C_{eq,H}}$$ **Eq. 9**

Where:

b_H is the Langmuir apparent dissociation constant for protons.

$C_{eq,H}$ is the equilibrium concentration of protons in the solution.

Other parameters refer to metal species. It is noticeable that these parameters (corresponding to the tested metal) in the standard Langmuir equation (Eq. 2) are pH-dependent and are actually only valid for one particular pH value. The extended Langmuir model takes into account differences in pH. Its parameters can be only obtained by non-linear regression analysis.

This approach was used by Ma and Tobin[123,173] to describe biosorption of Cr(III) Cu(II) and Cd(II) on peat. The model assuming a direct competition of metal ions and protons for biosorbent sites exhibited the best fit.

2.3.1.2.5 Ion exchange isotherm

Ion exchange models based on exchange equilibrium constants and separation factors have been introduced to fit and interpret the data obtained from both equilibrium[153] and dynamic[78] biosorption experiments. The classical ion exchange concept based on exchange equilibrium constants and separation factors was applied and a dimensionless relationship was obtained for a binary system. Schiewer and Volesky[153] chose such an approach for modelling of ionic strength and electrostatic effects in biosorption of divalent metal ions (Ca, Cd) and protons by *Sargassum* biosorbent. A combined equation was derived allowing direct calculation of cation binding without iterations. Only one parameter, the binding constant, had to be determined for each of metals. Using the parameters (such as amount of binding sites, proton binding constant etc.) obtained from pH titrations enabled to predict the effects of pH, ionic strength and Ca concentration on Cd binding.

The same approach used by Kratochvil et al.[144] for dynamic sorption of Cu and biomass regeneration in a fixed-bed column enabled to predict the system behaviour on the basis of proposed ion-exchange model.

2.3.1.2.6 Equilibrium model incorporating solution chemistry - HIEM model

The Hydrolyzed Ion Exchange Model (HIEM) was developed to describe ion-exchange based uranium biosorption on a *Sargassum* biosorbent.[77] In this particular case, the ion exchange based Schiewer's model did not successfully describe uranium uptake which exceeded the stoichiometric biomass binding capacity. The model is based on the ion exchange and incorporates the proton concentration and the hydrolysis equilibrium constants into the basic model equation in addition to the easily measured total uranium concentration. As a result, the equilibrium uranium uptake can be calculated from the total uranium concentration and proton concentration in solution at pH controlled conditions. The uranium speciation was incorporated in the model. It was demonstrated that the model is capable to predict the equilibrium sorption status from the initial conditions.

2.3.1.2.7 Comparison of biosorption performance

When using the Langmuir equation (most cases), the sorption performance is quantified in two parameters - the maximum uptake (q_{max}) and b coefficient. The q_{max} is applicable, when the characteristic q_{max} sorption plateau appears. The high sorbate-sorbent affinity is also desirable as it reflects a good uptake values at low concentrations (C_f). This is characterized by a steep rise of the isotherm curve close to its origins. Performance in this region is reflected in the Langmuir coefficient b.

The comparison of single-sorbate sorption performances should be preferably done upon the complete sorption isotherm curves. In order for an exact comparison, they should be performed under the same experimental conditions (e.g. pH, temperature, ionic strength). For example, it is essential to compare sorption performance under the same pH; when pH is changing during sorption (uncontrolled, unbuffered solutions) the modelling of the system using the Langmuir equation is not appropriate and the comparison of experimental data is difficult.[86] Another aspect is that the optimal pH value for the best performance of one sorbent may not be the same one as for the best performance of another one.
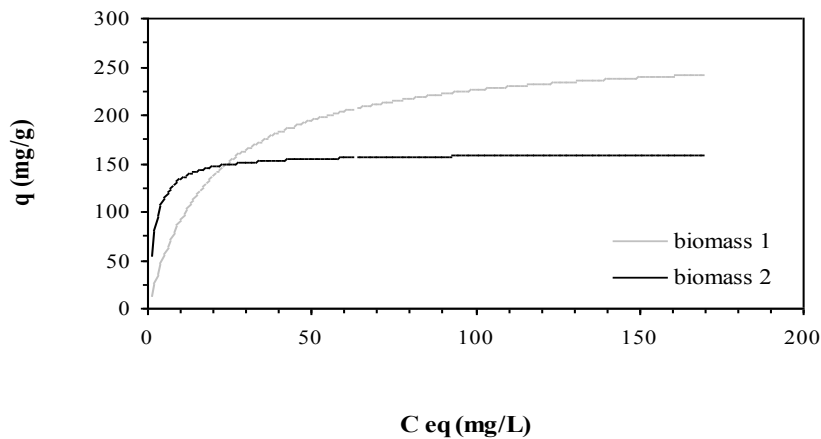
Figure 7 Comparison of two isotherm equilibrium plots

As an illustration, two hypothetic isotherms corresponding to two different biomass types are compared in Figure 7. The selection of better sorbent depends on desired effect. When an eventual recovery of the sorbate is in play, the highest possible saturation of the sorbent is desired even at high equilibrium concentrations and so biomass 1 would be chosen since it exhibits higher uptake capacities. While if the sorbent is supposed to work at low

residual sorbate concentrations (e.g. if the maximum concentration of a pollutant is regulated) the initial part of the sorption curve is in concern. Consequently, even if one of two compared sorbents performs lower q_{max}, but gives higher b value (the case of biomass 2), it could be more suitable because it performs higher sorption uptake in lower equilibrium concentrations.

2.3.2 Sorption kinetics

For a proper understanding of a sorption process it is equally important to know the equilibrium and the kinetics of such a process. Kinetics, in its literal sense, deals with changes in chemical properties in time and is concerned especially with rates of changes. The equilibrium analysis is fundamental for the evaluation of the affinity or capacity of a sorbent. However, thermodynamic data can only predict the final state of a system from an initial non-equilibrium mode and provides so the information about the final state of the system.

It is therefore important to determine how sorption rates depend on the concentrations of sorbate in solutions and how are these rates affected by the sorption capacity or by the characteristics of the sorbent in terms of kinetics.

Various models were involved in description of biosorption kinetics. Among them, equations based on solution concentration (first-order and second-order reversible reactions, first-order and second-order irreversible reactions, pseudo-first-order and pseudo-second – order reactions) as same as equations based on the sorption uptake capacity (the Lagergren's pseudo-first-order and the Ho's pseudo-second-order reactions) were employed.

2.3.2.1 Lagergren's first-order reaction relationship

Lagergren[154] proposed a rate equation for the sorption of solutes from a liquid solution. It may be represented as follows:

$$\frac{dq_t}{dt} = k_1\left(q_{eq} - q_t\right)$$

<div align="right">Eq. 10</div>

Where:

k_1	is the rate constant of pseudo-first-order biosorption, $[\text{min}^{-1}]$
q_{eq}, q_t	denote the uptake at equilibrium and at time t, respectively, $[\text{mg g}^{-1}, \text{mmol g}^{-1}]$.

After integration, while applying boundary conditions $q_t=0$ at $t=0$ and $q_t=q_t$ at $t=t$ a following expression is obtained:

$$\log\left(q_e - q_t\right) = \log\left(q_e\right) - \frac{k_1}{2.3}t$$

<div align="right">Eq. 11</div>

A plot of left side expression against t should give a straight line to confirm the applicability of the kinetic model. Azizian[155] has derived the same relationship by different method and reported that the k_1 constant is a combination of adsorption and desorption rate constants and is not the intrinsic adsorption rate constant which was mistakenly reported in the literature.

2.3.2.2 Ho's pseudo second-order-reaction relationship

Another model for the analysis of sorption kinetics is a pseudo-second-order equation developed by Ho et al.[156,157,158] The rate law is expressed as follows:

$$\frac{dq_t}{dt} = k_2 \left(q_{eq} - q_t \right)^2$$

<div align="right">Eq. 12</div>

Where:

k_2	is the rate constant of sorption, [g (mg min)$^{-1}$]
q_e	is the amount of sorbate sorbed at equilibrium, [mg g^{-1}]
q_t	is the amount of sorbate sorbed at any time, [mg g^{-1}]

Separating the variables in the Eq. 12 gives:

$$\frac{dq_t}{(q_e - q_t)^2} = k_2 dt$$

<div align="right">Eq. 13</div>

Integrating subsequently Eq. 13 for the boundary conditions t=0 to t=t and q=0 to q=qt gives:

$$\frac{1}{q_{eq} - q_t} = \frac{1}{q_{eq}} + k_2 t$$

<div align="right">Eq. 14</div>

This is the integrated rate law for a pseudo-second-order reaction. Eq. 14 can be rearranged to obtain a linear form:

$$\frac{t}{q_t} = \frac{1}{k_2 q_{eq}^2} + \frac{1}{q_{eq}} t$$

<div align="right">Eq. 15</div>

The plot of t/q_t versus t gives a straight line with the slope of $1/k_2 q_{eq}^2$ and the intercept of $1/q_{eq}$. The equilibrium uptake (q_{eq}) and sorption rate constant (k_2) could be evaluated from the slope and intercept, respectively.

Azizian[155] has derived the same relationship using different method and showed that the observed rate constant (k_2) is a complex function of the initial concentration of solute (C_0). The author proved further that when the initial concentration of solution was high, the sorption process obeyed pseudo-first-order kinetics, and when the initial concentration of solute was low, then the process was of pseudo-second-order. He also concluded that for systems whose sorption kinetics obeys the pseudo-first-order model, the observed rate constant (k_1) was a linear function of the initial concentration of solute in solution; while its slope and intercept were adsorption and desorption constants, respectively. For the systems which obeyed the pseudo-second-order model the observed rate constant (k_2) was a complex function of initial concentration of solute.

2.3.2.3 Diffusion phenomena in biosorption kinetics

Prior to the proper biosorption reaction, the sorbate has to be transported from the bulk of the solution to the sorption sites. Following transport steps were identified[72] and are illustrated in Figure 8:

- Step 1 – metal transfer from the bulk of solution to the boundary film layer on surface of the sorbent particle
- Step 2 – transfer of the metal from the boundary film to the surface of the sorbent
- Step 3 – transfer of the metal from the surface to the intraparticle active sites
- Step 4 – uptake of metal ion on the active sites, via complexation, sorption and intraparticle precipitation phenomena
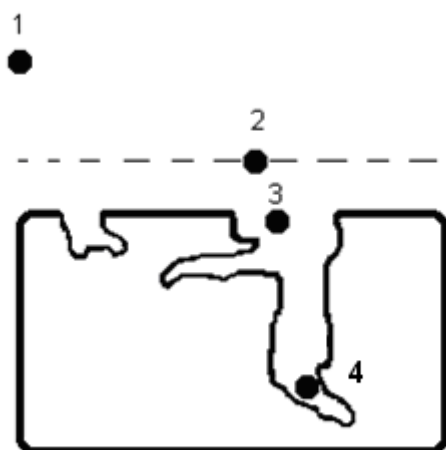
Figure 8 Transport phenomena in biosorption kinetics[159]

The overall rate of the process is determined by the slowest of the described phases. The proper sorption mechanism is generally a rapid, non-limiting phase (step 4). The transport in the bulk of solution (step 1) is done by convection and any concentration differences are constantly levelled out by agitation (under the condition of sufficient agitation, of course). Agitation, however, affects neither the interior of the sorbent particle nor the liquid layer which adhere to the particle surface. Within the particle and through this layer, the so-called film transport can occur by diffusion only.

Though there exist two potential rate-determining steps:

- Particle diffusion – interdiffusion of ions within the particle itself (step 3)
- Film diffusion – interdiffusion in the adherent film (step 2).

Either step can be rate-controlling. The process is controlled by particle diffusion, when the film diffusion is much faster than particle diffusion and the concentration differences in the film are instantaneously levelled out. Thus the concentration gradient exists only in the particles. In the case of film diffusion controlled process, the diffusion within the particle is instantaneous and the gradient exist only in the film layer. In the intermediate case the rate may be affected by both steps.[160]

The mathematical theory of diffusion assumes that the rate of transfer of diffusing substances through unit area of a section is proportional to the concentration gradient measured normal to the section, i.e. Fick's first law, and the gradient of concentration along X axis is given by Fick's second law. For a complete modelling of sorption kinetics it would be necessary to take into account not only these diffusion equations, derived from the Fick's laws, but also boundary conditions, including the sorption isotherm that controls the

equilibrium at the solid/liquid interface and the reaction kinetic equation, when necessary.[141] This usually results in a very complex system of equations, which cannot be solved analytically. However, it is possible to simplify the solving method by separating diffusion steps (film and intraparticle diffusion).[86, 228]

2.3.2.3.1 External mass transfer diffusion model

This model is also called the boundary method[161] and expresses the evolution in the concentration of the solute in the solution, C_t (mg L^{-1}), as a function of the difference in the concentrations of the metal ion in the solution, C_t, and at the particle surface, C_s, (mg L^{-1}). The change of solute concentration is solution should obey the following equation[162,163]:

$$\frac{dC_t}{dt} = -\beta_L S(C_t - C_s)$$

Eq. 16

Where:

β_L is mass transfer coefficient, [m s^{-1}]

S is specific surface area, [m^{-1}].

The coefficients could be determined when several assumptions are applied:

- C_s negligible at *t=0*,
- concentration in solution tending to the initial concentration C_0
- negligible intraparticle diffusion.

Then the Eq. 16 can be simplified to:

$$\left(\frac{dC_t/C_0}{dt}\right)_{t\to 0} = -\beta_L S$$

Eq. 17

And the solution is:

$$-\ln\frac{C_t}{C_0} = \beta_L S t$$

Eq. 18

Eq. 18 is a linear relationship. The slope of this plot gives the global coefficient. This is generally applied on the first period of sorption experiment curve.

Assuming smooth, spherical particles, the surface area for mass transfer, *S*, can be obtained from *m* (solid concentration), using the equation:

$$S = \frac{6m}{d_p\rho(1-\varepsilon)}$$

Eq. 19

m	is concentration of solid in solution, [mg L^{-1}]
d_p	is particle diameter, [m]
δ	is particle density, [kg m^{-3}]
ε	is particle voidage, [-].

2.3.2.3.2 The intraparticle mass transfer diffusion – Weber & Morris model

In diffusion studies, rate processes are usually expressed in terms of the square root of time (i.e. in the form of the curve q=f(t$^{0.5}$). The overall shape of these curves is related to several phenomena, but the initial linear portion is attributed to intraparticle diffusion. The gradient of the linear portions of plots was defined as a rate parameter K. Although the parameter does not have the usual dimensions of a rate constant (mg g^{-1} min$^{-0.5}$), it is characteristic of rate of the adsorption process in its beginning.

This simple intra-particle diffusion model proposed by Morris and Weber[163] is of the following form:

$$q = Kt^{0.5}$$

<div align="right">**Eq. 20**</div>

Where:

q	is the amount of sorbed metal ion at time t, [mmol g^{-1}]
t	is the time, [s]
K	is the diffusion coefficient in the solid, [mmol g^{-1} s$^{1/2}$].

K is determined from the plot q=f(t$^{0.5}$) only for the initial linear period of time.

McKay and Poots[164] demonstrated that, for dye uptake by wood particles, the plots were linear in the region between 5 – 20% of removal and that the dye adsorption on wood particles was controlled by intraparticle diffusion although a boundary layer resistance was experienced in the early stages of adsorption. The same conclusion was done by McKay et al.[165] for the adsorption of a basic dye on silica gel.

Zhang and Bai[166] studied the mechanism and kinetics of humic acid adsorption onto chitosan-coated granules. Based on the Fick's diffusion law, the amount of adsorption by diffusion controlled dynamics as a function of time can be given according to Siqueira et al.[167]:

$$\Gamma(t) = 2C_0 \sqrt{Dt/\pi}$$

<div align="right">**Eq. 21**</div>

Where:

$\Gamma(t)$	is the amount of adsorbed sorbate per unit surface area of the adsorbent at time
t	is the time of the experiment
C_0	is the initial concentration of the adsorbate in the bulk solution
D	is the diffusion coefficient.

To convert Γ(t) to an adsorbed amount based on per unit weight of adsorbents, the specific surface area, S, should be known. Thus, the equation can be revised to give:

$$\mathbf{q(t)} = \mathbf{2C_0S\sqrt{Dt/\pi}}$$ **Eq. 22**

Where:

$q(t)$ is the amount of sorbate adsorbed per unit weight, $[mg.g^{-1}]$

This equation indicates that under a diffusion controlled mechanism a plot of $q(t)$ versus $t^{0.5}$ would follow a linear relationship. The values of D are determined from the slopes of the straight lines. This is analogue to the method of Morris and Weber.[163]

2.3.2.3.3 *The intraparticle mass transfer diffusion – Urano & Tachikawa model*

Another kind of intraparticle diffusion model was proposed by Urano and Tachikawa.[168] and Urano et al.[169] In this model the sorption rate is considered to be independent of the stirring speed and external diffusion to be negligible relative to the low overall sorption rate. The model is given by the following equation:

$$\mathbf{f\left(\frac{q}{q_{max}}\right) = -\left[log\left(1-\left(\frac{q}{q_{max}}\right)^2\right)\right] = \frac{4\pi^2Dt}{2.3d_p^2}}$$ **Eq. 23**

Where:

q_{max}, q are the solute concentrations in the solid at t and t→∞, $[mmol.g^1]$

d_p is the particle diameter, $[m]$

D is the diffusion coefficient in the solid, $[m^2\ s^{-1}]$

The linearization is carried out using the initial time of contact between 0 and 120 minutes.

2.3.3 Multi component sorption equilibrium

Industrial effluents usually contain number of components. Regarding potential industrial application of biosorbents, it is essential to test their behaviour in multicomponent systems. In these systems, reciprocal interference and competition for adsorption sites may occur. Multicomponent sorption depends on the number of metals competing for sorption sites, their combinations, their concentrations, order of metal addition, residence time etc. ossible interaction effects exist between metals themselves in the solution and the interactions with the surface depend particularly on the sorption mechanism. The reversibility/irreverisibility of the binding may also occur.

The effect of other metallic ions (or anionic co-ions) on the performance of one-metal sorption has been assessed in several studies by showing the difference from the original (one-metal) sorption when a known concentration of contaminants was introduced. Two different results were obtained. Kuyucak and Volesky[170] observed only a minor effect of co-ions on original uptake of gold by *Sargassum natans*. While significant negative effect of zinc and copper was observed for cadmium sorption by *Ascophyllum nodosum*.[171]

However, this approach offers only very superficial information on the actual sorption process, whose true equilibrium relationships are reflected in the isotherm where the final (residual) concentration of the sorbates in the solution are the ones that really matter. A better approach to the evaluation of multi-ion sorption phenomenon is to use the relationship reflecting the respective equilibrium base effects. A two metal system can be evaluated graphically by using three-dimensional plotting of the sorption isotherm surface, whereby the second metal residual concentration is also used and both metal uptake values are summed, representing the total uptake on the vertical axis. The limitation of this approach is obvious because the effects of the third of subsequent metallic species on the sorption performance cannot be depicted graphically.[172] Instead, a multi-parameter mathematical approach has to be taken to describe, evaluate and hopefully predict the performance of these complex multi-metal sorption systems.

For this purpose so-called extended (or competitive) models derived from single component Langmuir or Freundlich isotherm equations were developed. Langmuir competitive model has the following form (Eq. 24).

$$q_{i,eq} = \frac{a_i C_{i,eq}}{1 + \sum_{j=1}^{N} b_j C_{j,eq}}$$

Eq. 24

Where:

a_i, b_j are derived from the corresponding individual Langmuir isotherms.

Due to the complex nature of metal-biosorbent interactions and the strong influence of parameters such as ionic strength and the overall composition of the solution on the binding constants derived from simple Langmuir and Freundlich isotherm relationships, these constants are not the "true" thermodynamics constants, but are highly dependent on specific experimental conditions as illustrated in previous chapters.

Eq. 24 was used in many studies for the description of competition between metal ion and protons. For instance, the ideal Langmuir competitive isotherm assuming a 1:1 stoichiometry has the form of Eq. 9.

Ma and Tobin[173] investigated uptake and competition effects of Cr(III), Cu(II), and Cd(II) present in binary systems (Cr-Cd, Cr-Cu, Cu-Cd) during biosorption on peat. Several models were proposed with differing basic assumptions regarding different binding mechanisms. Their applicability to the empirical data was tested. The optimum model was subsequently used to generate three-dimensional biosorption surfaces, which allowed extrapolation and interpolation of uptake and competition effects. Ma and Tobin observed that the presence of co-ions inhibited uptake of individual metals by up to 70%.

Another approach was chosen by Sag Y. et al.[174], who presented the use of the competitive Freundlich model restricted to binary mixtures as follows:

$$q_{1,eq} = \frac{a_1^0 C_{1,eq}^{b_1^0 + b_{11}}}{C_{1,eq}^{b_{22}} + a_{12} C_{2,eq}^{b_{12}}}$$

Eq. 25

$$q_{2,eq} = \frac{a_2^0 C_{2,eq}^{b_2^0 + b_{22}}}{C_{2,eq}^{b_{22}} + a_{21} C_{1,eq}^{b_{21}}}$$

Eq. 26

Where the a_i^0 and b_i^0 (i=1, 2) are derived from the individual Freundlich isotherms (k and 1/n, respectively). The six other parameters (b_{11}, a_{12}, b_{12}, b_{22}, a_{21} and b_{21}) are correction coefficients.

Pagnanelli et al.[175] proposed to use the modified Langmuir model including interaction terms η_i which were characteristic of each metal and depended on the concentrations of the other ions in solution. Authors have compared the applicability of this model with the competitive Freundlich model for the biosorption of copper and cadmium by *Arthrobacter* sp. *b*iomass and concluded that for a two metal systems the Freundlich modified model was better than the Langmuir one.

Ho and McKay[176] showed also the use of an extended Langmuir equation with a competition term and incorporated interaction factors which performed high agreement with experimental data (copper, nickel biosorption onto peat).

More sophisticated models were developed for specific and particular biosorption cases. Such as the approach chosen by Jeon and Holl[177], who described heavy metal sorption equilibria for aminated chitosan. The sorption material was considered to act as a weakly basic anion exchanger. A Lewis acid/base interaction with heavy metal ions was considered while an equivalent amount of anions had to be co-adsorbed to maintain electroneutrality in both the liquid and the resin phase. Hydrogen ions were preferred over heavy metals and strong acids. Therefore, the uptake of heavy metal salts developed as a competitive sorption of heavy metal and strong acids. Authors prepared a surface complexation model based on the concept of surface charge generated from amphoteric surface sites of the solid phase capable to react with cationic or anionic species from the liquid phase to form ion pairs at the surface (called surface complexes).

Prediction of binary and multi-component systems required the numerical solution of systems of coupled nonlinear equations including the conditions of electroneutrality in the liquid and adsorbent phases, mass balances for each species etc. The model reflected well the affinity of the sorbent for the acid and the two metal species (Cu and Ni). Because of the strong preference, the amount of copper ions adsorbed was almost the same in the ternary system as in the binary system. For the less preferred nickel ions, however, the loading was smaller than in the binary case. Thus, the effect of nickel ions on the uptake of copper ions was small, whereas the influence of copper on the uptake of nickel was considerably greater.

Juang and Shao[178] proposed an alternative method using the mass balance equations and the mass action law for description of cadmium, zinc and nickel uptake by cross-linked chitosan. In this case it was important to know the stoichiometry of the complex ligand-metal. The basic assumptions of this model were:

- protons and metal ions compete for the same binding groups (i.e. –NH$_2$ group)
- the binding of amine groups with protons is always equimolar
- the average number of aminogroups bound with one metal ion is fixed over the whole pH range
- all types of possible binding sites have the same affinity to each metal ion.

The model was first developed for a single metal system and then extended to a multi-metal system, but this extension did not give satisfactory results.

A different approach was chosen by Tzesos et al.[179], who presented the results of metal competition in a multi-metal biosorption system with two different strains of *Pseudomonas sp.* as biosorbents compared on the basis of their Pearson's classification. The Pearson's classification in the three broad categories (i.e. soft, hard and border line elements) is based on the chemical coordination characteristics of the elements. Yttrium ions and uranium ions were selected as the representatives of the hard group. Yttrium ions form complexes preferentially with ligands having oxygen as a donor atom. Uranium, commonly present in solution in the uranyl complex ionic form behaves rather like divalent, accordingly to form readily complexes with oxygen donor ligands too. Palladium, silver and gold belong to soft element coordinating preferentially with ligands of decreasing electronegativity. Nickel belongs to the borderline class presenting and intermediate coordination behaviour.

Significant competition effects were observed for metals belonging to the same class. For metals belonging to different classes, their biosorptive uptakes were not significantly

affected by the presence of a co-ion, while borderline elements were affected by the presence of co-ions.

2.3.4 Biosorption in dynamic continuous mode

There are two diametrically different systems that could be used for the assessment of continuous – flow sorption dynamics: the fixed-bed reactor and the continuous-flow stirred tank reactor. Both can exist in different configurations and modifications featuring various process pros and cons. The probably most efficient configuration of the system is traditionally associated with the fixed-bed approach.[171]

The use of biomass in powdered form as presented in above chapters reveals some problems, such as difficulty in the separation of fine biomass particles after biosorption and mass loss during regeneration process. Low mechanical strength and small particle size of used biosorbent make it difficult to use in column applications because of the potential clogging of the column.

To solve these problems, dead biomass is usually immobilized in a biopolymeric or polymeric matrix used as a supporting material. Immobilization may improve biomass performance and biosorption capacity, increase mechanical strength and facilitate separation of biomass from pollutant-bearing solution.

Nevertheless, the use of immobilized biomass has also a number of disadvantages. Firstly, it increases the costs of the process. Secondly, the immobilization affects adversely the mass transfer kinetics. The number of binding sites is reduced since the majority of sites lies within the bead. So a good support material used for immobilization should be rigid, chemically inert and cheap. It should as well bind cells firmly, have high loading capacity and have a loose structure for overcoming diffusion limitations.

2.3.4.1 Biosorption in column mode

For continuous operations with immobilized biomass, the most convenient configuration is that of a packed column, much like that used for ion exchange. Packed bed column is an effective arrangement for cyclic sorption/desorption. It allows efficient utilization of the sorbent capacity and results in a better quality of the effluent.

Continuous packed bed sorption has also a number of process engineering advantages including high yield operations and relatively easy scaling up from a laboratory scale procedure.

The process of metal biosorption in a fixed bed column is influenced by:

- Sorption equilibrium

- Sorption particle mass transfer

- Flow pattern through the packed bed.

The overall performance of flow-through column is strongly related to the length and shape of the adsorption zone of the column. This zone develops between the section of the column which is already saturated and the section that still contains fresh biosorbent. The saturation of the bed within the transfer zone varies from zero (on the front of the zone) to the full saturation. As the loading of the biosorbent progresses, the zone moves along the column in the direction of the liquid flow with a certain velocity which is predominantly determined by the sorbate loading, sorbent capacity and column feed rate.

When the adsorption (saturation) zone reaches the end of a column, the metal concentration in the outlet stream increases sharply and the useful time of the column is over. This moment is called the *breakthrough point*. The time before the breakthrough occurs is the *service time* of the column. A typical breakthrough curve is illustrated in Figure 9. These parameters are the most important for designing the process. It directly affects the feasibility and economics of the sorption process. It is relatively easy to determine experimentally these values, but they are very dependent on column operating conditions.
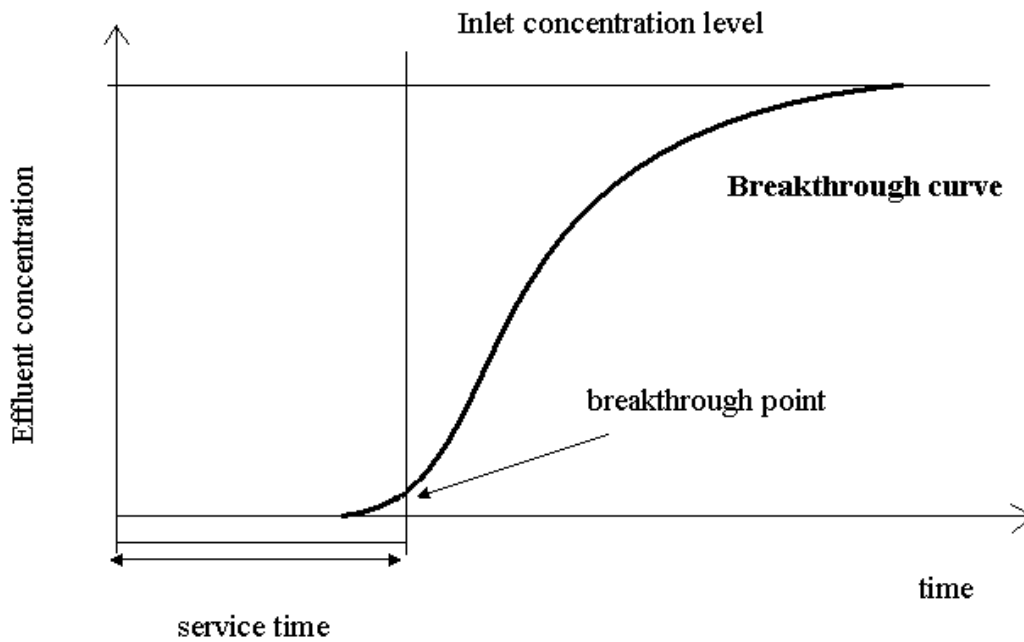
Figure 9 Breakthrough curve description

At the breakthrough point a portion of column contains the transfer zone with only partially saturated sorbent in it. Obviously, the shorter is the adsorption zone in the column, the longer is the column service time and the larger is the fully utilized sorbent portion inside the column.[144] The longer the transfer zone, the more sorbent ends up being not fully utilized. For the economical optimization of the process it is important to minimize the length of the transfer zone and increase thus the sorbent utilization.

The steeper is the breakthrough curve, reflecting the length of the transfer zone, the more efficient is the overall utilization of the sorbent in the column. A comparison of two breathrough curves is displayed in Figure 10. An unfavourable breakthrough curve (curve number 1) is flat and trailing, indicating a long transfer zone inside the column. On the opposite hand, a favourable breakthrough curve (curve number 2) is characterized by a steep and sharp slope, showing the effective utilization of the biosorbent material inside the column.
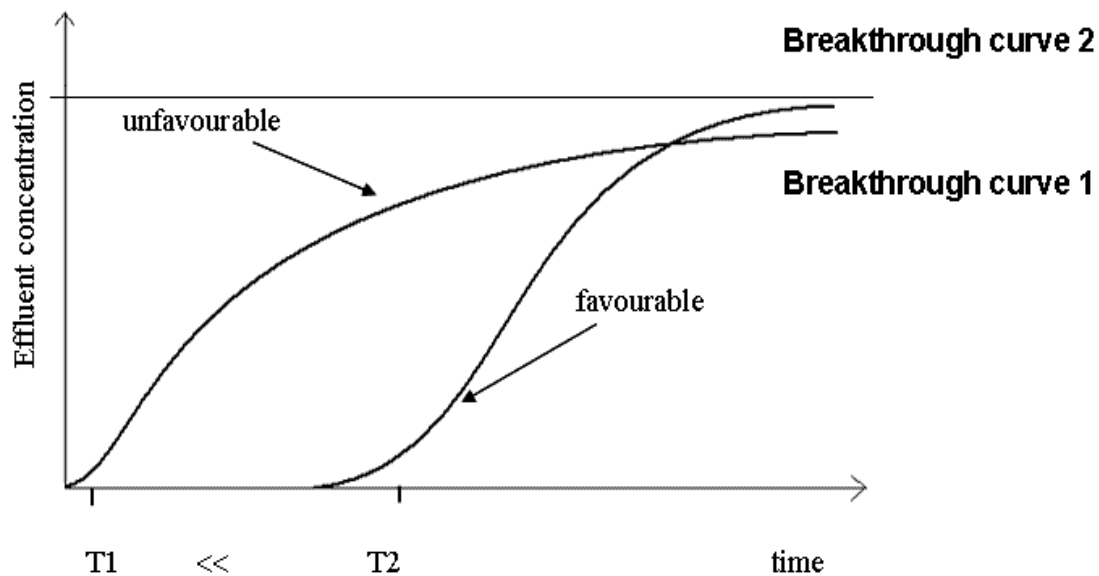
Figure 10 Comparison of favourable and unfavourable breakthrough curve

The link between equilibrium sorption behaviour and the column breakthrough curve is that according to the theory of chromatography, different parts of the transfer zone move with different speeds depending on the shape of the equilibrium isotherm for the given sorbent.

More sophisticated handling of experimental data is required to predict and explain the breakthrough curves for different sorption column operation scenarios as illustrated in the following chapter.

2.3.4.1.1 The breakthrough curve modelling

Developing a model to describe accurately the dynamic behaviour of adsorption in a fixed bed system is inherently difficult. Since the concentration of the adsorbate as the feed moves through the bed, the process does not operate at steady state. Therefore successful design of a column adsorption process requires prediction of:

- Concentration-time profile (breakthrough curve)
- Fundamental transport equations (material balance between solid and liquid)

The fundamental transport equations for a fixed bed are usually written in the following form:

$$\varepsilon \frac{\partial C_b}{\partial t} + U_0 \left(\frac{\partial C_b}{\partial Z} \right) + (1 - \varepsilon) \left(\frac{\partial q}{\partial t} \right) = E \left(\frac{\partial^2 C_b}{\partial^2 Z} \right)$$

Eq. 27

Where:

q	is the contaminant concentration in the sorbent at time t, [mg L^{-1}]
C_b	is the contaminant concentration in solution, [mg L^{-1}]
Z	is the column depth, [cm]
ε	is the void fraction in the bed, [-]
U_0	is the superficial velocity, [cm min^{-1}]
E	is the dispersion coefficient, [cm^2 min^{-1}].

And the mass balance of the adsorbed bed can be written as follows:

$$(1 - \varepsilon) \left(\frac{\partial q}{\partial t} \right) = r$$

Eq. 28

Where

r	is the adsorption rate, [mg L^{-1} min^{-1}]

The adsorption rate depends on the mechanism responsible for adsorption, which can be controlled by mass transfer from the bulk solution to the surface of the adsorbent. Alternatively, it can be also controlled by diffusion and reaction within the adsorbent particles.

All these equations are differential and usually require complex numerical methods to solve. Because of this, various simple mathematical models were developed to predict the dynamic behaviour of the column and these models are cited below.

2.3.4.1.2 The Adams-Bohart model

The fundamental equation describing the relationship between C_{eff}/C_{in} and time in a flowing system was established by Adams and Bohart[180] for the adsorption of chlorine on charcoal. Nevertheless, its overall approach can be applied successfully in quantitative description of other systems. The model assumes that the adsorption rate is proportional to both the residual capacity of the sorbent and the concentration of the sorbate species. The model is used for the description of the initial part of the breakthrough curve.

The mass transfer obeys the following equations:

$$\frac{\partial q}{\partial t} = -k_{AB} q C_b \qquad\qquad \textbf{Eq. 29}$$

$$\frac{\partial C_b}{\partial Z} = -\frac{k_{AB}}{U_0} q C_b \qquad\qquad \textbf{Eq. 30}$$

Where:

k_{AB} is the kinetic constant, [L mg^{-1} min^{-1}].

If following assumptions are taken into account:

- The concentration field is considered to be low, e.g. effluent concentration $C_{eff}<0.15C_{in}$
- For $t\rightarrow\infty$
- $q\rightarrow N_0$, where N_0 is the saturation concentration,[mg L^{-1}],

the equation is obtained with parameters k_{AB} and N_0:

$$\ln \frac{C_{eff}}{C_{in}} = k_{AB} C_{in} t - k_{AB} N_0 \frac{Z}{U_0} \qquad\qquad \textbf{Eq. 31}$$

Where:

C_{eff}, C_{in} are the effluent and inlet concentrations, respectively.

The values describing the characteristic operational parameters of the column can be determined from a plot of C_{eff}/C_{in} against t at a given bed height and flow rate.

2.3.4.1.3 The Wolborska model

This model is based on mass transfer equations for diffusion mechanism used for the description of adsorption dynamics in the range of the low-concentration breakthrough curve.[181] The mass transfer in the fixed bed sorption is described by the following equations:

$$\frac{\partial C_b}{\partial t} + U_0 \left(\frac{\partial C_b}{\partial Z} \right) + \left(\frac{\partial q}{\partial t} \right) = D \left(\frac{\partial^2 C_b}{\partial^2 Z} \right)$$ Eq. 32

$$\frac{\partial q}{\partial t} = -v \left(\frac{\partial q}{\partial Z} \right) = \beta_a \left(C_b - C_s \right)$$ Eq. 33

Where:

C_s	is the contaminant concentration at the solid/liquid interface, [mg L^{-1}]
D	is the axial diffusion coefficient, [cm^2 min^{-1}]
v	is the migration rate, [cm min^{-1}]
β	is the kinetic coefficient of the external mass transfer, [min^{-1}].

According to Wolborska's assumptions:

- $Cs \ll C_b$
- $v \ll U_0$
- Negligible axial diffusion $D \rightarrow \infty$ as $t \rightarrow 0$

The solution can be approximated to:

$$\ln\frac{C}{C_0} = \frac{\beta_a C_0}{N_0}t - \frac{\beta_a Z}{U_0}$$

$$\beta_a = \frac{U_0^2}{2D}\left(\sqrt{1+\frac{4\beta_0 D}{U_0^2}}-1\right)$$

Where:

β_0 is the external mass transfer coefficient with negligible axial dispersion coefficient D.

Wolborska observed that in short beds or at high flow rates of solution through the bed, the axial diffusion is negligible and $\beta_a=\beta_0$. The migration velocity of the steady-state front satisfies the relation, known as Wicke's law:

$$\nu = \frac{U_0 C_0}{N_0 + C_0}$$

The expression of the Wolborska solution is equivalent to the Adams-Bohart relation if the coefficient k_{AB} is equal to β_a/N_0. So the plotting of $ln\ C/C_0$ versus t would also give information on this model.

2.3.4.1.4 The Thomas model

Thomas model was traditionally used to predict the maximum adsorption capacity of an adsorbent in order to predict the concentration-time profile for the effluent. The model has the following form[182]:

$$\frac{C_{eff}}{C_{in}} = \frac{1}{1 + \exp\left(\frac{k_{Th}}{Q}\left(q_0 X - C_{in} V_{eff}\right)\right)}$$

Eq. 37

Where:

k_{Th}	is the Thomas rate constant, [mL min^{-1} mg^{-1}]
q_0	is the maximum solid-phase concentration of the solute, [mg g^{-1}]
X	is the amount of sorbent in the column, [g].

The linearized form of the Thomas model is as follows:

$$\ln\left(\frac{C_{in}}{C_{eff}} - 1\right) = \frac{k_{Th} q_0 X}{Q} - \frac{k_{Th} C_{in}}{Q} V_{eff}$$

Eq. 38

The kinetic coefficient k_{Th} and the adsorption capacity of the bed q_0 can be determined from a plot of *ln [(C_{in}/C_{eff})-1]* against the time at a given flow rate or versus the flow rate.

This model belongs among the most frequently used models in column performance theory. It assumes Langmuir kinetics of adsorption-desorption and no axial dispersion. The primary weakness of this model is that its derivation is based on second order reaction kinetics. Adsorption is usually not limited by chemical reaction kinetics but is often controlled by interphase mass transfer.

2.3.4.1.5 The Clark model

Clark[183] defined a new model based on the Freundlich isotherm relationship and the mass transfer concept.

$$\mathbf{U}_0 \frac{\mathbf{dC}_b}{\mathbf{dZ}} = \mathbf{K}\left(\mathbf{C}_b - \mathbf{C}_{eq}\right)$$

Eq. 39

Where

K is the mass transfer coefficient, [min^{-1}].

This model leads to a system of equation that must be solved by non-linear regression analysis.

2.3.4.1.6 The Yoon and Nelson model

Yoon and Nelson developed a relatively simple model for the adsorption and breakthrough of adsorbate vapours or gases onto activated charcoal.[184] The model is based on the assumption that the rate of decrease in the probability of adsorbate molecule is proportional to the probability of adsorbate breakthrough on the adsorbent.

The Yoon and Nelson model is not only less complicated than other models, but also requires no detailed data concerning the characteristics of adsorbate, the type of adsorbent, and the physical properties of adsorption bed.

For a single-component system it can be expressed as follows:

$$\ln \frac{\mathbf{C}_{eff}}{\mathbf{C}_{in} - \mathbf{C}_{eff}} = \mathbf{k}_{YN}\mathbf{t} - \tau\mathbf{k}_{YN}$$

Eq. 40

Where:

k_{YN} is the rate constant, [min^{-1}]

τ is the time required for 50% adsorbate breakthrough, [min]

t is the breakthrough (sampling) time, [min]

The calculation of theoretical breakthrough curves for a single-component system requires the determination of the parameter k_{YN} and τ for the adsorbate of interest. These values may be determined from available experimental data. The approach involves a plot of $ln\ C_{eff}/(C_{in}-C_{eff})$ versus sampling time. If the theoretical model accurately characterizes the experimental data, this plot will result in a straight line with slope of k_{YN} and intercept τk_{YN}.

All these models were applied to experimental data obtained for dynamic studies performed on fixed bed column for phenol biosorption by immobilized activated sludge by Aksu and Gonen[185] to predict the breakthrough curves and to determine the column kinetic parameters. The initial region of breakthrough curve was defined by the Adams-Bohart (or Wolborska) model at all flow rates and inlet phenol concentrations studied, while the full description of breakthrough could be accomplished by all other models only at higher flow rates and higher inlet phenol concentrations.

Han et al.[186] used the Thomas model to describe copper and lead sorption corn chaff in a fixed bed column. It was found that the model described adequately the sorption behaviour.

Naja and Volesky[187] studied the multi-metal biosorption in a fixed bed flow-through column. Biomass of brown seaweed *Sargassum fluitans* was used for this purpose. The ion exchange model adapted for multi-metal systems was proposed. The model consisted of a coupled system of partial differential, ordinary differential and algebraic equations describing the dynamics of the multi-component ion exchange in a flow-through fixed-bed.

3 Materials and Methods

Raw materials (industrial fungi) used in this study were issued from Czech industrial partners. *Penicillium oxalicum* var. Armeniaca was supplied by Ascolor Biotec (Pardubice, Czech Republic) and *Tolypocladium* sp. by Ivax Pharmaceuticals (Opava, Czech Republic). Both biomass types (*Penicillium oxalicum* var. Armeniaca and *Tolypocladium* sp.) constituted a fermentation waste by-product originated from food and pharmaceutical industry, respectively.

3.1 *Tolypocladium sp.*

Tolypocladium sp. is a genus of fungi used in pharmaceutical industry to produce a cyclosporine-type antibiotic.[188,189,190] Cyclosporine is a known immunosuppressive agent utilized in organ transplantations and in the treatment of autoimmune diseases.[191] It has also antifungal, anti-parasitic and anti-inflammatory effects.[192]

Tolypocladium sp. - Mycelium sterilae MS 2929 used in our study, was derived from a microorganism of the Czech Collection of Mircoorganisms CCM 8184 by the producer and was employed in antibiotic production. Growing conditions of the fungus were submerged fermentation procedure. The antibiotic was isolated from the biomass by methanol extraction after the fermentation process. The biomass was then stripped by steam and finally dried. Actually, the sorbent material was a denaturized product resulting from the action of methanol on proteins (during solvent extraction) and from the steam treatment.

The material was considered cleaned from residual fermentation by-products, fungal pigments and sugar residues. Biomass sample obtained for our experiments was issued from fermentation plant R&D laboratory and not directly from the industrial process. The sample was of black colour, loose and easy to handle. For these reasons, it was used as supplied (after grinding and sieving). It will be referenced T-sample. Figure 11 shows the macroscopic aspect of the material.

Figure 11 *Tolypocladium sp.* **biomass**

The dry matter content of original material supplied reached 30 % for *Tolypocladium* material according to the producer. This value could not have been checked as the material material was supplied in dry form.

3.2 *Penicillium oxalicum var.armeniaca*

P. oxalicum var. Armeniaca (Czech Collection of Microorganisms N° 8242, CCM 8242) was industrially used for the production of a red food pigment Arpink Red™ - dyeing molecule for meat, sweets and diary products.

Several genera of fungi are known for production of such pigments.[193] The fungus *Monascus* has been used traditionally in East Asia to produce a red food pigment.[194] Ogihara et al.[195,196] described recently the production of similar pigments by a fungus isolated from soil and identified as belonging to *Penicillium* sp. The use of a local strain of *Penicillium oxalicum* for a production of milk-clotting and caseinase enzymes was reported by Hashem.[197,198]

The biomass was also cultivated under submerged conditions. The pigment (anthraquinone type) is an exogenous secondary metabolite of *P. oxalicum* var. Armeniaca that is usually extracted from the culture media after removal of suspended biomass.

The pigment (molecular weight 378) is of a dark red to black colour in a powder form giving blood red solutions. UV/VIS spectrometry of its water solution showed 2 maxima at 498 nm (A1) and at 425 nm (A2). The determined quality marker is A1/A2 ratio ranging

between 1.1 – 1.5. The pigment is soluble in water, acetic acid, egg white, ethanol, methanol and butanol and only partially soluble in acetone, while it is insoluble in hexane, ether, benzene and carbon tetrachloride. It is interesting to observe that the pigment forms insoluble chelates with metals. The pigment is stable in aqueous solutions in the range of pH 4-9, while it precipitates below pH 3.5.

Penicillium fungi were frequently used in biosorption. The removal of dyes was studied by Zhang et al.[199] and metal ions by Fourest et al.[53], Holan and Volesky[52].

3.2.1 *Penicillium* biomass pre-treatments

Penicillium biomass was obtained as a raw filtration cake without any pre-treatment. At first, the dry matter content of original material supplied by industrial partners was determined. It was found that, the material had a high content of water and that dry matter constituted only 17% by weight. The aspect of the biomass clearly indicated that pigments residues remained at the surface of the biomass (see Figure 12) and the material tended to decay very quickly.

Figure 12 *Penicillium oxalicum var. Armeniaca* biomass

For these reasons, the raw material was directly subjected to different cleaning procedures, which conditions are summarized in Table 1. Even though the pigment is soluble in water, simple water rinsing was not sufficient to remove it from the surface of biomass (sample P1). As the pigment is equally soluble in alcohols, ethanol rinsing was performed, but failed also, as the pigment remained on the biomass surface (sample P2).

Sample number	Cleaning treatment	Effect
P1	Demineralised water	Colour remained
P2	Ethanol + demineralised water	Colour remained
P3	NaOH (10 M, boiling temperature, 3 hours) washed up to neutral pH Filtered and dried (fluidized bed dryer)	No colour remained
P4	NaOH (1 M, boiling temperature, 3 hours), washed up to neutral pH , filtered and dried (fluidized bed dryer)	No colour remained
P4FD	NaOH (1 M, boiling temperature, 3 hours), washed up to neutral pH, filtered and dried (freezed dried)	No colour remained

Table 11 Details of experimental conditions for *Penicillium* biomass pretreatment

So an alkaline treatment was carried out in order to remove the pigment residues. The alkaline treatment was often reported in the literature to prepare effective biosorbents from the fungal mycelia.[135] The alkaline treatment is known to promote deacetylation of chitinous fraction, proteins dissolution, removal of soluble glucans and hydrolysis of lipids.[200,201,202,203]

Two different NaOH concentration levels (1M and 10M NaOH) were selected for a treatment at boiling temperature and both of them led to a complete decolourization of the biomass as shown in Figure 13.

After the treatment, the biomass was carefully washed on a Buchner funnel using vacuum filtration until the filtrate reached neutral pH. The samples were subsequently dried using fluidized bed dryer (samples P3 and P4 and also samples P1 and P2) or freeze-dried (sample P4FD). The sorption capacities of samples P4 and P4FD were compared to check the influence of drying procedure.

Although both alkaline treatments led to desired decolourization (see Figure 13), the prepared samples were visually slightly different as illustrated in Figure 14. The sample P3 was of a pink-beige colour, while the sample P4 was more beige.

Figure 13 Different appearance of prepared Penicillium samples (numbers correspond to samples P1, P3, P4, respectively)
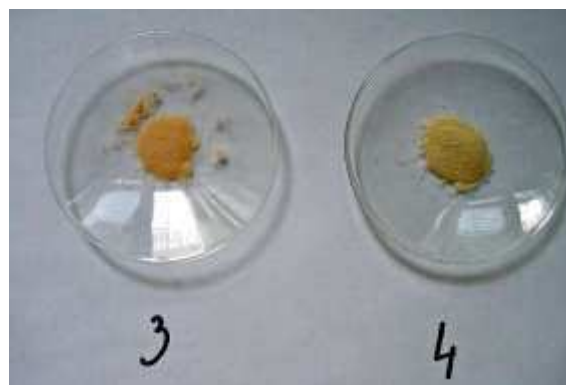
Figure 14 Comparison of appearance of biomass samples P3 and P4 according to their treatment

On the other hand the treatment led to a significant loss of organic matter and equally to a significant production of an alkaline filtrate. The yield (on the dry matter basis) did not exceed 20-30%, according to treatment, respectively. Taking into account a very low dry matter content of original material (17%), only about 35 – 50 grams of biosorbent could be prepared from 1 kg of original biomass.

To avoid possible misinterpretation of experimental results due to the presence of remaining pigments on samples P1 and P2 (possible formation of insoluble metal chelates), biosorption experiments were only performed using P3, P4 and P4FD samples. All the samples were subjected to grinding and sieving to separate the biomass in 5 fractions of the following sizes: G1 < 125 μm < G2 < 250 μm < G3 < 355 μm < G4 < 510 μm < G5 < 750 μm. In most cases, unless specified (investigation of the effect of sorbent size), the G1 size-fraction was used for sorption experiments.

3.3 Biomass characterization

To characterize the sorption materials several analyses were performed. Carbon, hydrogen and nitrogen contents were determined by elemental analysis. Infrared spectra of original materials, prepared biosorbents and metal saturated biosorbent samples were studied. The density, specific surface, pore distribution and their volume were measured.

3.3.1 Elemental analysis

The elemental analysis was performed using a Perkin-Elmer 2400 automatic elemental analyzer and the main characteristics – C, H and weight percentages - were determined and are summarized in Table 12. The experimental procedure used for elemental analysis did not allow the direct determination of oxygen content.

Sorbent sample	C(%)	H(%)	N(%)	C/N molar ratio
P1	48.1	7.6	4.4	13
P2	43.4	7.1	5.1	10
P3	43.0	7.8	3.3	15
P4	44.8	7.3	3.1	17
T	51.9	8.0	6.5	9

Table 12 Elemental analysis of sorbent materials

The results demonstrate that the composition significantly changed regarding the treatment of *Penicillium* derived samples. This is particularly evident for the nitrogen content. After the treatment with ethanol (sample P2), *Penicillium* biomass lost a significant percentage of carbon (from 48% to 43%), while the nitrogen content slightly increased (from 4.4% to 5.1%). On the contrary hydrogen content slightly decreased (from 7.6% to 7.1%). Ethanol is well known as a denaturizing agent and this may explain the C/N ratio decrease (from 13 to10).

After the treatment with boiling sodium hydroxide solutions (samples P3 and P4) a great change in their elemental composition was observed. The carbon content tended to the same values as for the ethanol treated sample (43.0% and 44.8% for P3 and P4 samples, respectively), while the nitrogen content had an opposite tendency. Its content decreased to 3.3 and 3.1, for P3 and P4 samples, respectively. These results contrast with the observation of Spanelova et al.[204] made on the treatment of *Aspergillus niger* waste biomass by concentrated NaOH solutions where N content increased after alkaline treatment.

The C/N molar ratio significantly increased to 15 with highly alkaline solution and to 17 with 1M solution. The treatment of biomass with boiling NaOH solutions is known as a deproteinizing operation. This procedure is commonly employed for the preparation of

chitin/chitosan from crustacean shells[141]. A treatment at room temperature with concentrated NaOH allows removing protein materials, while at boiling temperature the treatment with NaOH is expected to promote the deacetylation of chitin (acetylglucosamine polymer) to chitosan (glucosamine polymer) according to Figure 15. The increasing degree of deacetylation is traditionally considered a favourable parameter for the chelating ability of chitosan materials.[141,205]
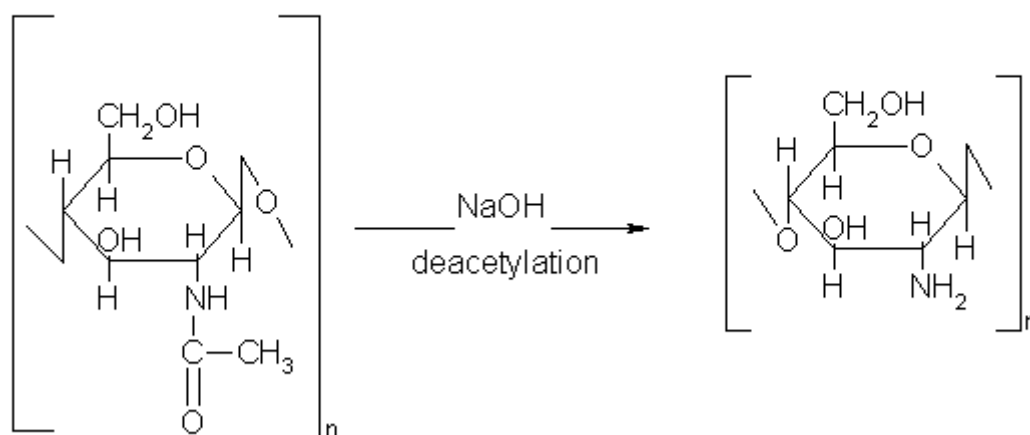
Figure 15 Deacetylation of chitin

The composition of the *Tolypocladium* material differs significantly from the composition of the *Penicillium* - derived materials. Both carbon and nitrogen contents are higher, up to 51.9% and 6.5% respectively, but the C/N molar ratio is lower (9). This is significantly lower than in the case of alkali treated P-samples, but very close to the values obtained for alcohol treated material (P2 sample). It is worth to note that the T-sample was also alcohol (methanol) treated and this treatment was followed a steam stripping (heat treatment).

3.3.2 Physical characterization

The density, the specific surface and the pore volume and size of P3 and T samples were determined. Helium-air picnometry using Micrometrics multivolume pycnometer 1305 was used to determine the samples densities. This method is often employed in determining of bulk densities of solid materials (metal oxides, catalysts, activated charcoal etc.) as it is non-

destructive, quick and reliable. The sample is put in a chamber, which is subsequently pressurized with a gas, preferably helium. Subsequent gas expansion in a precisely measured volume results in a pressure drop. The sample volume and density are then easily calculated.

The textural characteristics were obtained from nitrogen physisorption using Micrometrics ASAP 2020 device. The specific surface area, mean cylindrical pore diameters and adsorption pore volume were measured. The BET specific surface area was calculated by using the standard Brunauer, Emmett and Teller method on the basis of the adsorption data. The pore size distributions were calculated applying the Barrett-Joyner-Halenda (BJH) method to the adsorption branches of isotherms. The results are summarized in Table 13.

Biomass sample	Density	BET Specific surface area	Pore volume	Pore size
	$[g.cm^{-3}]$	$[m^2\ g^{-1}]$	$[cm^3\ g^{-1}]$	[nm]
P3	1.34	1.19	-	-
T	1.32	1.23	0.0018	17

Table 13 Physical characteristics of P3 and T samples

BET specific surfaces of both P3 and T samples are comparable to the specific surfaces of other biosorbents (Bayramoglu et al.[58]). Nevertheless these values are inferior to specific surfaces reported for other materials, since specific surfaces manifold higher were reported for carbon black[206] (170 $m^2\ g^{-1}$) and activated carbon[207] (ranging between 116 and 469 $m^2\ g^{-1}$). Due to a poor porosity of the P3 sample the pore volume and pore size were not determined. The protocols of these measurements are attached in Appendix.

3.3.3 Infra-red spectroscopy

FT-IR spectra of original materials were obtained using a Nicolet 740 spectrometer with a resolution of 2 cm^{-1} using 32 scans and the OMNIC software version 4.1 for numerical treatment of spectra. Analyses were performed on KBr discs. Carefully dried biomass was mixed with KBr and dried under vacuum before being conditioned in the form of thin discs under a mechanic pressure. Final concentrations of sorbent in the powder were close to 0.1% by weight.

Figure 16 shows FT-IR spectra of *Penicillium* derived sorbents. The FT-IR spectra clearly demonstrate that different functional groups are present on the biosorbents.
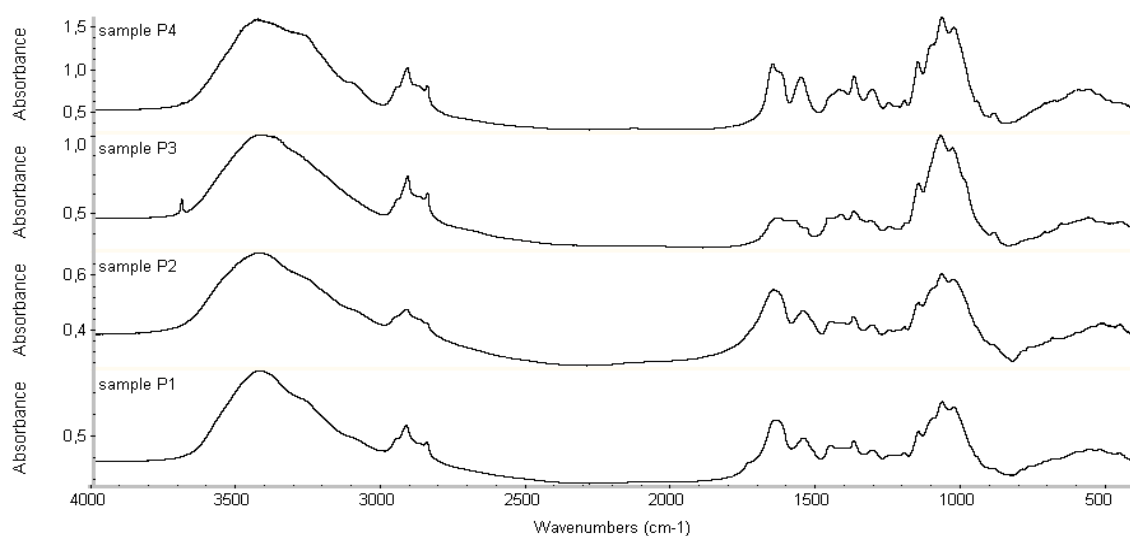
Figure 16 FT-IR spectra of *Penicillium* derived samples

The large band around 3400 cm^{-1} attributed to –OH groups masks the relevant information in the range 3500-3000 cm^{-1}. In the range 3000-2800 cm^{-1} the bands are representative of symmetric (2920 cm^{-1}) and asymmetric (2850 cm^{-1}) stretching of CH_3 and CH_2.

Figures 17 – 18 show the spectra of P3 sample and T sample (selected as the best sorbents for target metals, which will be illustrated in following chapters), respectively. A large band with several peaks was observed between 1200 cm^{-1} and 800 cm^{-1} (namely at 1080 and 1030 cm^{-1}). These bands were attributed to polysaccharide ring according to Schmitt and Flemming[208]. This band is present both in T and P3 spectra.
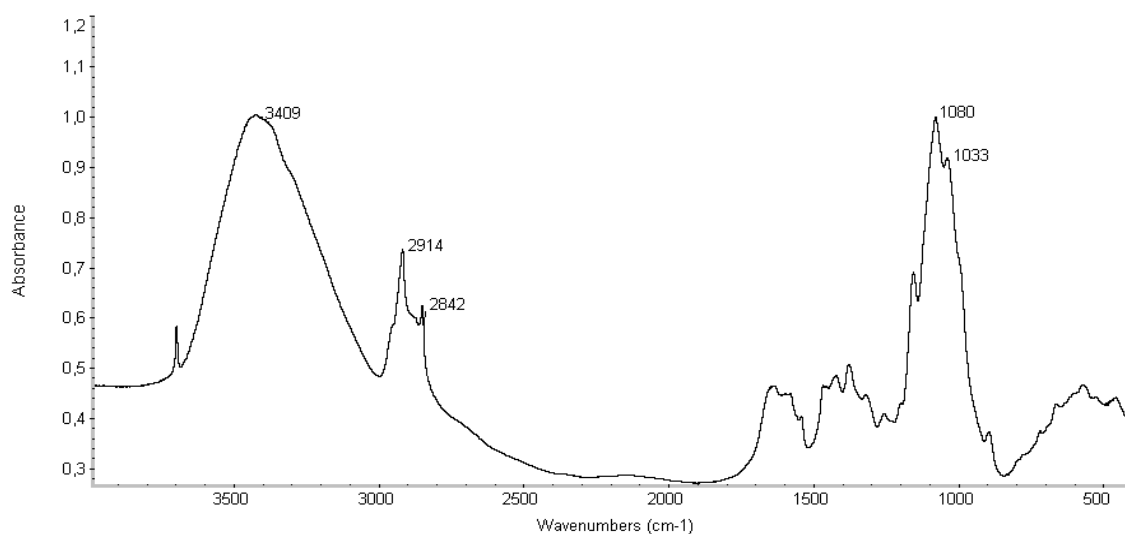
Figure 17 FT-IR spectrum of P3 sample
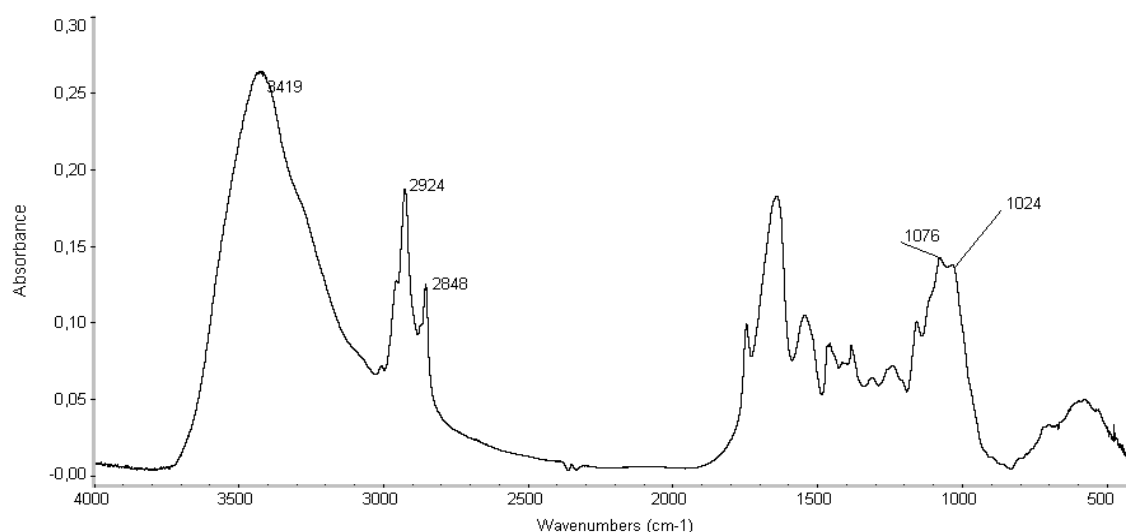
Figure 18 FT-IR spectrum of T sample

The most interesting information of these FT-IR spectra are found in the range of wavenumbers 1800- 400 cm^{-1} and the most significant differences between the spectra of T-sample and P3 sample are visible in the region 1800 – 1200 cm^{-1} (see Figure 19).
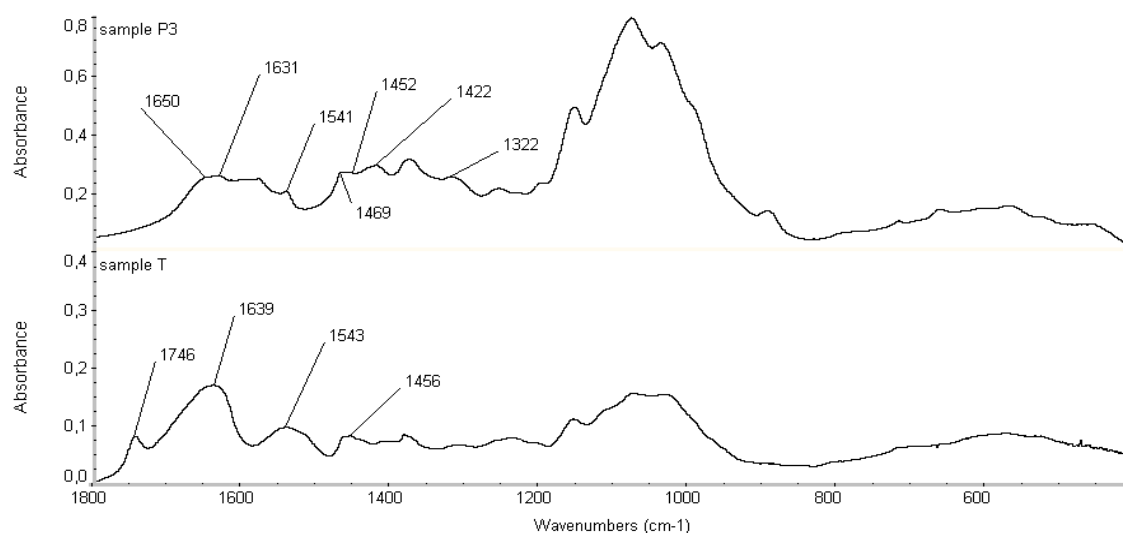
Figure 19 Comparison of FT-IR spectra of samples P3 and T – detail 1800-400 cm^{-1}

A peak was observed at 1745 cm^{-1} on T spectrum. This peak attributed to carbonyl stretch in carboxylate groups (un-ionized) or ester groups did not appear on P3 sorbent. T sorbent was also characterized by a wide band located around 1640 cm^{-1}. This band was attributed to Amide I (-C-O stretching coupled with –N-H deformation mode) band by Park et

al.[57] and Yee et al.[209] A large band observed at 1545 cm^{-1} was attributed to Amide II (-N-H deformation coupled to –C=N- deformation) band[57], typical for protein structure. Around 1460 cm^{-1} –CH$_2$ bending vibration was observed.

The spectrum of P3 biosorbent was very close to the spectrum of chitin/chitosan materials.[210] Three weakly resolved bands were observed in the range 1700-1500 cm^{-1}. The peak and a shoulder at 1650 and 1630 cm^{-1} were attributed to Amide I band (in chitin or proteins –C-O stretching coupled to-N-H deformation) associated to O-H-O bending of bound water. The peak that was observed at 1545 cm^{-1} was attributed to Amide II band (-N-H, -C-N and structure of proteins). The band at 1600-1580 cm^{-1} was attributed to amine groups; however, the presence of acetyl groups (incomplete deacetylation) resulted in weakly resolved bands, due to the superimposition of bands caused by amide vibrations. The presence of amine groups is usually confirmed by the presence of a shoulder around 3265 cm^{-1}, however, this peak is frequently hidden by vibrations of –OH groups, like in our case. Several peaks at 1472-1468, 1458 and 1430 cm^{-1} can be attributed to vibrations of pyranose –C-H bending and –O-H bending. At 1316 cm^{-1} the peak corresponds to –C-O-H bending coupled with -CH$_2$ deformation. This may also correspond to the Amide II band (-N-H deformation mode coupled with –C=O and –C=N- stretching modes). These series of bands are characteristic of biomass constituted of chitin-based materials and/or proteins.[210]

As already mentioned several changes appeared on *Penicillium* samples submitted to different treatments (reported in Table 11) and are illustrated in Figure 16. While the initial material (P1) was characterized by the presence of weakly resolved peak at 1743 cm^{-1} (attributed to carboxyl/carbonyl groups – see Figure 20), this peak disappeared with alcoholic and alkaline treatments.

Alkaline treatment is usually carried out to remove proteins from biomass in order to produce chitin and chitosan materials. The treatment with NaOH allows removing proteins and most of non-chitosan-like materials (except mineral compounds that should be removed by acidic treatment). In case of alkaline treatments at high temperatures, chitin material is converted to chitosan by deacetylation. This may explain that samples P3 and P4 were characterized by FT-IR spectra very close to those obtained with chitosan samples partially deacetylated.
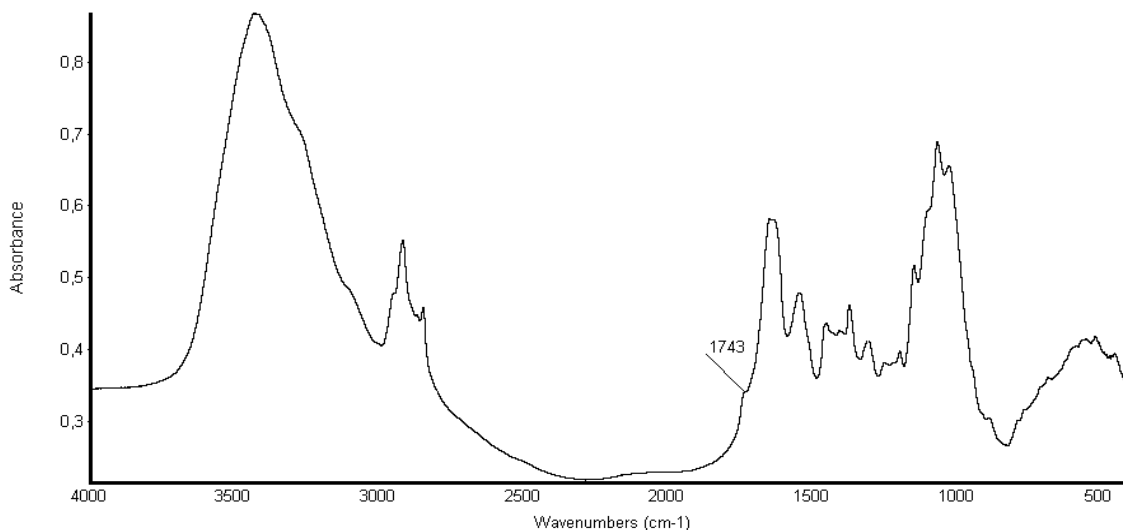
Figure 20 FT-IR spectrum of P1 sample

It is interesting to observe that P4 material remained insoluble in weakly acidic solutions, indicating that a fraction of acetamido groups was not completely deacetylated, while P3 material was partially soluble at pH 2 and pH 3 (analogy to chitosan – soluble in mineral acids). P3 and P4 samples correspond to different extents of deacetylation resulting in a change in the spectrum in the range $1650 - 1550$ cm^{-1}. At strong NaOH concentration (sample P3) high deacetylation of the biomass resulted in the shift of the 1554 cm^{-1} band and the appearance of the shoulder at 1580 cm^{-1} representative of amine groups (see Figure 21).
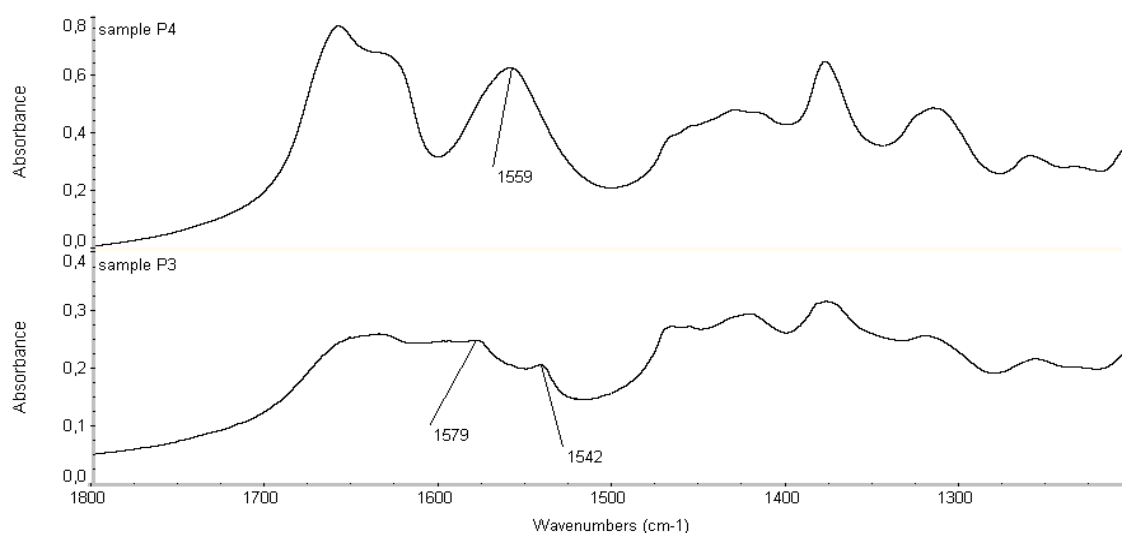
Figure 21 Comparison of FT-IR spectra of samples P3 and P4 – detail 1800-1200 cm^{-1}
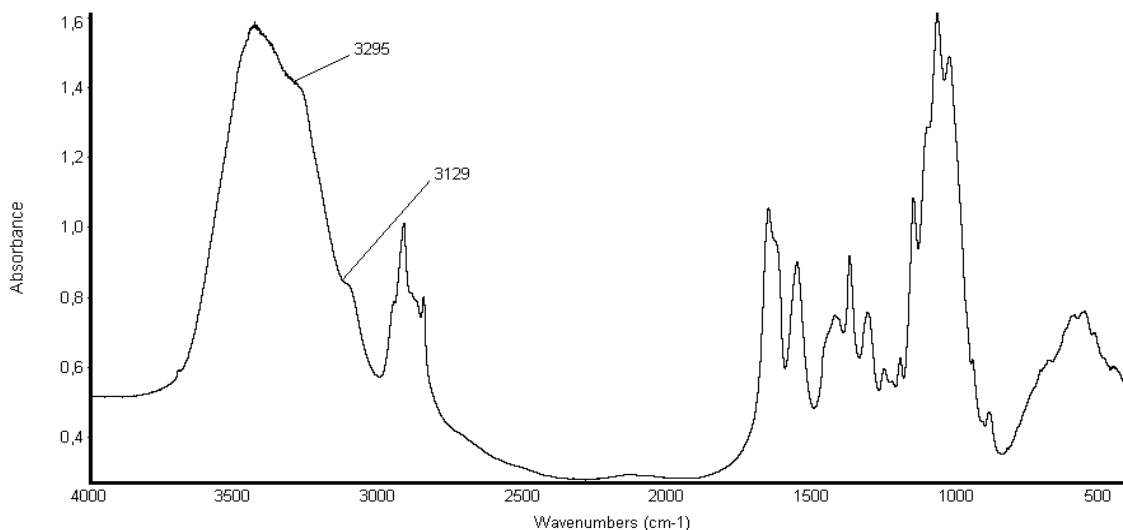
Figure 22 FT-IR spectrum of sample P4

P4 sorbent was characterized by the presence of two shoulders at 3297 and 3136 cm^{-1} (see Figure 22) that are less visible on the spectrum of P3 sorbent. These bands may be attributed to amide A and amide B bands[211]. This indicates that the degree of deacetylation was lower for P4 than for P3, consistently with solubility properties. The spectrum of P3 was close to that of chitosan while that of P4 (using less drastic deacetylation conditions) was similar to that of chitin-like materials.

Samples P1 and P2 were coloured fungal samples indicating that the anthraquinone dye was not completely removed from the biomass. This may also explain the presence of a peak at 1741 cm^{-1} on the original material and the presence of wide band at 1650 cm^{-1} with a small weakly resolved shoulder at the same wavenumber on sample P2 (the superimposition of vibration bands for amide and carbonyl groups may explain the weakly resolved broad band). Sample P2 was coloured indicating that anthraquinone dye remained on the biomass; though the dye is soluble in alcohol, the treatment was not sufficient for a perfect cleaning of the sorbent. This alcoholic treatment is suspected to remove lipid fraction but was dot sufficient to completely remove carboxylic or carbonyl groups (as evidenced by the width of the band close to 1660 cm^{-1}). The N content was significantly greater than that present in alkali-treated samples indicating that the fraction of sorbent removed during the alkaline treatments contained significant amount of nitrogen containing molecules such as proteins.

3.3.4 *Tolypocladium* material for column experiments

For column experiments the *Tolypocladium* biomass in granulated form originated directly from the industrial fermentation process was supplied by the producer. The *Tolypocladium* biomass was immobilized on FW14 Celatom diatomaceous (infusorial) earth (by Eagle Picher, Nevada, USA) during the filtration procedure. A partially wet sample of this material was supplied for our experiments. Several treatments, experiments and analyses were performed before the column arrangement with such a material was tested.

The supplied material was of greyish-black colour, loose and easy to handle. The shape of particles was rather spherical ranging from quite big beads to nearly powder form. Beads were quite hard and stable under manual mechanical pressure.

At first, after careful drying, a sieving analysis was performed. The results are displayed in Table 14 and Figure 23. The examples of each size fraction are presented in Figure 24. Seven different size fractions were prepared as follows: <1mm(B2)<2.5mm(B3)<3.15mm(B4)<5.0mm(B5)<5.6mm(B6)<8mm(B7)<B8. Nearly 80% of beads were inferior in size to 5 mm, approximately 30% of beads had diameter in the range of 5 – 3.15 mm and another 30% in the range of 2.5 – 1mm. The mesh size of sieves was selected according to the size of available sieves. Additionally, a fraction (called B1) was later prepared by dividing B2 fraction into two fractions (B1 ranging from 0 to 0.5 mm and B2 ranging from 0.5 to 1.0 mm).

Size fraction	Weight	%
[mm]	[g]	-
B2	<1.0	16	6.5
B3	1.0 – 2.5	26	10.5
B4	2.5 – 3.15	11	4.4
B5	3.15 – 5.0	70	28.2
B6	5.0 – 5.6	27	10.9
B7	5.6 – 8	67	27
B8	>8	31	12.5
Total		248	100

Table 14 Bead size analysis
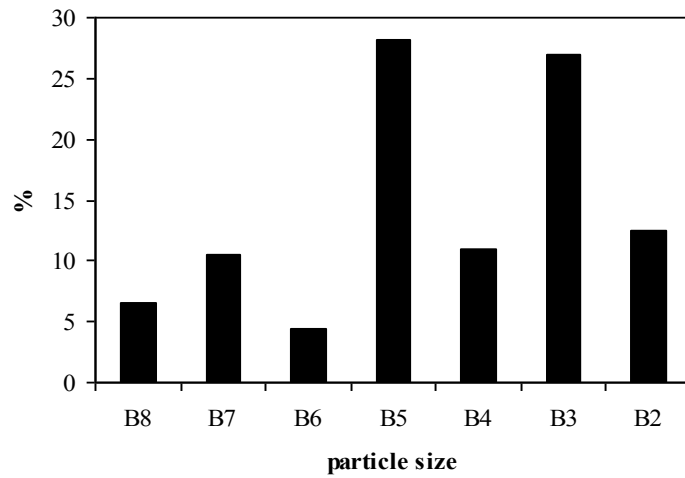
Figure 23 Sieving analysis – size distribution of beads
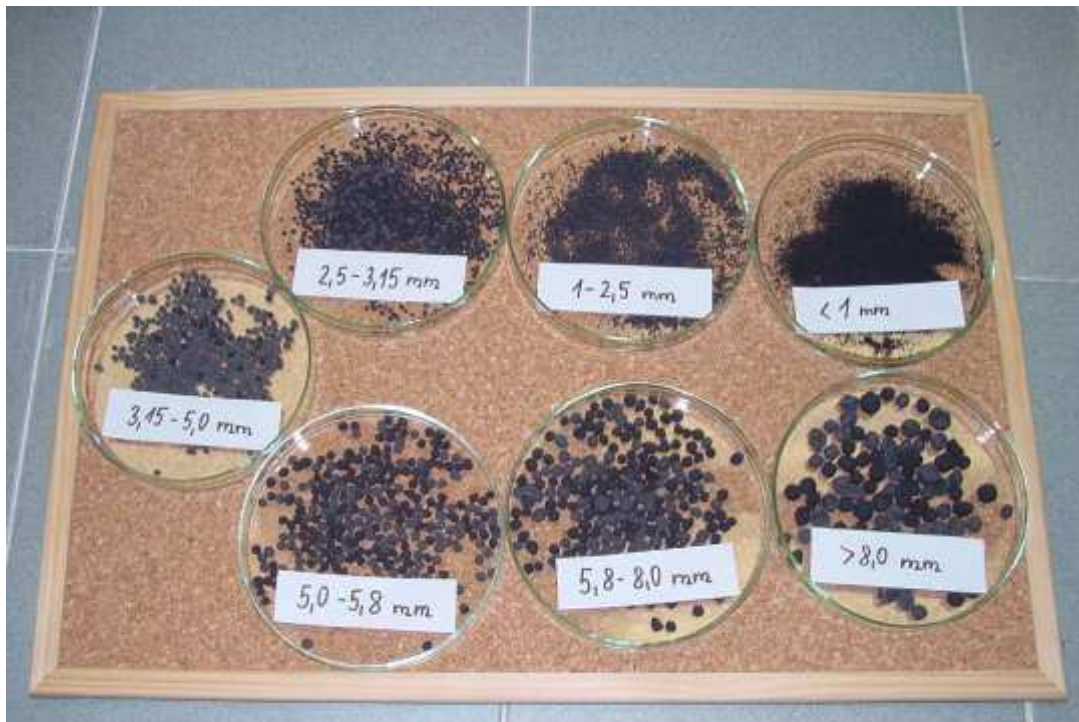
Figure 24 Size fractions of immobilized *Tolypocladium* sp.

According to our industrial partner the percentage of diatomite should be approximately 30%. This entry was verified in two different ways. All seven size fractions were calcinated at 550°C in a furnace up to a constant weight in order to determine the amount of inorganic matter in the samples. The results are summarized in Table 15. The

calcinated residues of all samples as same as samples of 3 smallest fraction (<1mm (B1), 1 - 2.5mm (B2), 2.5 – 3.15mm 5(B3)) of the original material were analysed by XRF method (X-ray fluorescence) for determination of inorganic materials.

Size fraction	Calcination residue (%)
B2	26.2
B3	29.8
B4	30.3
B5	30.5
B6	31.9
B7	31.5
B8	29.9

Table 15 Calcination residues

For the majority of fractions the residue percentage was in the range of 30%, except the smallest size fraction where the value was slightly lower - 26%. The differences between samples before and after calcinations are illustrated in Figure 25.
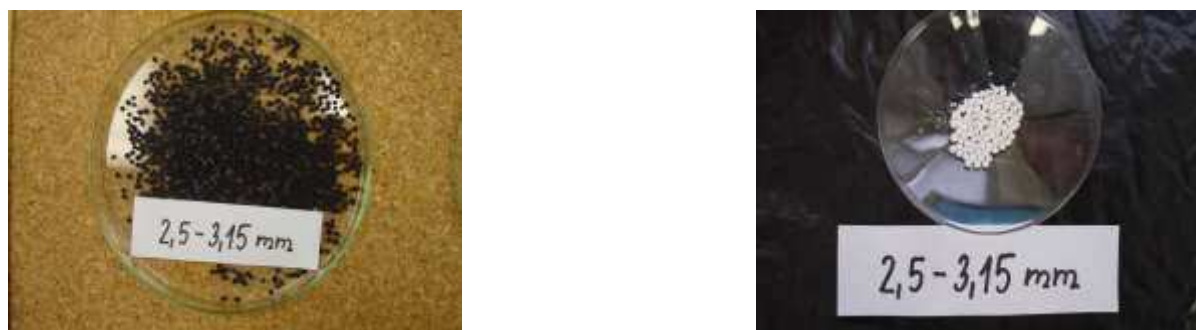
Figure 25 Sample of biomass size fraction 2.5 – 3.15 mm before (left) and after calcination (right)

The results of XRF analysis in the form of oxides of calcinated residues are displayed in Table 16. The amount of analyzed matter was in the range from 91 – 98%, which indicates good calcinations of biomass samples. The immobilization agent is mainly composed of silicon dioxide (approx. 80%), and the rest being the oxides or other compounds of iron, aluminium, sodium, magnesium, phosphorus, potassium and calcium.

Size fraction	Analyzed matter	%									
	%	**Na₂O**	MgO	Al₂O₃	**SiO₂**	**P₂0₅**	K₂O	CaO	TiO₂	Fe₂O₃
B2	98.4	**3.9**	0.5	2.8	**82.0**	**5.8**	2.6	0.8	0.2	1.4
B3	96.4	**4.0**	0.4	2.8	**83.1**	**5.0**	2.2	0.8	0.2	1.4
B4	98.1	**4.0**	0.4	2.8	**83.8**	**4.9**	2.1	0.8	0.2	1.4
B5	91.4	**4.1**	0.4	2.8	**83.1**	**4.9**	2.1	0.8	0.2	1.5
B6	97.8	**4.0**	0.4	2.8	**83.5**	**4.8**	2.0	0.8	0.2	1.5
B7	96.1	**4.0**	0.4	2.8	**83.5**	**4.7**	2.1	0.8	0.2	1.5
B8	95.8	**4.0**	0.4	2.8	**82.8**	**5.2**	2.2	0.8	0.2	1.5

Table 16 XRF analysis of calcinated residues

The results of XRF of original samples (small size fractions as the bigger beads were impossible to powder with the help of a mortar and a pestle) are summarized in Table 17.

Size fraction	Analyzed matter	%										
	%	**Na₂O**	MgO	Al₂O₃	**SiO₂**	**P₂0₅**	S	Cl	K₂O	CaO	TiO₂	Fe₂O₃
B2	39.5	**2.4**	0.4	2.9	**76.0**	**7.8**	2.0	0.1	4.7	1.5	0.3	2.3
B3	42.4	**2.5**	0.4	2.8	**77.0**	**7.1**	1.8	0.1	4.0	1.3	0.3	2.4
B4	43.5	**2.5**	0.4	2.7	**78.0**	**6.9**	1.7	0.1	3.9	1.3	0.3	2.3

Table 17 XRF analysis of original samples

The results are not entirely comparable to the results of calcination experiments. The analyzed matter amount for the smallest size fraction was 39.5% of presented sample, while the calcinated residue was only 26% in this case. The same discrepancy was observed for the two other samples. But it should be taken into account, that there appeared some elements during this analysis that were not observed before, namely sulphur, chlorine and higher amount of phosphorus. Although sulphur, chlorine and phosphorus can create inorganic compounds such as sulphates, sulphides, chlorides or phosphates, the fact that these elements are not found in calcinated samples (or found in a lesser extent) should signify that these elements are involved in organic compounds that were eliminated during the calcination. The elementary analysis of these materials was performed again to verify this hypothesis; unfortunately, the chlorine and phosphorus content could not have been determined due to their low concentrations (see Table 18). It is worth to note that both the original elemental and

the infrared analyses of the biomass without diatomite material did not revealed such a presence.

Size fraction	N(%)	C(%)	H(%)	S(%)	P(%)	Cl(%)
B2	5.3	38.0	5.4	0.5	x	x
B3	5.1	36.7	5.3	0.3	x	x
B3	5.0	36.0	5.3	0.3	x	x

Table 18 Elemental analysis of *Tolypocladium* granulated material

If the elemental analysis of the original powdered sample is compared with the above results (after subtracting the content of diatomite), it can be stated that the C, H and N contents correspond, so the composition of produced biomass seemed to be stable.

3.4 Sorption procedures

The first part of the sorption study was subdivided into three particular experiments. At first a preliminary study of pH influence was performed. This study served to select the optimum pH for the sorption experiments and equally to test the sorption properties of sorption materials and to eliminate the less efficient sorbents. This step was followed by a determination of sorption isotherms and monitoring of sorption kinetics.

This first part of the work was followed by experiments performed in binary metal systems, where the metal-metal-sorbent interactions were studied, and the experimental work was concluded by experiments performed at dynamic system with a fixed-bed column.

3.4.1 Study of pH influence

The metal solutions were prepared by dilution from stock solutions (concentration 1g Me L^{-1}) prepared using chloride salts of mercury (HgCl$_2$, Riedel de Haen, Germany), of lead (PbCl$_2$, Fluka, Switzerland) of cadmium (CdCl$_2$.H$_2$O, Merck, Germany) and potassium dichromate (K$_2$Cr$_2$O$_7$, Lachema-Chemapol, Czech Republic).

The study of pH influence on sorption properties was performed by mixing a known amount of sorbent sample with metal solution at selected pH for 72 hours on a shaker. There

was no pH control during the process, if not indicated otherwise. The final pHs of suspensions were noted, solutions were filtered and analyzed for residual metal concentrations. Sorbent dosage was fixed at 300 mg L^{-1}, while the initial metal concentration was 50 mg L^{-1}. Biomass free blanks were always used as controls. The biomass blanks were solutions containing the same concentration of metal at the selected experimental pH without biomass. These solutions were treated in the same manner as the biomass suspensions (3 days of agitation, ambient temperature). Their final pH and metal concentrations were determined afterwards. The blanks were prepared to check the possibility of metal precipitation due to the experimental pH, to verify the evolution of pH without the presence of biomass and they were also used as initial values (initial concentration) for evaluation of results.

A second set of experiments was performed with pH control. During the sorption procedure, pH was regularly monitored and controlled to the standard value. Additionally, a last series of experiments was performed to verify the eventual precipitation of metal due to the release of organic or mineral matter from biomass at optimum pH. Therefore, the biosorbents were pre-conditioned in water of the optimum pH for 3 days, the biomass was then removed by filtration and the filtrate was used to prepare the solution (by dilution of the stock solution). After metal addition, the solution was mixed for 24 hours, filtered and the metal concentrations were compared to calculated values (from dilution factor). This last set of experiments was to confirm whether the precipitation of metal occurs due to the release of organic matter and/or pH effect. Such a problem was observed by Spanelova et al.[104] for the recovery of lead using waste biomass of *Aspergillus niger* from citric acid production plant, where the presence of oxalate residues leached during the sorption experiments induced lead precipitation in the form of lead oxalates.

3.4.2 Sorption isotherm determination

In the case of sorption isotherms, solutions at appropriate pH (selected according to the results of the previous experiments) were prepared at different initial concentrations (typically 10 – 100 mg Me L^{-1}), while the biosorbent concentration was fixed at a constant value (300 mg sorbent L^{-1}). The operational mode was maintained as in the previous set of experiments (e.g. 3 days of contact on a shaker, final pH measurement, filtration and determination of residual metal concentration). The uptake was calculated according to the

mass balance equation (Eq. 1) and Langmuir (Eq. 41) and Freundlich (Eq. 42) equations in their linearized forms were used to describe experimental data.

$$\frac{C_f}{q} = \frac{1}{bq_{max}} + \frac{C_f}{q_{max}}$$ **Eq. 41**

Where:

q is the amount of adsorbed metal per unit weight of biosorbent, [mg g^{-1}]

q_{max} is the maximum sorbate uptake under the given experimental conditions, [mg g^{-1}]

C_f is the remaining (or equilibrium - C_{eq}) metal ion concentration in solution, [mg L^{-1}]

b is the coefficient related to the affinity between the sorbent and sorbate, [L mg^{-1}].

$$\ln q = \ln k + \frac{1}{n} C_f$$ **Eq. 42**

Where:

k is an empirically determined constant being related to the maximum binding capacity [L g^{-1}]

n is an empirically determined constant related to the affinity or binding strength, [dimensionless]

C_f is the remaining (or equilibrium – C_{eq}) metal ion concentration in solution, [mg L^{-1}]

3.4.3 Sorption kinetics

The sorption kinetics was also monitored using a standard procedure. One litre of metal solution at given metal concentration at selected pH was mixed with sorbent at chosen

sorbent dosage for 72 hours. Samples of suspensions were withdrawn at regular time intervals, immediately filtered and analyzed for residual metal concentration. The whole experiment was performed at constant temperature. Three reactors were usually run at the same time.

Several sets of experiments were carried out. The influence of initial metal concentration was tested, therefore the sorbent dosage was fixed (300 mg L^{-1}) and the metal concentration varied. Three experiments were run simultaneously at three metal concentration levels (20, 50 and 100 mg Me L^{-1}, respectively).

The influence of sorbent dosage was tested also (which means fixed metal concentration and varied sorbent dosage – 100, 300, 500 mg sorbent L^{-1}, respectively).

Finally, the influence of biosorbent particle size was examined. Both sorbent and metal concentration were fixed (50 mg Me L^{-1}, 300 mg sorbent L^{-1}, respectively), but the sorbent size varied (5 sorbent sizes tested).

The experimental data were visualised in form of plots and mathematically described using kinetics order equations and the diffusion phenomena influence was examined according to simple models described in chapter 2.3.2.3.

3.4.4 Bimetallic systems

Biosorption experiments in bimetallic systems were also performed in order to determine the influence of the presence of other metals, and to evaluate possible competition and inhibition effects on the process efficiency. More specifically, the influence of lead and cadmium presence on mercury sorption was examined.

The experiments were typically performed at varying concentration of one metal and constant addition of the second metal at the optimum initial pH of the first metal. The sorption isotherms were determined and compared to single metal systems.

3.4.5 Column experiments

Column studies were performed in following experimental arrangement. A glass column of inner diameter of 2 cm and height of 15 cm was wet packed with *Tolypocladium* beads of selected fraction size. The dry bed height was 8 cm, but the material tended to swell

and increase its volume. A complementary experiment was performed. A 10 mL volumetric cylinder was filled with 5 mL of beads and refilled with water, after 2 days of hydration the swelling phenomenon induced an increase of the bed volume to 8 mL.

Monometallic (Cr(VI) or Hg) solutions at its optimum pH were pumped through the column in a down flow direction in case of hexavalent chromium and in up flow direction in case of mercury by a peristaltic pump. With the regard to the column diameter, only beads of diameter inferior to 2.5 mm were used. At the beginning a down flow of the liquid was chosen due to easier experimental layout, but as technical problems occurred during the experiments (i.e. level decrease etc.) the up flow direction was later adopted. Samples were collected at regular intervals by a fraction collector and analyzed for metal contents. The experimental arrangement is illustrated in Figure 26.
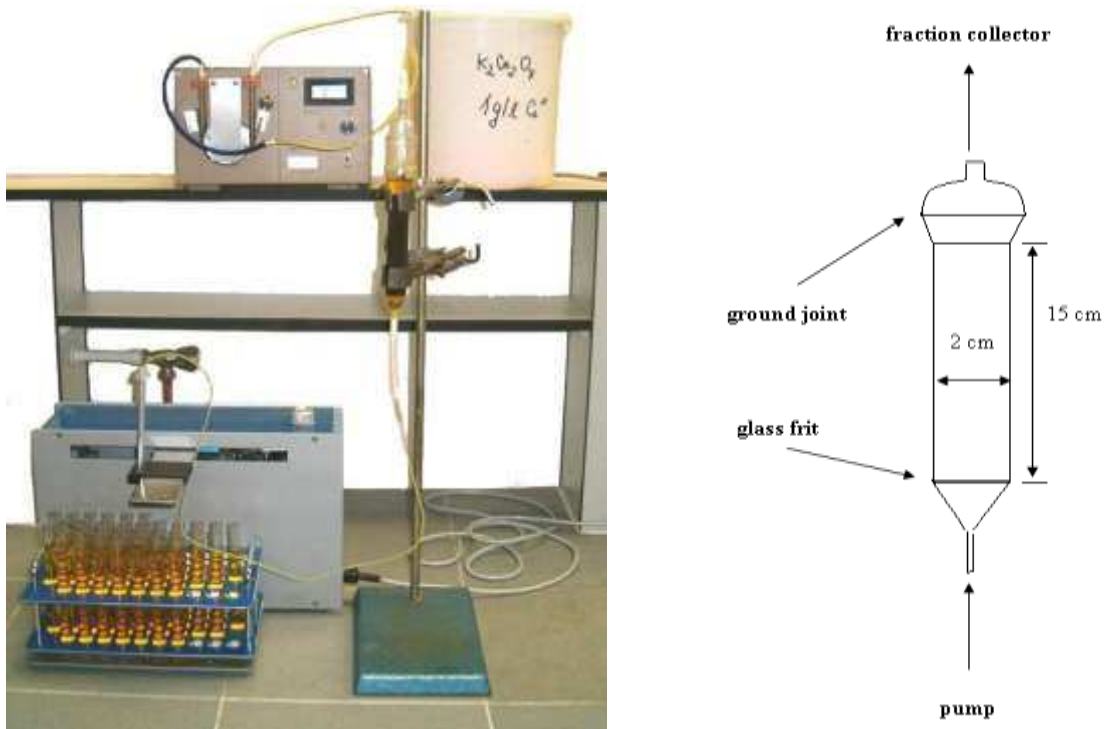
Figure 26 Column experimental arrangement for hexavalent chromium dynamic sorption

The column experiment was once terminated when the ratio of effluent to influent metal concentration reached certain stable value.

3.4.6 Analytical methods

Cadmium, mercury and lead concentrations were determined by inductively coupled plasma atomic emission spectrometry (using a JY 2000 spectrometer, Jobin-Yvon, Longjumeau, France). Total chromium concentration was determined by atomic absorption spectrometry (using atomic absorption spectrometer GBC SensAA, GBC, Australia) and hexavalent chromium content was determined spectrophotometrically[212] at 540 nm after colorimetric reaction with 1,2-diphenylcarbazide (supplied by Fluka, Switzerland).

The analytical standards used for determination of calibration curves were supplied by Carlo Erba (Italy) for Cd, Hg and Pb analyses and by Analytika s.r.o (Czech Republic) for Cr analyses. The calibration curves were prepared ranging between $0 - 100$ mg Me L^{-1} in case of mercury, lead, cadmium and total chromium, while ranging only between $0 - 1$mg Me L^{-1} in case of hexavalent chromium due to high sensitivity of the colorimetric method. Consequently, the samples had to be diluted prior to their analysis.

The samples were in general analyzed only once, but only the results with standard deviation lower than 1% were considered relevant (taking into accountant that atomic absorption spectrometer and ICP atomic emission spectrometer perform every analysis three times). In the case of the spectrophotometrical method, the samples were also analyzed only once, nevertheless the results were verified by occasional repetition and very good repeatability was found (standard deviation inferior to 3%). The differences between hexavalent and total chromium amounts were not considered significant when inferior to 5%.

3.4.7 Comments on experimental procedure

The experiments were not repeated by default, but in every series of experiment one experiment was performed in duplicate to verify the repeatability of results (see the exampleof mercury sorption isotherm using P3 sorbent at initial pH5 performed in duplicate in Figure 224 *in Appendix G) and satisfactory repeatability of results was found (as shown in* Figure 225 *where the data were statistically treated). Similar repeatability was obtained for other experiments performed in duplicates. According to these results, we have deduced a standard deviation corresponding to less than 8% for all experiments.*

Taking into account the heterogeneity of the biosrbent materials, we have considered that variability due to experimental procedure (solution preparation, sorbent weighing, and

analyses) was less than the variability due to biomass heterogeneity. We will consider that variations less than 8% are not significantly different.

4 Results and discussion

4.1 Selection of pH and sorbent materials

The precipitation test with released material from biomass revealed systematically negative indicating that the removal of metals only proceeded by sorption process and not by an artefact mechanism of precipitation due to pH increase or interactions with dissolved compounds.

4.1.1 Mercury

Figure 27 shows sorption efficiency obtained with sorbents P3, P4, P4FD and T for initial pH (uncontrolled) varying between pH 2 and pH 7. The sorption of mercury below pH 4 was negligible, regardless of the sorbent. This phenomenon, observed for metallic cations biosorption, was often described in the literature[65,63] and is known as a so-called *adsorption edge*. This lack of cationic biosorption below pH 4 is traditionally attributed to the competition for sorption sites between protons and metal cations.

It is worth to note that at pH 2 and pH 3 the sorbent P3 could not be used since the material tended to dissolve (pH 2) and to form colloid particles (pH 3). As the sorbent was prepared using a very drastic alkaline treatment and by analogy with the procedure used for chitin deacetylation, it is possible to suggest that this treatment led to the production of a chitosan-like material that was only partially deacetylated (as indicated by FTIR spectra) but was partially soluble in acidic solutions (analogy with chitosan – soluble in mineral acids solutions[141]). Less strong alkaline treatment is not expected to produce an extensive deacetylation of chitin-like material. The resulting material is thus expected to be less favourable for metal chelation.
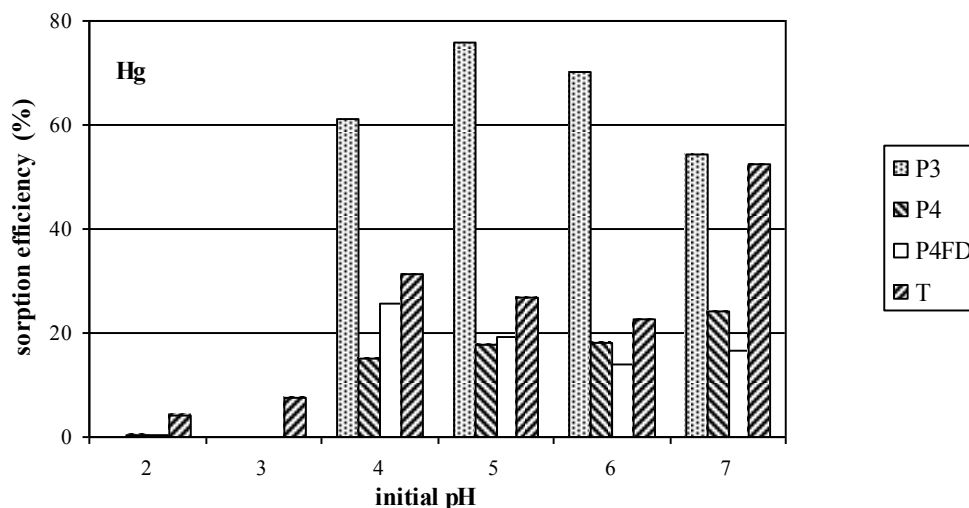
Figure 27 Influence of initial pH (uncontrolled) on Hg sorption efficiency using biosorbents P3, P4, P4FD and T (initial concentration: 50 mg L^{-1}, sorbent dosage: 300 mg L^{-1})

Best sorption appeared when initial pH was 4 or higher. This result is common to all four tested sorbents. In the range of pH 4 -7 the sorption efficiency was hardly affected by pH in case of P-samples. On the contrary in the case of T-sample, a significant increase in sorption efficiency was observed at pH 7. This fact could be explained by the decrease in proton – metal sorption competition. As at increased pH, the proton competition for sorption sites decreases, the affinity of the sorbent for metal cations could increases.

Obviously the highest sorption efficiency was observed for P3 sample. Under selected experimental conditions this efficiency was 2-3 times higher compared to other materials. This significantly greater efficiency may be explained by the drastic deacetylation treatment used for biomass cleaning.

The relatively weak effect of pH in nearly neutral pH range may be explained by the "buffering" effect of the biomass. As shown on Figure 28, the final pH remained stable for initial pH below 4. While for initial pH ranging between pH 4 and pH 6, the equilibrium pH stabilized around pH 6 for sorbents P4 and P4FD (no effect of drying procedure) and around pH 6.7 for sorbent P3. When the initial pH was set to 7, sorbents P4 and P4FD weakly affected the pH of the solution, while sorbent P3 increased the pH to 8.3.
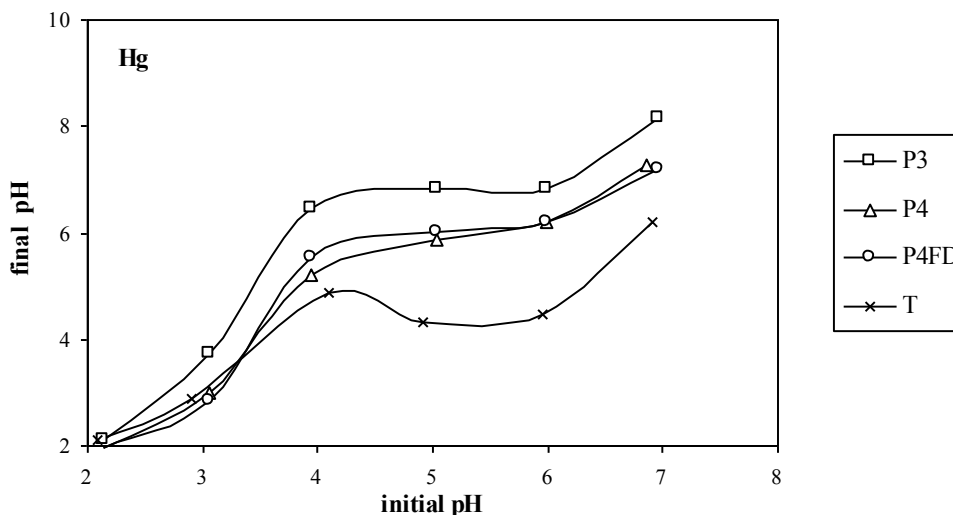
Figure 28 pH variation during Hg sorption using biosorbents P3, P4, P4FD and T (initial concentration: 50 mg L^{-1}, sorbent dosage: 300 mg L^{-1})

For sorbent T, pH variations were significantly different. For solutions at initial pH4, the pH rose to 5, while for solutions at pH 5-7 the equilibrium pH tended to decrease (from 6 to 5 and from 7 to 6.5). The difference in the acid-base behaviour of the sorbents can be explained by the differences in the treatments to which they were subjected. P-samples were alkali-treated and a part of this base (although a careful rinsing) could have remained on the biomass surface and hence be progressively released during the sorption process causing so the pH increase. The pH variation may also be related to proton sorption.

On the contrary biosorbent T was not subjected to such a treatment and pH variations were less important. The slight acidification of the solution may result from a different mechanism of metal sorption. If an ion exchange process is involved in the uptake of mercury, protons may be released causing pH decrease. This is consistent with the FTIR analysis of biosorbent T that revealed the presence of carboxylic groups. When the pH is below the pK$_a$, protons on carboxylic groups may be exchanged with cations (as describe for algal interactions with metal ions in chapter 2.2.1.6). It is interesting to note that in acidic solutions (pH below 4) the colour of the solution changed in the presence of sorbent T due to a partial release of organic material.

Basically, the highest sorption was obtained with sorbent P3 with equilibrium pH close to 6.5 (corresponds to initial pH 5). Under selected experimental conditions the sorption efficiency exceeded 75%. For other P-samples, the sorption efficiency did not exceed 30%. With sorbent T the sorption efficiency increased to 55% when the initial pH was set to pH 7, so the sorption efficiency was comparable to that obtained for P3 biosorbent.

It is worth to note that due to acid-base properties of T sample the equilibrium solution reached pH 6.5, which was the optimum equilibrium pH for P3 sample.

The increase in solution pH during the sorption process was significant with sorbent P3. Therefore, a complementary set of experiments was performed with pH control. Figure 29 shows that in most cases pH control revealed unfavourable with a slight decrease in sorption efficiency while the pH was maintained constant by regular acid addition.
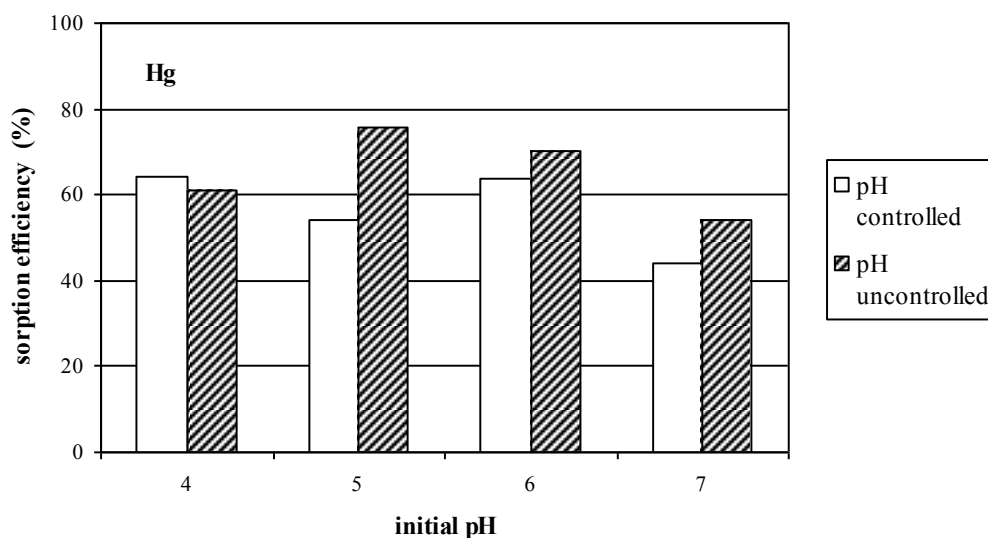
Figure 29 Influence of pH on Hg sorption efficiency using biosorbent P3 (initial concentration: 50 mg L^{-1}, sorbent dosage: 300 mg L^{-1})

In the case of Reactive Black 5 sorption using chitosan material[92], the influence of pH on dye removal was significantly altered when the acid-base properties of the sorbent were controlled by an acidic pre-conditioning of the polymer. The pre-conditioning allowed to reduce pH variation during the sorption process, at the expense of a loss in sorption properties. Similar results were obtained in our work; controlling the pH by acid or base addition generally decreased uptake performance.

Table 19 summarizes mercury (II) speciation at four different pH values. The speciation was calculated by the Visual MINTEQ programme ver. 2.5[213] (free software for calculations of metal speciation, solubility equilibria etc.). PH 3 corresponds to initial pH at which a negligible mercury sorption was observed. PH 5 and pH 7 correspond to optimum initial pHs for P3-sample and T-sample respectively. PH 6.5 is the final (equilibrium) pH observed in both systems. Total dissolution of salt used for solution preparation and no metal

precipitation were predicted by the programme, thus the observed concentration decrease can only be ascribed to biosorption process.

It is well indicated in the below table, that the majority of species is present in a non-ionic form all along the tested pH range and so the interaction with biomass function groups should also be of a non-ionic character. The same observation was made by Herrero et al.[112] for mercury sorption by macroalgal biomass of *Cystosteira baccata*.

It is equally evident, that with increasing pH the amount of hydroxo-complexes (Hg(OH)$_2$ and HgClOH (aq)) increases too, while at pH 3 the majority of mercury(II) exists in the form of HgCl$_2$ (aq). However, the speciation modelling did not give any indication of the possible biosorption mechanisms, even though the existence of optimum equilibrium pH (pH 6.5) may be related to mercury speciation and increasing amount of hydroxo-complexes. Nevertheless, it may also be related to acid-base properties of biosorbent samples.

Component	Species	% of total component concentration			
		pH$_i$			pH$_f$
		3	5	7	6.5
Cl$^-$	Cl$^-$	12.6	18.3	68.1	50.6
	HgClOH (aq)	0.1	5.5	21.1	22.5
	HgCl$^+$	0.1	0.1	-	26.8
	HgCl$_2$ (aq)	87.1	76.0	10.7	0.1
	HgCl$_3^{-1}$	0.1	0.1	0.1	
Hg^{2+}	**Hg(OH)$_2$**	-	**0.4**	**39.6**	**17.9**
	HgClOH (aq)	**0.2**	**12.6**	**48.2**	**51.3**
	HgCl$^+$	0.3	0.2	-	0
	HgCl$_2$ (aq)	**99,4**	**86.7**	**12.2**	**30.6**
	HgCl$_3^{-1}$	0.1	0.1		0.1

Table 19 Mercury speciation at different pHs (temperature 20°C, initial concentration 50 mg Hg L^{-1}, prepared by dissolving HgCl$_2$)

4.1.2 Chromium

Since chromate ions are readily reduced in acidic solutions, the systematic determination of Cr(VI) and Cr(III) was necessary for both correct description and appropriate interpretation of binding mechanism. Results obtained for the P-samples (P3 and

P4) are summarized in Figure 30. According to previously published results, the range of initial pH was enlarged and varied between pH 1 and pH 8. Sample P4FD was no longer used as the pre-testing on mercury and cadmium confirmed no influence of drying procedure.
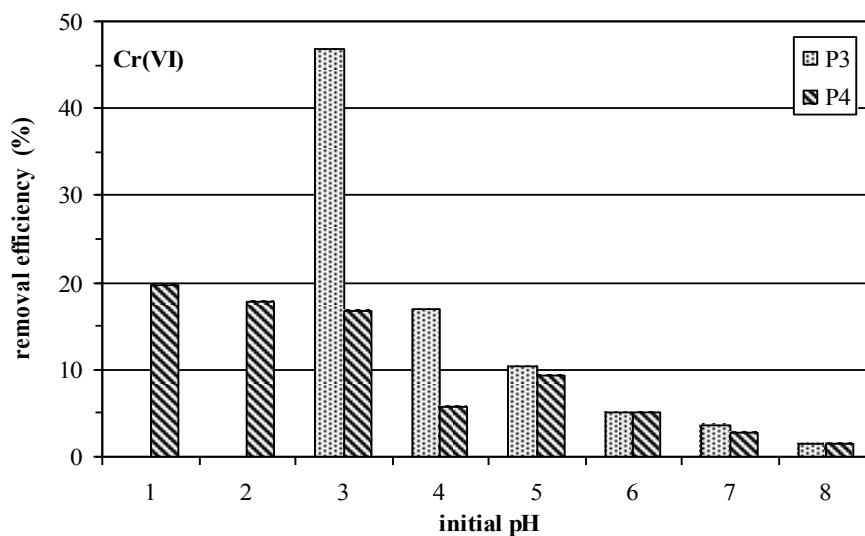
Figure 30 Influence of initial pH (uncontrolled) on Cr(VI) sorption efficiency using biosorbents P3 and P4 (initial concentration: 50 mg L^{-1}, sorbent dosage: 300 mg L^{-1})

Several similarities with mercury sorption were found. Obviously, the P3 sample exhibited higher sorption efficiency at the same experimental conditions. The results for P3 sample at initial pHs 1 and 2 could not be displayed as the sorption material tended to dissolve at these pHs, but surprisingly on contrary with the observation made with mercury, it was stable at initial pH 3. Actually this pH revealed as the optimum pH for chromium biosorption as almost 50% of hexavalent chromium were sequestered from the solution.

The chromium uptake efficiency decreased with increasing pH of the solutions. This trend was observed for both of the sorbent samples, regardless of the higher sorption capacity of P3 sample. The same phenomenon was often described in the literature.[97,55] No significant difference between the hexavalent chromium and total chromium content was detected.

The contact of biomass with metal solution significantly changed the pH of the solution. The same tendencies (shown in Figure 31) can be observed for both P3 and P4 sorbents.
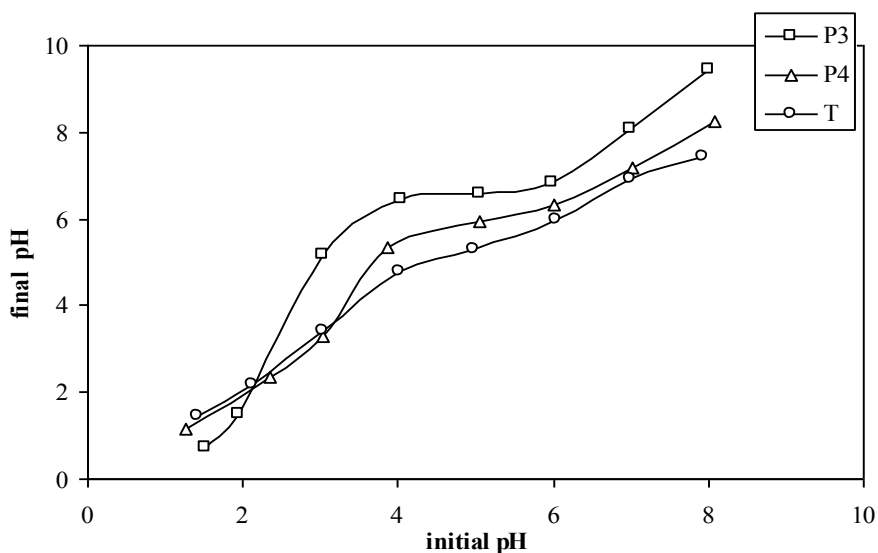
Figure 31 pH variation during Cr sorption using biosorbents P3, P4 and T (initial concentration: 50 mg L⁻¹, sorbent dosage: 300 mg L⁻¹)

The pH of the solutions tended to increase all over the tested range. Nevertheless, the trend was more pronounced in the case of P3 sample between initial pH 3 and pH 6, where the pH tended to increase towards neutral values. When sample P4 was used, the equilibrium pH remained close to the initial values in the range of pH from 1 to 3 and then between 7 and 8. In the slightly acidic area (in the range from 4 to 6) the biomass also increased the pH of the solutions towards the neutral values. The experiment with controlled pH was not performed in this case as the final pH at initial pH 3 was close to 5 and there was no possibility of metal precipitation at this pH and as in addition the previous experiments with pH control revealed unfavourable. In the case of T sample no significant pH changes within the sorption process were observed, whereas the maximum change was 0.5 unit as illustrated in Figure 31.

The results for *Tolypocladium* sorbent are summarized in Figure 32. In comparison to the *Penicillium* derived samples there was a significant difference between hexavalent chromium and total chromium final content in the solution. Approximately 30% of hexavalent chromium was removed from the solution at pH 2 and 1, which corresponds to approximately 15% decrease of total chromium content in the solution at pH 2 and 12% at pH 1. The highest sorption efficiency (for both of chromium forms) was obtained at the former pH, which was selected as an optimum for further experiments. In this case also, the sorption capacity decreased with increasing the pH.
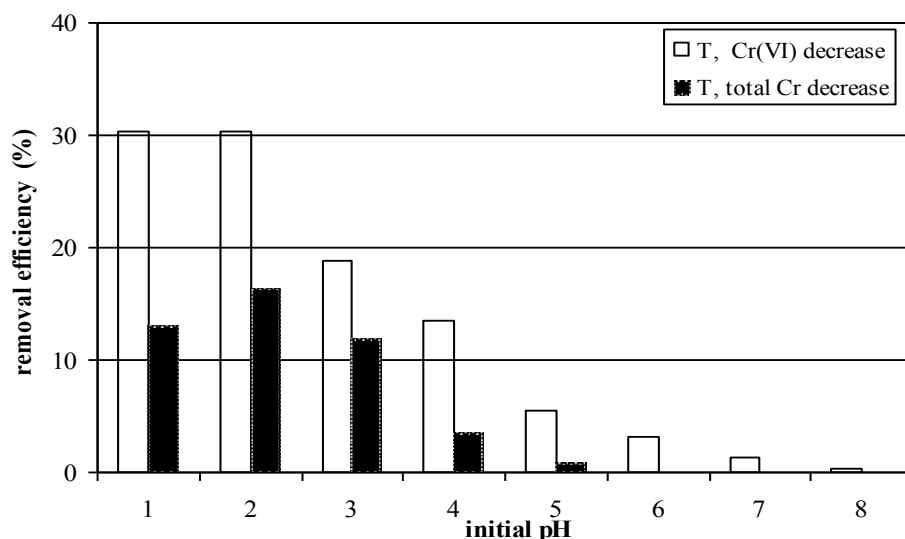
Figure 32 Influence of initial pH (uncontrolled) on Cr(VI) and Cr$_{total}$ sorption efficiency using biosorbent T (initial concentration: 50 mg L^{-1}, sorbent dosage: 300 mg L^{-1})

Table 20 summarizes hexavalent chromium speciation under selected experimental conditions. The majority of Cr(VI) exists in the form of HCrO$_4^-$ in the acidic region (pH 2 - 5). This anionic form should consequently interact with the biomass sample via the different mechanisms described in chapter 2.2.1.8. Electrostatic interaction between chromate anion and protonated functional groups on the biomass surface is probably the mechanism in the case P3 sample. However, the table does not take into account the possible effect of metal reduction at acidic pH, which was partially the case of T sample.

Component	Species	% of total component concentration		
		pH		
		2.0	5	8
K$^+$	K$^+$	100	100	99.7
	KCrO$_4^-$	-	-	0.3
Cr(VI)	**CrO$_4^{2-}$**	-	**3.2**	**96.8**
	KCr$_2$O$_7^-$	0.1	0.1	-
	KCrO$_4^-$	-	-	0.6
	HCrO$_4^-$	**95.4**	**89.7**	**2.6**
	H$_2$CrO$_4$ (aq)	0.4	-	-
	Cr$_2$O$_7^{2-}$	4.1	7.0	-

Table 20 Hexavalent chromium speciation at different pHs (temperature 20°C, initial concentration 50 mg Cr(VI) L^{-1}, prepared by dissolving K$_2$Cr$_2$O$_7$)

4.1.3 Cadmium

The sorption behaviour of the tested biosorption materials was similar to that found for mercury. The results are displayed in Figure 33.
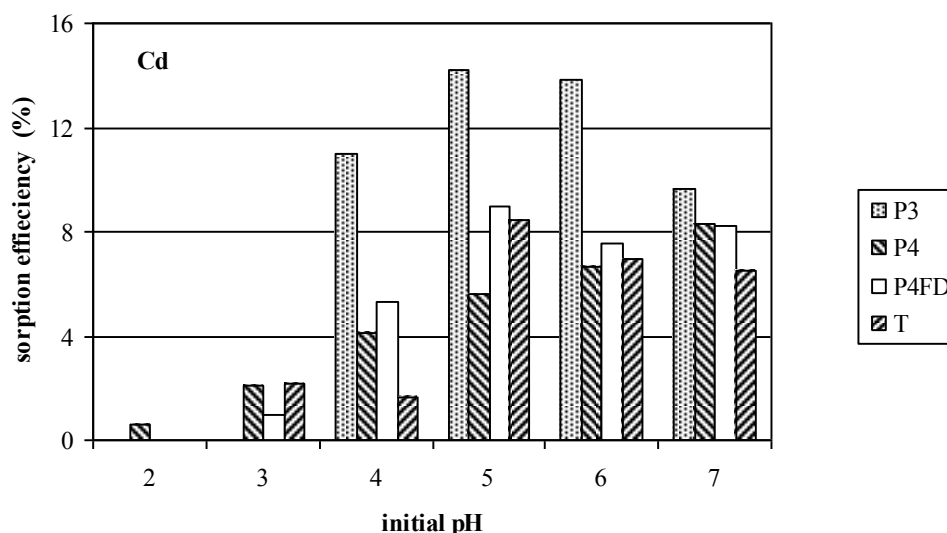
Figure 33 Influence of initial pH (uncontrolled) on Cd sorption efficiency using biosorbents P3, P4, P4FD and T (initial concentration: 50 mg L^{-1}, sorbent dosage: 300 mg L^{-1})

Following similarities were observed:

a) Weak sorption performance at pH below 4

b) Better sorption obtained with sorbent P3 (though the differences were less marked than in the case of Hg removal)

c) Optimum pH range between pH 5 and pH 6 for sorbent P3

d) Comparable sorption efficiencies when the initial pH was in the range pH 4 – pH 7.

However, a significant difference in sorption efficiency was observed, whereas this efficiency did not exceed 14%.

Figure 34 shows pH variation during cadmium sorption. The pH remained almost constant when the initial pH was below 4 and it increased strongly during sorption when the initial pH was set to pH 4 and tended to level off at the value of 6.5 for P4 and P4FD sorbent and at 7.3 for P3 sorbents.
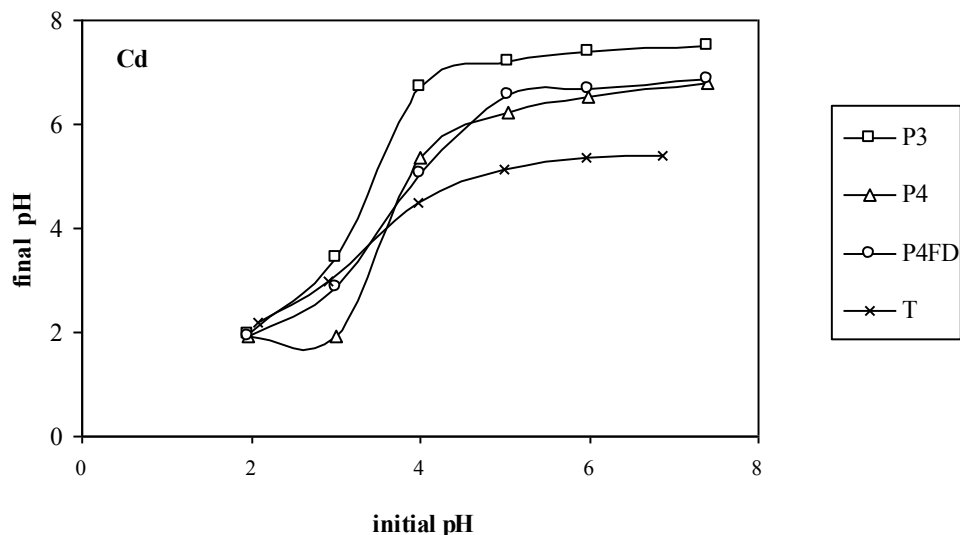
Figure 34 pH variation during Cd sorption using biosorbents P3, P4, P4FD and T (initial concentration: 50 mg L^{-1}, sorbent dosage: 300 mg L^{-1})

In the case of sorbent T, the equilibrium pH tended to level off at the value of 5.5, which is also consistent with the trends observed in the case of mercury sorption on sorbent T.
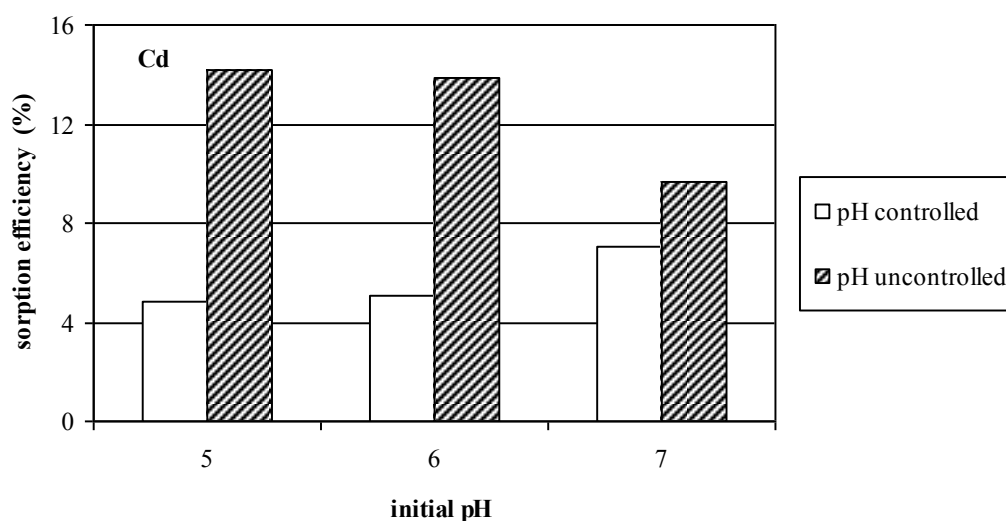
Figure 35 Influence of pH on Cd sorption efficiency using biosorbent P3 (initial concentration: 50 mg L^{-1}, sorbent dosage: 300 mg L^{-1})

Figure 35 shows on sorbent P3 that the pH control significantly decreased sorption performance (between 2 and 3 times), expect for pH 7, where the loss in sorption efficiency did not exceed 20%.

Table 21 summarizes the cadmium speciation at different solution pH calculated by Visual MINTEQ ver. 2.5. Total dissolution of salt used for solution preparation and no metal precipitation were predicted by the programme, thus the observed concentration decrease can only be ascribed to biosorption process.

It is well illustrated that the metal is present only in its simple cationic form in the range of pH tested in our experiments. Thus the direct interaction between Cd^{2+} and biomass functional groups is expected. The metal speciation is hardly influenced by the solution pH and so the existence of optimum sorption pH cannot be explain by occurrence of different cadmium forms and should be only dependent of ionic form of biomass sorption groups and their interaction with the metal.

Component	Species	% of total component concentration		
		pH$_i$		pH$_f$
		3	5	8
Cl^-	Cl^-	96.8	96.7	96.8
	$CdCl^+$	3.2	3.3	3.2
Cd^{2+}	Cd^{2+}	**93.8**	**93.6**	**93.2**
	$CdCl^+$	6.2	6.4	6.4
	$CdOH^+$	-	-	0.4

Table 21 Cadmium speciation at different pHs (temperature 20°C, initial concentration 50 mg Cd L^{-1}, prepared by dissolving CdCl$_2$.H$_2$O)

4.1.4 Lead

Based on results obtained with other metal ions, experiments were limited to biosorbents P3 and T and the pH range was restrained between pH 4 and pH 6 (Figure 36). The pH range was restrained because at lower pH than pH 4 P3 sample tended to dissolve and at higher pH there was a possibility of lead precipitation. The initial lead concentration was also decreased (to 10 mg L^{-1}) to prevent the possible lead precipitation at higher metal concentrations.

For biosorbent P3, the sorption efficiency remained almost constant between pH 4 and 6. This fact may be correlated to pH variation as illustrated in Figure 37. The pH strongly increased (for example pH 3 was shifted to pH 6) and the pH tended to level off around pH

6.5, regardless of the initial pH when set between pH 4 and 6. This effect limits the impact of pH variation on sorption efficiency with biosorbent P3.
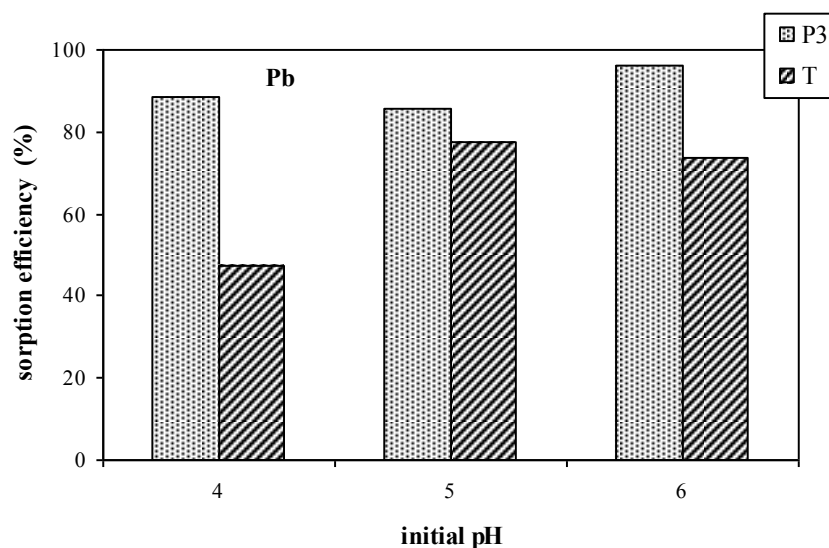
Figure 36 Influence of initial pH (uncontrolled) on Pb sorption efficiency using biosorbents P3 and T (initial concentration: 10 mg L^{-1}, sorbent dosage: 300 mg L^{-1})

For biosorbent T, the sorption efficiency increased above pH 4 and tended to level off above pH 5. As already observed the pH tended to decrease and stabilized around pH 4.5, when the initial pH was set between pH 3 and 6. Sorption efficiency under selected experimental conditions (i.e. with lower metal concentrations than with Hg, Cd and Cr) reached the values in the range 80 to 95% for all three values of pH for P3 sample. pH 5 was selected as optimum for both sorbents. The efficiency was high enough (85%) and the equilibrium pH low enough to prevent the possible precipitation for sorbent P3 and it reached up to 77% for sorbent T.
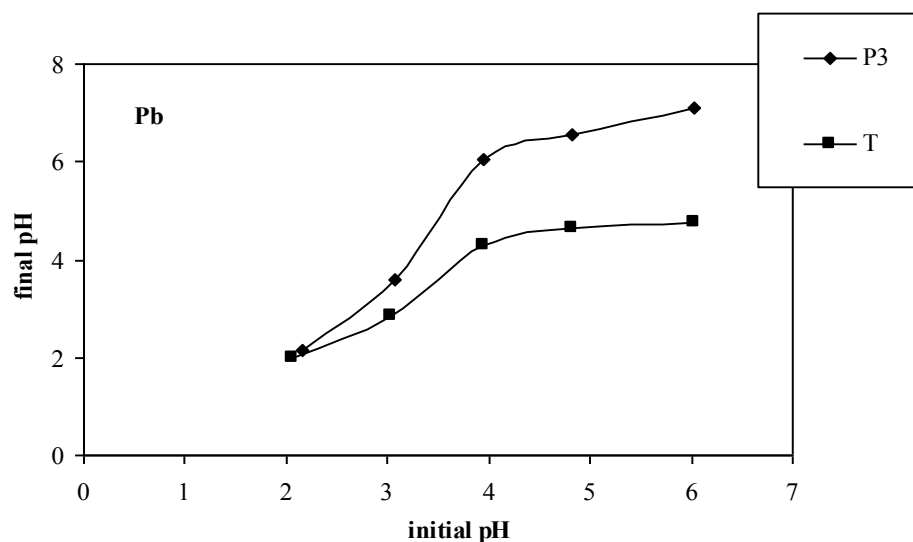
Figure 37 pH variations during lead biosorption (initial concentration: 10 mg L^{-1}, sorbent dosage: 300 mg L^{-1})
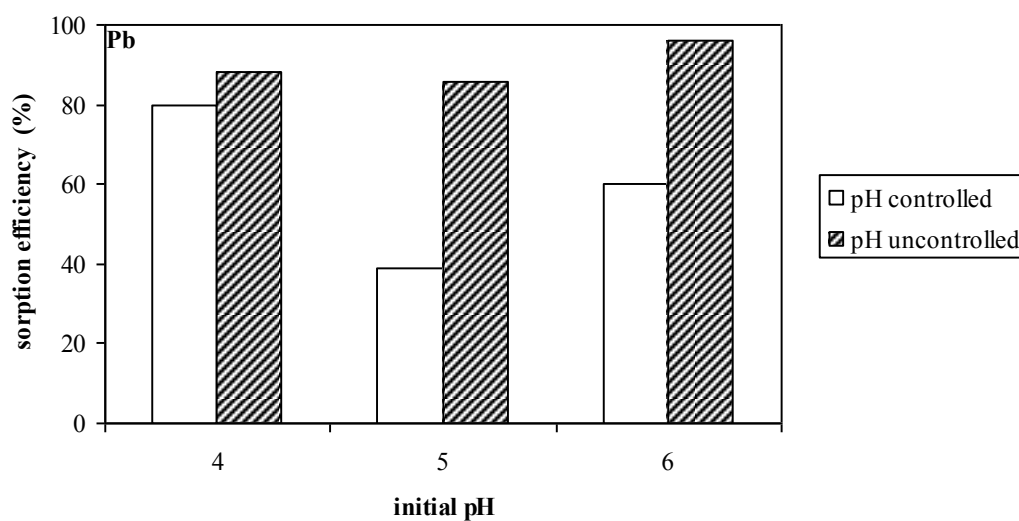
Figure 38 Influence of pH on Pb sorption efficiency using biosorbent P3 (initial concentration: 10 mg L^{-1}, sorbent dosage: 300 mg L^{-1})

The experiments with pH controlled were also performed in the case of P3 sample (Figure 38). It appears obvious that pH control decreased sorption efficiency as already observed with other metal ions.

Table 22 summarizes the lead speciation and similarly to cadmium, lead appears predominantly as a simple cation in the solution under selected experimental conditions. Total dissolution of salt used for solution preparation and no metal precipitation were predicted by

the programme, thus the observed concentration decrease can only be ascribed to biosorption process.

Component	Species	% of total component concentration		
		pH_i		pH_f
		5.0	6.3	8.8
Cl^-	Cl^-	99.8	99.9	100.0
	$PbCl^+$	0.2	0.1	
Pb^{2+}	Pb^{2+}	**99.5**	**95.8**	**5.3**
	$PbOH^+$	**0.2**	**3.9**	**69.5**
	$Pb(OH)_2$ (aq)	-	-	16.3
	$Pb(OH)_3^-$	-	-	0.1
	$Pb_3(OH)_4^{2+}$	-	-	8.8
	$Pb_4(OH)_4^{4+}$	-	-	-
	$PbCl^+$	0.3	0.3	-

Table 22 Lead speciation at different pHs (temperature 20°C, initial concentration 10 mg Cr(VI) L^{-1}, prepared by dissolving PbCl$_2$)

4.1.5 Conclusion

The control of solution pH systematically decreased the sorption efficiency for sorbent P3. This sorbent acts like a "buffering" agent tending to increase the pH close to pH 6, certainly due to the release of NaOH that was not completely removed from the biomass within the cleaning process despite the careful rinsing up to neutral pH.

The drastic treatment with NaOH (10M) revealed more efficient than the treatment with less concentrated alkali. The analogy with chitin deacetylation procedure may explain that the conversion of the biomass with alkaline treatment is more efficient for deacetylation of chitin present in the cell wall of fungi. Biosorbent T showed generally lower sorption efficiencies than biosorbent P3, though greater than those obtained with P4 material. Significantly different acid-base behaviour was observed with T sample. The pH of biomass-metal suspension tended to decrease indicating that a possible release of protons took place in the sorption process. According to these results and consistently with the chemical characterization of the biosorbents it is possible to suggest that biosorption on biosorbent T

may occur on carboxylic functions with simultaneous proton release, while with biosorbent P3 the sorption could involve chelation on amine groups of chitosan-like material.

4.2 Sorption isotherms

Due to the negative impact of pH control on the sorption performance, experiments were only performed with uncontrolled pH. The final pH was recorded at the end of the experiments. The amount of sequestered metal is displayed in following figures as a function of equilibrium concentration and the equilibrium pH is superimposed on the isotherm plot. The presentation of equilibrium pH together with the sorption capacity contributes to validate data and modelling hypothesis.

4.2.1 Mercury

Figures 39 and 40 the sorption isotherms for mercury using the best sorbents, i.e. P3 and T at their optimum initial pH, i.e. pH 5 and pH 7, respectively. Table 23 shows the parameters for Langmuir and Freundlich models.
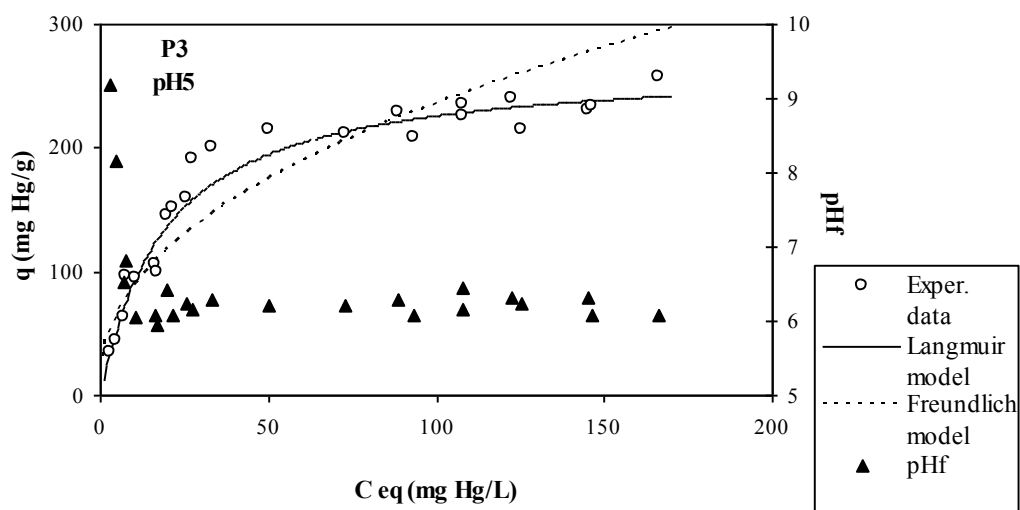
Figure 39 Hg sorption isotherm for biosorbent P3 at initial pH5
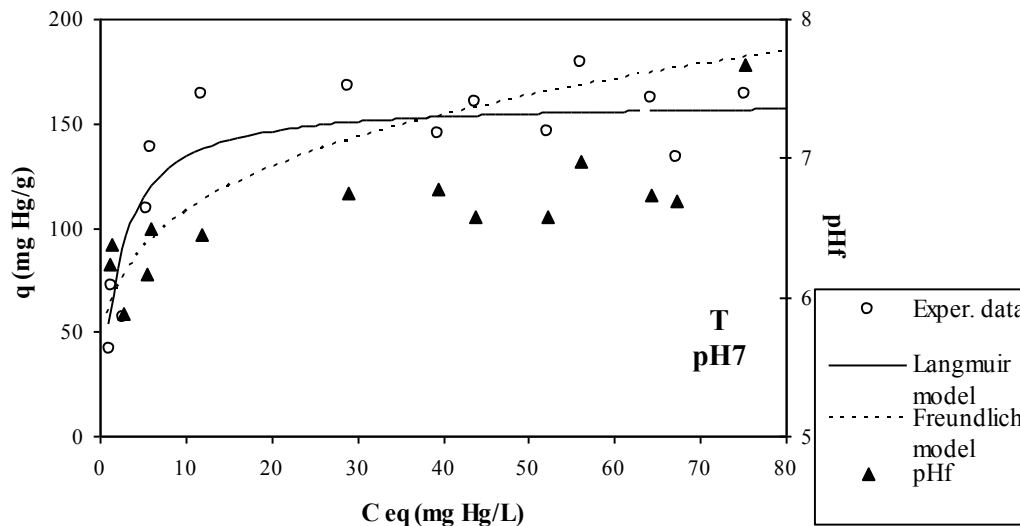
Figure 40 Hg sorption isotherm for biosorbent T at initial pH7

The shape of the isotherms, characterized by a steep initial slope with a quasi-linear trend followed by a plateau is very similar to the favourable Langmuir-type isotherm. It is thus expectable to find that the correlation between experimental data and the mathematical fitting is significantly better using the Langmuir equation. The initial slope of the curve is given by the parameter $q_{max}b$. The higher is this initial slope, the greater is the affinity of the material for target metal ion. In the case of the Freundlich equation the greater is the coefficient n the higher is the affinity of the sorbent for the metal.

sample	pH_i	Langmuir						Freundlich		
		q_{max}		b		$q_{max}b$	R^2	k	n	R^2
		[mg g^{-1}]	[mmol g^{-1}]	[L mg^{-1}]	[L mmol^{-1}]	[L g^{-1}]	-	[L g^{-1}]	-	-
P3	5	269	1.34	0.07	14.04	18.8	0.988	32	2.3	0.868
T	7	161	0.80	0.50	80.50	80.5	0.973	59	3.9	0.730

Table 23 Sorption isotherms using biosorbents P3 and T for Hg – model parameters

In the case of biosorbent P3, the maximum sorption capacity at monolayer coverage, deduced from the model was very high, i.e. 269 mg g^{-1}, it means 1.34 mmol g^{-1}, while the coefficient b was low, i.e. 0.07 L mg^{-1} (or 14 L mmol^{-1}). These data clearly demonstrate that biosorbent P3 has a great capacity for mercury.

In the case of biosorbent T, the maximum sorption capacity was significantly lower than for biosorbent P3 (161 mg g^{-1} or 0.8 mmol g^{-1}), while the coefficient *b* was significantly greater (0.5 L mg^{-1} or 80.5 L mmol^{-1}). *Tolypocladium* waste revealed a less favourable sorbent

for mercury than *Penicillium* alkali-treated material. This result confirms the trends observed in the study of pH effect. Nevertheless, the parameter $q_{max}b$ is higher for T sorbent indicating better sorption behaviour at low mercury concentrations.

It is interesting to observe that in the concentration range investigated in this work the maximum mercury sorption capacity tended experimentally to 240 mg g^{-1}, which means only 90% of the theoretical maximum sorption capacity at monolayer coverage (q_{max}) derived from Langmuir equation for biosorbent P3. While for biosorbent T, the experimental and theoretical values of maximum sorption capacities were comparable (around 160 mg g^{-1}). The higher efficiency of biosorbent P3, compared to biosorbent T, may be related to:

a) a different sorption mechanism as already suggested

b) and/or different densities of sorption sites on the biomass.

Carboxylic groups can be classified as hard bases (Pearson's HSAB theory) and preferentially react with hard acids, while amine groups are usually classified as soft bases that easily react with soft acids such as Hg^{2+}. Providing the suggested mechanisms for mercury sorption by P3 and T sorbents are truly interactions with amine and carboxylic functions, respectively, the highest affinity of P3 (versus T) for mercury uptake was expectable.

Nevertheless, the interpretation of these differences is rather difficult because of diversity of sorption sites, possible treatment effects on the structure of sorbent materials, density of sorption sites and accessibility and availability of these sites. These sites may also be engaged in hydrogen bonds or linked to other cell wall components.

4.2.2 Chromium

Figures 41 and 42 show chromium sorption isotherms when using P3 and T biosorbents samples at their optimum initial pH, i.e. pH 3 and pH 2, respectively. Table 11 reports the parameters for Langmuir and Freundlich equations.
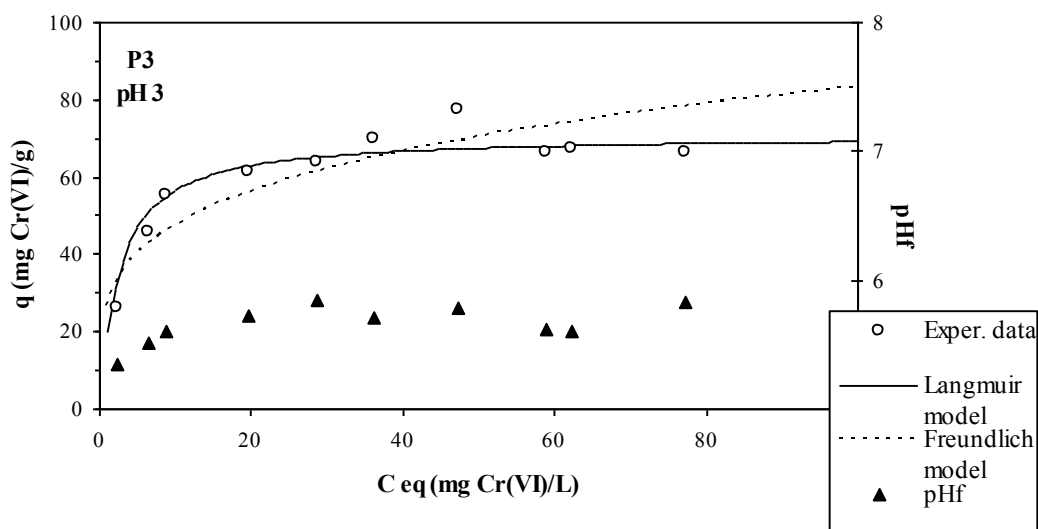
Figure 41 Cr(VI) sorption isotherm for sorbent P3 at initial pH 3

In case of P3 sample, both Langmuir and Freundlich equations were successfully applied to fit the experimental data. Nevertheless the Langmuir equation fitted better experimental data in this case. The maximum sorption capacity at monolayer coverage derived from the Langmuir model reached 71 mg g^{-1}, corresponding to 1.36 mmol g^{-1}, which is a value close to that obtained for mercury with the same material. The coefficient b was 0.39 L mg^{-1} (20.28 L $mmol^{-1}$), which is of the same order of magnitude (in molar units) as the one of mercury. The value of parameter $q_{max}b$ was several times higher for P3 sample over the T biosorbent. These data clearly demonstrate that the material has equally a high affinity and capacity for hexavalent chromium. The values of hexavalent chromium equilibrium concentration were identical to those of total chromium, thus there was no reduction observed in this suspension system. This finding seemed to confirm, that the probable biosorption mechanism was electrostatic attraction.
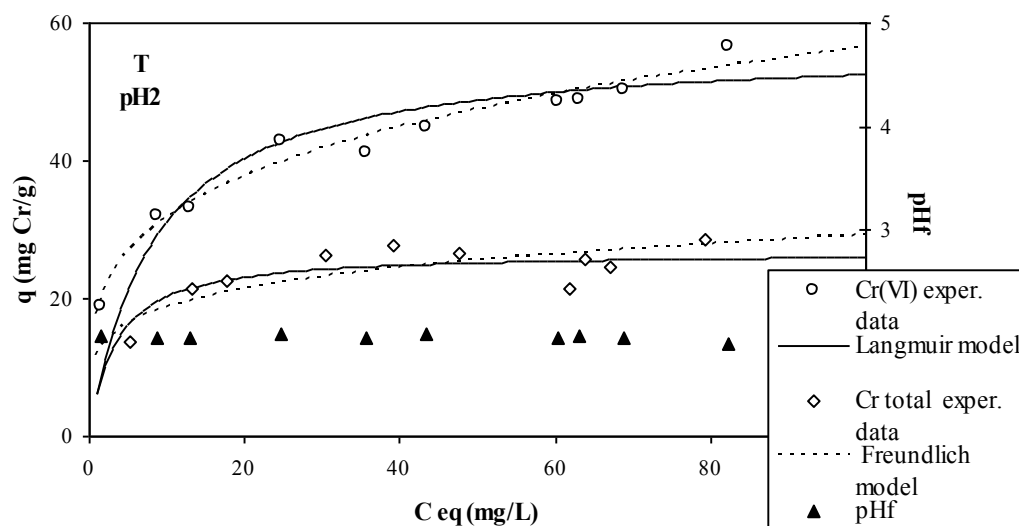
Figure 42 Cr sorption isotherms for sorbent T at initial pH 2

In the case of T sample (Figure 42), a hexavalent chromium isotherm as well as a total chromium sorption isotherm were determined. The maximum hexavalent chromium sorption capacity was lower than for biosorbent P3 (57 mg g^{-1} or 1.09 mmol g^{-1}) and the coefficient *b* was also lower (0.12 L mg^{-1} or 6.24 L mmol^{-1}).

But as already mentioned in the previous chapter and illustrated in Figure 42 the decrease of hexavalent solution concentration was not accompanied by the decrease of total chromium concentration due to the phenomenon of partial chromium reduction. Approximately only 50% of chromium was completely removed from the liquid phase.

sample	metal	pH$_i$	Langmuir						Freundlich		
			q$_{max}$		b		q$_{max}$b	R^2	k	n	R^2
			[mg g^{-1}]	*[mmol g^{-1}]*	[L mg^{-1}]	*[L mmol^{-1}]*	[L g^{-1}]	-	[L g^{-1}]	-	-
P3	Cr(VI)	3	71	*1.36*	0.39	*20.28*	27.7	0.990	26.8	4.1	0.810
T	Cr(VI)	2	57	*1.09*	0.12	*6.24*	6.8	0.980	17.7	4.0	0.981
	Cr$_{total}$	2	27	*0.52*	0.31	*16.12*	8.4	0.955	11.9	5.1	0.650

Table 24 Sorption isotherms using biosorbents P3 and T for Cr – model parameters

4.2.3 Cadmium

The sorption of cadmium is much less favourable than that obtained for mercury and chromium. The sorption isotherms shown in Figures 43 - 44 confirm the trends observed on the impact of pH on sorption efficiency.
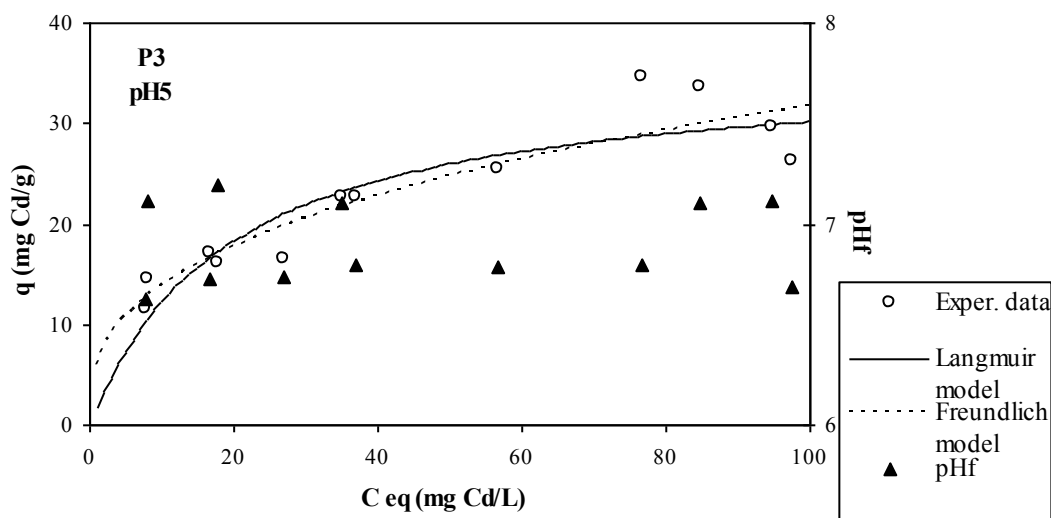
Figure 43 Cd sorption isotherm using sorbent P3 at initial pH 5
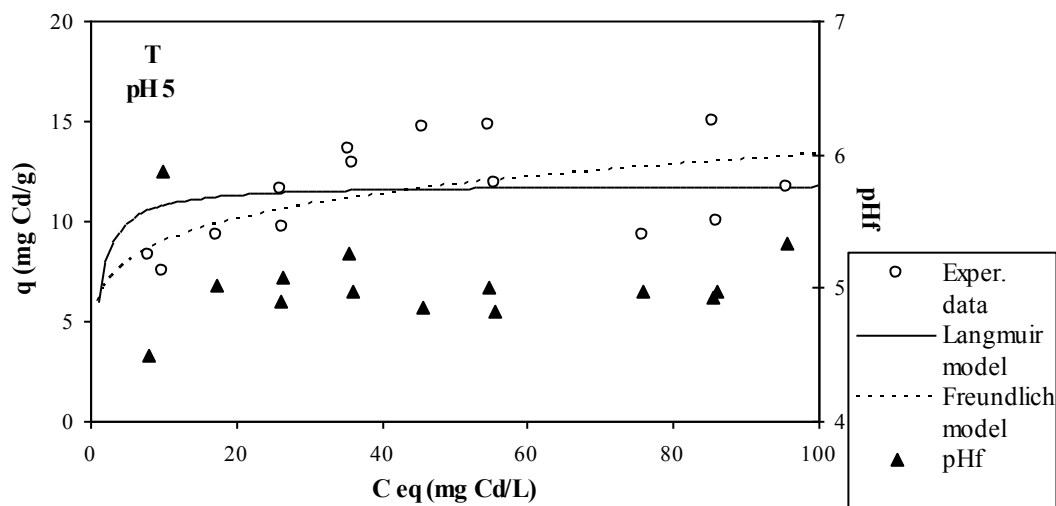
Figure 44 Cd sorption isotherm for sorbent T at initial pH 5

Maximum sorption capacity calculated from Langmuir equation, that fitted better the experimental data than Freundlich equation, did not exceed 36 mg g^{-1} (or 0.32 mmol g^{-1}) for biosorbent P3. This is about four times lower than the levels reached with mercury. The sorption capacity was even lower for biosorbent T, the maximum sorption capacity did not exceed 12 mg g^{-1} (or 0.11 mmol g^{-1}). This is even three times lower than for biosorbent P3.

Another great difference between biosorbents P3 and T is related to the affinity coefficient *b*, which was quite low for P3 sample and twenty times greater for T sample as illustrated in Table 25.

sample	pH$_i$	Langmuir						Freundlich		
		q_{max}		b		q_{max}b	R^2	k	n	R^2
		[mg g^{-1}]	*[mmol g^{-1}]*	[L mg^{-1}]	*[L mmol^{-1}]*	[L g^{-1}]	-	[L g^{-1}]	-	-
P3	5	36	*0.32*	0.05	*5.62*	1.8	0.929	6.0	2.8	0.895
T	5	12	*0.106*	1.03	*115.8*	12.2	0.894	6.0	5.8	0.372

Table 25 Sorption isotherms using biosorbents P3 and T for Cd – model parameters

The affinity of biosorbent P3 for cadmium is of the same order of magnitude than that for mercury. In the case of cadmium sorption the maximum sorption capacity found experimentally roughly corresponded to the values calculated from Langmuir model. The maximum sorption capacity at monolayer coverage tended to the maximum sorption capacity obtained experimentally. According to the Langmuir theory it would mean that all sites available for sorption were occupied under these experimental conditions.

Assuming the same hypothesis and the same precautions on the interpretation as for mercury, higher sorption capacity of P3 sample (than T sample) confirm the preferential sorption of this weak acid for weak base functional groups (i.e. amine functions).

4.2.4 Lead

In the case of lead uptake, maximum sorption capacities were of the same order of magnitude as for cadmium if compared on the basis of molar units (Figures 45-46 and Table 26), and significantly lower than those found for mercury and chromium (5-6 times lower).
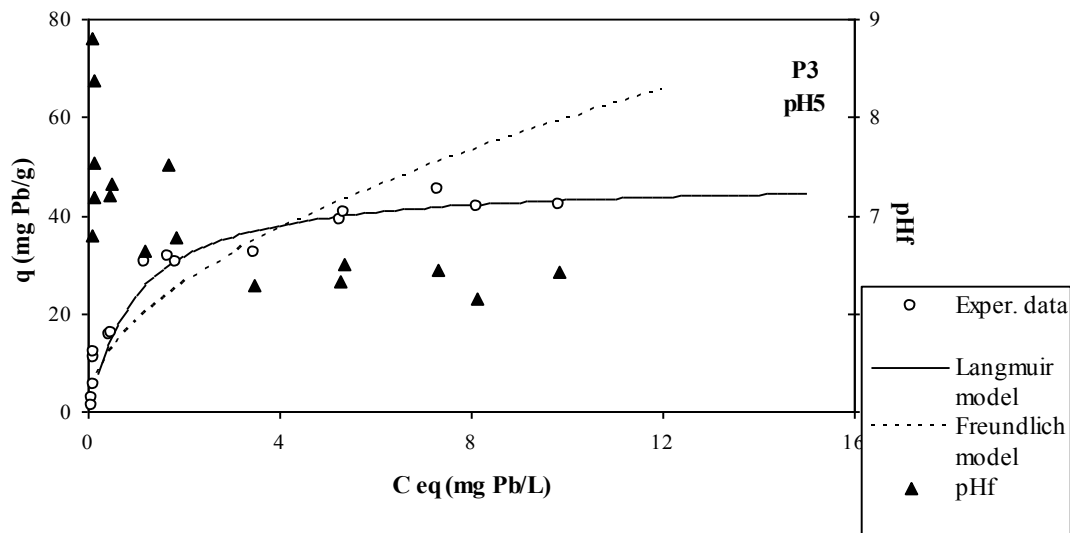
Figure 45 Pb sorption isotherm for sorbent P3 at initial pH 5

The Langmuir model fitted again better experimental data than the Freundlich equation. The maximum sorption capacity given by the experimental plateau rose up to 47 mg g^{-1} for biosorbent P3, which is 20 % below the theoretical value, obtained from q$_{max}$ of the Langmuir equation; while it did not exceed 28 mg g^{-1} for biosorbent T. The theoretical and experimental values were again consistent in the case of the latter sorbent sample.
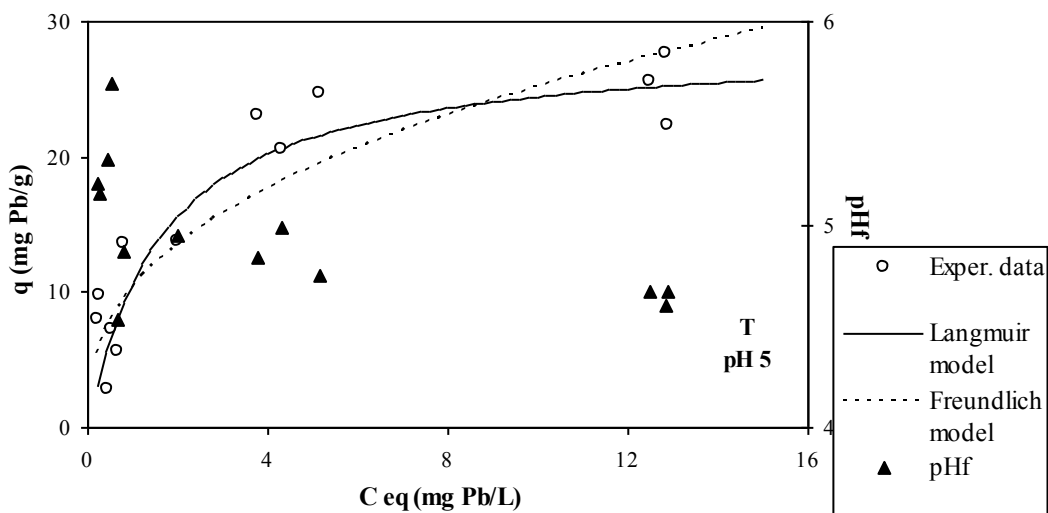
Figure 46 Pb sorption isotherm for sorbent T at initial pH 5

The affinity coefficient was more favourable for sorbent P3 than for sorbent T. Nevertheless, based on molar units the affinity coefficients obtained with lead were the highest compared to mercury and cadmium.

126

sample	pH$_i$	Langmuir						Freundlich		
		q$_{max}$		b		R^2	q$_{max}$b	k	n	R^2
		[mg g^{-1}]	*[mmol g^{-1}]*	[L mg^{-1}]	*[L mmol^{-1}]*	-	[L g^{-1}]	[L g^{-1}]	-	-
P3	5	47	*0.23*	1.01	*209.3*	0.976	47.9	18.2	1.9	0.800
T	5	28	*0.14*	0.61	*126.4*	0.945	17.3	10.3	2.6	0.680

Table 26 Sorption isotherms using biosorbents P3 and T for Pb – model parameters

Lead is part of the borderline classification according to Pearson's rules, while mercury and cadmium are classified among weak acids. In the case of mercury and cadmium, their soft acid character caused the greater affinity for amine functions over the carboxylic groups (as assumed for the identification of reactive groups). In the case of lead the functional groups do not have pre-defined reactivity and the fact that biosorbent P3 is better than biosorbent T cannot be attributed to the functional groups we assume to be present on the biomass.

4.2.5 Conclusion

The sorption isotherms confirmed the observation and pre-selection that was made upon the results of the study of pH influence. The sorption isotherms allowed determining the maximum sorption capacities, which is usually the first criterion for biosorbent ranking and the affinity of the material for target metal. Regarding maximum sorption capacities the biosorbent P3 clearly shows greater affinity for each individual metal (Hg, Cr, Cd and Pb) than biosorbent T.

The alkali-treatment may have strongly increased the accessibility and availability of sorption sites, as well as their density. Indeed, the strong alkaline treatment operated with NaOH (10M) removes proteins and glucanes and it contributes to the deacetylation of chitin-based materials under the boiling conditions. Therefore, amine groups can readily react with metal cations.

The alcohol treatment used for the extraction of antibiotics from *Tolypocladium* mycelia only contributes to denature the proteins but do not remove inert materials, which results in lower density of sorption sites. Additionally, it does not make the reactive sites more accessible, as they could be engaged in bonds with other cell wall constituents.

If the comparison is based on the maximum uptake capacity derived from Langmuir model in mass units the following order is obtained for P3 sorbent: Hg>>Cr>Pb>Cd, while if the comparison is based on molar units the order changes significantly to: Hg≅Cr>Cd>Pb.

The same comparison for sorbent T is as follows: Hg>>Cr_{total}>Pb>Cd in mass units and Hg> Cr_{total}>Pb>Cd in molar units.

If the values of coefficient *b* are compared the following ranking is obtained for biosorbent P3 (in decreasing order): Pb>>Cr>>Hg≅Cd based on mass units, while Pb>>Cr>Hg>Cd based on molar units. For biosorbent T the ranking is of following order: Cd>Pb>Hg>Cr_{total} in mass units, while Pb>Cd>Hg> Cr_{total} in molar units.

The sorption capacities of both tested materials towards mercury and chromium were on the upper boundary of the range reported in the literature (as summarized in Table 3 for mercury and in Table 4 for chromium), while the sorption capacities obtained for cadmium and lead were only mediocre (as illustrated in Table 6 for cadmium and in Table 8 for lead).

4.3 Interactions of metals with P3 and T sorbent

Various methods of instrumental analysis could reveal the information about the metal – biosorbent interactions. Different electron microscopic methods (coupled with a microanalysis apparatus) are useful in determining the distribution of the metal throughout the cell structure. The Fourier-transform infrared (FTIR) spectroscopy has a crucial role in obtaining structural and bonding information. Nuclear magnetic resonance spectroscopy could also be used, but this technique is more expensive and requires special sample preparation. Furthermore the NMR spectra of biomaterials are often difficult to interpret. The information on valence states of the metals and on nature of attachment between biomolecules and metals can also be obtained by the means of X-ray photoelectron (XPS) spectroscopy.

The FTIR technique was used in the present study to investigate the nature of interactions between biosorbent samples and the target metals. The SEM analysis coupled with EDX microanalysis was used to study the morphology of samples and distribution of biosorbed metals within the biosorbent particles.

4.3.1 Infrared spectroscopy results

The biomass samples were put in the contact with metal solutions at their optimum pH for 36 hours. Sorbent dosage and metal concentration were selected to obtain maximal saturation of biosorbents. The saturated biomass samples were then separated by filtration, washed several times with deionised water, dried and finally carefully separated from the filter. The FTIR analysis was then performed according to previously described procedure (chapter 3.3.3, page 88). In the case of hexavalent chromium biosorption, protonated materials (conditioned at optimum pH of the experiment without the presence of chromium) were analyzed too.

Taking into account the low sorption capacities of these biosorbents for some of the target metals (Cd, Pb), the intensity of the vibrations that are affected by the presence of the metals may be very low or even non-detectable. For P3 sorbent, Figure 47 shows that FTIR spectra were only significantly affected in the range 1800-1500 cm^{-1}. The decrease of intensity of bands at 3400 cm^{-1} (-OH groups of water), 2920 and 2850 cm^{-1} (symmetric and asymmetric stretching of CH$_3$), 1080 cm^{-1} and 1033 cm^{-1} (C-H vibrations corresponding to polysaccharide ring) was also observed and similar behaviour was described in literature[215]. Nevertheless, this decrease does not reveal any valuable information about the biosorption mechanism and will not be discussed further.
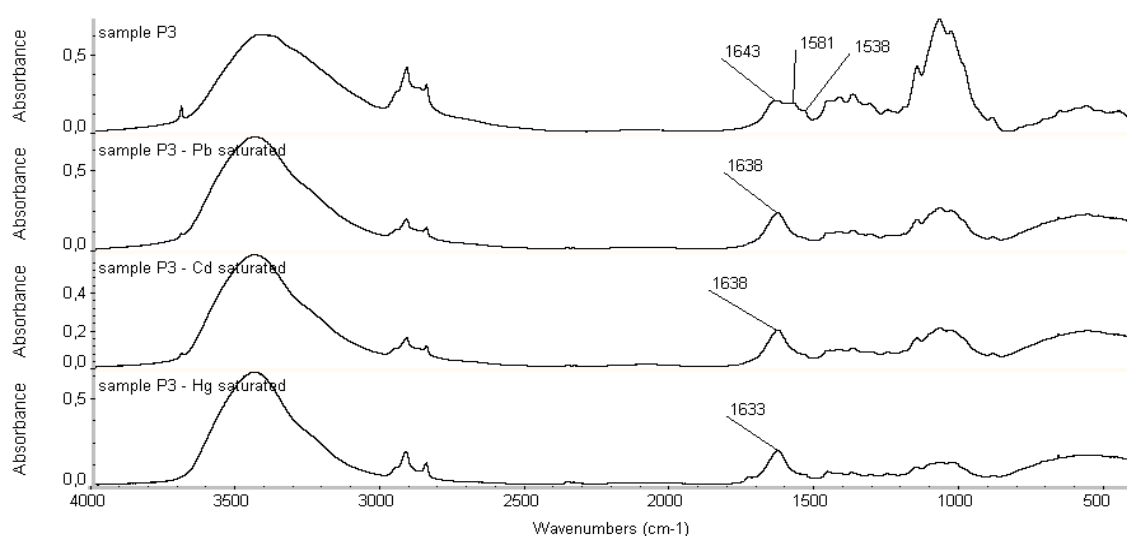
Figure 47 FTIR spectra of metal saturated P3 samples

The peak at 1580 cm^{-1} (corresponding to amine group) disappeared and the intensity of the band at 1540 cm^{-1} (ascribed to Amide II) was drastically decreased. The disappearance of the band at 1580 cm^{-1} indicates that the amine group was involved in the binding of the metals. This is consistent with the process used for biomass treatment that led to the predominance of amine groups (due to alkaline extraction and deacetylation). Surprisingly in the case of Hg uptake a band appeared at 1735-1730 cm^{-1} (Figure 48). This band is traditionally ascribed to carbonyl group (stretching), but carboxylic groups were not present in the original material. According to Lien-Vien et al.[214], adsorption band of acid chlorides carbonyl stretching can also appear in this region. This might supports the hypothesis of the biomass interaction with Hg(Cl)$_2$ or HgCl(OH) species (in case of amide group interaction with these species).

Additionally, the binding of the metals was followed by a decrease in the width of the band at 1650-1630 cm^{-1} that was attributed to the superimposition of two bands on the spectrum of the original material. It seems that the peak at 1650-1660 cm^{-1} (Amide I) was significantly decreased due to metal binding for all tested metals. In this area the vibrations were attributed to amide bands conjugated with OH bending from water. This could indicate that OH groups could be involved in the binding or the stabilization of metal-biomass binding.
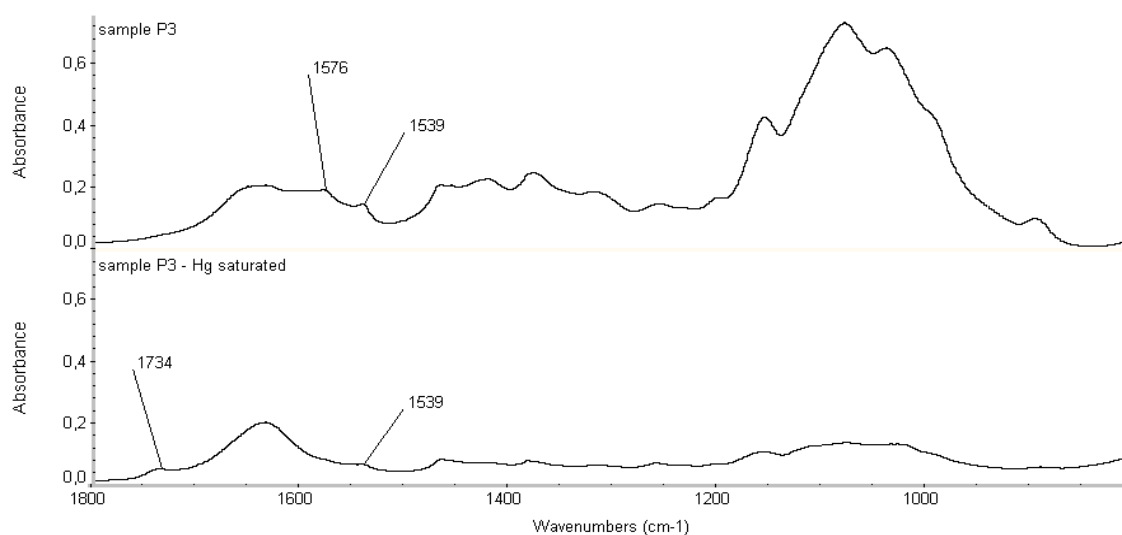
Figure 48 Detail of comparison of P3 and P3 – Hg saturated FTIR spectra (1800 – 600 cm^{-1})

In the case of T biosorbent, the FTIR spectra were almost unaffected by the binding of metals (Figure 50). The relative intensities of the bands at 1743 cm^{-1} (carbonyl group – stretching) and 1380 cm^{-1} (in-plane bend of C-OH[214]) were only slightly decreased, which is not as evident from Figure 50, but the decrease was confirmed when the spectra were

subtracted (not shown). This could support the hypothesis that metal binding occurred by interaction with carboxylic groups. According to Lien-Vien et al.[214], when a salt is made of a carboxylic acid, the C=O and C-O bonds of the acid are replaced by two equivalent (or nearly equivalent) "bond-and-a-half" bonds and the asymmetric stretch is consequently seen at 1650 – 1540 cm^{-1}. In the case of saturated T-sorbent samples an increase of intensity was observed for a band at 1640 cm^{-1}, which may be another proof of the proposed mechanism.

It is interesting to observe that in T biosorbent the nitrogen content was significantly higher than in other biosorbents (Table 12, page 86) but this nitrogen was involved in bonds with other compounds (probably amino acids) that made the nitrogen groups not available for binding of metals.
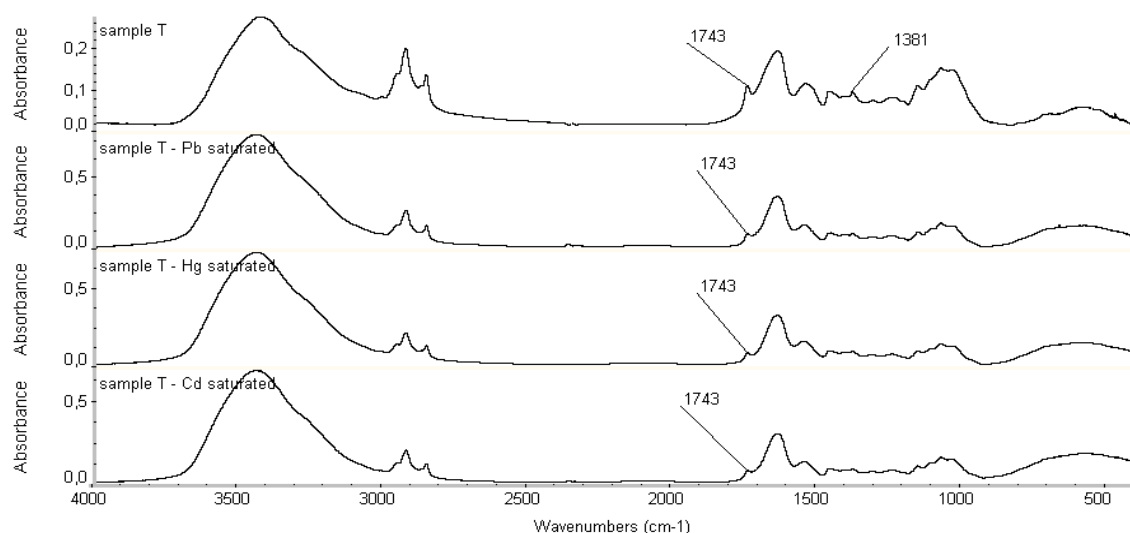
Figure 49 FTIR spectra of metal saturated T samples
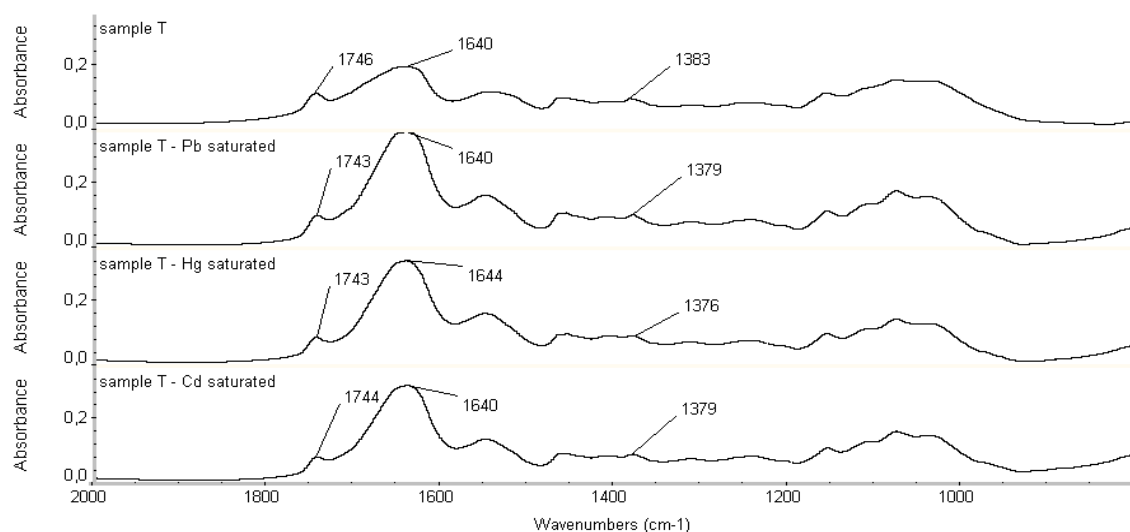
Figure 50 Detail of FTIR spectra of metal saturated T samples (2000 – 800 cm^{-1})

Kapoor and Viraraghavan[136] identified three different amide absorption bands (at 1646, 1558 and 1377 cm^{-1}) on alkaline treated *Aspergillus niger* biomass, whereas a carbonyl stretching of a carboxylic group (carbonyl stretching vibration) was also found at 1733 cm^{-1}. The biomass functional groups were subsequently blocked according to different treatments and these modified biomass samples were subjected to biosorption experiments. Lead biosorption appeared to be more sensitive to modifications of the carboxylic group than of amine group, while cadmium and copper showed the inverse trend. However, the saturated biomass samples were not studied by the means of infrared spectroscopy to support these conclusions.

Askhenazy et al.[215] investigated the functional groups involved in lead biosorption by acetone-washed yeast biomass of *Saccharomyces uvarum* (brewery waste). XPS showed that both amine and carboxyl groups can be involved in the procedure. A significant difference in the nitrogen peak before and after lead adsorption was observed confirming so that nitrogen containing groups participated in the process. Nevertheless the oxygen peak in XPS spectrum was shifted after lead biosorption, indicating involvement of oxygen from carboxyl group in lead uptake. Meanwhile the photoacoustic IR spectra of lead exposed biomass showed a change in symmetrical stretch of the carboxylate group, which shifted from 1405 to 1375 cm^{-1}. This shift was attributed to a change in the counter-ion associated with the carboxylate anion. This suggests that acidic groups, especially carboxylates, contributed to the metal uptake. The conclusion was drawn that carboxyl groups were the dominant species in the lead biosorption mechanism, but nitrogen containing groups also interacted with lead.

The main differences between the original P3 sample spectrum and its protonated and chromium saturated forms spectra appeared also in the range 1650 – 1400 cm^{-1}. The peak at 1580 cm^{-1} (corresponding to amine groups) disappeared completely both in the protonated and the metal saturated samples spectra (Figure 52). The intensity of the peak at 1540 cm^{-1} (Amide II) decreased significantly in the spectrum of the protonated sample and nearly disappeared when the biomass sample was saturated with chromium. This may be the proof of metal-amine group participation in chromium biosorption, supporting so the electrostatic attraction mechanism (see the mechanism scheme for chitin in Figure 51).
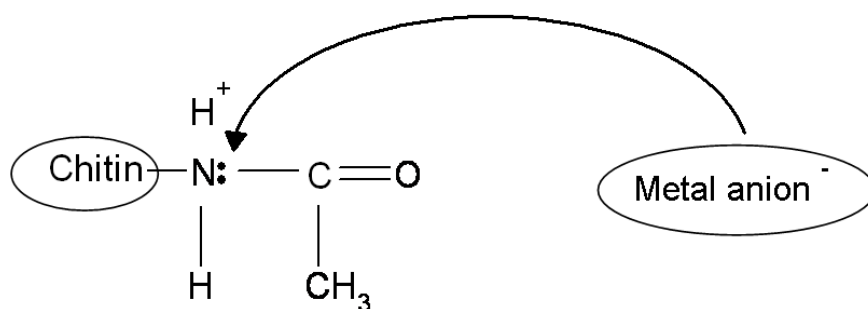
Figure 51 Scheme of electrostatic attraction mechanism

The absorption band at 1640 cm^{-1} (corresponding to vibrations of C=O bond in amide group) was shifted to 1630 cm^{-1}, but its intensity remained unchanged. The peak at 1376 cm^{-1} present in the original P3 sample spectrum possibly corresponding to C-N stretching band[214], was slightly shifted to 1382 cm^{-1} in its protonated and metal saturated spectra. Additionally, it became very sharp in the protonated spectrum and its intensity decreased in the chromium saturated sample spectrum.

Figure 52   Detail of comparison of protonated, chromium saturated and original P3 spectra (2000 – 400 cm^{-1})

Volesky[216] reported the existence of a band at 950 cm^{-1} corresponding to CrO$_3$ on the spectrum of acid-washed crab shell (AWUS) material saturated with hexavalent chromium. AWUS is a chitin based material and it was characterized by adsorption bands at 1450 cm^{-1} (Amide II) and at 1739 cm^{-1} (carbonyl stretching). These bands disappeared from the chromium saturated FTIR spectrum indicating so the involvement of amide group in Cr

adsorption (Figure 51). However the existence of a band at 950 cm^{-1} was not confirmed in our case. Bayramoglu et al.[58] studied the hexavalent chromium biosorption on *L. sajor-caju* fungus and reported its FTIR spectra (original, heat and acid treated). The presence of amine groups in the material was confirmed, but unfortunately, the saturated material spectrum was not presented in their study. Bai and Abraham[118] studied hexavalent chromium uptake by *Rhizopus nigricans* and reported that spectral analysis before and after Cr binding indicated – NH group involvement in Cr(VI) binding. A substantial decrease in the absorption intensity of –NH bending (1539-1651 cm^{-1}) and –NH stretching (3388 cm^{-1}) was reported, confirming so electrostatic attraction between protonated amines of the cell wall and anionic chromate species (at acidic pH). Malkoc et al.[217] reported important shifts of absorption bands corresponding to bonded –OH or/and stretching –NH groups together with C-OH of carboxylic group after hexavalent chromium sorption by waste pomace from olive oil factory.

Park et al.[57] studied hexavalent chromium reduction process on non-viable *Aspergillus niger* and compared the FTIR spectra of its protonated and chromium saturated forms. The band around 1740 cm^{-1} (C=O stretching) slightly disappeared from the chromium-loaded biomass, while the peak around 1650 cm^{-1} (C=O chelate stretching) became larger. After the chromium was desorbed, the FTIR spectrum became similar to that of the protonated biomass. It was thus suggested that the carboxyl groups were involved in the binding. Meanwhile, the peak around 1570 cm^{-1} increased after Cr(VI) biosorption, but did not reappear after chromium desorption, since the absorption peaks in the range of 1530-1650 cm^{-1} correspond to –NH bending, it was assumed that the amino groups might be also involved in biosorption process.

In the case of T sample, the FT-IR spectra remained almost unaffected by protonation and chromium binding (Figure 53). The relative intensity of the band at 1746 cm^{-1} decreased slightly, while the band at 1640 cm^{-1} (Amide I) remained unchanged. This could support our hypothesis that metal binding occurs by an interaction with carboxylic group. A decrease of intensity of band at 1381 cm^{-1} (C-OH bending) was observed in spectrum of protonated biomass, which possibly corresponds to dissociation of carboxyl group. The intensity of this band re-increases in saturated spectrum, but the corresponding peak became narrower and sharper. These findings suggest different sorption mechanisms in case of T sorbent, especially when the reduction phenomenon was observed during batch sorption. If the hypothesis of combined biosorption/reduction mechanism is correct, the biomass had to be oxidized. The

decrease in intensity of carbonyl stretching band may be the sign of an oxidation process, whereas the oxidation product could be only carbon dioxide.
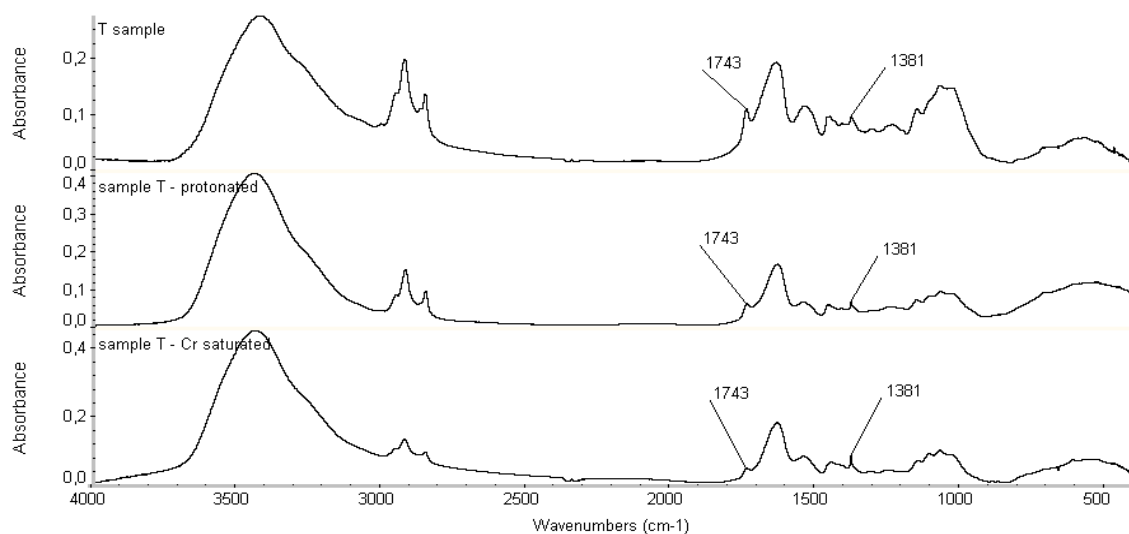
Figure 53 Comparison of protonated, chromium saturated and original T spectra

4.3.2 SEM microscopic observations

The surface structure of the original biomass samples and the metal saturated samples was examined by scanning electron microscope (SEM). The SEM analysis was performed by FEI Quanta 200 (FEI Company) in both secondary electrons and backscattered electrons mode and was coupled with energy-dispersive X-ray analysis (using Inca energy program 350 for the treatment of data).

Energy dispersive X-ray spectroscopy (EDX) is a method used to determine the energy spectrum of X-ray radiation. Especially the backscattered electrons may be used to detect the contrast between areas with different chemical compositions. This can be observed when the average atomic number of the regions is different.

Within SEM analysis, a number of particle images was reviewed for each analyzed sample, it was therefore possible to identify particle types and morphologies specific for each sample. SEM image of P3 and T samples are shown in Figure 54 and Figure 55, respectively. The surface of P3 sample seemed to be smooth and regular. The white spots in Figure 54 were identified as quartz impurities. On the other hand, sample T seemed to be porous in comparison with P3 sample.
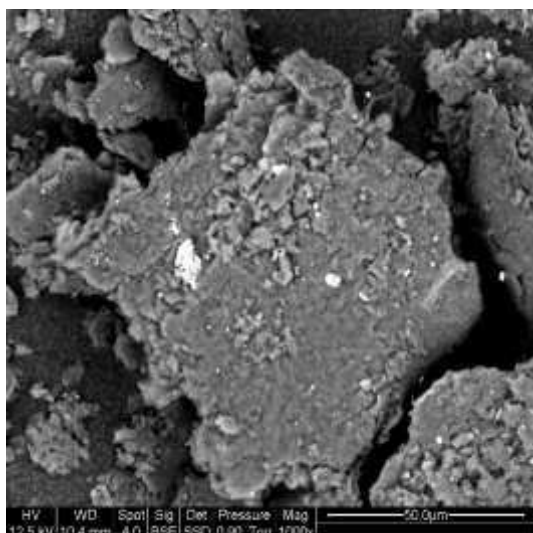
Figure 54   SEM image of original P3 sorbent (BSE mode – magnification 1000)
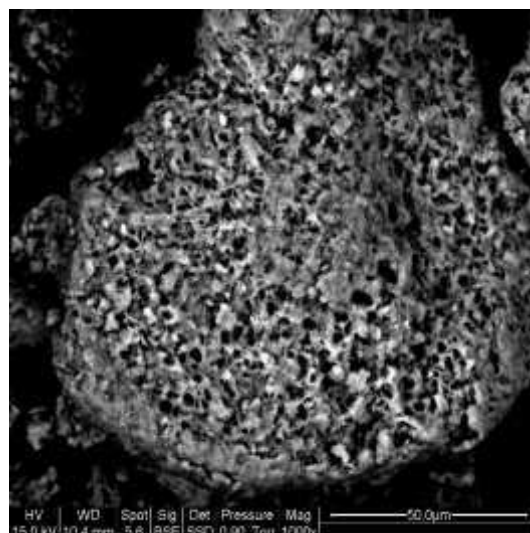
Figure 55 SEM image of original T sorbent (BSE mode – magnification 1000)

When metal saturated samples were subjected to microscopic analyses, several interesting observations were done. The surface of mercury saturated P3 sample (Figure 56) resembled to a sponge and was slightly lighter (less dark) than the original material. On the surface of T sample, spherical microcrystallites were found. These microcrystallites were identified as mercury (Figure 58), whereas the analysed point is indicated by an arrow in Figure 57. With the exception of carbon and oxygen, no other elements were identified in the sample, supporting so the hypothesis of ion-exchange mechanism on carboxyl groups of sample T.
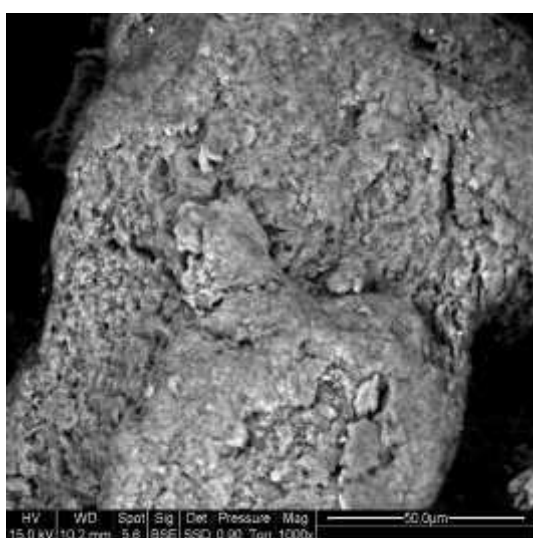
Figure 56   SEM image of mercury saturated P3 sorbent (BSE mode – magnification 1000)
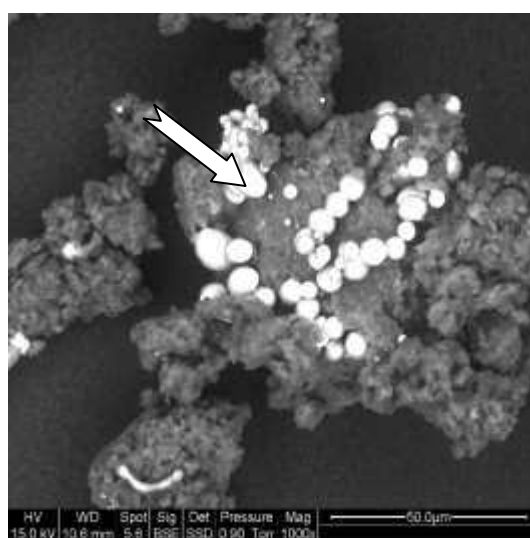
Figure 57 SEM image of mercury saturated T sample (BSE mode – magnification 1000)

136
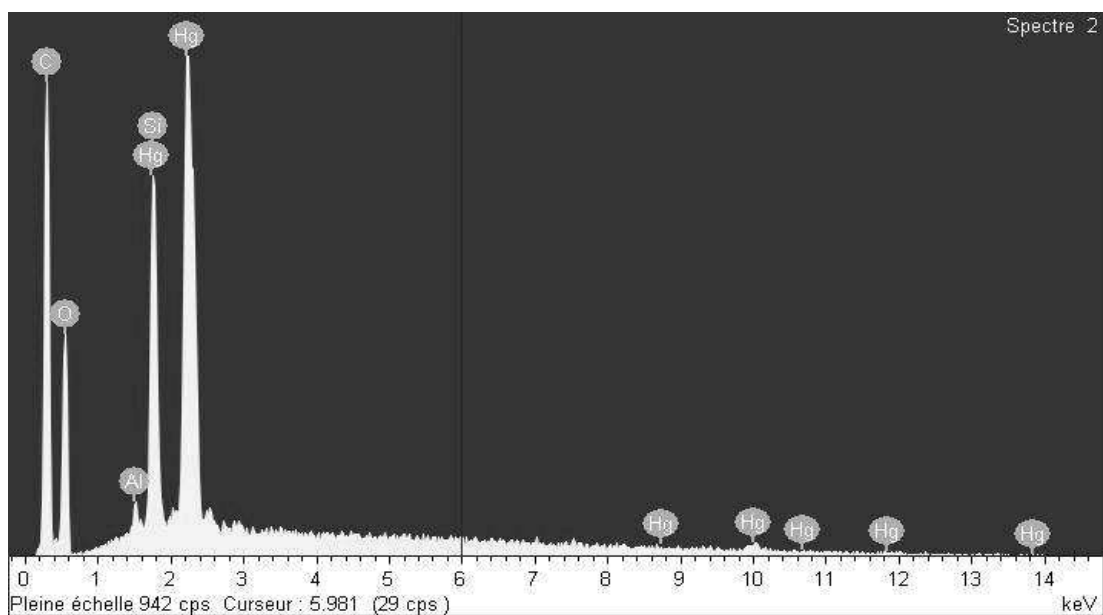
Figure 58 EDX spectrum of mercury saturated T sample

Similar mercury crystalline structures were observed by other researchers. Kumaresan et al.[218] presented a novel approach in preparing mercury(II)cadmium(II)telluride (MCT) based semiconductors. Mercury and cadmium were electrodeposited on thin titanium film and these films were then analyzed by SEM. SEM images revealed the existence of a so-called "cauliflower" morphology of deposited metals (see Figure 59). The average grain size was approx. 1.22 μm (Figure 60). The structures in images of mercury rich MCT films resembled to structures observed in the present study (see Figure 61 corresponding to MCT film and Figure 62 corresponding to mercury saturated biosorbent).

Moreno et al.[219] observed analogical crystalline structures on the mercury contaminated samples from the proximity of Almadén mercury mine. These structures were identified as cinnabar (HgS), $Hg_6Cl_3O(OH)$ and metallic mercury. Whereas Patil et al.[220] studied preparation of nanocrystalline mercury sulphide thin films by ionic layer adsorption and reaction and observed spherical HgS nano-crystallites formation in SEM images.
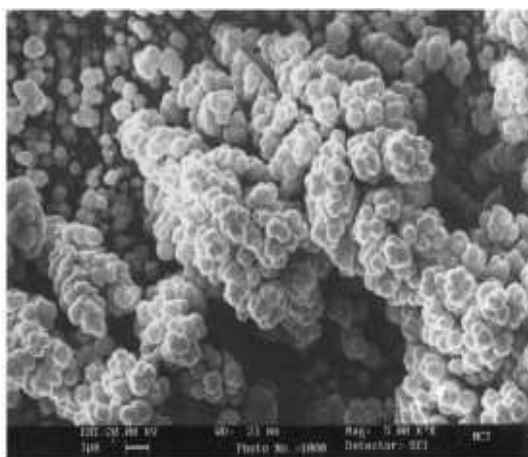
Figure 59 Surface of mercury rich MCT film (Kumaresan et al., 1999)[218]
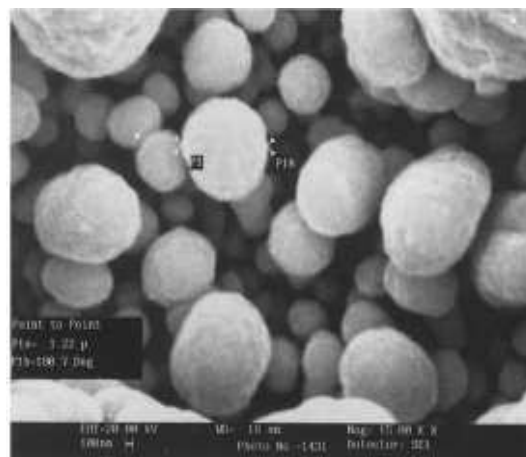
Figure 60 Grain size of mercury rich MCT film (Kumaresan et al., 1999)[218]
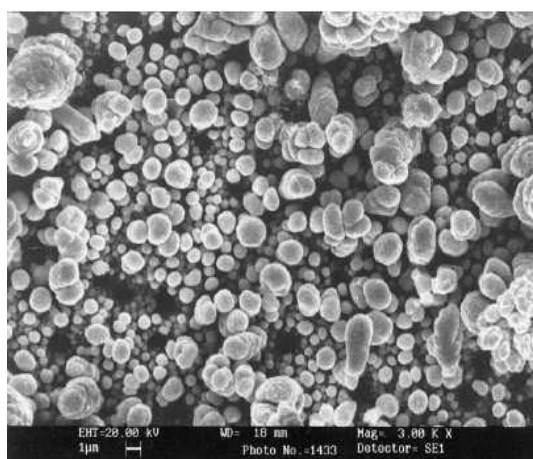
Figure 61 Porous deposition of MCT at lower thickness (Kumaresan et al., 1999)[218]
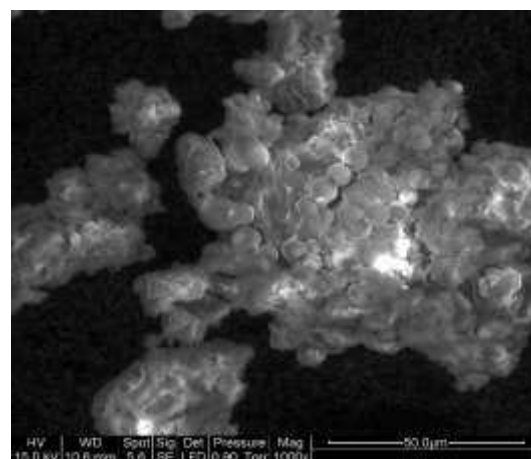
Figure 62 SEM image of mercury saturated T sample (SE mode – magnification 1000)

At higher magnification (5000) it was observed that the surface of P3 samples was covered by abundant, regularly distributed white spots. These spots were identified as mercury (Figure 63), whereas the analysed point is indicated by an arrow in Figure 63. Contrary to T sample, chlorine was also found in sample P3 (EDX spectrum in Figure 65). This finding supports the hypothesis of interaction between complexed mercury species ($Hg(Cl)_2$ and $HgCl(OH)$) and amine (or amide) groups present in P3 sample. In addition to spherical crystalline structure observed in Figure 57, analogical white spots were also found at higher magnification on the surface of T sample (Figure 64), but these spots seemed to be dislocated in a less regular manner.
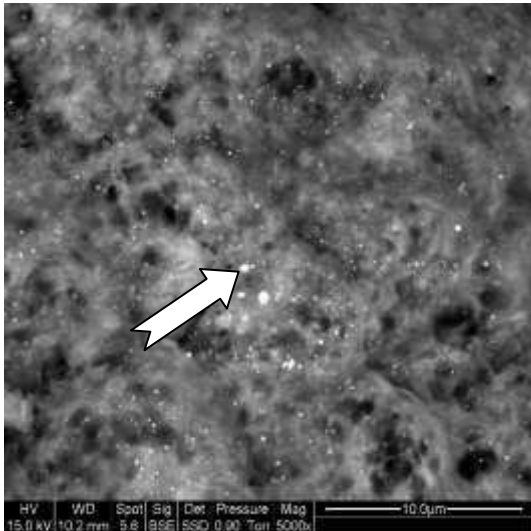
Figure 63 SEM image of mercury saturated P3 sorbent (BSE mode – magnification 5000)
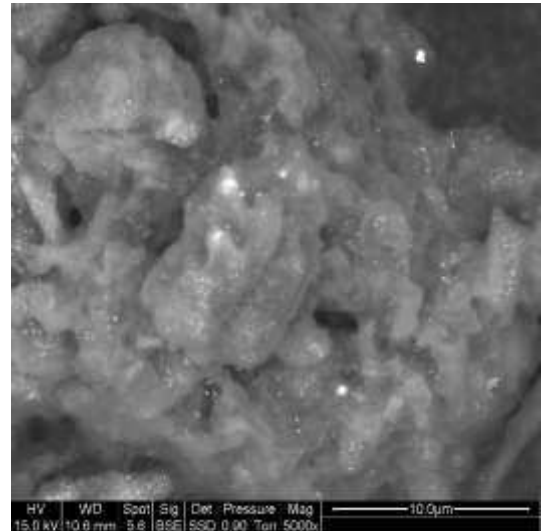
Figure 64 SEM image of mercury saturated T sample (BSE mode – magnification 5000)
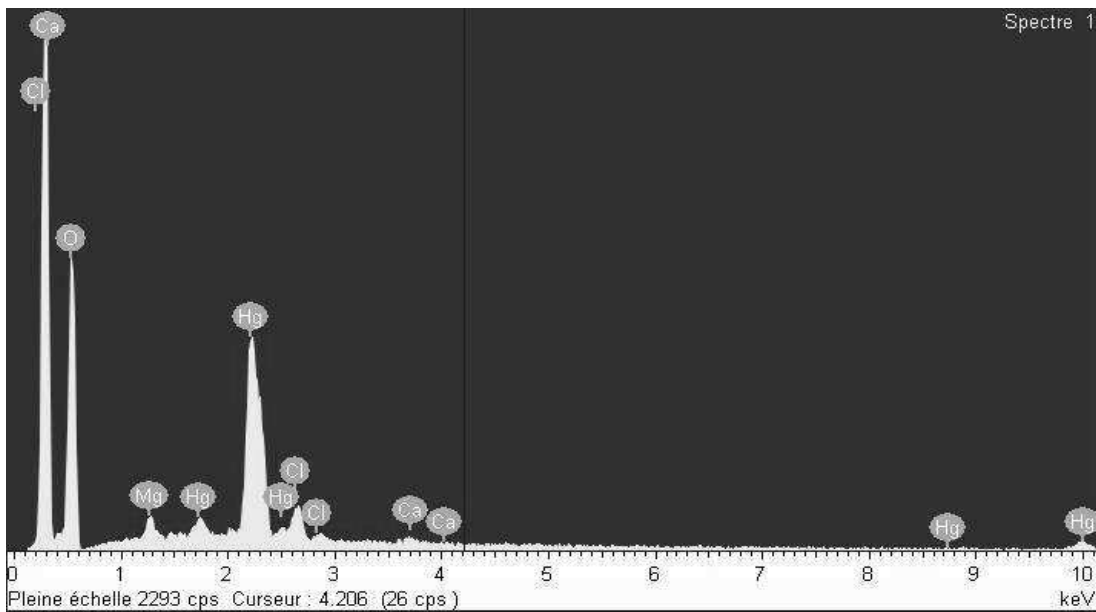
Figure 65 EDX spectrum of mercury saturated P3 sample

Cadmium presence was much less visible on the surface of both samples (Figures 66-67), certainly due to its lower molecular weight and due to its lower sorption capacity. Nevertheless cadmium was identified by EXD elemental analysis (Figures 68 – 69). The analyzed areas are indicated by white squares in SEM images of cadmium saturated samples.
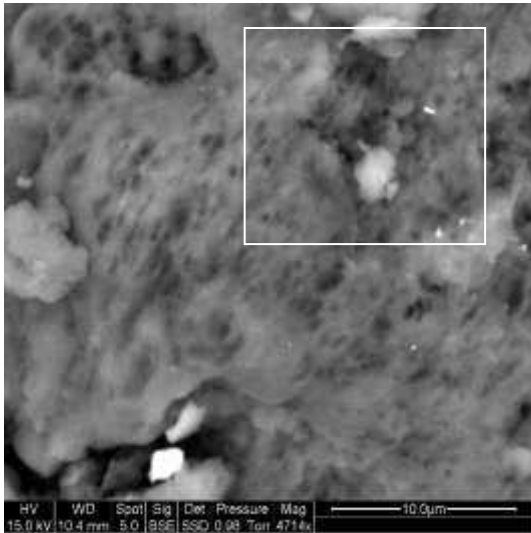
Figure 66 SEM image of cadmium saturated P3 sorbent (BSE mode – magnification 4714)
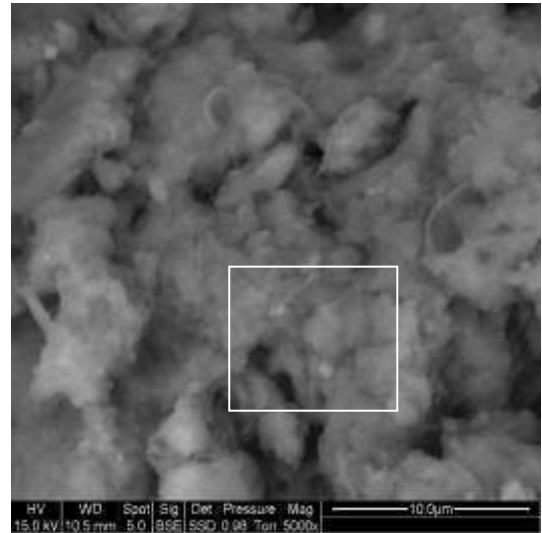
Figure 67 SEM image of cadmium saturated T sample (BSE mode – magnification 5000)
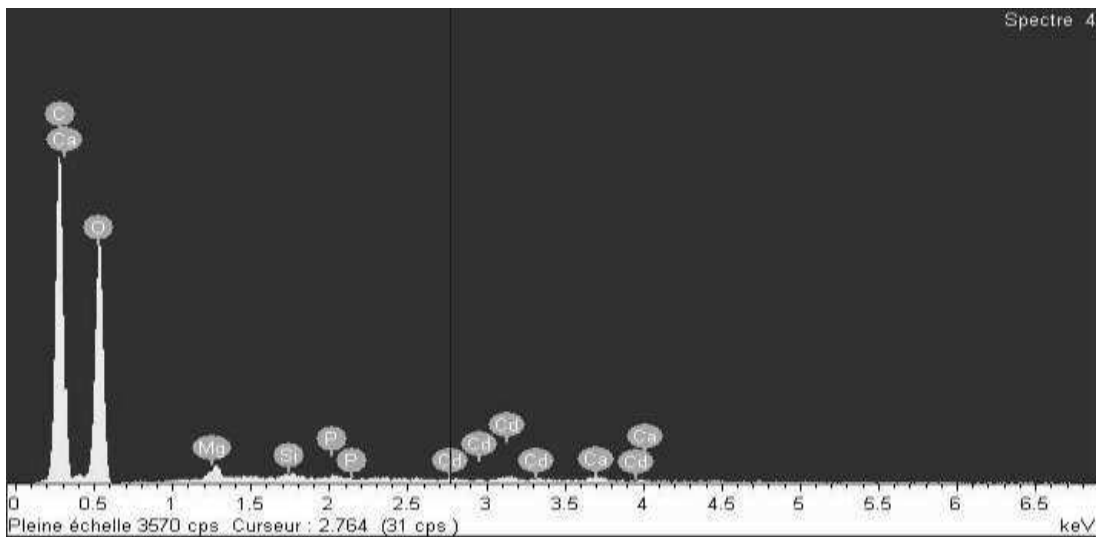
Figure 68 EDX spectrum of cadmium saturated P3 sample
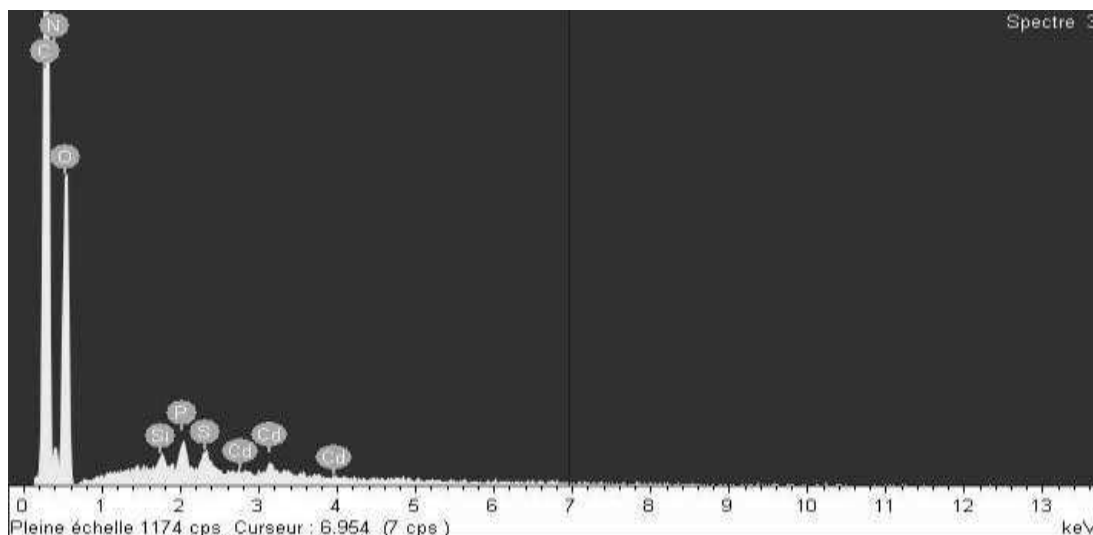
Figure 69 EDX spectrum of cadmium saturated T sample

The differences between the original and saturated samples revealed less evident due to lower molecular weight of chromium (Figure 70 corresponding to P3 sample and Figure 71 corresponding to T sample). Nevertheless EDX analyses confirmed chromium presence on entire surface of the particles (Figures 72 – 73). Analysed area indicated by a white square (Figure 70) and a white arrow (Figure 71). It is worth to note that the differences between original and saturated samples were visible even by eye, since the biosorbent changed the colour within the sorption process.

SEM images of both samples indicated that the surface was covered by light nodules. This effect is visible better in Figure 71, due to higher magnification of the image. The whitish nodules formation was observed by Eiden et al.[221] for chromium saturated chitin and chitosan and it was called Eiden-Jewell effect. Malkoc et al.[217] also reported that pores and surface of pomace (olive oil industry waste) after hexavalent chromium adsorption were covered by chromium and the surface biosorbent became smooth.
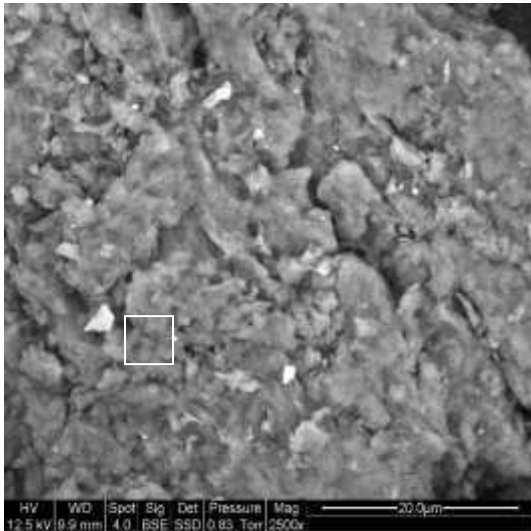
Figure 70 SEM image of chromium saturated P3 sorbent (BSE mode – magnification 2500)
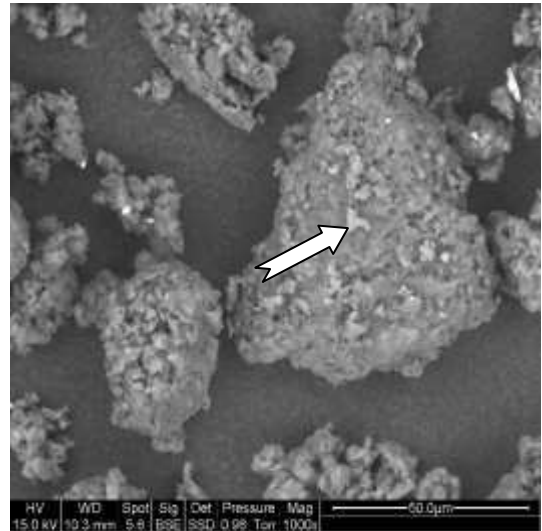
Figure 71 SEM image of chromium saturated T sorbent (BSE mode – magnification 1000)
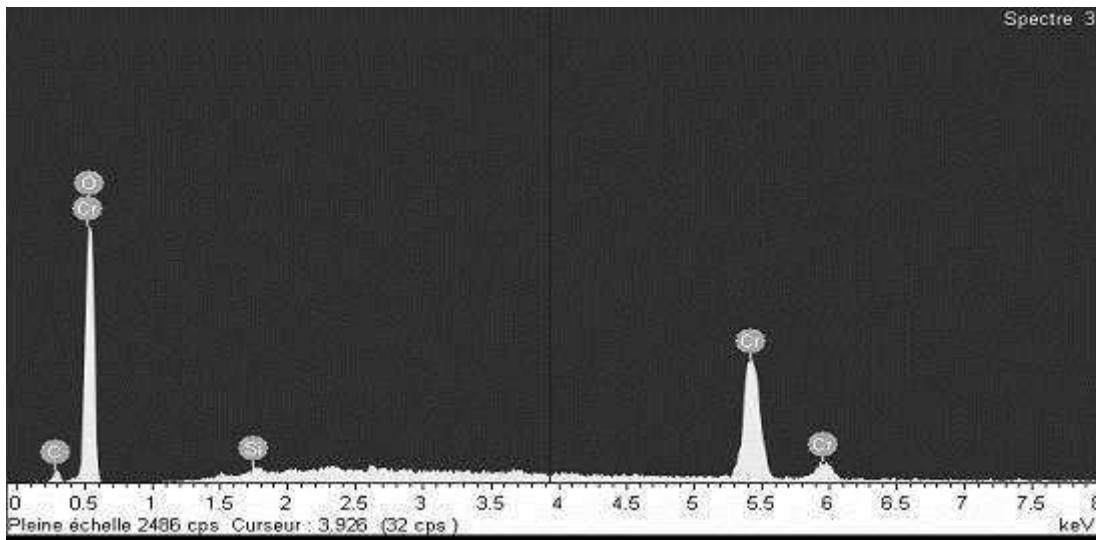
Figure 72 EDX spectrum of chromium saturated P3 sample
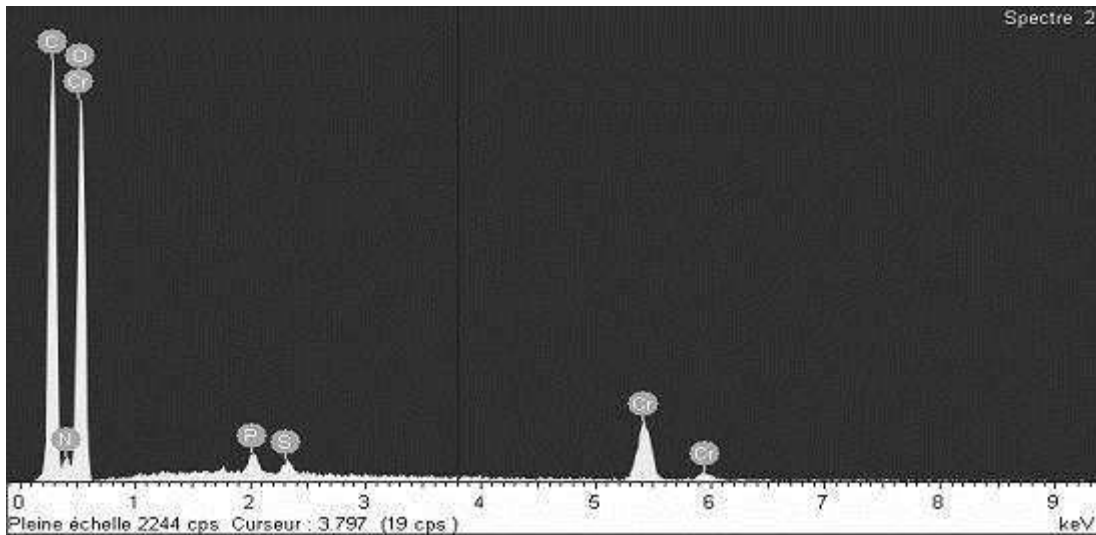
Figure 73 EDX spectrum of chromium saturated T sample

Lead saturated samples performed differently. White islands (zones) are visible in Figure 74 corresponding to P3 samples. These islands were identified as lead (Figure 76) and this observation supports the hypothesis of microprecipitation mechanism in case of lead. Eiden et al.[221] reported similar images for lead biosorption by chitin and chitosan. While in the case of T sorbent (Figure 75), distinct small white spots were found and were identified as lead (Figure 77). Tunali et al.[222] found that in the case of lead biosorption by *Bacillus* biomass, the material surface was sponge-like and was covered by a layer of lead. Sponge-like surface was observed in case of T sample at lower magnification (not shown).
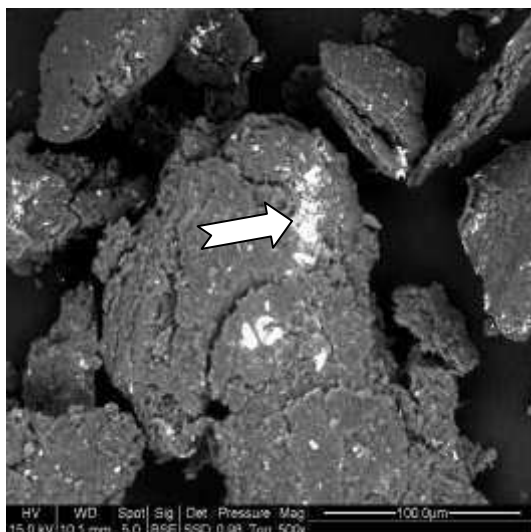
Figure 74 SEM image of lead saturated P3 sorbent (BSE mode – magnification 500)
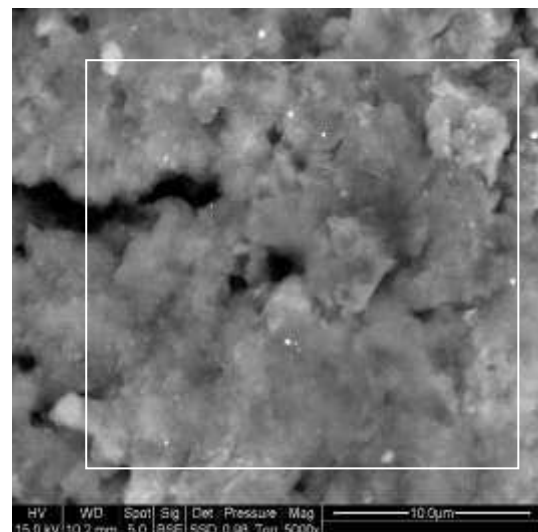
Figure 75 SEM image of lead saturated T sorbent (BSE mode – magnification 5000)
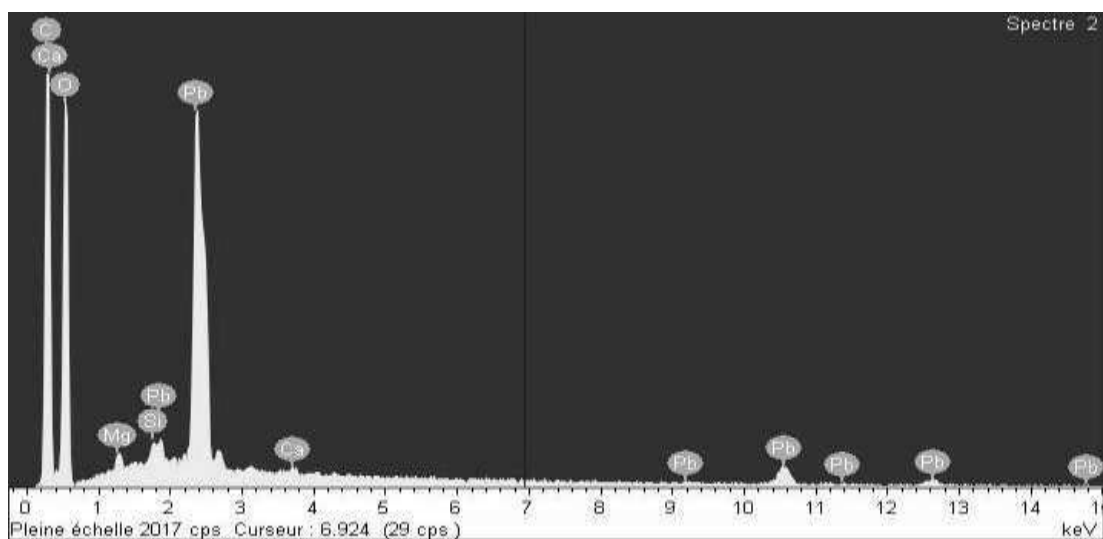
Figure 76 EDX spectrum of lead saturated P3 sample
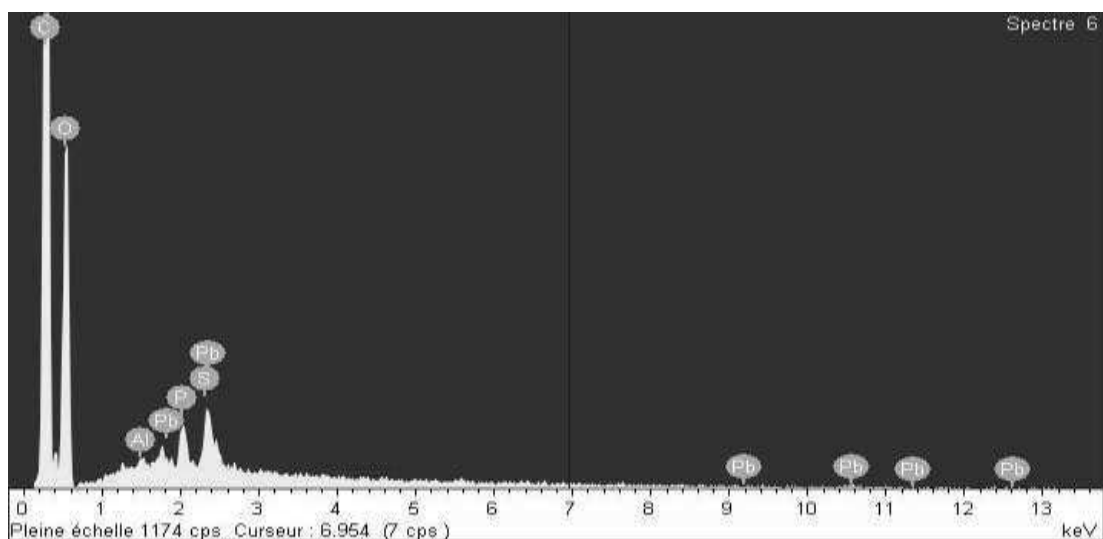
Figure 77 EDX spectrum of lead saturated T sample

4.3.3 Conclusion

The use of instrumental analyses enabled to confirm the hypotheses formulated in previous chapters. At first, the metal saturated samples were subjected to FTIR analysis. In the case of P3 sample, the adsorption bands corresponding to amine or amide groups were modified. A decrease in their intensity, their shifts and even disappearance were observed in the presence of the target metals confirming so the hypothesis of metal chelation on nitrogen containing groups. Beside this, a peak, not found in the original spectrum, appeared in the

FTIR spectrum of mercury saturated sample. It is highly probably, that this adsorption band corresponds to adsorption of chloro- or hydroxo- complex of mercury(II).

For T sample, the changes in the FTIR spectra were less evident. Only the relative intensity of the band corresponding to a carbonyl of a carboxyl group decreased. Thus the ion exchange on carboxyl group was not excluded as the biosorption mechanism in the case of T sample. Chromium saturated T sample did not help to clarify the possible mechanism of the combined sorption/reduction mechanism, though the carboxyl group may probably participate in this process.

The target metals were found on the surface of each tested biosorbent samples by scanning electron microscope. It was possible to quantify their amount on SEM images visually and this amount appeared to be proportional to the sorption capacities reported earlier. According to the best sorption performance towards mercury, this metal was found in abundance on the surface of both biosorbents. While in the case of the T sample spherical nanostructures formation was observed and these structures were similar to those displayed in literature, in the case of P3 sample numerous spots of much smaller size were observed together with chlorine. The visual identification of chromium and cadmium was more difficult due to their lower atomic numbers; nevertheless their presence was confirmed by EDX microanalysis. Concerning lead, well distinct white zones (islands-like) were found on the surface of P3 sample, supporting so the hypothesis of microprecipitation phenomenon. However, distinct small spots of lead were found on the surface of T sample.

4.4 Monitoring of sorption kinetics

Application of Langmuir and Freundlich isotherm equations on experimental data enabled to determine the equilibrium parameters specific for each sorbate-sorbent couple as well as some trends observed in general (ranking of biosorbents sorption behaviour regarding their maximum sorption capacities and affinities towards tested metals, better sorption performance of P3 sorbent towards all tested metals etc.).

The objective of this part of work was to observe the evolution of the concentration decrease in the system as a function of time, to describe the process by means of kinetic order relationships and to determine the transport mode responsible for the control of the process. This was particularly important for identifying the limiting steps and the parameters to be improved in order to achieve an optimum efficiency of the biosorption process. The influence

of several experimental parameters (initial metal concentration – C_i, sorbent dosage - SD, particle size - d_p) on sorption kinetics was investigated.

The same phenomenon was observed all along all performed sorption experiments. Sample T was immediately dispersed in the bulk of solution after its addition, while on the contrary the dispersion of sample P3 was much slower. The material tended to form lumps aggregating in the vortex of the suspension system after the contact with solution. These lumps dispersed progressively within the first 60 – 90 minutes of experiments. A manual disintegration of lumps with a spatula was efficient to a certain degree (creating smaller lumps, which dispersed faster). Decreasing the agitation speed in order to interfere the vortex creation did not reveal suitable. Even though this operation led to a vortex reduction, it led, indeed, to settling of a part of material due to an insufficient agitation. It was found that a worsen dispersion of P3 sorbent was more due to a certain hydrophobicity of the material and not due to vortex creation. This behaviour may have played an important role in the control of diffusion mechanisms of the process.

4.4.1 Mercury

The highest sorption capacities were so far obtained for mercury for both P3 and T biomass samples. Therefore a lot of attention was given to its uptake kinetics considering the impact of parameters such as C_i, SD and d_p.

4.4.1.1 Influence of metal concentration

At first the influence of initial metal concentration on mercury biosorption kinetics was investigated. Kinetic decay curves (residual/initial metal concentration ratio) were plotted versus time using P3 and T sorbent samples (Figures 78 and 79, respectively). The sorbent dosage was fixed at 300 mg L^{-1} and three different values of mercury concentration were tested (20, 50, 100 mg Hg L^{-1}, respectively).
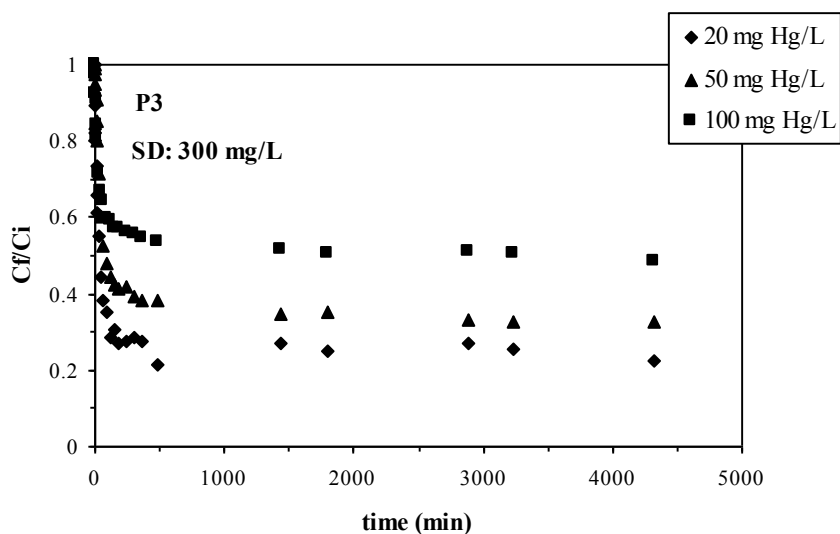
Figure 78 Influence of mercury concentration on sorption kinetics (pH$_i$=5, P3 sample, 300 mg sorbent L^{-1})
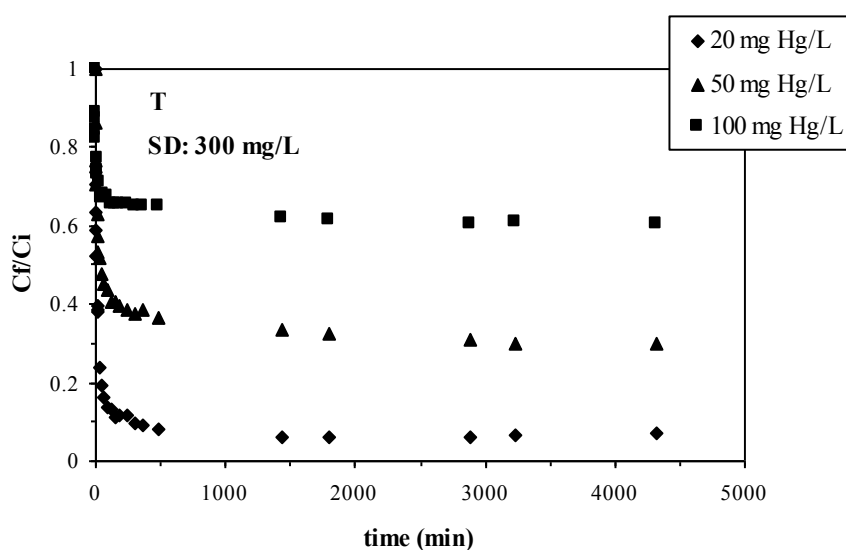
Figure 79 Influence of mercury concentration on sorption kinetics (pH$_i$=7, T sample, 300 mg sorbent L^{-1})

At fixed sorbent dosage and increasing solute concentration (i.e. increasing sorbate to sorbent ratio) lower sorption efficiency is usually obtained. This is easily explained by the fact that the solute ions occur in excess to sorbent particles. It was thus expectable to find the efficiency of the process decreasing with the increase in the mercury concentration.

The sorbent efficiency at initial concentration 100 mg Hg L^{-1} was higher for P3 sorbent, 50% compared to 40% for sorbent T. At the initial concentration 50 mg Hg L^{-1} the sorption efficiencies were comparable for both sorbents (70%). Surprisingly, an inverse trend

was observed at initial concentration 20 mg Hg L^{-1}. Sorbent T exhibited sorption efficiency as high as 94%, while sorbent P3 reached only 80%. This phenomenon could be easily explained in relation to the results of sorption isotherm modelling. The value of coefficient b (derived from Langmuir isotherm relationship) was several times higher for T sorbent than the value corresponding to P3 sample. According to Kratochvil et al.[144] and as illustrated in Figure 7 (page 56) the sorbent - sorbate affinity is reflected in the value of this coefficient. The higher is this value, the higher is the initial slope of the isotherm plot and the better is the sorption behaviour at low equilibrium concentrations. This fact explains very well obtained experimental results.

Some discrepancies between the results of isotherms and equilibrium points of uptake kinetics were also observed. The process efficiencies were in general slightly lower than those expected according to the maximum sorption capacities derived from the Langmuir isotherm relationship (especially in the case of P3 material). While a good accordance was observed at the lowest concentration level, these discrepancies were increasing with increasing initial metal concentration. It should be mentioned, that in the case of P3 sorbent the uptake capacities at saturation level obtained experimentally reached only 90% of the calculated value (derived from Langmuir model).

Two different relationships presented in chapter 2.3.2 were tested to describe mercury biosorption kinetics, namely the Lagergren's pseudo first order reaction rate equation (further referred as Lagergren's equation) (Eq. 11, page 58) and the Ho's pseudo second order reaction rate equation (further referred as Ho's equation) (Eq. 15, page 59). Both of them were used in their linearized forms. The application of the Ho's equation resulted in a reasonable fit (Table 27), while very low correlation coefficients were obtained for the Lagergren's model fit and thus these data are not presented.

For both biomass samples the value of rate constant (k_2) decreased drastically when the initial concentration was increased from 20 to 50 mg Hg L^{-1}. This indicates that the rate of biosorption process decreased with increasing initial concentration. However, the values were comparable for initial concentrations 50 and 100 mg Hg L^{-1} (see Table 27). The increasing trend in q_e values and decreasing parallel trend in k_2 values were also observed by Ho et al.[157] for competitive sorption of heavy metals by sphagnum moss peat.

Biosorbent	C_i	k_2	g_e	R^2
	[mg L^{-1}]	[10^{-5} g mg^{-1} min^{-1}]	[mg g^{-1}]	-
P3	20	164.0	51.5	1
	50	19.3	111.4	1
	100	16.9	154.9	0.999
T	20	232.1	68.3	1
	50	39.0	110.9	1
	100	39.0	126.9	1

Table 27 The effect of initial metal ion concentration on mercury biosorption kinetics at 300 sorbent L^{-1} – pseudo second-order reaction-rate fit (C_i: initial metal ion concentration, k_2: rate constant, g_e: metal ion removal capacity at equilibrium, R^2: correlation coefficient)

The excellent fit of the Ho's equation is shown in Figures 80 and 81. Lines in figures represent the modelling of experimental data with the appropriate equation. To illustrate the excellence of the fit an example of the linearization is shown in Appendix B by plotting the t/q_t ratio versus time (Figures 146 – 147). However, the Ho's equation fitted significantly better the experimental data for P3 sorbent in the region 0 – 240 minutes (corresponding to 4 hours of experiments) than in the case of T sorbent. On the contrary, the equilibrium was well described by this equation for both biosorbents.
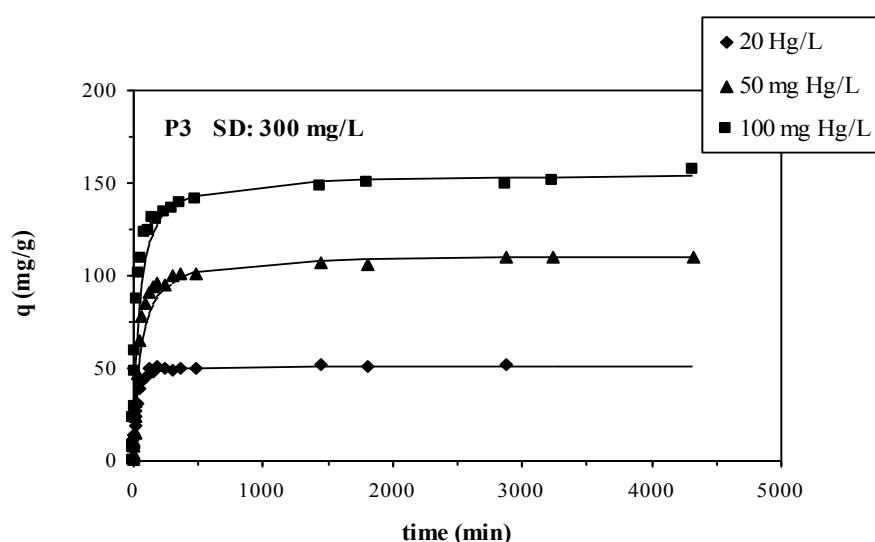
Figure 80 Influence of mercury concentration on sorption kinetics – pseudo second order rate equation fit (pH$_i$=5, P3 sample, 300 mg sorbent L^{-1})
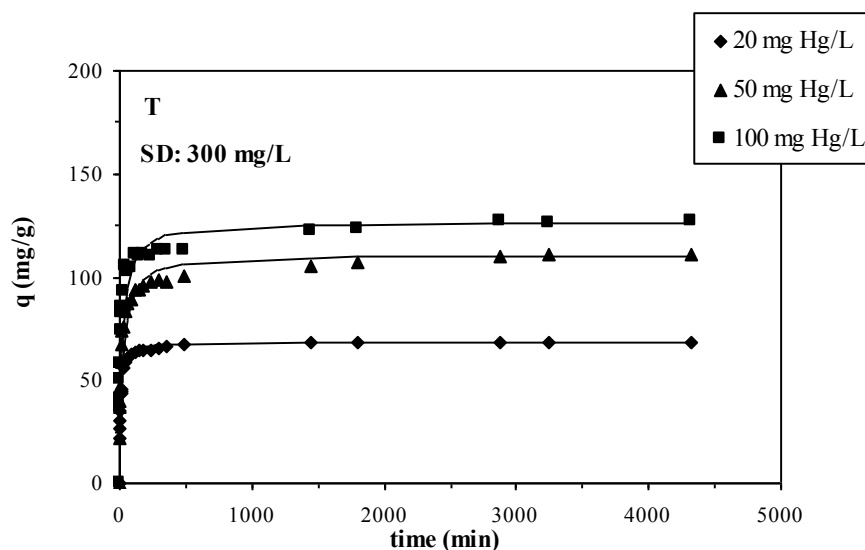
Figure 81 Influence of mercury concentration on sorption kinetics – pseudo second order rate equation fit (pH$_i$=7, T sample, 300 mg sorbent L^{-1})

The Ho's equation was often used to describe experimental data and it was successfully applied to mercury sorption on activated carbon[223], lead and cadmium sorption on *Aspergillus niger* biomass[63], copper and lead sorption on peat[156] and Remazol Black B dye sorption on *Rhizopus arrhizus* biomass[224].

To determine the transport mode responsible for the control of biosorption kinetics three equations previously described in the chapter 2.3.2.3 (page 60) were selected to fit the experimental data. These are namely the external mass transfer model (Eq. 18, page 63), Weber and Morris (W&M) (Eq. 20, page 64) and Urano and Tachikawa (U&T) (Eq. 23, page 65) relationships dealing with the intraparticle mass transfer and diffusion. Single independent models were chosen in order to estimate the relative influence on experimental results.

A good correlation of the experimental results with the models would indicate that diffusion mechanisms were controlling the sorption kinetics. Calculated correlation coefficients varied between 0.92 and 0.99 for P3 sample and 0.76 and 0.96 for T sample. This correlation is presented in Appendix B (Figures 148 - 158)in the form of a plot of time versus logarithm of C$_f$/C$_i$ corresponding to external mass transfer model, in the form of a plot of square root of time versus q (W&M model) and as a plot of f(q$_t$/q$_m$) as a function of time (U&T model).

The calculations were performed for the first 20 minutes of experiments for the external mass transfer diffusion model and for the first 60 minutes for the intraparticle mass transfer diffusion models according to the conclusions made in chapter 2.3.2.3.

Biosorbent	External mass transfer model			Intraparticle mass transfer models			
				W&M		U&T	
	C_i	β_L	R^2	K	R^2	D	R^2
	[mg L^{-1}]	[10^{-5} m min^{-1}]	-	[mg g^{-1} min$^{-0.5}$]	-	[10^{-10} m^2 min^{-1}]	-
P3	20	5.9	0.922	5.4	0.992	7.1	0.989
	50	2.9	0.963	10.6	0.950	4.2	0.939
	100	3.0	0.978	16.1	0.969	4.5	0.980
T	20	11.0	0.762	6.9	0.884	9.9	0.967
	50	7.2	0.870	10.5	0.892	6.1	0.929
	100	3.4	0.796	12.3	0.883	7.2	0.904

Table 28 Effect of initial mercury concentration on the diffusional constants (SD 300 mg L^{-1})

An increase in the initial metal concentration resulted in a decrease in the external mass transfer coefficient β_L and in an increase in the intraparticle mass transfer rate K (W&M). Increasing the metal concentration in the solution seemed to reduce the diffusion of mercury ions in the boundary layer and to enhance the diffusion in the solid.

As evident from the decay curves (Figures 78 - 79) the process proceeded in two different phases. The initial fast decrease in the concentration corresponded approximately to the first 6 hours of experiment. The strong affinity between mercury and biosorbent samples led to a rapid concentration decrease in the solution and this decrease resulted subsequently in a drop of the concentration gradient in the boundary layer. Thus the flux of the mass transfer between the liquid and the solid was reduced and the overall rate of the process was decreased, since the concentration gradient is the driving force of the external mass transfer.

The process at 20 mg Hg L^{-1} was probably controlled only by the surface sorption as the gradient decreased quickly. On the contrary for the higher concentrations, the gradient remained sufficiently high after the saturation of the surface to push the sorbate to penetrate and diffuse inside the sorbent particle. This second phase was characterized by a very slow concentration decrease and lasted up to 24 hours. Thus the sorption process could be divided into two stages, the first rapid step being controlled by mass transport from the liquid film to

the sorbent surface and the second slow step controlled by the sorbate diffusion inside the solid particles. So with the increasing initial concentration the intraparticle transfer was playing the major role, while at low concentrations the process seemed to be controlled mainly by the external mass transfer rate.

The same conclusions were obtained by Jansson-Charrier et al.[225] for vanadium sorption on chitosan and by Guibal et al.[226] for uranium sorption on a modified chitosan. The calculated coefficients were of the same order of magnitude as those reported by Jansson-Charrier[225].

The U&T model also fitted well the experimental data contrary to Jansson-Charrieret al.[225], who reported a non-linear distribution of experimental points, which was not really the case here as illustrated in Figure 170 (Appendix B). For P3 sample the coefficient D derived from this model was nearly two times higher for initial concentration 20 mg Hg L^{-1}, while the values obtained for the two other initial concentration were comparable. For sample T the values of coefficient D were of following order: $D_{20}>D_{100}>D_{50}$ (subscripts correspond to the initial metal concentration). However these coefficients were of the same order of magnitude. Moreover the values of coefficient D were very close for both sorbents. It is expectable that the diffusion coefficients in the biomass should be independent of the solute concentration. The observed variations may be due to external diffusion and the modelling of the process that artificially separated external and intraparticle mass transfer.

Figure 82 and Figure 83 display the plots of the residual/initial metal concentration ratio versus time using P3 and T sorbent samples, respectively, at initial sorbent dosage 100 mg L^{-1}. The same range of concentration was held (20, 50, 100 mg Hg L^{-1}, respectively). These experimental conditions correspond to less favourable solid/liquid (S/L) ratio. This allows taking into account the impact of sorbent saturation.
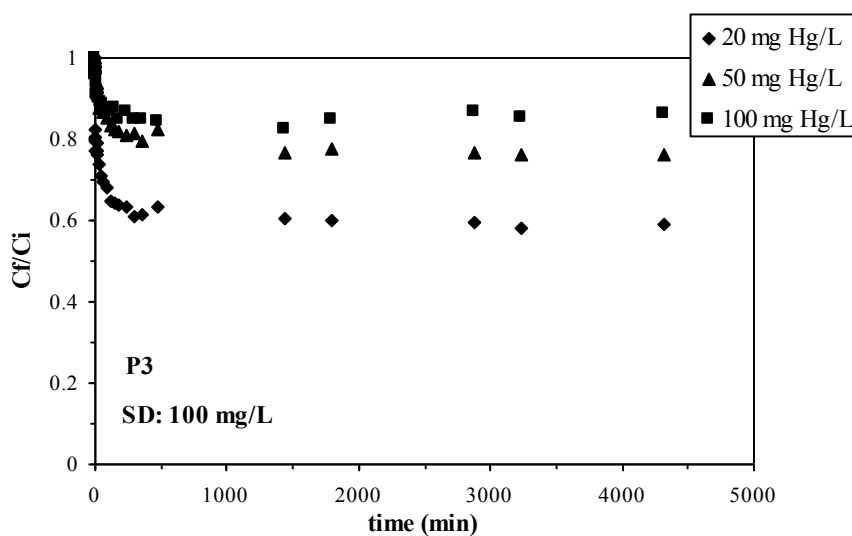
Figure 82 Influence of mercury concentration on sorption kinetics (pH$_i$=5, P3 sample, 100 mg sorbent L^{-1})
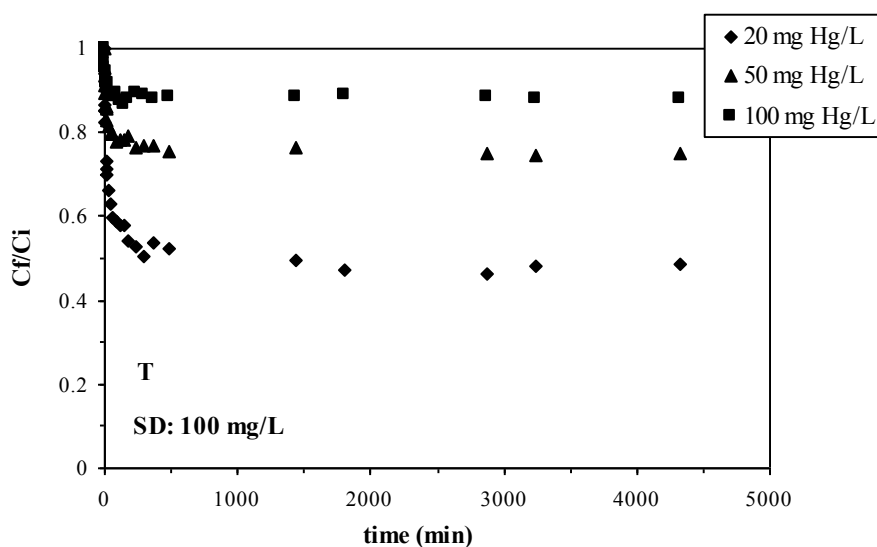
Figure 83 Influence of mercury concentration on sorption kinetics (pH$_i$=7, T sample, 100 mg sorbent L^{-1})

As in the case of previous sorbent dosage the efficiency of the process increased with decreasing mercury concentration, even though the overall efficiency remained low due the lower sorbent dosage. The sorption efficiencies at 100 and 50 mg Hg L^{-1} were comparable for both sorbents (10 and 25%, respectively), whereas at the initial concentration 20 mg Hg L^{-1} sorbent T exhibited higher sorption efficiency (50%) than sample P3 (40%), although this phenomenon was not so pronounced as in the previous case.

153

Ho's equation fitted again well experimental data. As this fact was clearly illustrated in the case of sorbent dosage 300 mg L^{-1}, the results are presented only in Appendix B (Table 54).

Table 29 summarizes the results of the modelling of mass transfer and diffusion phenomena. A logarithmic dependence of experimental data was obtained with sorbent P3 at initial concentration 20 mg L^{-1}, which resulted in a low fit to all three models. Taking into account the low values of R^2 indicating a bad fitting of experimental data, any discussion of the trends reveals difficult.

On the contrary, a decreasing trend of β_L values was observed for T biosorbent with increasing initial mercury concentration, while the K parameter continuously increased with increasing initial metal concentration. This trend confirms the increasing effect of intraparticle diffusion with the increase in solute concentration. No influence of tested parameter on the values of coefficient D was found, while they were all of the same order of magnitude.

Biosorbent		External mass transfer diffusion		Intraparticle mass transfer model			
				W&M		*U&T*	
	C_i	β_L	R^2	K	R^2	D	R^2
	[mg L^{-1}]	[10^{-5} m min^{-1}]	-	[mg g^{-1} min$^{-0.5}$]	-	[10^{-10} m^2 min^{-1}]	-
	20	5.8	0.323	5.3	0.655	3.7	0.860
P3	50	3.2	0.840	8.2	0.935	2.5	0.884
	100	3.0	0.830	0.8	0.931	3.7	0.933
	20	12.3	0.828	8.9	0.929	5.2	0.968
T	50	6.3	0.820	11.4	0.915	7.2	0.934
	100	3.1	0.700	13.5	0.837	8.5	0.724

Table 29 Effect of initial mercury concentration on the diffusional constants (SD 100 mg L^{-1})

The last dosage tested corresponded to 500 mg L^{-1} and the plots of experimental results are displayed in Figures 84 – 85.
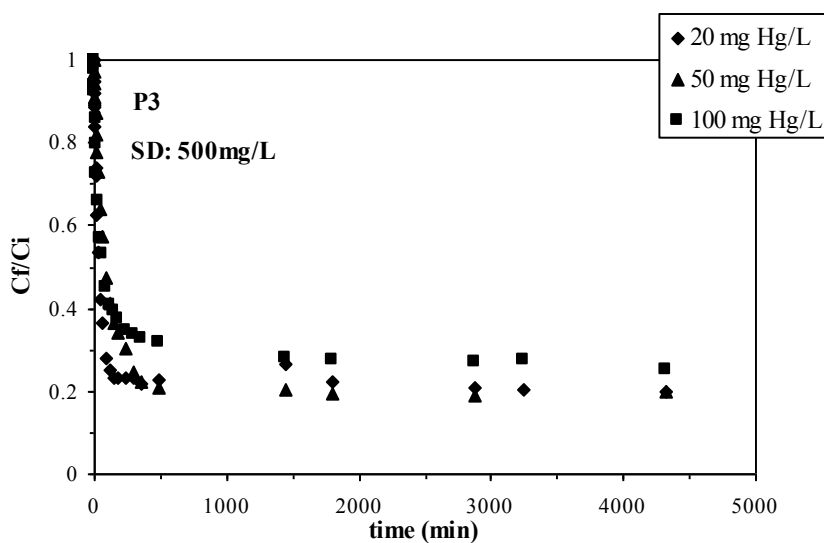
Figure 84 Influence of mercury concentration on sorption kinetics (pH$_i$=5, P3 sample, 500 mg sorbent L^{-1})
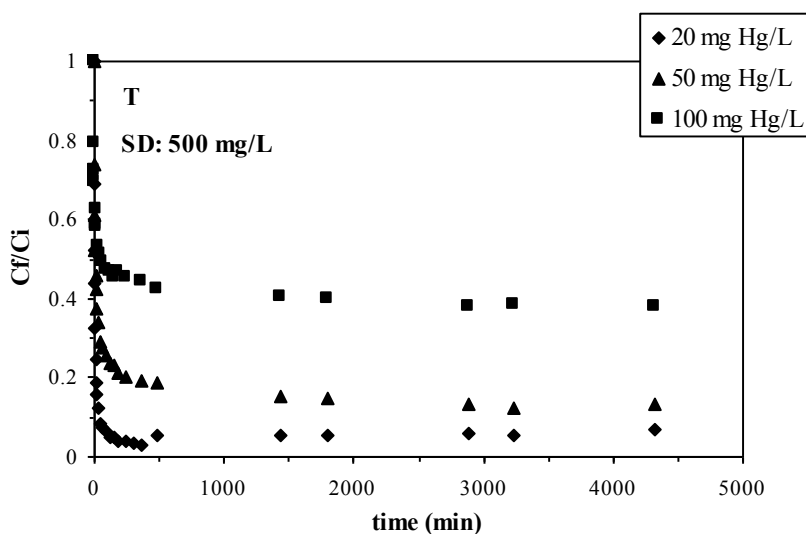
Figure 85 Influence of mercury concentration on sorption kinetics (pH$_i$=7, T sample, 500 mg sorbent L^{-1})

A different behaviour was observed for the two sorbent samples. The efficiency ranging between 75% and 80% was obtained with P3 sample, regardless of the initial concentration. It seemed that the sorbent material was in excess to sorbate molecules, which provoked a very rapid drop of the concentration gradient. This rapid drop of gradient probably resulted in a purely surface sorption and thus a complete saturation of sorbent seemed not to be achieved.

155

The question why in such case the efficiency did not approach 100% would reveal completely logic. Two possible answers could be found. Firstly, the final (equilibrium) concentrations were very low and as already mentioned, P3 sample revealed less efficient under such experimental conditions. Secondly, the observed phenomenon could be related to mercury speciation. The pH of mercury - P3 material suspensions tended to level off at pH 6.5 within the biosorption experiments. At this pH and concentration 100 mg Hg L^{-1} seventy percent of mercury exists as hydroxo and hydroxo-chloro complexes, while the rest of mercury exists in the form of $HgCl_2$ (speciation not shown). It is thus possible, that P3 material interacted preferentially with mercury hydroxo- or hydroxo- chloro complexes and the rest of mercury present in solution was inaccessible for biosorption by this material. Nevertheless, no physical confirmation for the second hypothesis was obtained.

On the opposite hand a regular trend was observed with sorbent T. The highest efficiency was found for the initial metal concentration 20 mg L^{-1} (93%) and it decreased with increasing metal concentration to 87% and 62% for 50 and 100 mg Hg L^{-1}, respectively. A longer time to reach the equilibrium was observed together with the lower efficiency for both of the latter concentrations. This would correspond to the conclusion made for the previous sorbent dosage, assuming that the sorption process took place in the entire particle after the surface saturation, which resulted in a rate decrease and prolonged time to reach the equilibrium when the mercury ions had to penetrate inside the particles.

Table 30 summarizes the results obtained for diffusion phenomena modelling.

Biosorbent		External mass transfer diffusion		Intraparticular mass transfer model			
				W&M		*U&T*	
	C_i	β_L	R^2	K	R^2	D	R^2
	[mg L^{-1}]	[10^{-5} m min^{-1}]	-	[mg g^{-1} $min^{-0.5}$]	-	[10^{-10} m^2 min^{-1}]	-
	20	2.8	0.975	3.3	0.984	6.3	0.986
P3	50	1.8	0.905	5.2	0.966	2	0.977
	100	2.6	0.968	13.3	0.969	3.4	0.987
	20	13.4	0.872	3.8	0.767	16	0.930
T	50	6.6	0.804	7.9	0.826	7.1	0.901
	100	1.4	0.688	10.5	0.818	6.6	0.915

Table 30 Effect of initial mercury concentration on the diffusional constants – results (sorbent dosage 500 mg L^{-1})

No influence of initial concentration on the value of the external mass transfer coefficient was found for P3 sample, while the values were of the same order of magnitude. With sample T the coefficient decreased with increasing initial concentration.

Concerning the intraparticular mass transfer models, the coefficient K (W&M model) increased with increasing initial metal concentration in the case of both sorbent samples. With the U&T model the diffusion coefficient values were of the same order of magnitude for P3 sample, while it decreased with increasing initial metal concentration from 20 to 50 mg L^{-1} and stabilized above 50 mg L^{-1} in the case of T sample.

4.4.1.2 Sorbent dosage influence

The second step in these experiments was to verify the biosorbent dosage influence at different initial metal concentrations. This is another way to present the data obtained in the previous section in order to visualize the impact of this critical parameter. Figures 86 and 87 display the plots of the residual/initial metal concentration ratio versus time using P3 and T sorbent samples, respectively. The initial metal concentration was fixed at 20 mg L^{-1} and the influence of three values of sorbent dosages was tested (100, 300, 500 mg L^{-1}, respectively).
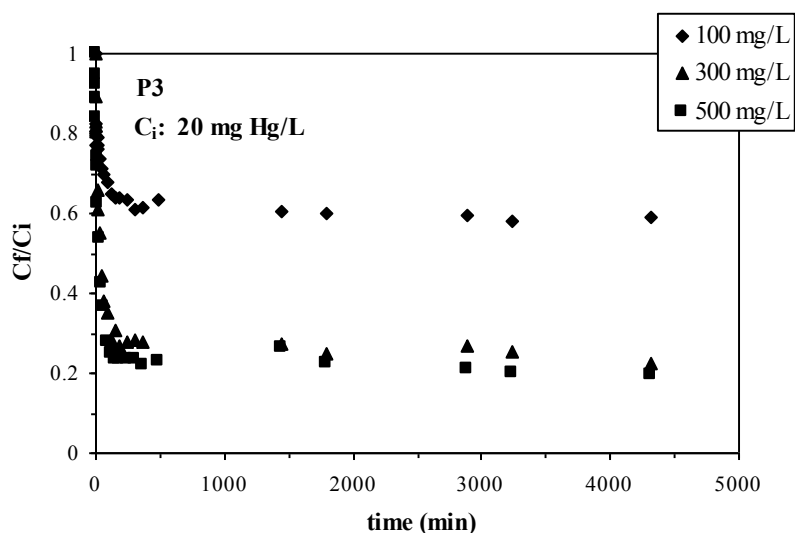
Figure 86 Influence of sorbent dosage on mercury sorption kinetics (pH$_i$=5, P3 sample, 20 mg Hg L^{-1})
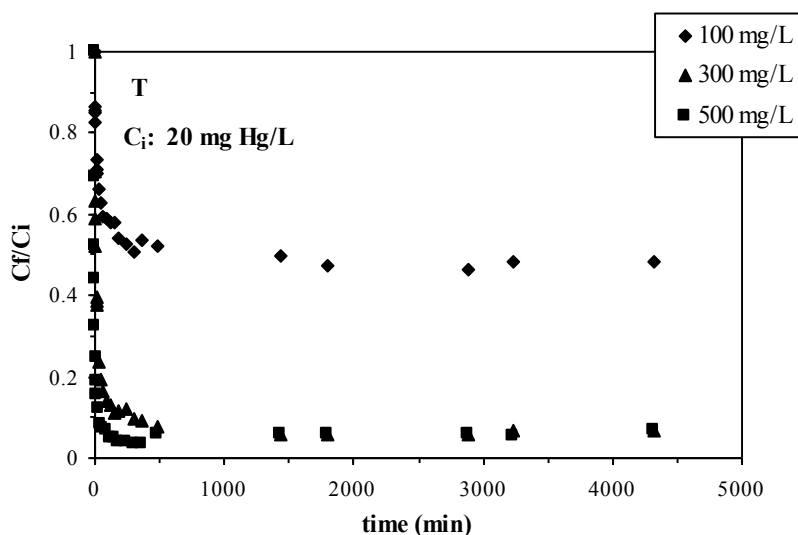
Figure 87 **Influence of sorbent dosage on mercury sorption kinetics (pH$_i$=7, T sample, 20 mg Hg L^{-1})**

The same trend is noticeable in both figures. The efficiencies obtained with 300 and 500 mg sorbent L^{-1} were high and very close in the case of both biosorbent samples. Nevertheless, the efficiency of P3 sample reached only 80%, while that of T sample was as high as 95%. It is evident that increasing the sorbent dosage beyond 300 mg L^{-1} did not induce higher sorption efficiency. For sorbent dosage 100 mg L^{-1} the sorption efficiency attained 40% for P3 sample and 50% for T sample. The trend of higher sorption efficiency obtained with T sample at low mercury concentration was already mentioned, whereas this behaviour was more pronounced at higher sorbent dosages.

Figures 88 and 89 present the decay curves at initial mercury concentration 50 mg L^{-1} using P3 and T sorbent samples, respectively. A significant difference between the efficiency of the dosage 100 mg sorbent L^{-1} and the two other dosages is still evident for both sorbent samples. At the former dosage the efficiency reached only 20% for both biomass samples, while it ranged between 75% and 80% for the two higher dosages for both biosorbents.
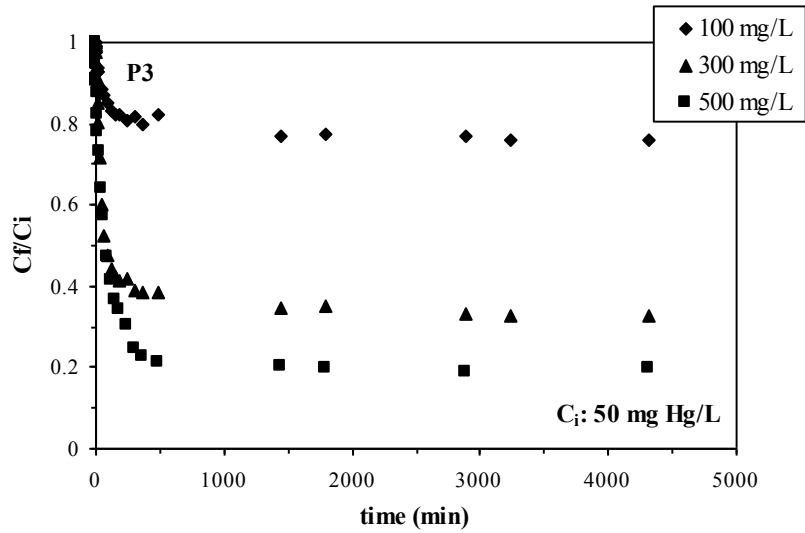
Figure 88 Influence of sorbent dosage on mercury sorption kinetics (pH$_i$=5, P3 sample, 50 mg Hg L^{-1})
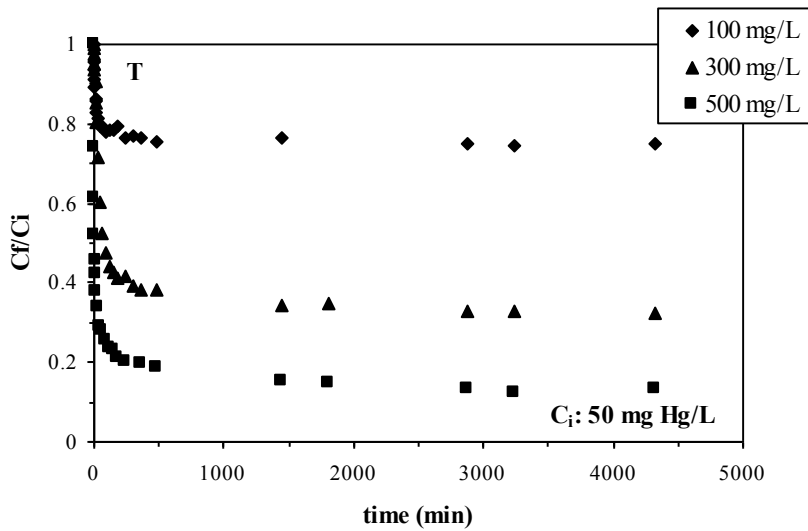
Figure 89 Influence of sorbent dosage on mercury sorption kinetics (pH$_i$=7, T sample, 50 mg Hg L^{-1})

Finally, Figure 90 and Figure 91 show the plots at the initial metal concentration fixed at 100 mg L^{-1} and the three different values of sorbent dosages tested (100, 300, 500 mg L^{-1}, respectively).
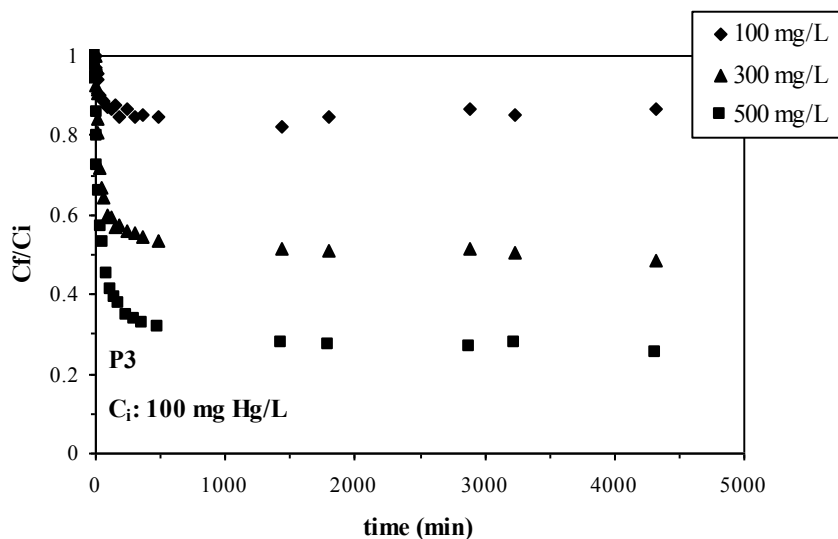
Figure 90 Influence of sorbent dosage on mercury sorption kinetics (pH$_i$=5, P3 sample, 100 mg Hg L^{-1})
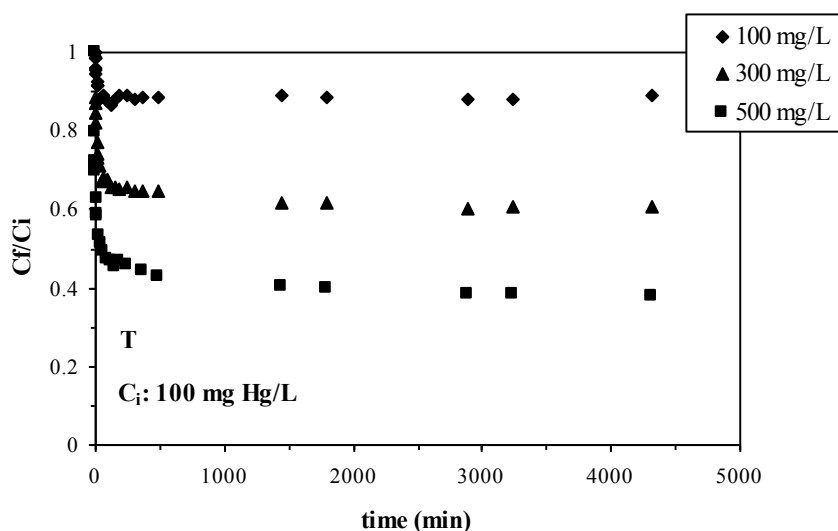
Figure 91 Influence of sorbent dosage on mercury sorption kinetics (pH$_i$=7, T sample, 100 mg Hg L^{-1})

Even at the highest mercury concentration tested the sorption behaviour of both biomass samples resembled, but the differences between individual sorbent dosages were well pronounced. The highest efficiency was observed for the highest sorbent dose and it decreased with decreasing dose (70, 50, 20 % and 60, 40 and 10% for P3 and T samples, respectively). In this case, the P3 sample performed higher efficiencies at all three sorbent levels.

As illustrated in the previous chapter, mercury biosorption on both sorbent materials followed second order kinetics. Ho and Ofomaja[158] reported that for lead ions sorption on palm kernel fibres values of k_2 constant increased with increasing sorbent dosage, while values of q_e decreased. Similar trend was found in the present study at initial metal concentration 20 mg Hg L^{-1} (Table 55, page 291). In the case of the two other tested sorbent dosages, the findings corresponded to the observations done on the basis of the decay curves (results summarized in Table 56, page 292 corresponding to 50 mg Hg L^{-1} and in Table 57, page 292 for 100 mg Hg L^{-1}).

The effect of tested parameter on mass transfer control in the system at 20 mg Hg L^{-1} is summarized in Table 31. The interpretation of experimental data for P3 sample revealed to be difficult due to low correlation coefficients at 100 mg sorbent L^{-1}. In the case of T sample, coefficient β_L was of the same order of magnitude for both of tested samples and thus no influence of sorbent dosage was found on the external mass transfer at low mercury concentration. On the contrary, coefficient K (W&M model) decreased, while the coefficient D (U&T model) increased with the increase in sorbent dosage. The decrease of K coefficient is in conformity with the hypothesis of predominant surface sorption at higher sorbent dosage.

Biosorbent		External mass transfer model		Intraparticular mass transfer model			
				W&M		U&T	
	SD	β_L	R^2	K	R^2	D	R^2
	[mg L^{-1}]	[10^{-5} m min^{-1}]	-	[mg g^{-1} min$^{-0.5}$]	-	[10^{-10} m^2 min^{-1}]	-
	100	5.8	0.323	5.3	0.655	3.7	0.860
P3	300	5.9	0.922	5.4	0.992	7.1	0.989
	500	2.8	0.975	3.3	0.984	6.3	0.986
	100	12.3	0.828	8.9	0.929	5.2	0.968
T	300	11.0	0.762	6.9	0.884	9.9	0.967
	500	13.4	0.872	3.8	0.767	16.0	0.930

Table 31 Effect of sorbent dosage on the diffusional constants – results (initial metal concentration 20 mg Hg L^{-1})

Table 32 summarizes the effect of sorbent dosage on diffusion of mercury at the initial concentration 50 mg Hg L^{-1}.

Biosorbent		External mass transfer model		Intraparticular mass transfer model			
				W&M		*U&T*	
	SD	β_L	R^2	K	R^2	D	R^2
	[mg L^{-1}]	[10^{-5} m min^{-1}]	-	[mg g^{-1} min$^{-0.5}$]	-	[10^{-10} m^2 min^{-1}]	-
P3	100	3.2	0.840	8.2	0.935	2.5	0.884
	300	2.9	0.963	10.6	0.95	4.2	0.939
	500	1.8	0.905	5.2	0.966	2.0	0.977
T	100	6.3	0.820	11.4	0.915	7.2	0.934
	300	7.2	0.870	10.5	0.892	6.1	0.929
	500	6.6	0.804	7.9	0.826	7.1	0.901

Table 32 Effect of sorbent dosage on the diffusional constants (initial metal concentration 50 mg Hg L^{-1})

Coefficient β_L decreased slightly with the increase in the sorbent dosage in the case of P3 sample, whereas in the case of T sample the coefficient value was not affected by the tested parameter. The effect on the rate of intraparticle diffusion was not apparent. The values of *K* parameter for both biomass samples were close for the initial sorbent dosage 100 and 300 mg sorbent L^{-1}, while the values corresponding to 500 mg sorbent L^{-1} were significantly lower. This is coherent with the previous observations (Figures 88 and 89). No influence of tested parameter was realised for diffusion coefficient *D*, while the values were of the same order of magnitude for both biosorbents.

The influence of increasing sorbent dosage on external mass transfer coefficient at 100 mg Hg L^{-1} is summarized in Table 33. The values obtained for P3 samples remained of the same order of magnitude, which may signify that the change of the tested parameter did not affect the rate of the process. For the same sorbent sample an important increase of *K* parameter was observed with the increase in sorbent dosage from 100 mg L^{-1} to 300 mg L^{-1}, whereas above this dosage the value tended to level off. The coefficient *D* maintained approximately the same value for all three tested biosorbent dosages.

In the case of T sample both β_L parameter and *K* parameter appeared not to be affected by the increase in sorbent dosage. The same trend was observed for *D* coefficient (i.e. the same order of magnitude for all tested levels of sorbent dosage). But the interpretation of the data remained difficult regarding quite low correlation coefficients in the case of T sample, as the dependence of the investigated parameters revealed rather logarithmic.

Biosorbent		External mass transfer model		Intraparticular mass transfer model			
				W&M		U&T	
	SD	β_L	R^2	K	R^2	D	R^2
	[mg L^{-1}]	[10^{-5} m min^{-1}]	-	[mg g^{-1} min$^{-0.5}$]	-	[10^{-10} m^2 min^{-1}]	-
	100	3.0	0.830	0.8	0.931	3.7	0.933
P3	300	3.0	0.978	16.1	0.969	4.5	0.980
	500	2.6	0.968	13.3	0.969	3.4	0.987
	100	3.1	0.700	13.5	0.837	8.5	0.724
T	300	3.4	0.796	12.3	0.883	7.2	0.904
	500	1.4	0.688	10.5	0.818	6.6	0.915

Table 33 Effect of sorbent dosage on the diffusional constants (initial metal concentration 100 mg Hg L^{-1})

4.4.1.3 Influence of particle size

The influence of this parameter is considered crucial in the classical adsorption theory. The particle size reveals as a key parameter, when the physical sorption plays the dominant role, since the physisorption process is very sensitive to the specific surface of the sorbent. It is common knowledge that increasing the sorbent size leads to the decrease of the specific surface, which affects physical adsorption negatively. However, the chemisorption process is considered to be less sensitive to this parameter.

Figure 92 and Figure 94 display the effect of this parameter on mercury biosorption for P3 and T sorbents, respectively. Slightly different behaviours were observed.

In the case of P3 sample (Figure 92), the highest sorption efficiency was observed for the smallest size fraction G1. Surprisingly, the G5 fraction exhibited a very close efficiency. Other fractions behaved nearly the same in the first stage of the process, whereas the decrease in mercury concentration was slower in comparison to G1 fraction. Nevertheless, it seemed that the equilibrium was attained at the same time as for G1 fraction, though the efficiency of the process was slightly lower in the case of G2, G3 and G4 fraction.
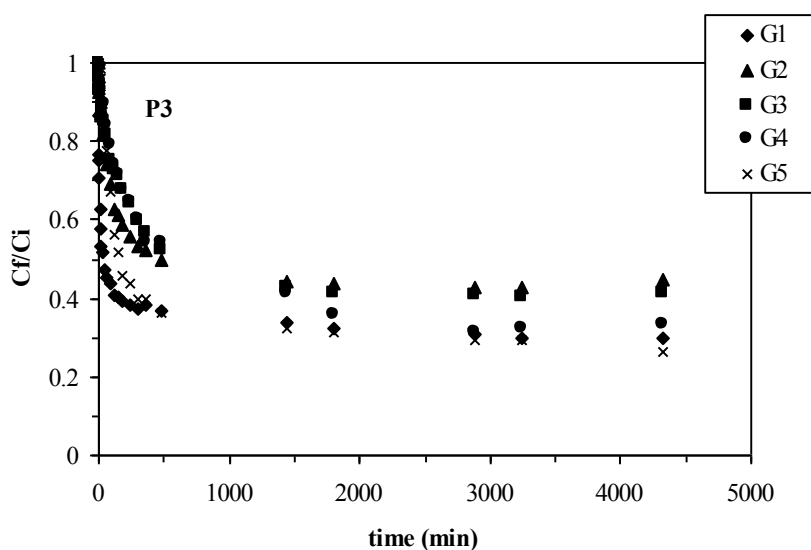
Figure 92 Influence of sorbent particle size on mercury biosorption (pH$_i$=5, P3 sample, 50 mg Hg L^{-1}, 300 mg sorbent L^{-1})

The details are displayed in Figure 93, where the first 8 hours of experiment are presented. From this figure it is apparent that there was a great difference in the rate of biosorption. The fastest decrease in concentration was observed for G1 fraction, which attained an apparent equilibrium after 4 hours of experiment. G5 fraction reached this equilibrium with the same efficiency after 5 hours and the other fractions followed this behaviour and attained the equilibrium only after 6 hours of experiment and with lower efficiency of the process.

The irregularities observed in the case of the G5 fraction can be explained by the apparently big size of the particles and their possible heterogeneity or an insufficient separation during the sieving process, which could have resulted in sticking of smaller particles on the surface of G5 particles. The possibility of disintegration of particles within the agitation process can neither be excluded.
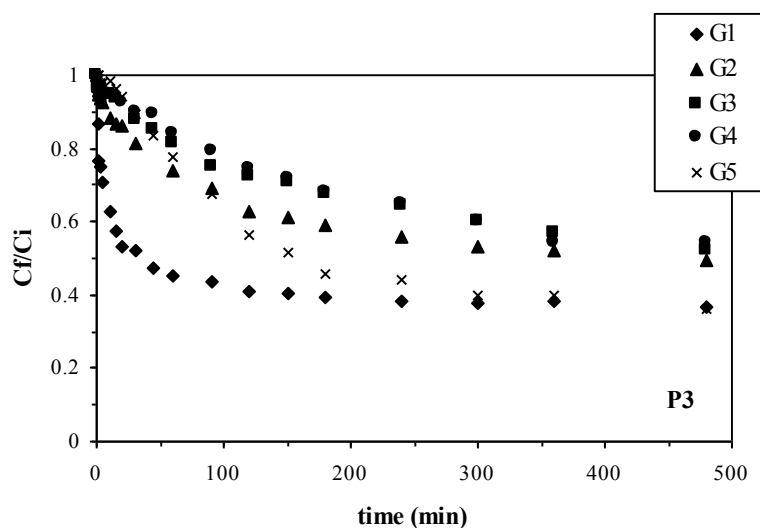
Figure 93 Influence of sorbent particle size on mercury biosorption – detail first 8 hours of experiment (pH$_i$=5, P3 sample, 50 mg Hg L^{-1}, 300 mg sorbent L^{-1})

Figure 94 shows the same dependence for T sample. In this case more regular behaviour was observed and the influence of particle size seemed to be even more pronounced. The highest efficiency was obtained for G1 fraction. For the other fractions the concentration decrease was slower but alike for all four remaining fractions. The main differences were observed in biosorption efficiency in the second slower phase of the process.
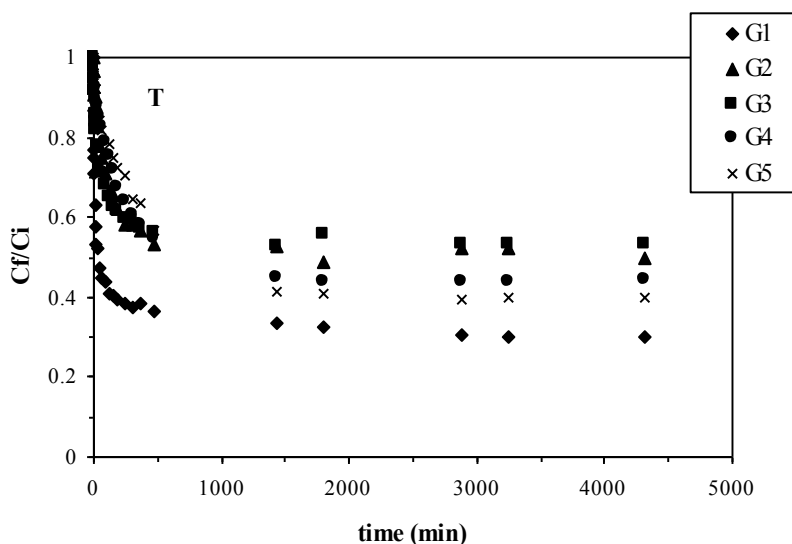
Figure 94 Influence of sorbent particle size on mercury biosorption (pH$_i$=7, T sample, 50 mg Hg L^{-1}, 300 mg sorbent L^{-1})

The details for the first 8 hours of the experiment are displayed in Figure 95. Very similar behaviour was observed for G2 and G3 fraction and then again for G4 and G5 fractions. Such a phenomenon was also observed by Jansson-Charrier for the vanadium sorption by chitosan.[225]
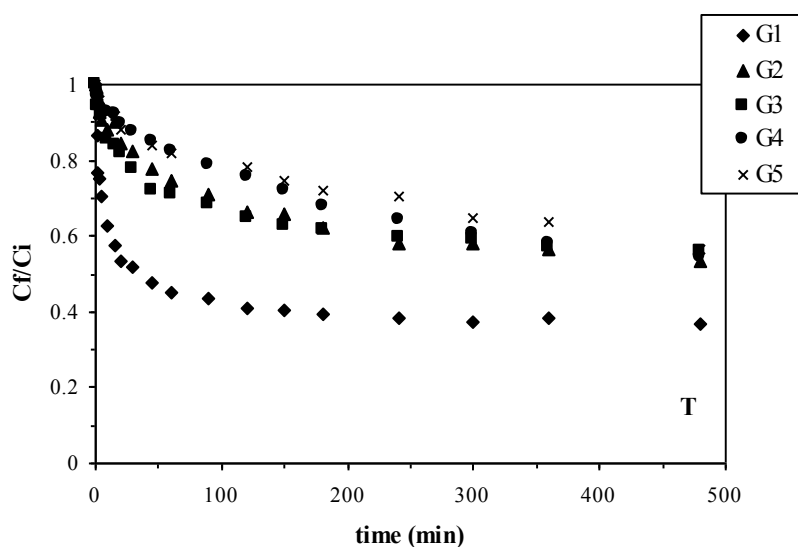
Figure 95 Influence of sorbent particle size on mercury biosorption – detail first 8 hours of the experiment (pH$_i$=7, T sample, 50 mg Hg L^{-1}, 300 mg sorbent L^{-1})

Even in this case, the biosorption process followed second order kinetics, while the Ho's equation described well the experimental data (Table 58, page 293). The value of k2 constant decreased with increasing sorbent size for both samples with the exception G2 fraction for P3 sample, which gave a value close to that of G1 fraction and G3 fraction for sorbent T, which gave also the value close to that of G1 fraction of T sample. These fits are represented in Figure 172 and Figure 173 shown in Appendix B. The decreasing values of k$_2$ parameter indicate the decrease in biosorption rate. This correlates with the observations done on the basis of the decay curves.

The obtained diffusion coefficients were summarized in Table 34. The values of external mass transfer coefficient decreased with increasing sorbent particle size for P3 sample, whereas these values remained stable for T sample, with exception of G1 fraction (which reached a value approximately three times higher).

The decreasing trend was also noted for *K* coefficient of the Weber and Morris model (with the exception of G5 fraction of P3 sample). It worth to point out, that the *K* values

corresponding to G2 and G3 fractions of T sample were very close as well as the values corresponding to G3 and G4 of the same material. This confirms the observation performed on the basis of the decay curves.

Biosorbent	d_p	External mass transfer model		Intraparticular mass transfer model			
				W&M		*U&T*	
		β_L	R^2	K	R^2	D	R^2
		[10^{-5} m min^{-1}]	-	[mg g^{-1} min$^{-0.5}$]	-	[10^{-10} m^2 s^{-1}]	-
	G1	2.9	0.963	10.6	0.950	4.2	0.939
	G2	1.9	0.873	5.3	0.993	5.8	0.992
P3	G3	1.0	0.569	3.6	0.957	4.9	0.971
	G4	0.9	0.840	2.9	0.946	5.2	0.918
	G5	0.7	0.878	4.4	0.873	19.9	0.888
	G1	7.2	0.870	10.5	0.892	6.1	0.929
	G2	1.8	0.795	5.2	0.971	7	0.982
T	G3	2.7	0.934	6.6	0.986	26.6	0.988
	G4	1.3	0.892	3.6	0.984	10.6	0.995
	G5	1.3	0.812	3.2	0.967	16.5	0.960

Table 34 Effect of sorbent dosage on the diffusional constants – results (initial metal concentration 50 mg Hg L^{-1}, sorbent dosage 300 mg L^{-1})

On the contrary, the coefficient *D* of Urano and Tachikawa model remained stable for G1 - G4 size fraction of P3 sample and increased suddenly for G5 fraction. For T sample its value varied between 6.1 – 26.6 10^{-10} m^{2}s^{-1} regardless of tested parameter. No visible trend was observed. However, for both P3 and T samples the coefficient D remained within the same range of values.

Jansson-Charrier[225] observed that particle size of chitosan had an important effect on the sorption rate. The increased particle diameter resulted in longer time to reach the equilibrium. The evolution of the diffusion coefficients for the various models was non linear and non proportional. The initial external diffusion rate was increased by lowering the particle size of the sorbent; in the same conditions the intraparticle diffusion rate (W&M) was decreased. This is opposite to our findings, since both coefficients increase with decreasing particle size.

Guibal et al.[226] reported that uranium sorption on glutamate glucan was controlled by intraparticle diffusion as the increasing particle size resulted in a decrease in sorption rate together with extended time before the equilibrium was reached in the system. This was explained by authors by the fact that with increasing particle size the metal ion has indeed a greater intraparticle distance to diffuse before the polymer becomes saturated. The sizes of particles used by each author were comparable to sizes used in this study.

Hellferich[227] showed that for a film diffusion controlled process, the rate is inversely proportional to the particle diameter; while for intraparticle diffusion controlled process it is proportional to the second power of the diameter.

4.4.1.4 Conclusion

The decrease in sorbent/sorbate ratio resulted in the decrease in the efficiency of the process. The P3 sample exhibited in general higher sorption efficiencies than T sample with the only exception at initial concentration 20 mg Hg L^{-1}, where a reverse trend was observed.

The influence of sorbent dosage was not the same at all investigated mercury concentration levels. As expected the increase in sorbent dosage resulted in an increase in sorption efficiency, but at the lowest mercury concentration the T sample revealed more efficient at all three dosages. The efficiencies were comparable for both biomass samples at 50 mg Hg L^{-1}, while the P3 sample was more efficient at the initial concentration 100 mg Hg L^{-1}.

The process followed pseudo second order reaction kinetics and the Ho's equation fitted well the experimental data. The values of constant k_2 decreased and the value of constant q_e increased with the increasing initial concentration. While different trends were observed, when the influence of sorbent dosage was investigated. Regular behaviour was found when the effect of particle size was investigated. Rate constant k_2 decreased with increasing particle diameter, while q_e constant remained stable.

Table 35 recapitulates trends observed when the diffusion phenomena were studied.

Biosorbent	Tested parameter	External mass transfer model	Intraparticle diffusion model	
			W&M	**U&T**
		β_L	**K**	**D**
		$[m\ min^{-1}]$	$[mg\ g^{-1}\ min^{-0.5}]$	$[m^2\ min^{-1}]$
	increasing C_i	decrease	increase	no influence
P3	increasing SD	no influence	NS	no influence
	increasing d_p	decrease	decrease	no influence
	increasing C_i	decrease	increase	no influence
T	increasing SD	no influence	decrease	no influence
	increasing d_p	NS	decrease	NS

Table 35 Effect of tested parameters on diffusion phenomena within mercury biosorption (NS – non significant results)

For each sorbent sample the increase in concentration resulted in the decrease in external transfer rate, while parallely the rate of intraparticle transfer increased. On the other hand the D coefficient (U&T model) was not affected by the tested parameters, even though the model fitted well experimental data.

It was difficult to discuss the effect of the sorbent dosage. Different behaviours were obtained at different concentration levels.

Whereas the influence of particle sizes was clearly distinguished, but remained difficult to explain. Both external and intraparticle transfer rate constants decreased with the increase of particle diameter, while the diffusion coefficient D was not affected.

When Biots number ($B_i=\beta_L d_p/D$) was calculated from the ratio of the rate of external mass transfer to intraparticle mass transfer, the obtained values were lower than one indicating that the overall rate of the process was controlled by the rate of external diffusion.

4.4.2 Hexavalent chromium

The analyses of both forms of chromium (Cr_{total} and Cr(VI)) were performed all along all kinetics experiments and these values were continuously compared. If not indicated otherwise, the results presented in this chapter correspond to the hexavalent chromium

amount. The results corresponding to the total chromium amount are displayed only when a discrepancy between these two values was observed.

4.4.2.1 Influence of initial metal concentration

The influence of initial hexavalent chromium concentration was investigated at first. Figures 96 and 97 present the plots of the residual/initial metal concentration ratio versus time using P3 and T sorbent samples, respectively. The sorbent dosage was fixed at 300 mg L^{-1} and three different values of hexavalent chromium concentration were tested (20, 50, 100 mg Cr(VI) L^{-1}). The experimental conditions were maintained similar to those used in the case of mercury.

The efficiency of the process decreased with increasing chromium concentration for both biosorbent samples, but this decrease was not proportional to the increase in concentration. Close results were obtained at initial concentrations 50 and 100 mg Cr L^{-1} (25 and 14%, respectively) with P3 sample. Additionally, these values were slightly lower than those expected according to results of isotherm determination. This would indicate that the process took place solely on the surface of biosorbent's particles and not in its entire volume and was probably more influenced by the boundary layer thickness and consequently by the concentration gradient.

Surprisingly, an efficiency reaching 100% was observed at initial concentration 20 mg L^{-1}. Though, a turbidity of the solution was observed from the 420th minute of the experiment. This turbidity was provoked by a partial dissolution of P3 sorbent material, while creating a colloid in the solution (as described in chapter 4.1.2). The phenomenon was undoubtedly responsible for the high efficiency observed. It is worth to note that although the final hexavalent concentration approached zero, the total chromium concentration remained stable around the value of 7 mg Cr_{total} L^{-1}. Hence, this process could be connected with the reduction phenomenon. To prevent this behaviour (dissolution of sorbent) the experiments were not performed with sorbent dosage 100 mg L^{-1} as a low sorbent dosage at low experimental pH seemed to be susceptible to such a process and thus these phenomena did not occur later.
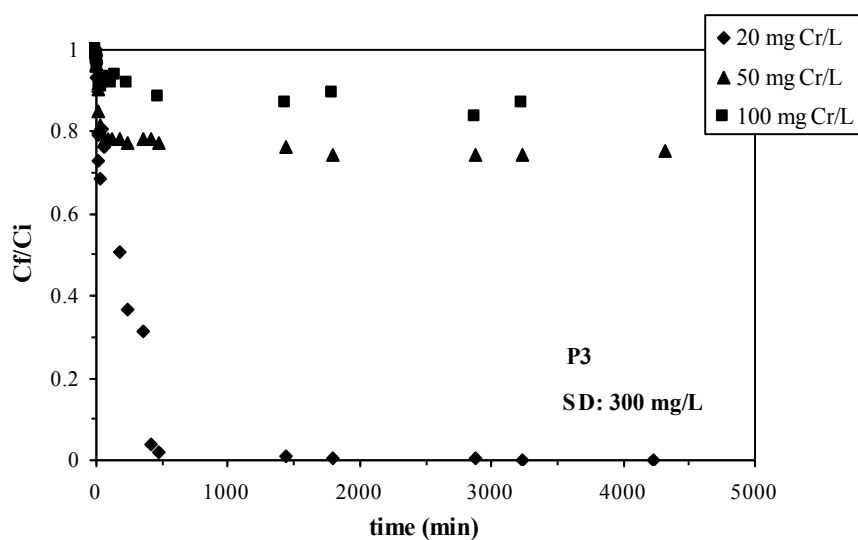
Figure 96   Influence of hexavalent chromium concentration on sorption kinetics (pH$_i$=3, P3 sample, 300 mg sorbent L^{-1})

Very close sorption efficiencies (approx. 25%) were obtained for T sample in the case of initial concentrations 50 and 100 mg Hg L^{-1} as well (details in Figure 97). Nevertheless, the system at 50 mg L^{-1} reached the equilibrium earlier. On the opposite hand, a very high efficiency (80%) was found at the initial concentration 20 mg L^{-1}. As indicated in Figure 97, the process did not even attain its equilibrium in this case as the actual concentration of the solution was still decreasing, despite a very long contact time. However, the equilibrium was clearly attained for the two other concentration levels tested.

The observed efficiencies were very close to the values expected according to the maximum sorption capacity derived from the Langmuir equation. Hence, it could be assumed that the sorbent was saturated (or close to saturation) at the three tested concentration levels.

When T sample was used a discrepancy between hexavalent (Figure 97) and total chromium (Figure 98) content was detected in agreement with the observations done within the previous experiments.
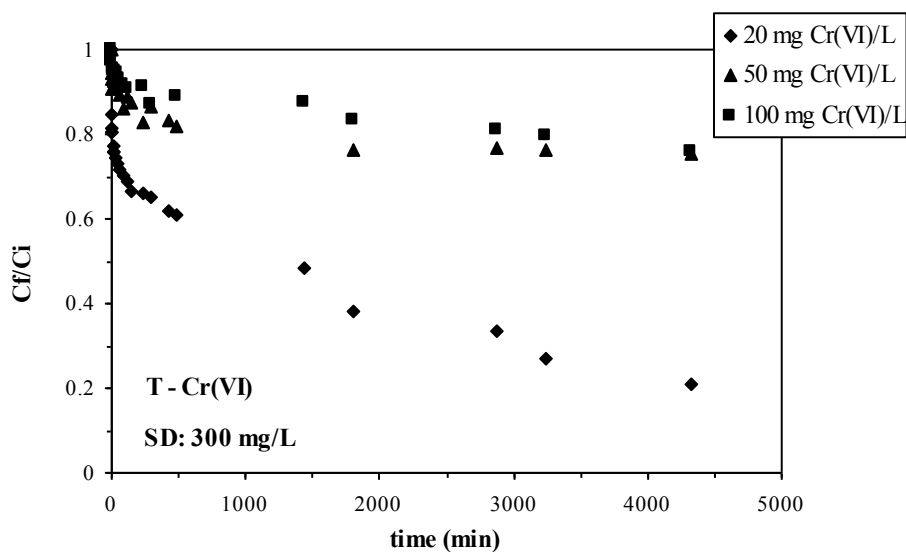
Figure 97 **Influence of hexavalent chromium concentration on sorption kinetics (pH$_i$=2, T sample, 300 mg sorbent L^{-1})**
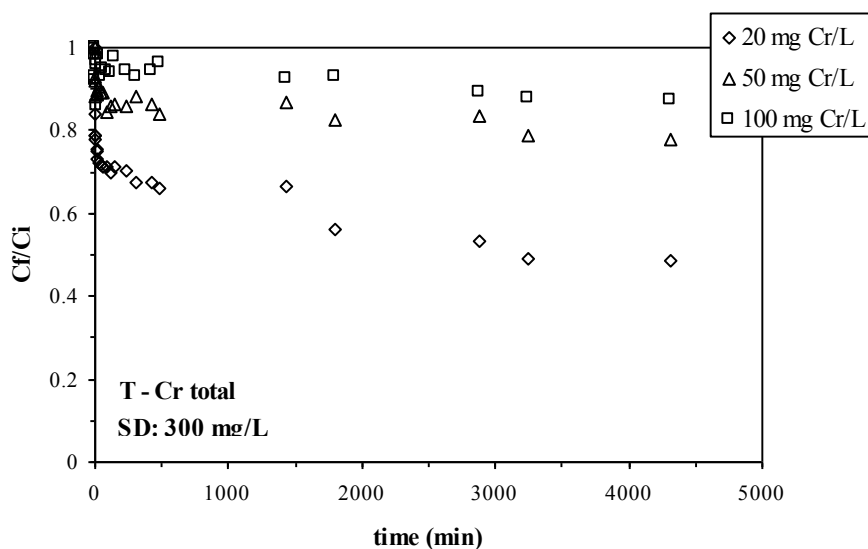
Figure 98 **Influence of total chromium concentration on sorption kinetics (pH$_i$=2, T sample, 300 mg sorbent L^{-1})**

Chromate anions are known as a strong oxidizing agent. When present in surface waters they can be easily reduced by ferrous ions, sulphides, humic acids and other organic matter containing SH functional group.[28] Acidic environment promotes such a process. As reported in chapter 2.2.1.8 and confirmed within our experiments the hexavalent chromium biosorption takes place solely in acidic solutions. The proper mechanism of this process is not clear and several hypotheses were proposed – namely electrostatic attraction between

protonated sorption sites and anionic metal species[55], reduction[120], combined process of reduction and sorption[37,122].

The determination of biosorption isotherms enabled to describe the equilibrium in system, where both forms of chromium (Cr^{3+}, Cr(VI)) were identified, while kinetics experiments enabled to observe the evolution of their contents as a function of time. The markedly highest difference was found at initial concentration 20 mg Cr(VI) L^{-1} and this fact is illustrated in Figure 99. A simultaneous decrease of both values was found in the first period, but the hexavalent chromium decrease continued at a higher rate than the total chromium decrease. It is likely, that the total chromium decrease attained its equilibrium, while its hexavalent content did not. The decrease in total chromium content is undoubtedly connected with the sorption phenomenon, while the difference between these two values has to be related to the reduction process. This would signify that during the first period the system was governed by sorption process as chromium was completely removed from the liquid phase. Whereas, after this first period the sorption process attained its equilibrium (negligible decrease in total chromium concentration), while the hexavalent chromium content continued to decrease, certainly due to a reduction process. Its worth to note that neither precipitation nor colour change were observed during the experiment and the suspension remained yellow.
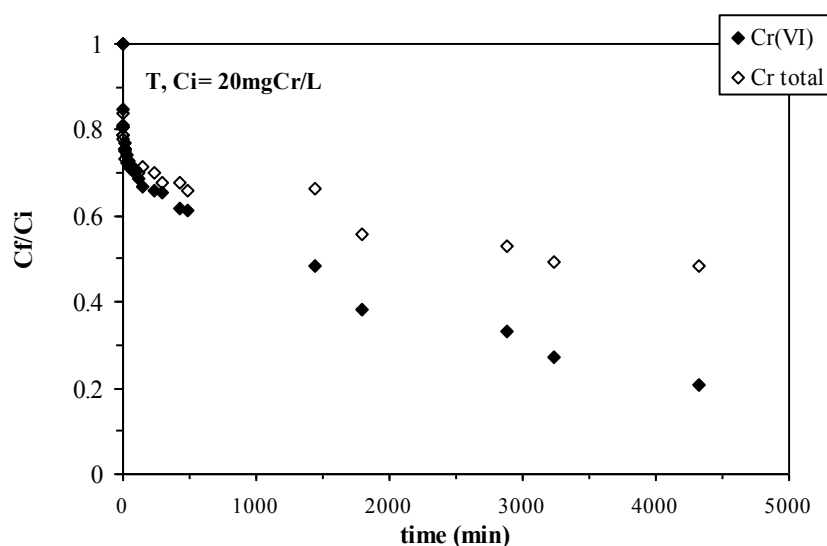
Figure 99 Comparison hexavalent/total chromium decrease (sorbent T)

Kratochvil et al.[37] suggested the hypothesis of a combined-ion exchange – redox process based on simultaneous or subsequent uptake of $HCrO_4^-$ anion by a process similar to

ion exchange on weak anion resins and its reduction (details in Figure 6, page 34). In such a system, the biomass has to enable the reduction of hexavalent chromium. The pH of the system seemed to play a crucial role in the process. According to Kratochvil et al. the uptake of chromium from solutions by biomass was maximized at a pH value low enough to shift the equilibrium of the anion-exchange reaction to the right, but still high enough to be in the vicinity of $pH_{critical}$ so that the reduction of $HCrO_4^-$ to Cr^{3+} did not dominate the system. If this hypothesis is valid, it could explain the obtained results. Furthermore Cabatingan et al.[122] also reported a simultaneous sorption/reduction process. They observed that the biosorption and reduction were two parallel processes occurring at different rates and they proved that both processes were coupled in a parallel way.

It is worth to note that the higher was the sorbent/sorbate ratio the higher discrepancy between hexavalent and total chromium content was observed. So a high sorbent/sorbate ratio seems to support the reduction process. This phenomenon will be illustrated further in the next chapter.

The Ho's and the Lagergren's equations were again applied to experimental data in order to describe the kinetics of the process. When the Ho's relationship was employed, a good correlation with experimental results was obtained as illustrated in Table 36 and displayed in Figures 158 - 159 for both P3 and T sorbent, respectively. Figures 158 - 159 and the linearized plots of experimental data are listed in Appendix D (Figures 160 - 161).

Irregular evolution of model parameters was found for both sorbent samples. Results corresponding to initial concentration 20 mg L^{-1} (P3 sample) were not considered relevant due to the partial dissolution of the sorbent and colloid formation, which made the discussion of results for P3 sample rather difficult.

Several conclusions could be drawn from the comparison of data corresponding to hexavalent and total chromium removal by T sorbent. The k_2 parameter followed the same trend for both chromium forms; however, its values were higher for total chromium and did not differ as much. While all three values of q_e parameter were very close, but in general lower than the values corresponding to hexavalent chromium uptake. The highest discrepancy was observed for the initial concentration 100 mg L^{-1}.

Biosorbent		C_i	k_2	g_e	R^2
		[mg L^{-1}]	[10^{-5} g mg^{-1} min^{-1}]	[mg g^{-1}]	-
P3		20	14.2	58.8	0.996
		50	91.5	42.4	0.999
		100	41.8	40.7	0.998
T	*Cr(VI)*	20	12.9	47.7	0.974
		50	26.6	41.1	0.996
		100	7.1	73.2	0.953
	Cr$_{total}$	20	29.4	35.6	0.983
		50	36.5	34.2	0.979
		100	26.7	38.3	0.992

Table 36 The effect of initial metal ion concentration on chromium biosorption kinetics at 300 sorbent L^{-1} – pseudo second-order reaction-rate fit (C_i: initial metal ion concentration, k_2: rate constant, g_e: metal ion removal capacity at equilibrium, R^2: correlation coefficient)

When Lagergren's equation was fitted to experimental data quite satisfactory correlation coefficients were obtained. Although this fact usually signifies a good fit, the model tended to under-predict the experimental data as illustrated in Table 59 presented in Appendix D.

Concerning the evaluation of the limiting step of the chromium biosorption, the same relationships were used for the determination of the diffusion rates and related coefficients as in the case of mercury. The results are summarized in Table 37.

Biosorbent			External mass transfer model		Intraparticular mass transfer model			
					W&M		*U&T*	
		C_i	β_L	R^2	K	R^2	D	R^2
		[mg L^{-1}]	[10^{-5} m min^{-1}]	-	[mg g^{-1} min$^{-0.5}$]	-	[10^{-11} m^2 min^{-1}]	-
P3		20	5.9	0.987	2.0	0.656	3.9	0.346
		50	2.1	0.975	5.4	0.970	91.1	0.983
		100	1.0	0.980	4.6	0.968	59.7	0.974
T	Cr(VI)	20	2.4	0.500	1.7	0.681	6.7	0.739
		50	0.9	0.561	1.8	0.700	9.7	0.700
		100	0.6	0.793	2.6	0.912	4.7	0.910

Table 37 Effect of sorbent dosage on the diffusional constants (initial metal concentration 300 mg Cr L^{-1})

Results corresponding to initial concentration 20 mg L^{-1} (P3 sample) were not considered relevant due to the partial dissolution of the sorbent and colloid formation, which had to influence the diffusion process certainly. The fact that there was no dissolution observed at higher metal concentration seemed to signify that the presence of metal somehow stabilized the sorbent. By the way, the biosorption process changed the colour of the sorbent from beige in the beginning to ochre at the end of experiments due to the presence of chromium on the biomass surface.

Despite this fact, the external diffusion coefficient β_L decreased significantly with the increase in initial metal concentration from 50 mg Cr(VI) L^{-1} to 100 mg Cr(VI) L^{-1}. On the opposite hand, the rate of intraparticle mass transfer (K) lowered only infinitesimally, whereas the value of coefficient D decreased markedly. It should be kept in mind that at 50 and 100 mg Cr(VI) L^{-1} the saturation of the sorbent material was not achieved and the process had to take place predominantly on its surface, so it was more sensitive to the effect of external mass transfer.

With T sorbent, low values of correlation coefficients make any reasonable interpretation of the results difficult. This low fit was not caused by a fluctuation of experimental data, but by the fact that the data revealed a rather logarithmic dependence instead of a linear one (corresponding plots listed in Appendix D). This may signify that the artificial separation of external and inparticular diffusions was not appropriate in this case or it may be due to combined sorption/reduction process.

Guibal et al.[228] investigated the sorption of two other anions (vanadate and molybdate) by chitosan beads and flakes and found that sorption kinetics was mainly controlled by intraparticle diffusion for beads, while for flakes the controlling mechanisms were both external and intraparticle diffusion. When metal anion concentration influence was tested, the β_L value varied inversely with the initial concentration (as a power of the initial molybdate concentration). For flakes it was decreasing by over an order of magnitude. It seemed that external diffusion contributed to the control of the rate, principally for flakes. Increasing the initial concentration reduced the contribution of external film resistance (the lower the intercept of W&M model, the thinner the boundary layer). On the opposite hand the variations of coefficient D did not follow any trend, but molybdate gave higher values than vanadate.

4.4.2.2 Influence of sorbent dosage

The influence of sorbent dosage was tested at only one concentration level (i.e. 50 mg Cr(VI) L^{-1}). Figures 100 and 101 represent the plots for P3 and T sorbent samples, respectively. The sorbent dosages corresponded to those used with mercury (100, 300, 500 mg sorbent L^{-1}).
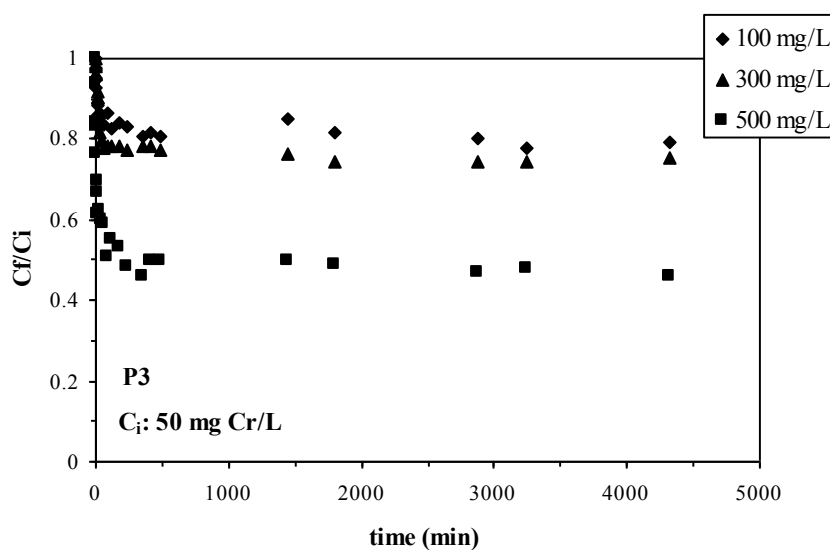
Figure 100 Influence of sorbent dosage on hexavalent chromium sorption kinetics (pH$_i$=3, P3 sample, 50 mg Cr(VI) L^{-1})

Contrary to the conclusions drawn for mercury, the sorption efficiencies for Cr(VI) at sorbent dosages 100 and 300 mg L^{-1} were comparable (approx. 20%) and much higher sorption efficiency was observed at 500 mg sorbent L^{-1} for P3 sample (55%). The sorption efficiency at 100 mg L^{-1} slightly exceeded the expected value, whereas it revealed to be slightly lower at 300 mg L^{-1} and at 500 mg L^{-1}.

Similar conclusions could be drawn on the behaviour of the T sample while only one difference was found. Apparently, the sorption system at 500 mg sorbent T L^{-1} did not attain the equilibrium during the experiment. This is illustrated in detail in Figure 102, where the hexavalent and total chromium concentration decreases are compared (500 mg sorbent L^{-1} and 50 mg Cr(VI) L^{-1}). It is obvious that the total chromium content levelled off after 30 hours of experiment, while the hexavalent chromium concentration was still decreasing. This was also the second case, where a significant discrepancy of these two values was observed. As already

suggested, it seems that a high sorbent to sorbate ratio (i.e. an excess of sorbent) promotes the reduction process.
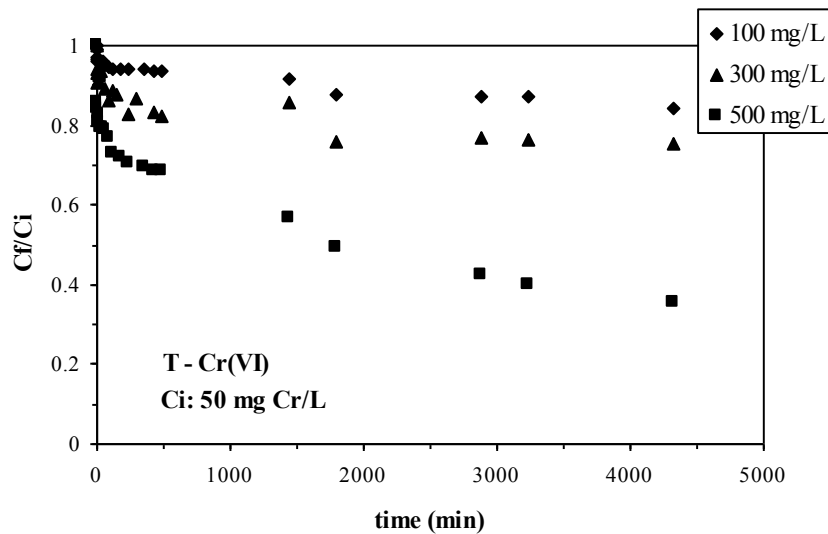
Figure 101 Influence of sorbent dosage on hexavalent chromium sorption kinetics (pH$_i$=2, T sample, 50 mg Cr(VI) L^{-1})
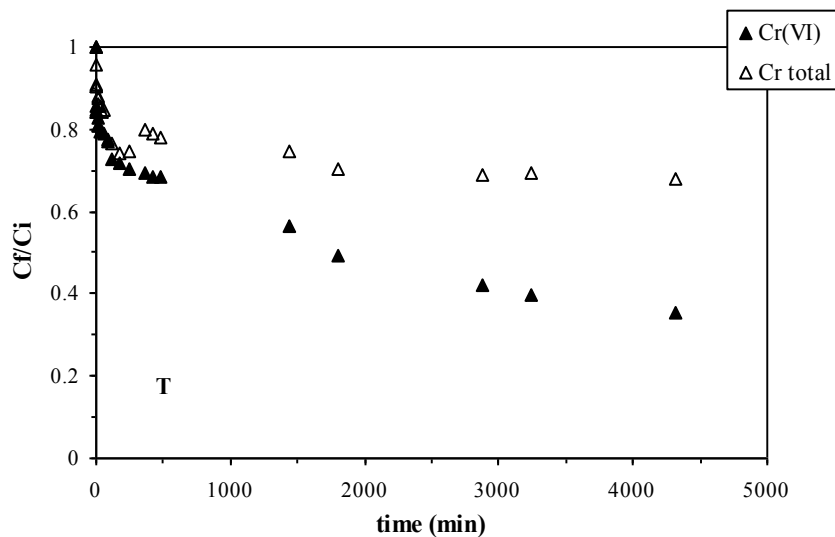
Figure 102 Influence of sorbent dosage on hexavalent chromium sorption kinetics – comparison of the efficiency Cr(VI)/Cr$_{total}$ (pH$_i$=2, T sample, 50 mg Cr(VI) L^{-1}, 500 mg sorbent L^{-1})

The comparison of corresponding parameters of Ho's equation revealed, that with both biomass samples the value of k_2 rate constant increased with the increasing sorbent dosage, while the value of q_e constant decreased. Nevertheless, the k_2 values corresponding to P3

sample were several times higher than the values corresponding to T sample (as illustrated in Figures 162 – 163 and summarized in Table 60 listed in Appendix D). When the total and hexavalent chromium decrease were compared, an increasing trend in their discrepancies was observed, which corresponds well to the previous conclusion.

Bayramoglu et al.[58] studied hexavalent chromium sorption on fungal biomass of *Lentinus sajor-caju* and investigated the influence of sorbent dosage on biosorption rate. An increase in the efficiency was found, but it was realized then after certain efficiency was reached, a further increment of the biomass dose did not provide sufficient improvement in efficiency. Lagergren's and Ho's equations were also used to fit experimental data, while the first order kinetics equation (Lagergren) described better the experimental data. An inverse conclusion was done in the present study.

When the diffusion phenomena were studied, the results obtained for T sample were non-exploitable due to the low correlation coefficients as illustrated in Table 38. The data revealed again a logarithmic dependence.

Biosorbent			External mass transfer model		Intraparticular mass transfer model			
					W&M		*U&T*	
		SD	β_L	R^2	K	R^2	D	R^2
		$[mg\ L^{-1}]$	$[10^{-5}\ m\ min^{-1}]$	-	$[mg\ g^{-1}\ min^{-0.5}]$	-	$[10^{-11}\ m^2\ min^{-1}]$	-
P3		100	5.2	0.836	9.9	0.872	46.0	0.869
		300	2.1	0.975	5.4	0.970	91.1	0.983
		500	3.7	0.888	5.5	0.852	57.7	0.831
T	**Cr(VI)**	100	0.1	0.382	2.2	0.614	4.7	0.642
		300	0.9	0.561	1.8	0.700	9.7	0.700
		500	1.0	0.429	1.6	0.589	5.1	0.632

Table 38 Effect of sorbent dosage on the diffusional constants (initial metal concentration 50 mg Cr L^{-1})

With P3 sample the influence of diffusion phenomena was not clear. The highest value of β_L corresponded to 100 mg L^{-1}, than followed 500 mg L^{-1} and the lowest value corresponded to 300 mg L^{-1}. The highest intraparticle transport rate was obtained also at 100 mg L^{-1}, while similar values were found for 300 and 500 mg L^{-1}. The highest diffusion coefficient *D* was obtained for sorbent dosage 300 mg L^{-1}, than followed 500 and 100 mg L^{-1}.

Sag and Aktay[151] studied hexavalent chromium biosorption onto chitin. They interpreted its kinetics in the scope of mass transfer and used the same models as in the present study. An increased uptake efficiency with increasing sorbent dosage was described and this was ascribe to increasing adsorption surface area, whereas the sorption capacity (mg Cr(VI) g^{-1} biomass) decreased. This trend was confirmed within our experiments too. A reduced rate of uptake process and, hence, a prolonged time to reach the equilibrium was found by authors. The external mass transfer coefficient and intraparticle diffusion coefficient D were not influenced by increasing sorbent dosage; though an important increase in intraparticle mass transfer rate (K value) was observed.

4.4.2.3 Influence of sorbent size

The influence of particle diameter on hexavalent chromium biosorption kinetics was also studied. Five fractions of different particle size were used as in the case of mercury. The significant influence of this parameter was apparently not found in this case (see Figures 103 and 105).
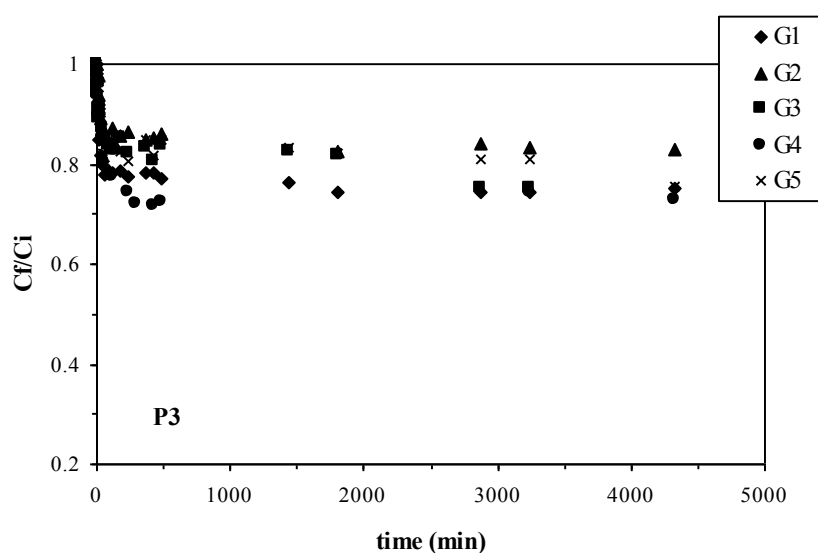
Figure 103 Influence of sorbent particle size on hexavalent chromium biosorption (pH$_i$=3, P3 sample, 50 mg Cr(VI) L^{-1}, 300 mg sorbent L^{-1})

Figure 104 reflects the process within the first 8 hours of experiment for P3 sample. Regardless of slight dispersion of experimental points, no significant effect of tested parameter was found. The G1 fraction exhibited slightly faster concentration decrease.
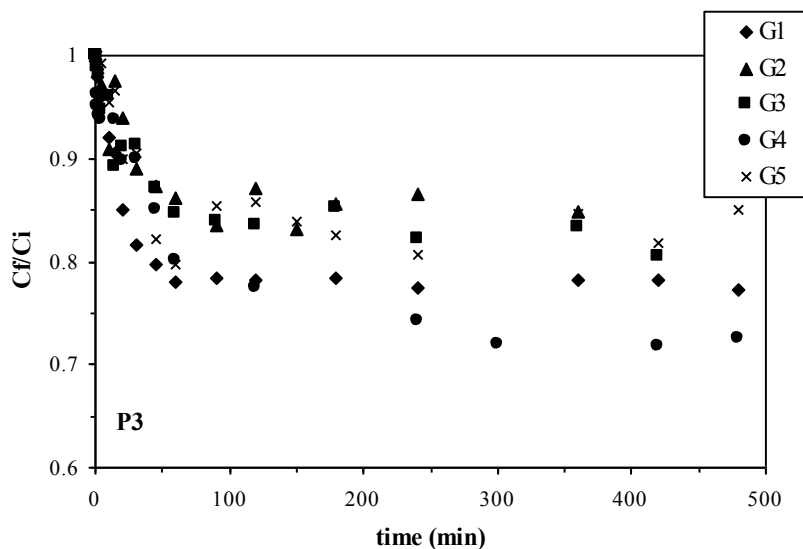
Figure 104 Influence of sorbent particle size on hexavalent chromium biosorption – detail first 8 hours of experiment (pH$_i$=3, P3 sample, 50 mg Cr(VI) L^{-1}, 300 mg sorbent L^{-1})

No significant effect of particle size was found either when T sample was used (Figure 105). The concentration decrease was slower than for P3 sample and it is not clear whether the equilibrium was really attained.
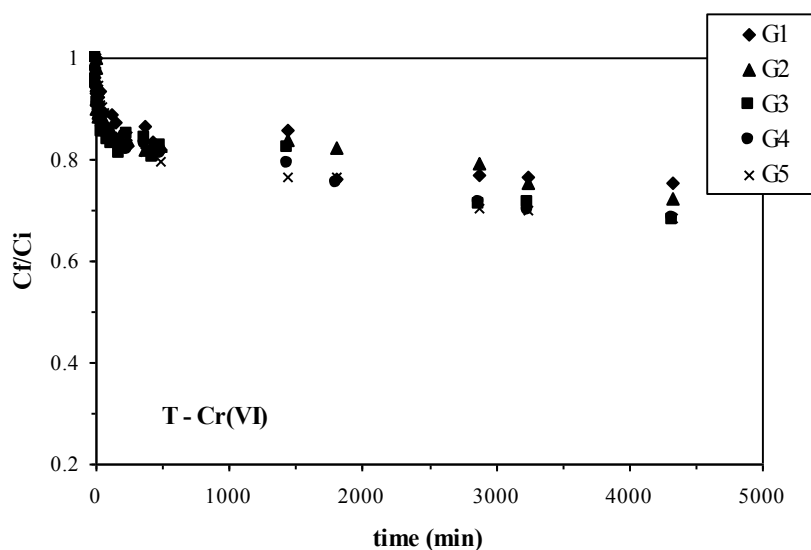
Figure 105 Influence of sorbent particle size on hexavalent chromium biosorption (pH$_i$=2, T sample, 50 mg Cr(VI) L^{-1}, 300 mg sorbent L^{-1})

The details are exposed in Figure 106, where the decay curves correspond to the first 8 hours of experiment. Regardless a slight fluctuation of experimental points no significant effect of particle diameter is obvious from the figure. The fact that chromium biosorption was not sensitive to the change of particle diameter and consequently to the change of surface area would signify that the overall process was not controlled by a phenomenon sensitive to specific surface.
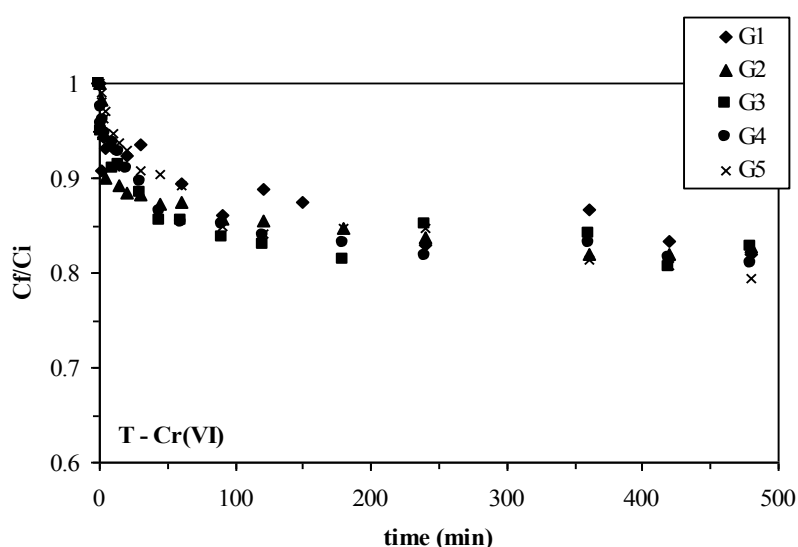
Figure 106 **Influence of sorbent particle size on hexavalent chromium biosorption – detail the first 8 hours of experiment (pH$_i$=2, T sample, 50 mg Cr(VI) L^{-1}, 300 mg sorbent L^{-1})**

The Ho's equation fitted well the experimental data in this case also, but no general trend was obvious in the results summarized in Table 61 (Appendix C). A big dispersion in the values of k$_2$ parameters was observed for P3 sample, while with T sample a slight decrease in the values was observed with increasing particle diameter.

When diffusion phenomena were studied, no general trend was found in obtained results. For P3 sample the external mass transfer coefficient reached the highest value for G1 fraction, while it was slightly lower and rather similar for other fractions. Low correlation coefficients were obtained for G2 fraction (dispersion of experimental points) and G4 fraction (logarithmic dependence of experimental data). Intraparticle mass transfer coefficient *K* reached similar values for G1 and G5 fractions and then again for G2, G3 and G4 fractions. Surprisingly and contrary to the findings done for mercury kinetics, a strong influence of tested parameter was observed for diffusion coefficient *D* (U&T model). Its values were

increasing exponentially with the increase in particle diameter. Similar behaviour was not found in the literature.

For T sample, no effect was found neither on the values of β_L coefficient nor on the values of K parameter. Whereas a significant influence of particle size on the values of D coefficient was also observed, even though this increase was less pronounced than for P3 sample.

Biosorbent		External mass transfer model		Intraparticular model			
				W&M		U&T	
	d_p	β_L	R^2	K	R^2	D	R^2
		[10^{-5} m min^{-1}]	-	[mg g^{-1} s$^{-0.5}$]	-	[10^{-11} m^2 s^{-1}]	-
	G1	2.1	0.975	5.4	0.970	91.1	0.983
	G2	1.2	0.495	3.5	0.816	272.5	0.911
P3	G3	1.5	0.831	3.3	0.910	234.7	0.909
	G4	1.0	0.657	3.5	0.914	683.0	0.868
	G5	1.4	0.836	5.7	0.940	2671.7	0.902
	G1	0.9	0.561	1.8	0.7	9.7	0.7
	G2	1.4	0.724	2.6	0.800	59.5	0.731
T	G3	1.5	0.765	3.1	0.954	125.3	0.949
	G4	1.0	0.843	2.8	0.986	258.6	0.991
	G5	0.9	0.883	2.3	0.969	301.3	0.962

Table 39   Effect of sorbent dosage on the diffusional constants – results (initial metal concentration 50 mg Cr(VI) L^{-1}, sorbent dosage 300 mg L^{-1})

Sag and Aktay[151] observed that for Cr(VI) sorption on chitin the values of both β_L coefficient and D coefficient slightly increased with increasing particle diameter, while the intraparticle transfer rate (K parameter) decreased. Moreover the coefficient values were of the same order of magnitude as in the present study. Authors concluded that the diffusion coefficients found in their study were slightly lower than those obtained in water or porous solids.

Guibal et al.[228] reported following observations for molybdate and vanadate sorption on chitosan beads and flakes. In the case of flakes, the variations with particle size were not appreciable. In the case of beads, the sorption rate decreased with increasing particle size as the time required to reach equilibrium significantly increased. The external transfer rate

decreased, while the external boundary layer thickness increased and the intraparticle transfer rate decreased only slightly with increasing bead size. Authors concluded that mass transfer in molybdate system was controlled by both intraparticle and external resistance for flakes and that the predominant control depended on the experimental conditions. When compared to molybdate, vanadate sorption was more rapid. All kinetics parameters were greater for molybdate than vanadate and this fact was more pronounced for beads. Flakes exhibited a similar behaviour for metals in terms of size effect. It appeared that for both metals the coefficient D remained independent of particle size for beads but not for flakes. It was concluded that the models described well the behaviour of beads, while they did not adequately represented flaked materials behaviour. However, this simplified approach was sufficient to give an evaluation of the parameter effect and to select which parameters controlled sorption kinetics.

4.4.2.4 Conclusion

The efficiency of the process decreased with increasing hexavalent chromium concentration, but as expected it increased with the increase in the sorbent dosage. In general, the process was less efficient than the mercury biosorption at selected experimental conditions. The process was also complicated by the partial reduction of hexavalent chromium to its trivalent form in case of T biosorbent, particularly at high sorbent dosage and low metal concentration.

The biosorption process followed very well the pseudo second order kinetics, while the pseudo first order reaction rate relationship largely under-predicted the experimental results, despite quite satisfactory correlation coefficients obtained.

Consistently with the findings done for mercury, the values of k_2 rate constant decreased with increasing initial concentration and increased with increasing sorbent dosage.

Very low correlation coefficients were obtained with T sample when diffusional models were applied to experimental data, which could signify that diffusion was not the rate limiting process or that the simplified modelling separating external and intraparticle diffusion is not appropriate for describing the system.

With P3 sorbent the results for the modelling of diffusion phenomena were also difficult to interpret. The size of the biosorbent particles (both samples) did not really affect both the rate and the efficiency of the process. Neither the external mass transfer rate nor the

K parameter (W&M model) were directly influenced by increasing particle size. According to these results, it was probable that the sorption process was not restricted to the surface of sorbent particles.

When Biots number was calculated from the ratio of the rate of external mass transfer to intraparticle mass transfer, the obtained values were lower than one indicating that the overall rate of the process was probably controlled by the rate of external diffusion.

4.4.3 Cadmium

Due to very low sorption capacities of both materials towards cadmium presented in the previous chapters a low efficiency of the process was expected for the biosorption kinetics experiments.

4.4.3.1 Influence of initial metal concentration

The influence of cadmium initial concentration was studied at first. Unfortunately, very unsatisfactory results were obtained. This fact was already indicated by the results of biosorption isotherms, where very low sorption capacities were found. The same experimental arrangement was used as in the case of mercury and chromium. The results are displayed in Figures 156 and 157 (Appendix C) as the plots of the residual/initial metal concentration ratio versus time using both P3 and T biosorbent samples, respectively. The sorbent dosage was fixed at 300 mg L^{-1} and three different values of cadmium concentration were tested (20, 50, 100 mg Hg L^{-1}, respectively).

The cadmium sorption was a very fast process completed within few minutes, but unfortunately very low sorption efficiencies were observed. The highest efficiency for P3 sample was found at initial cadmium concentration 20 mg L^{-1}, but it did not exceed 15% and reached only 13%, for other concentrations the efficiency was even lower. Indeed after two days of contact, the metal concentration in solution slightly increased. Furthermore some irregularities were observed, such as partial desorption of cadmium towards the end of the experiments. With T sample the sorption efficiency of the process was approximately the same as for the P3 sample.

4.4.3.2 Conclusion

Due to very low sorption efficiencies even at low concentration of cadmium the kinetics experiments with this metal were not continued. It would have been probably interesting to perform these experiments at lower cadmium concentration and with a very high sorbent dosage, which would lead to an increase in sorption efficiency. However, the objective of this study was to compare the biosorption behaviour at the same experimental conditions (if possible). Additionally, a large scale of materials exhibiting good sorption behaviour towards cadmium was presented in chapter 2.2.1.9. So it was decided to focus the attention on the other three metals yielding better results.

4.4.4 Lead

As already explained in chapter 4.1.4 to prevent the possibility of lead precipitation in case of an accidental increase of pH, lowered values of initial lead concentration were employed in this study (namely 5, 10 and 20 mg Pb L^{-1}). Despite the reduced concentrations, influence of similar parameters (C_i, SD, d_p) on lead biosorption was investigated as in the previous cases of mercury and chromium.

4.4.4.1 Influence of initial metal concentration

Firstly, the effect of initial lead concentration (C_i) was tested at three different sorbent dosage levels (SD: 100, 300, 500 mg L^{-1}). Figure 107 corresponds to an experiment performed with P3 biosorbent at sorbent dosage 300 mg L^{-1}. One common trend was observed all along all experiments performed with lead. As illustrated in Figure 107, a very rapid concentration decrease was observed within the first minutes of experiments, followed by a much slower decrease in following hours.
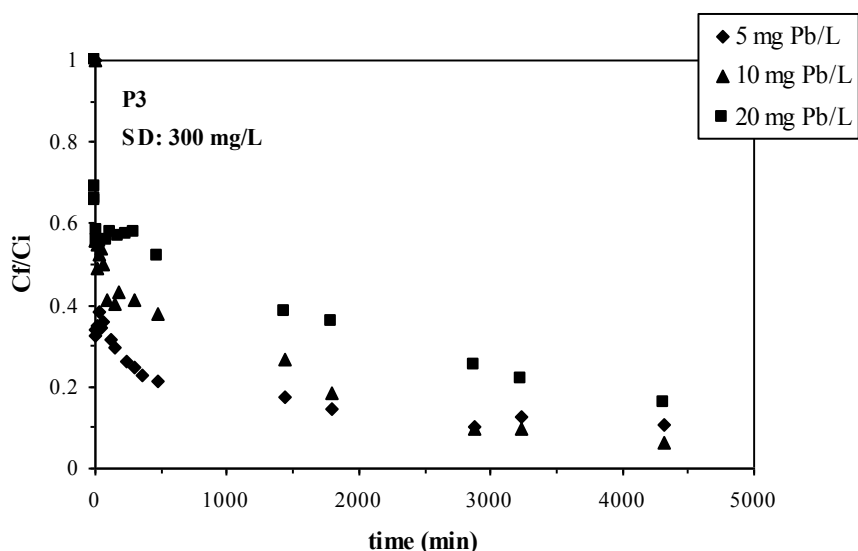
Figure 107 Influence of lead concentration on sorption kinetics (pH$_i$=5, P3 sample, 300 mg sorbent L^{-1})

This fast concentration drop was proportional to the initial concentration and corresponded to the decrease of 70% for 5 mg L^{-1}, 45% for 10 mg L^{-1} and 30% for 20 mg L^{-1}, respectively. Whereas the overall efficiency of the process reached 90% for both 5 mg L^{-1} and 10 mg L^{-1} and 80% for 20 mg L^{-1}. An interesting phenomenon was observed in the case of initial concentration 20 mg Pb L^{-1}, where quasi-equilibrium was established in the sorption system between 10th and 300th minute of the experiment. However, this equilibrium did not sustain and was followed by a further slow concentration decrease in the following stage of the process. This behaviour could be related to the phenomenon of lumps creation (described on page 145) and their slow dissolution. Assuming that lead biosorption was uniquely a surface process, the available surface sites became saturated quickly and quasi-equilibrium was established in the system. With the progressive disintegration of lumps new sorption sites became available and sorption process could continue. This hypothesis explains well the observed phenomenon; however, its confirmation was not obtained.
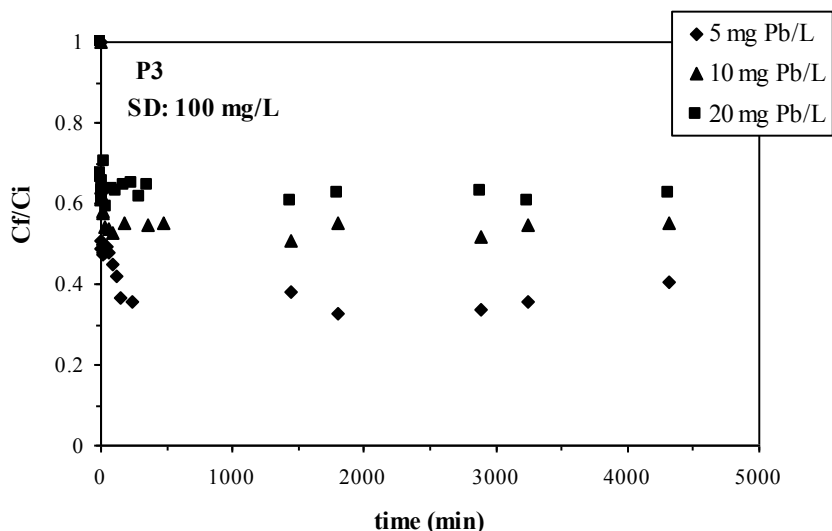
Figure 108 Influence of lead concentration on sorption kinetics (pH$_i$=5, P3 sample, 100 mg sorbent L^{-1})

Apart from lower sorption efficiency, similar sorption behaviour was observed for sorbent dosage 100 mg L^{-1} (Figure 108). This means a rapid concentration drop within the first minutes of experiment and slower decrease in the following period. Additionally, certain dispersion of experimental points was detected at the equilibrium stage. At lower sorbent dosage the formation of agglomerates was decreased and as a consequence the pseudo equilibrium stage was not observed.
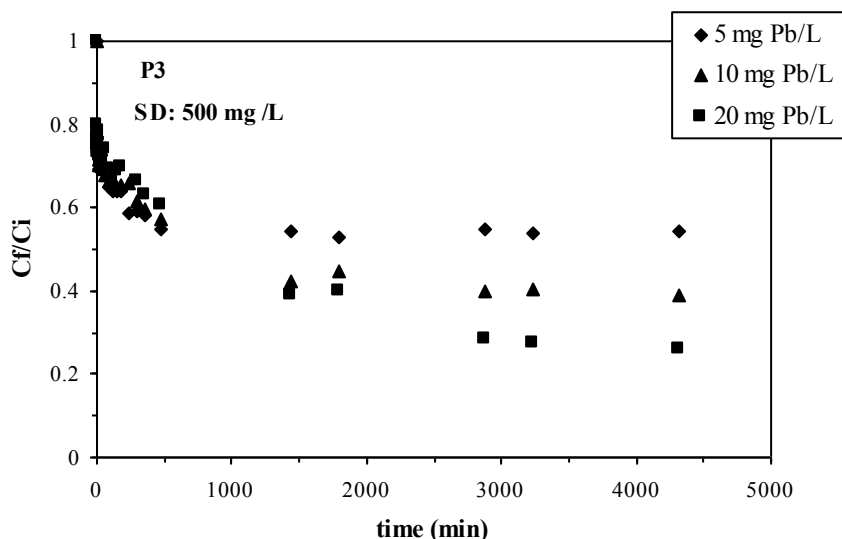
Figure 109 Influence of lead concentration on sorption kinetics (pH$_i$=5, P3 sample, 500 mg sorbent L^{-1})

Completely different behaviour was observed when the sorbent dosage was fixed to 500 mg L^{-1} (Figure 109). Simultaneous decrease of relative concentrations (C$_f$/C$_i$ ratios) was

observed during the first 8 hours (480 minutes) of experiment, while the main difference in the sorption behaviour was found in the second stage of the process. Surprisingly, the system corresponding to initial concentration 5 mg Pb L^{-1} attained its equilibrium first (after 8 hours) and with the lowest observed efficiency (45%). Meanwhile, the concentration decrease continued for systems at 10 and 20 mg Pb L^{-1}. After the equilibria were reached, the efficiencies as high as 60% (after 24 hours) and 75% were found (after 48 hours), corresponding to 10 and 20 mg Pb L^{-1}, respectively. The observed trend of efficiency increasing with increasing metal concentration was completely opposite to the previous observations done for mercury and hexavalent chromium. Furthermore, these findings contradict the logic trend of decreasing sorption efficiency with increasing sorbate/sorbent ratio. No explanation was found to clarify the results. Only if microprecipitation process on biomass surface sorption sites played an important role in the lead uptake, then the observed behaviour would fit the theory well, since the higher was the metal concentration, the higher efficiency was observed. It is thereby well known that the efficiency of precipitation process increases with increasing pollutant concentration. However no confirmation for this hypothesis was obtained.

Dispersion of experimental data was observed during all experiments performed with T sorbent, especially in the equilibrium part of decay curves (as illustrated in Figure 110 for the sorption system at 300 mg sorbent L^{-1}). This dispersion was probably related to the character of lead-biomass interactions. To avoid the possibility of an experimental mistake, these experiments were performed several times, however, the dispersion always occurred.

The rapid drop of concentration within the first minutes of contact was observed also for this biosorbent sample. The efficiency decreased with increasing metal concentration together with a shorter time, which was necessary to reach the equilibrium (300 minutes, 30 minutes and 20 minutes corresponding the initial concentrations 5, 10 and 20 mg Pb L^{-1}, respectively).
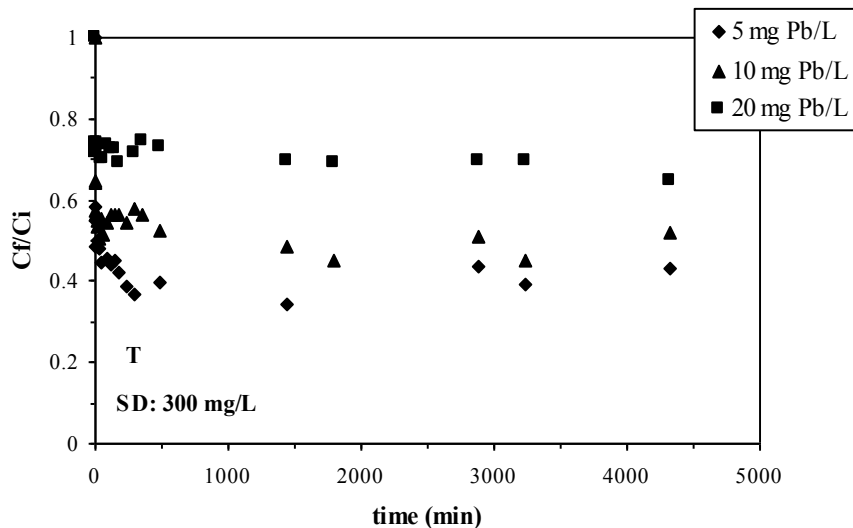
Figure 110 Influence of lead concentration on sorption kinetics (pH$_i$=5, T sample, 300 mg sorbent L^{-1})

Apart from lower sorption efficiency obtained with the lowest sorbent dosage 100 mg L^{-1} (Figure 190 shown in Appendix E), no significant changes in sorption behaviour were observed.

While for sorbent dosage 500 mg L^{-1} (displayed in Figure 111), an interesting behaviour was observed at initial lead concentration 5 mg Pb L^{-1}. In this particular case 100% uptake efficiency was reached. Another interesting observation was done for the sorption system at 20 mg Pb L^{-1} (presented separately in Figure 112), where an important concentration drop was observed within the first 30 minutes of the experiment, but this decrease was then stopped suddenly and a re-increase followed consequently between 30th and 300th minute. The equilibrium was finally established and the overall efficiency reached 45%. No explication was found to explain the observed phenomenon.
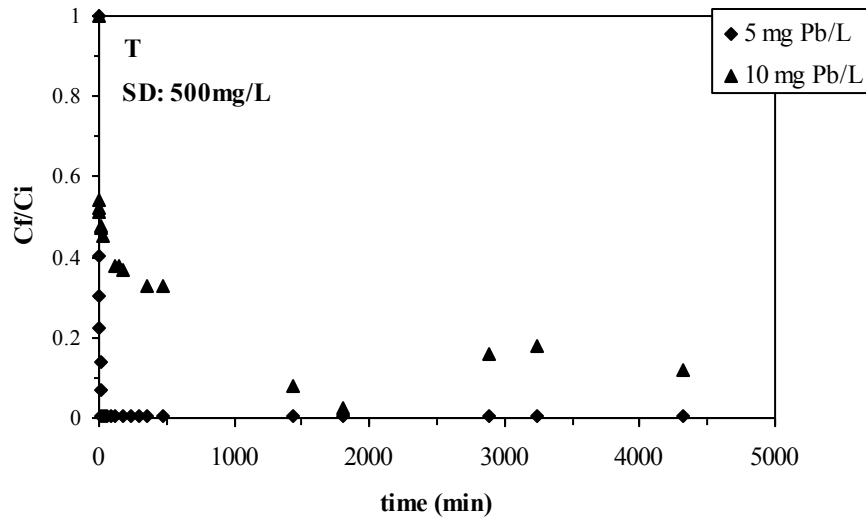
Figure 111 Influence of lead concentration on sorption kinetics (pH$_i$=5, T sample, 500 mg sorbent L^{-1})
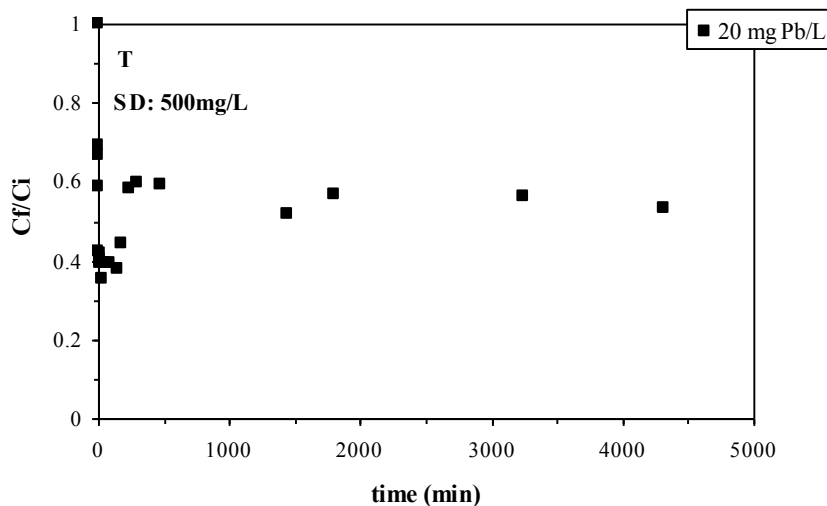
Figure 112 Influence of lead concentration on sorption kinetics (pH$_i$=5, T sample, 500 mg sorbent L^{-1})

The Lagergren's equation again failed to describe the experimental data, confirming that the process did not follow the first order kinetics. The results of Ho's equation application are summarized in Table 62 (page 305). Reasonably high correlation coefficients and behaviour of linearized plots indicated a good fit. The linearized plots are then shown in Figure 191 (P3 sorbent) and in Figure 192 (T sorbent). Nevertheless, the uptake curves calculated according to the modelling did not correlate experimental data (Figures 175 – 176). A poor correlation of obtained data was also observed for T biosorbent, but this could be caused by the fluctuation of experimental points.

Furthermore, it was not possible to investigate the role of diffusion phenomena as the selected models revealed inappropriate to describe the experimental data, especially due to the fast concentration drop within the first minutes of experiment. This fact is illustrated in Appendix E (Figures 177 – 182).

4.4.4.2 Influence of sorbent dosage

Similarly to the previous experiments, the second tested parameter was the influence of sorbent dosage (SD). Presentation of experimental data shown in chapter 4.4.4.1 while taking into account the influence of sorption dosage confirmed the irregularities observed in the previous chapter; however it did not contribute to clarify the observed results. Therefore the results will not be displayed.

4.4.4.3 Influence of particle size

The last tested parameter was the influence of particle size (d_p). The experiment was only performed with P3 sorbent as T sorbent presented undesirable fluctuation of experimental points and so made impossible any adequate interpretation. As already observed in the case of hexavalent chromium, the process seemed to be unaffected by increasing particle size (Figure 113). The fast concentration drop for all five size fraction used is well illustrated in Figure 114, where are displayed the first 8 hours of experiment.
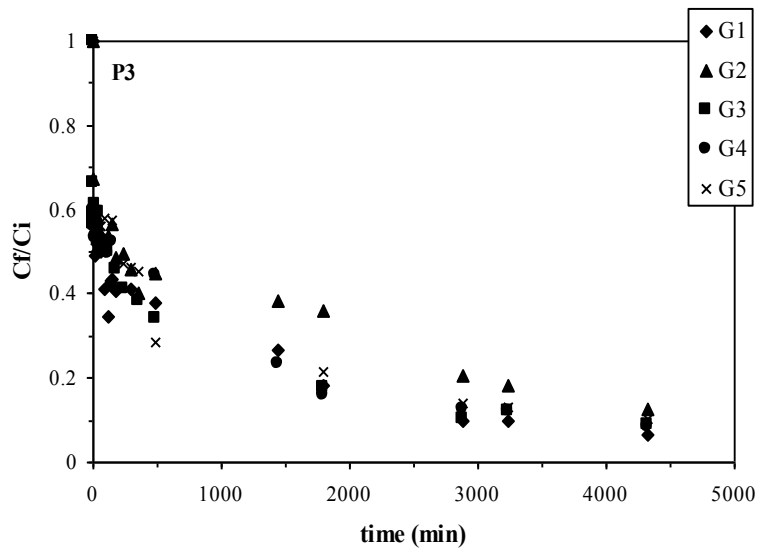
Figure 113 Influence of particle size on lead sorption kinetics (pH$_i$=5, P3 sample, 10 mg Pb L^{-1})
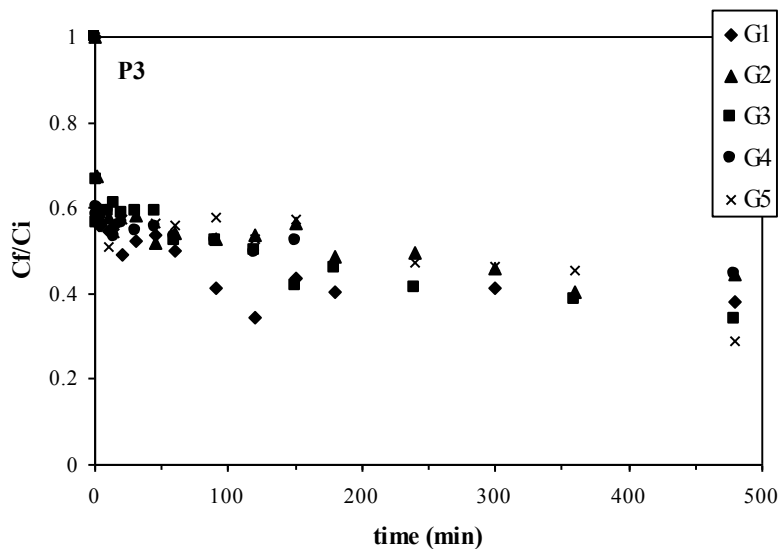
Figure 114 Influence of particle size on lead sorption kinetics (pH$_i$=5, P3 sample, 10 mg Pb L^{-1}) – detail corresponding to first 8 hours of experiments

4.4.4.4 Conclusion

The interpretation of experimental data obtained in kinetics experiments performed with lead was difficult. A very fast concentration drop within the first minute of experiment was observed for all concentration levels (both C$_0$ and SD) and both sorbent samples. Lagergren's relationship failed to describe the kinetics of the process. Whereas the Ho's equation was applicable and predicted well the equilibrium, but did not follow well the overall

form of uptake curves. A fluctuation of experimental points was often observed, especially in case of T sorbent.

The diffusion models used in previous chapter appeared inadequate this time.

4.4.5 Conclusion of kinetics results

The objective of this chapter was to observe the evolution of concentration (or more precisely of concentration decrease) in the system as a function of time, to describe the process by means of kinetic order relationships and to determine the transport mode responsible for the control of the process.

It was observed that the rate of biosorption decreased with increasing metal concentration and increasing particle diameter, while the influence of sorbent dosage was not clear. Biosorption process followed second order kinetics for mercury and chromium. Unsatisfactory results were obtained for cadmium and lead. While cadmium biosorption efficiency was too low under selected experimental conditions, several irregularities were observed during lead biosorption.

Mercury biosorption seemed to be controlled by film diffusion as its rate decreased with increasing concentration and increasing sorbent size. In the case of hexavalent chromium (P3 sample), the process seemed to be controlled by both intraparticle and film diffusion, the predominant control depending on the experimental conditions. Very low correlation coefficients were obtained for T sorbent. This may indicate that separation of film and intraparticle diffusion into two separate models was not appropriate or that diffusion was not the rate limiting process. Hexavalent chromium biosorption was not sensitive to change in sorbent size in both cases, which may signify that the process took place in the entire particle.

4.5 Sorption from bimetallic systems

As illustrated in the previous chapters, the best results were so far obtained for mercury and hexavalent chromium. The optimum pH for Cr(VI) binding lies far away from the optimum pH of other tested metals and therefore this metal was not included in these experiments. Meanwhile it was well described in the literature and confirmed within our

experiments, that cationic species do not sorb at acidic pHs and so their presence may not influence the uptake of anionic species from acidic solutions.

It was hence decided to focus the attention on mercury and to investigate the influence of cadmium and lead on mercury uptake for both P3 and T biosorbents. Four sets of experiments were prepared as described in Table 40. The experiments were performed according to the standard procedure described for monometallic sorption (3 days of contact on a shaker in a tempered room, pH_f determination, filtration and metal content determination by ICP-AES).

Sorbent sample	pH_i	C_i (Metal 1)	C_i (Metal 2)
P3	5	10 -100 mg Hg L^{-1}	1-20 mg Pb L^{-1}
T	5	10 – 100 mg Hg L^{-1}	1-20 mg Pb L^{-1}
P3	5	10 – 200 mg Hg L^{-1}	10 – 100 mg Cd L^{-1}
T	7	10 – 100 mg Hg L^{-1}	10 – 100 mg Cd L^{-1}

Table 40 Details of experimental procedure used for experiments with bimetallic solutions

If possible, the initial pH of suspension was adjusted to the optimum value common for both metals (in the case of P3 sorbent), which enabled the direct comparison of their reciprocal effect on the sorption of the second metal. When the optimum pH values differed (in the case of T sample), the initial pH was then adjusted to the optimum value corresponding to mercury. The only exception was done for Hg-Pb system using T sorbent, where the pH of the suspension was fixed to 5 in order to prevent lead precipitation at higher pH, since this precipitation may interfere the biosorption process and may devaluate the results of the experiments.

Although the solutions were prepared on mass concentration basis, the results are presented in molar units to facilitate the comparison between individual metals.

4.5.1 Influence of lead on mercury biosorption by P3 sorbent

The P3 material had to be re-prepared from the newly supplied biomass. Therefore the mercury isotherm (without presence of lead in solution, C_i ranging between 0 and 200 mg Hg L^{-1}) was repeated and the results were compared with the previous results (Figure 115). The re-prepared material exhibited slightly higher sorption capacities.
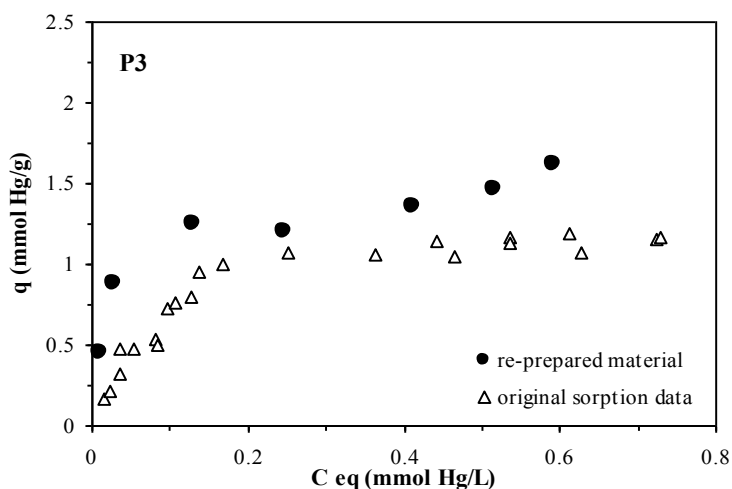
Figure 115 Comparison of Hg sorption isotherms for biosorbent P3 at initial pH 5

After lead addition, the shape of isotherms changed slightly (Figure 116), whereas their slopes were less steep when compared to the original isotherm. But no reduction in sorption capacity occurred and the influence of lead on mercury uptake was not observed. Nevertheless the comparison revealed difficult, since the saturation of the sorbent was not achieved in the tested concentration range.
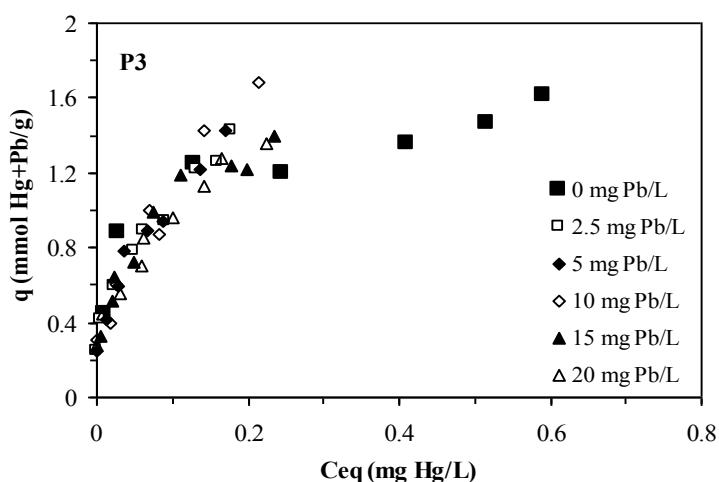
Figure 116 Hg sorption isotherms for biosorbent P3 at initial pH 5 and lead initial concentration ranging between 0 – 20 mg Pb L^{-1}

Figure 117 was prepared to clarify the influence of lead on the efficiency of the process. The corresponding sorption capacity (*q)* in absence of competing lead was referenced

as index 100. Mercury uptake was slightly enhanced at high mercury (100 mg Hg L^{-1}) and low lead initial concentrations (Hg/Pb ratio ranging from 40:1 to 5:1). The enhancement was in the range of 25 percent, but no relationship between the lead concentration and the percentage of sorption capacity increase was found. With decreasing mercury concentration (and increasing Hg/Pb ratio) the competition effect started to appear. Negligible decrease in mercury sorption capacity was observed in the case of initial concentration 50 mg Hg L^{-1}. The inhibition effect became more pronounced with further decrease in mercury concentration. Nevertheless, it did not exceed 30 percent. For example, at mercury-lead equimolar system the inhibition reached approximately 25 percent of the original sorption capacity. However, the sorption capacity varied within the range of 30% and the influence of lead on mercury uptake was not considered significant (in the studied concentration range).
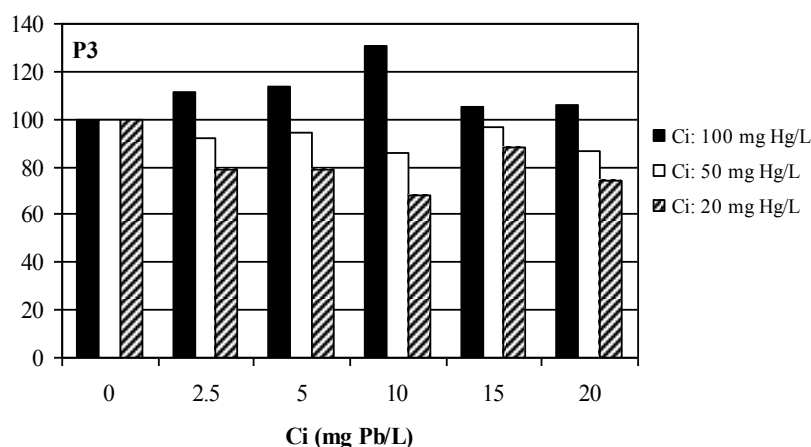
Figure 117 Effect of the presence of lead on mercury uptake by P3 sorbent at initial pH 5, initial mercury concentration 20, 50 and 100 mg L^{-1} and biomass dose 200 mg L^{-1}. The reference value 100 indicates mercury sorption in absence of competing lead

Herrero et al.[112] described also the enhancement effect of lead on mercury biosorption when using algal biomass of *C. baccata*. The presence of lead slightly enhanced mercury uptake (at SD 2.5 g L^{-1}, C_i = 50 mg Hg L^{-1} and C_i = 500, 1000 mg Pb L^{-1}) within the range of 20 percent, while it was slightly inhibited in the presence of copper. On the other hand, Herrero et al. observed that the uptake of mercury was unaffected by presence of cadmium, zinc, calcium and magnesium. The inhibition effect of copper was explained by its soft character and competition for the same sorption sites (according to Pearson's HSAB theory), whereas no explanation was proposed to clarify the effect of lead. Contrary to the present

results, Herrero et al. observed the enhancement effect in significant excess of lead. Thus it is possible that different phenomena caused the observed effect.

4.5.2 Influence of mercury on lead biosorption by P3 sorbent

As the experiments were run at the initial pH common for both metals, the influence of mercury on lead biosorption by P3 sorbent could have also been investigated. The lead isotherms (without mercury, C_i ranging between 0 and 20 mg Pb L^{-1}) are compared in Figure 118. The isotherm determined for the re-prepared P3 material corresponded well to the previous results.
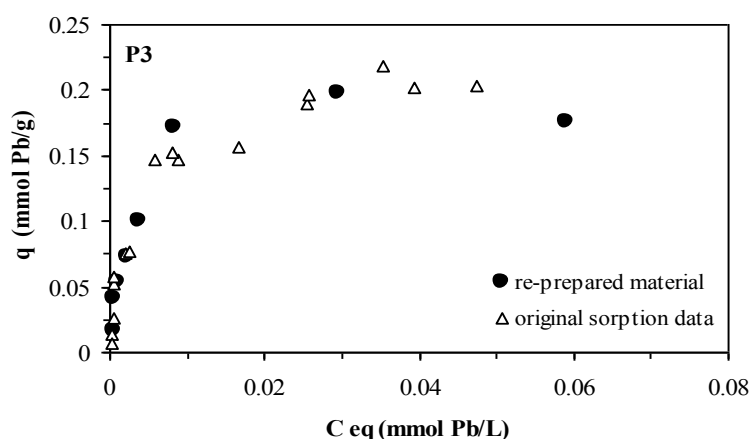
Figure 118 Comparison of Pb sorption isotherms for biosorbent P3 at inital pH 5

Contrary to the results obtained for mercury, biosorption of lead was significantly affected by the presence of mercury (Figure 119). The lead sorption capacity dropped by 30% compared to the original isotherm. However, the decrease was not proportional to the second metal concentration. Apparently, the reduction of sorption capacity was independent of mercury concentration. Figure 120 shows well, that the inhibition effect was not proportional to the decrease in Pb/Hg ratio and was approximately of the same order of magnitude all over the investigated concentration range.

198
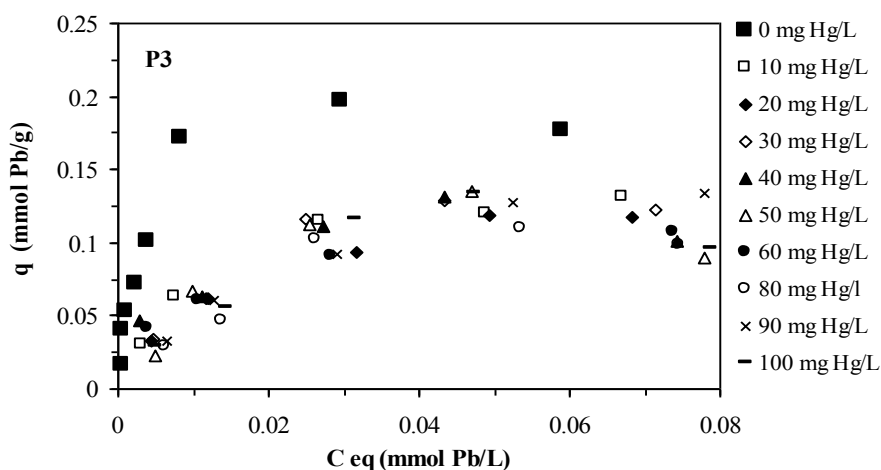
Figure 119 Pb sorption isotherms for biosorbent P3 at inital pH 5 and mercury concentration ranging between 0 – 100 mg Hg L^{-1}
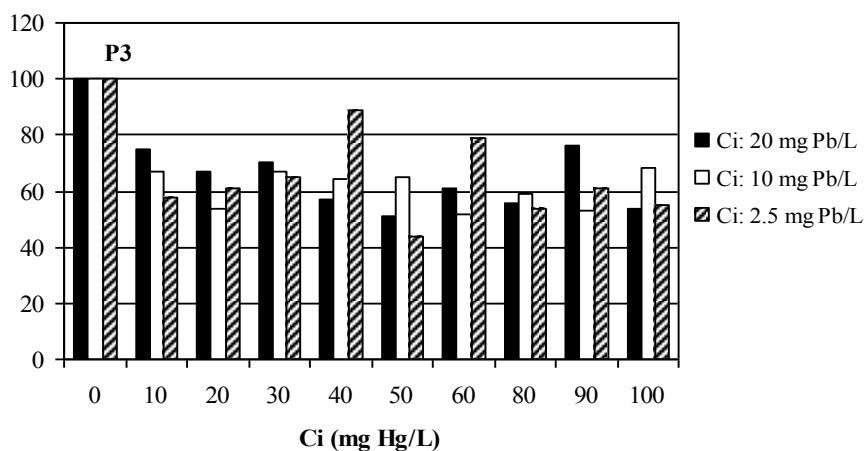
Figure 120 Effect of the presence of mercury on lead uptake by P3 sorbent at initial pH 5, initial lead concentration 2.5, 10 and 20 mg L^{-1} and biomass dose 200 mg L^{-1}. The reference value 100 indicates lead sorption in absence of competing mercury

4.5.3   Influence of lead on mercury biosorption by T sorbent

When mercury sorption in presence of lead was investigated using T sorbent, the initial pH was fixed to 5 (in order to prevent the lead precipitation at higher experimental pHs). Hence the mercury sorption isotherm at this pH had to be determined. Even though the

sorption material exhibited certain mercury sorption capacity at this pH, the obtained experimental data did not fit to any conventional isotherm relationship. Thereby the sorption data were not further presented in the form of sorption isotherm and only the influence on uptake efficiency was investigated (Figure 121). The same trend is apparent for three selected concentrations. At low lead concentration (2.5 mg Pb L^{-1}) the mercury uptake capacity seemed slightly induced, whereas a slight inhibition effect was observed with increasing second metal concentration, similarly to the mercury − lead system when P3 sorbent was used.
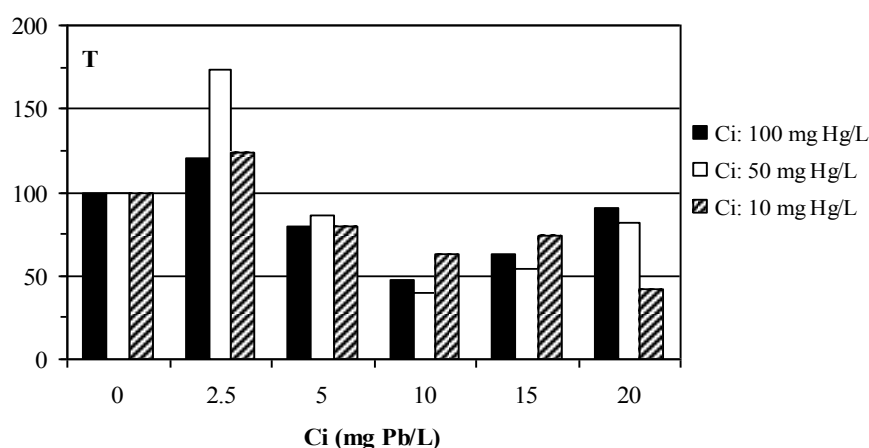
Figure 121 Effect of the presence of lead on mercury uptake by T sorbent at initial pH 5, initial mercury concentration 10, 50 and 100 mg L^{-1} and biomass dose 200 mg L^{-1}. The reference value 100 indicates mercury sorption in absence of competing lead

4.5.4 Influence of mercury on lead biosorption by T sorbent

In the case of T sorbent originally supplied material was used and pH 5 corresponded to lead optimum pH. Thus lead isotherm did not have to be verified and the sorption data were compared to the original sorption isotherm presented in chapter 4.2.4 (Figure 45, page 126). Even though the original sorption isotherm was of a classical favourable isotherm form, the shape of isotherms changed in the presence of mercury (Figure 122). Regardless of mercury concentration, the isotherms appeared to be flatter (nearly linear) without the typical plateau corresponding to sorbent saturation. No apparent inhibition or enhancement effect was observed and the differences from the single lead isotherm were only negligible. At lower

initial (and equilibrium) lead concentration, the presence of mercury seemed to reduce slightly lead uptake capacity, but with increasing lead concentration the trend became inverse (Figure 123). Nevertheless, the influence of mercury on lead biosorption was not significant, even if the latter metal was present in an excess to lead.
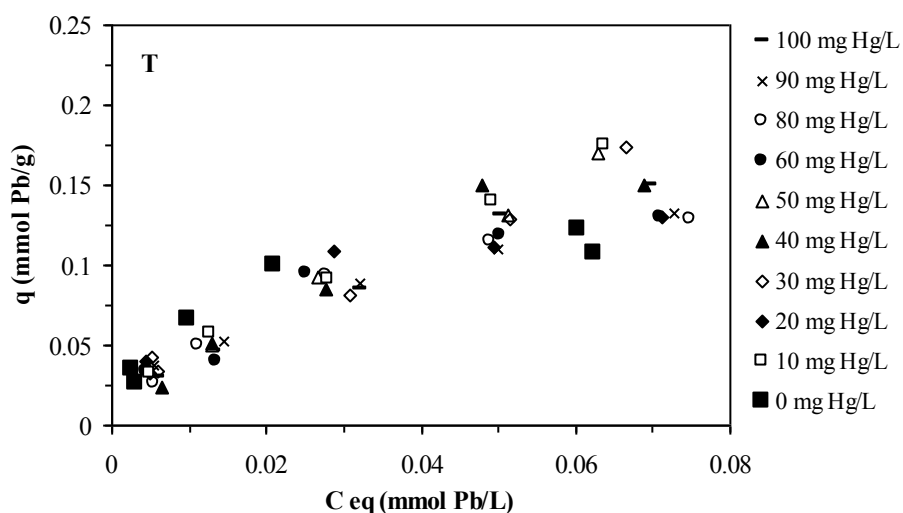
Figure 122 Pb sorption isotherms for biosorbent T at initial pH 5 and mercury concentration ranging between 0 – 100 mg Hg L^{-1}
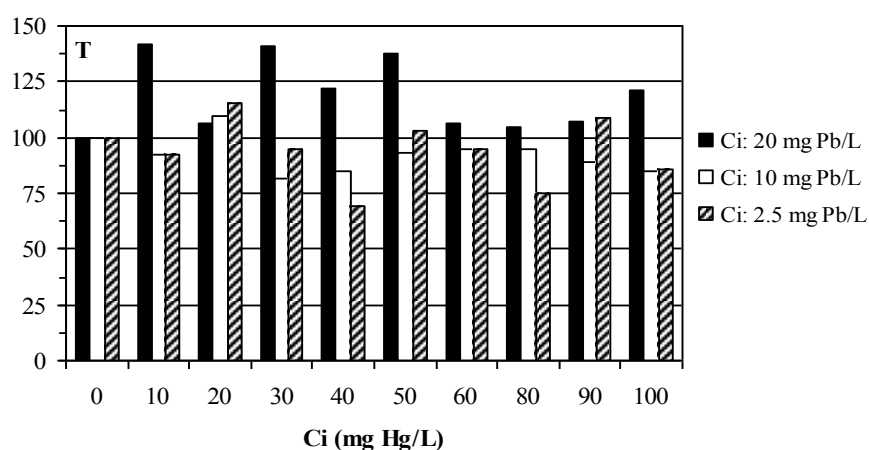
Figure 123 Effect of the presence of mercury on lead uptake by T sorbent at initial pH 5, initial lead concentration 2.5, 10 and 20 mg L^{-1} and biomass dose 200 mg L^{-1}. The reference value 100 indicates lead sorption in absence of competing mercury

Table 41 presents the results of mercury and lead speciation modelling performed by Visual MINTEQ programme. The initial pH of experiments was fixed to pH 5, but the evolution was observed during the experiments. Therefore the first column of the below table shows the speciation at the beginning of the experiments. Sorbent T tended to decrease the final pH, approximately to pH 4.5 (second column), whereas P3 sorbent shifted the final pH to pH 5.5 (third column). As illustrated in the Table 41, the majority of mercury species existed in a non-ionic form of $HgCl_2$ and the majority of lead existed as simple Pb^{2+} ion all over the tested experimental pH range. With increasing pH the amount of HgCl(OH) increased. No precipitation of tested metals was predicted by the programme, therefore the decrease in both metals concentrations may be related only to biosorption process.

Component	Species	% of total component concentration		
		pH_i	pH_f	
		5	4.5 (T)	5.5 (P3)
Cl^-	Cl^-	25.9	24.8	28.8
	HgClOH (aq)	1.6	0.6	4.3
	$PbCl^+$	0.1	0.1	0.1
	$HgCl^+$	-	-	-
	$HgCl_2$ (aq)	**72**	**74.2**	**66.6**
	$HgCl_3^-$	0.3	0.3	0.3
Hg^{2+}	$Hg(OH)_2$	-	-	0.3
	HgClOH (aq)	**4.3**	**1.5**	**11.3**
	$HgCl^+$	0.1	0.1	0
	$HgCl_2$ (aq)	**95.3**	**98.2**	**88.1**
	$HgCl_3^-$	0.3	0.3	0.3
Pb^{2+}	**Pb^{+2}**	**98.9**	**99.1**	**98.4**
	$PbOH^+$	0.2	0.1	0.6
	$PbCl^+$	0.9	0.9	1

Table 41 Mercury and lead speciation at different experimental pHs (temperature 20°C, initial concentrations 100 mg Hg L^{-1} and 20 mg Pb L^{-1}, prepared by dissolving $PbCl_2$ and $HgCl_2$)

The presence of amine and amide functional groups on the surface of sample P3 was previously identified and the interaction of these groups with the target metals was confirmed by FTIR analyses of saturated samples, which may signify that the lone electron pair (free electron doublet) of nitrogen was involved in the interaction with both metallic forms. The

participation of other sorption sites in the interaction with different metals was not confirmed. Thus the competition for the same site was expected during experiments with bimetallic solutions.

The highest sorption capacity in single metals systems was obtained for mercury, while the sorption capacities for lead and cadmium were much lower. Mercury sorption from bimetallic solution was only slightly influenced by the presence of lead. Thereby no competition effect was found and a high affinity and a selectivity of P3 sorbent to mercury were confirmed. On the other hand, lead sorption seemed to be significantly inhibited in the presence of mercury as illustrated below. Table 42 compares maximum sorption capacities at saturation levels on the molar basis between single and bimetallic systems. The total sorption capacities were obtained by summing the values corresponding to both metals. The total capacity obtained in bimetallic systems is only slightly below the theoretical value, while mercury uptake differs only slightly and lead uptake was significantly decreased in comparison to single metal system. This confirms high selectivity of P3 sorbent towards mercury and the inhibition effect of mercury on lead biosorption.

q (Hg)	q (Pb)	q (Hg+Pb)	q (Hg)	q (Pb)	q (Hg+Pb)
[mmol Hg g^{-1}]	[mmol Pb g^{-1}]	[mmol (Me) g^{-1}]	[mmol Hg g^{-1}]	[mmol Pb g^{-1}]	[mmol (Me) g^{-1}]
1.5	0.2	1.7	1.4	0.1	1.5
single metal system	single metal system	theoretic values obtained by summing single metal sorption capacities	bimetallic system at 20 g Pb L^{-1}	bimetallic system at 100 mg Hg L^{-1}	bimetallic system

Table 42 Inhibition effect in mercury - lead system using P3 sorbent

Mercury belongs to soft acids (according to Pearson's HSAB theory) as may so preferentially react with soft bases such as amine group. On the other hand, lead belongs among the borderline elements and is generally not expected to show such a preference. Additionally lead existed as a simple cation, while mercury was in a non-ionic form.

Tzesos et al.[179] related the interactions of metals to their classification according to Pearson's HSAB theory and observed that borderline elements were affected by the presence of either hard or soft elements, which was confirmed in the present study.

Concerning T sorbent, carboxylic groups were identified on its surface. The interpretation of saturated FTIR spectra was not as unambiguous as in the case of P3 sorbent.

The participation of carboxyl group in the binding was confirmed, while the interaction with nitrogen containing functional groups was not excluded.

According to Pearson' classification, carboxyl groups belong among hard basis and though the interaction with hard acid would be preferred. As mentioned above, mercury belongs among soft acid, while lead is a borderline element. Nevertheless, T sorbent showed a higher sorption capacity for mercury within single metal experiments.

Unfortunately, experimental data corresponding to mercury sorption in the presence of lead revealed un-exploitable, since a classical isotherm shape was not followed. Therefore maximum saturation uptake capacities cannot be compared. On the other hand, lead sorption did not appear to be inhibited by the presence of mercury and no competition effect was found.

The comparison of obtained results to the published data revealed to be difficult. Since a significant number of biosorbent materials was tested for uptake of a number of metals, it seemed impossible to find similar metals combination to compare with the present study. Nevertheless some studies are cited below to illustrate the diversity of published results.

Puranik and Paknikar[229] investigated the influence of cadmium, copper, cobalt and nickel on lead and zinc biosorption by both *Streptoverticillium cinnamoneum* and *Penicillium chrysogenum* biomass. Each of the biomasses exhibited preferential uptake of lead in a multi-metal situation. A reciprocal inhibition was observed for all binary systems containing zinc, while systems containing lead exhibited unequal inhibition. There was a reduction in co-cation uptake in the presence of either lead or zinc. The extent of inhibition in co-cation uptake in the presence of lead and zinc was lower at increasing co-cation concentrations. The effect of co-cations on sorption of lead was less pronounced than on zinc sorption.

The change of isotherm shape in the presence of second metal was also reported by Chassary[230], who evaluated competition effects between platinum and palladium species during sorption on chitosan. Chassary observed a change of isotherm shape from favourable form in the single metal system to nearly linear form in the presence of second metal. In single metal systems, chitosan showed higher sorption capacity for palladium over platinum. In binary systems, palladium was inhibited in the presence of platinum; nevertheless more important inhibition was realized for platinum in the presence of palladium. The same observation was done in the present study, where lead uptake was more influenced by the presence of mercury, than in the opposite case (for P3 sample).

4.5.5 Influence of cadmium on mercury biosorption by P3 sorbent

When cadmium was used as the second metal in the system, concentrations equivalent to those of mercury were used and therefore a better perception of competition effect was obtained. The single mercury isotherm (without presence of cadmium in solution) corresponds to Figure 115.

In the case of P3 sorbent, an inhibition effect of cadmium was observed on the first section of sorption isotherm (Figure 124), while an opposite effect was found with increasing cadmium concentration. The initial drop in sorption capacity is well visualized in Figure 125. At low mercury concentrations, the reduction in the range of 30 percent was observed, regardless of cadmium concentration. The inhibition effect of cadmium decreased with increasing initial mercury concentration. When initial mercury concentration was fixed to 100 mg L^{-1} (Hg/Cd molar ratio ranging from 20:1 to 2:1), the cadmium effect on mercury sorption became negligible. With a further increase of mercury concentration (150 mg Hg L^{-1}), a slight enhancement effect was found. Nevertheless, the enhancement/inhibition effects were within the range of 30%, like in the case of mercury-lead system, and the influence of cadmium was not considered to be significant.
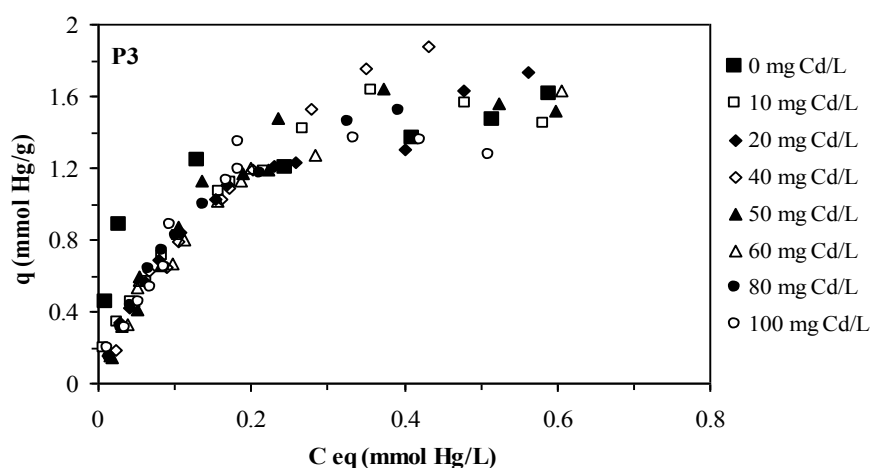
Figure 124 Hg sorption isotherms for biosorbent P3 at initial pH 5 and cadmium concentration ranging between 0 – 100 mg Cd L^{-1}
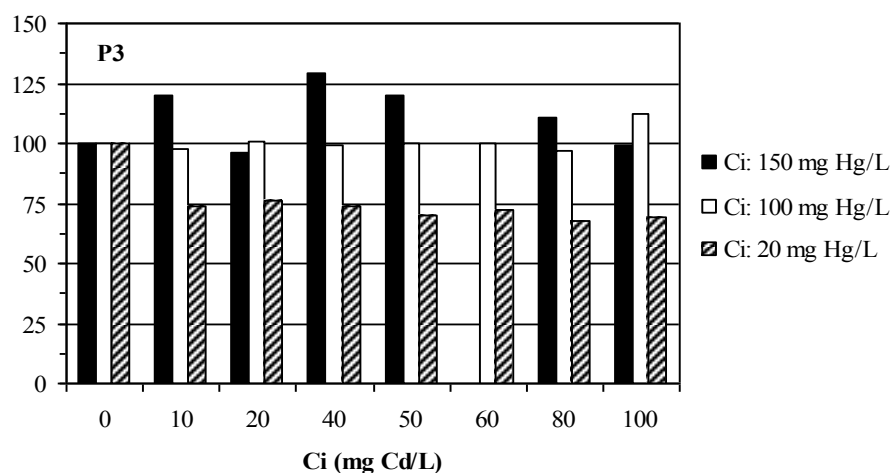
Figure 125 Effect of the presence of cadmium on mercury uptake by P3 sorbent at initial pH 5, initial mercury concentration 10, 100 and 150 mg L^{-1} and biomass dose 200 mg L^{-1}. The reference value 100 indicates mercury sorption in absence of competing cadmium

4.5.6 Influence of mercury on cadmium biosorption by P3 sorbent

The individual cadmium sorption isotherm was re-determined with the re-prepared P3 sorbent. The comparison between the original and repeated experimental data is displayed in Figure 126, whereas slightly higher sorption capacities were obtained for the re-prepared material.
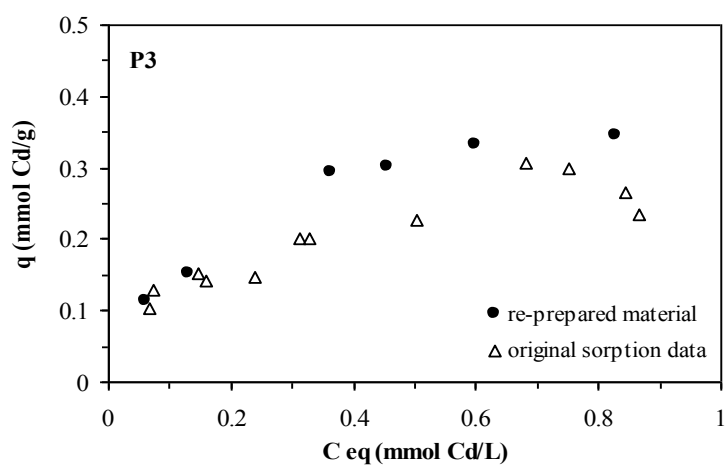
Figure 126 Comparison of Cd sorption isotherms for biosorbent P3 at initial pH 5

Slight inhibition effect of mercury at low cadmium equilibrium concentrations was found. Low equilibrium concentrations correspond to the first section of sorption isotherms, which were less steep than the corresponding single cadmium isotherm. With increasing mercury concentration, the differences in the second part of isotherm plots became more evident, since lower uptake capacities were attained at saturation of P3 sorbent (Figure 127 – corresponding to initial mercury concentration ranging between 0 – 100 mg Hg L^{-1}). Surprisingly, when the initial Hg concentration was further increased and ranged between 100 and 200 mg Hg L^{-1}, the inhibition effect seemed slightly reduced (Figure 128).
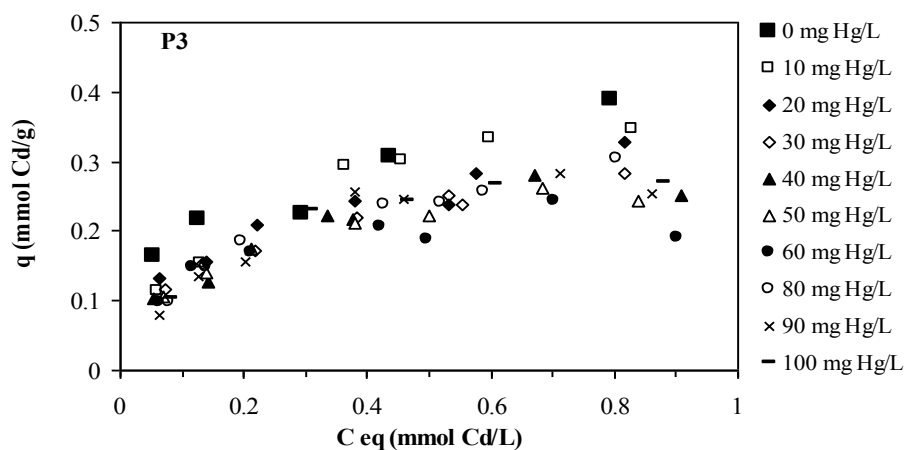
Figure 127 Cd sorption isotherms for biosorbent P3 at initial pH 5 and mercury concentration ranging between 0 – 100 mg Hg L^{-1}
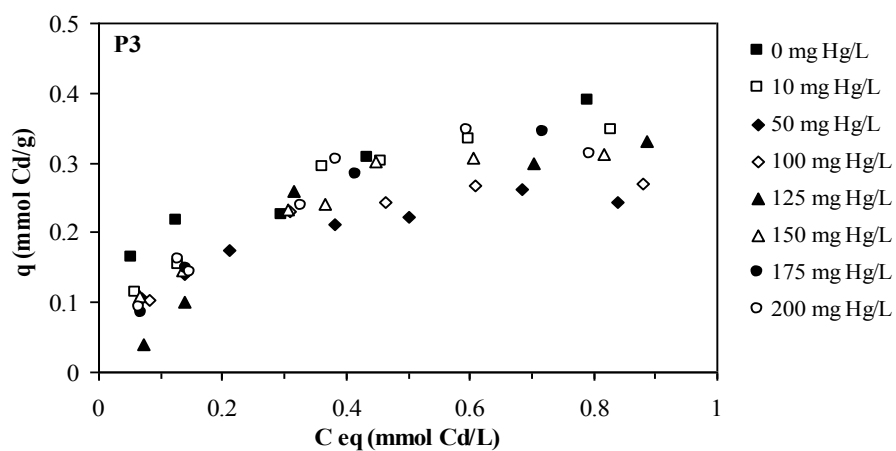
Figure 128 Cd sorption isotherms for biosorbent P3 at initial pH 5 and mercury concentration ranging between 0 – 200 mg Hg L^{-1}

When the data were displayed as the function of sorption capacity reduction, the previous observations were confirmed. The highest inhibition effect was observed at lowest cadmium concentration, which corresponded to lower slopes of sorption isotherms. Nevertheless, the relationship between inhibition extent and mercury concentration was not found. The inhibition continued to increase regularly with increasing mercury initial concentration up to 60 mg Hg L^{-1}. Beyond this concentration the uptake was only slightly reduced and the effect of mercury on cadmium biosorption became less pronounced.
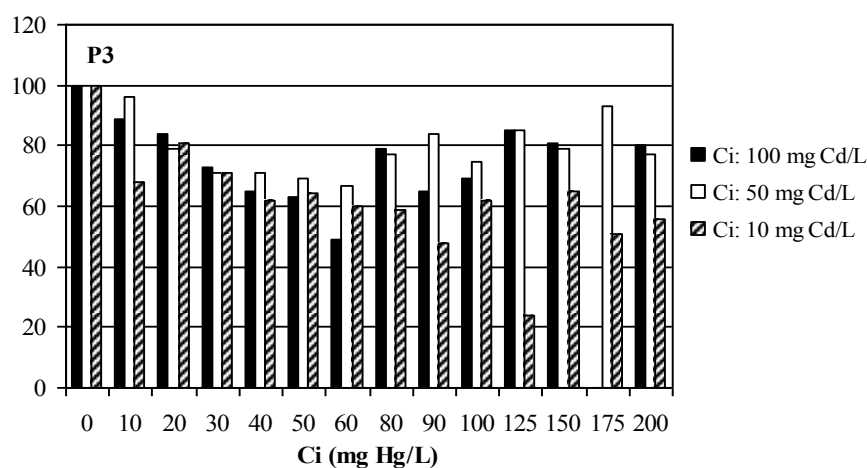
Figure 129 Effect of the presence of mercury on cadmium uptake by P3 sorbent at initial pH 5, initial cadmium concentration 10, 50 and 100 mg L^{-1} and biomass dose 200 mg L^{-1}. The reference value 100 indicates the cadmium sorption in absence of competing mercury

4.5.7 Influence of cadmium on mercury biosorption by T sorbent

In the case of T sorbent, the experiments were performed at initial pH 7. This was the optimum pH for mercury biosorption by T sorbent and so the sorption data were compared to Figure 40 (page 120, chapter 4.2.1).

An important inhibition effect of cadmium was observed from low concentrations levels (Figure 130) and this effect was even more pronounced at increased cadmium concentration levels. It seemed to be related to increasing cadmium concentration (especially at low mercury level).

The inhibition effect is displayed in Figure 131. The decrease in uptake capacity increased with increasing cadmium concentration. At equimolar system (50 mg Hg L^{-1} and 100 mg Cd L^{-1}) the inhibition reached 50 percent. Additionally, this decrease was proportional to cadmium concentration increase. The only exception concerns the highest mercury concentration (100 mg Hg L^{-1}) corresponding to an important excess of mercury over cadmium (Hg/Cd ratio ranging from to 20:1 to 2:1), where the inhibition effect was less pronounced.
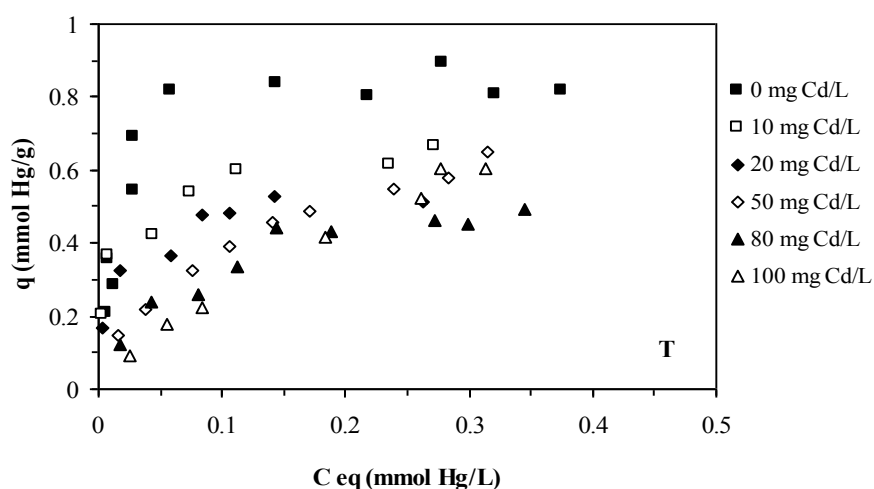
Figure 130 Hg sorption isotherms for biosorbent T at initial pH 7 and cadmium concentration ranging between 0 – 100 mg Cd L^{-1}
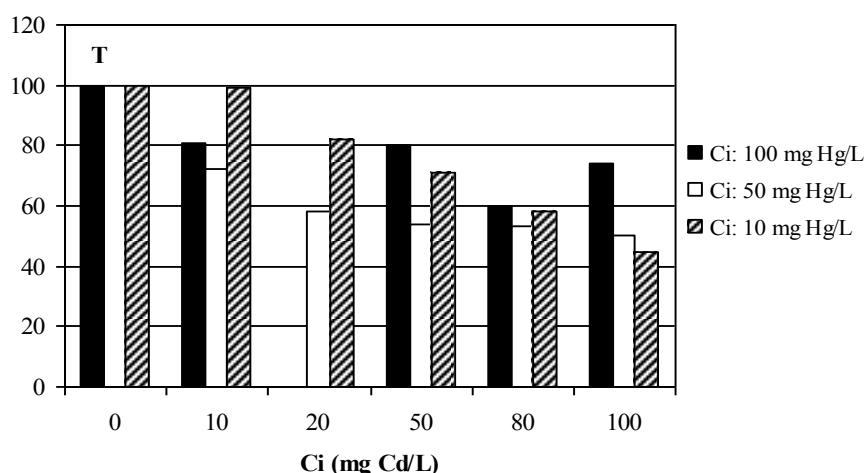
Figure 131 Effect of the presence of cadmium on mercury uptake by T sorbent at initial pH 7, initial mercury concentration 10, 50 and 100 mg L^{-1} and biomass dose 200 mg L^{-1}. The reference value 100 indicates mercury sorption in absence of competing cadmium

4.5.8 Influence of mercury on cadmium biosorption by T sorbent

Even though the previous experiments revealed that pH 7 was not the optimum pH for cadmium biosorption by T sorbent, the cadmium experimental data followed a classical isotherm shape (Figure 132).
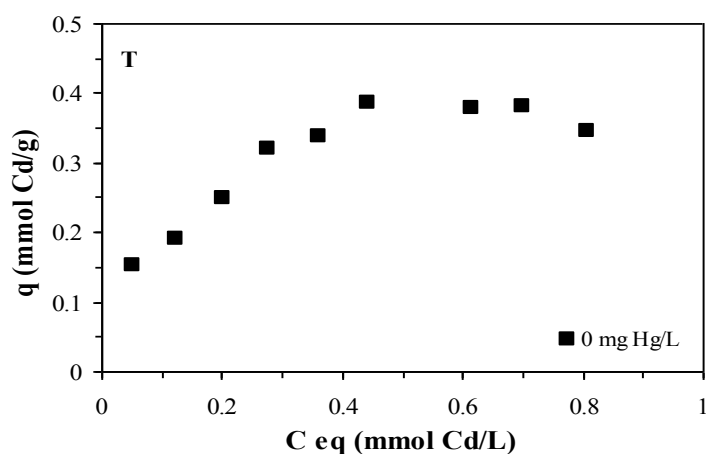
Figure 132 Cd biosorption isotherm using T sorbent at initial pH 7

Slight inhibition effect of mercury on cadmium sorption in bi-metallic systems is shown in Figure 133. The impact of mercury seemed to have a negligible effect on the first section of sorption isotherms, while the saturation plateaus (second section of the curve) were lowered significantly. This means that the influence of mercury was not significant at low cadmium concentration, whereas its influence was increasing with increasing cadmium concentration. These findings are confirmed in Figure 134.
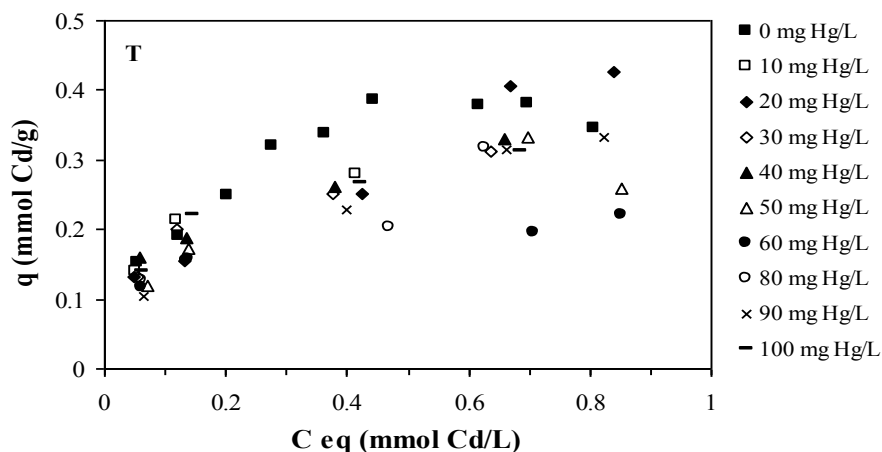
Figure 133 Cd sorption isotherms for biosorbent T at initial pH 7 and mercury concentration ranging between 0 – 100 mg Hg L^{-1}
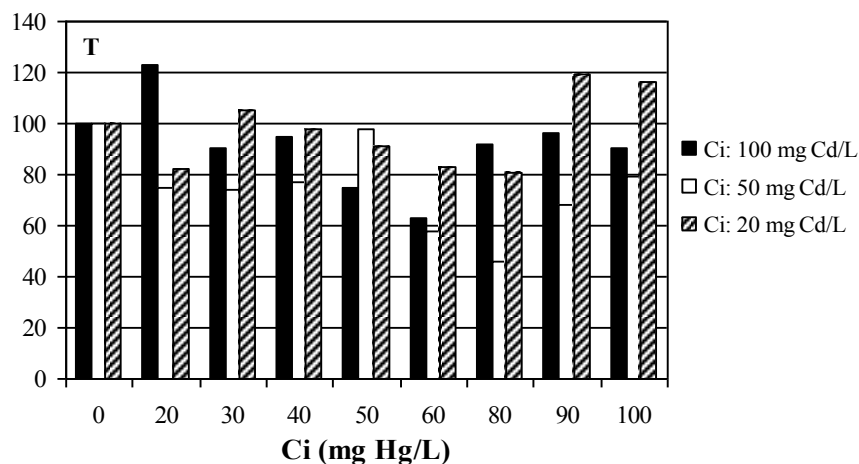
Figure 134 Effect of the presence of mercury on cadmium uptake by T sorbent at initial pH 7, initial cadmium concentration 20, 50 and 100 mg L^{-1} and biomass dose 200 mg L^{-1}. The reference value 100 indicates cadmium sorption in absence of competing mercury

Table 43 presents the results of mercury and cadmium speciation modelling performed by Visual MINTEQ programme. The initial pHs of experiments were fixed to pH 5 for P3 sorbent and to pH 7 for T sample and therefore the speciation at these pH values is presented in the below table. Since T sorbent tended to decrease pH and P3 sample had the opposite tendency to shift pH to higher values, pH of both systems tended to stabilized around pH 6

(last column in Table 43). At this pH, the majority of mercury species existed in a non-ionic form of $HgCl_2$ and the majority of cadmium existed as simple Cd^{2+} ion. No precipitation of tested metals was predicted by the programme, therefore the decrease in both metals concentrations may only be related to biosorption process.

Component	Species	% of total component concentration		
		pH_i		pH_f
		5 (P3)	7 (T)	6 (P3 and T)
	Cl^-	**72.4**	**76.6**	**72.9**
	$HgCl_4^{2-}$	-	-	-
	HgClOH (aq)	0.1	3.6	0.6
Cl^-	$CdCl^+$	4	4.2	4
	$CdCl_2$ (aq)	0.1	0.1	0.1
	$HgCl_2$ (aq)	22.5	14.9	21.6
	$HgCl_3^-$	0.9	0.6	0.9
	$Hg(OH)_2$		3.1	0.1
	$HgCl_4^{2-}$	-	-	-
Hg^{2+}	HgClOH (aq)	0.5	31.1	4.7
	$HgCl_2$ (aq)	**96.9**	**64**	**92.7**
	$HgCl_3^-$	2.6	1.8	2.5
	Cd^{2+}	**83.3**	**82.5**	**83.2**
Cd^{2+}	$CdCl^+$	16.5	-	16.6
	$CdCl_2$ (aq)	0.2	17.2	0.2

Table 43 Mercury and cadmium speciation at different experimental pHs (temperature 20°C, initial concentrations 100 mg Hg L^{-1} and 100 mg Cd L^{-1}, prepared by dissolving CdCl$_2$ and HgCl$_2$)

According to Pearson's HSAB classification, both cadmium and mercury belong among soft acids and may so preferentially bind to a soft base (such as amine group). Meanwhile the interaction of amine (or amide) groups was identified as the only sorption site in P3 sorbent. In case of T sorbent, the carboxyl group was likely the only sorption site, which took part in biosorption process. The observed decrease of pH was probably associated to carboxyl group dissociation.

According to Tzesos et al.[179], elements belonging either to hard or soft classes (Pearson's HSAB theory) exhibit competition effects among members of their class.

In the present study an important competition effect was observed only in the case of T sorbent. When P3 sample was used, the mercury uptake seemed to be unaffected by the presence of cadmium and the sorption of cadmium from the same bimetallic solutions was only slightly inhibited in the presence of mercury, as illustrated below. Table 44 compares maximum sorption capacities at saturation levels on the molar basis between single and bimetallic systems. The total sorption capacities were obtained by summing the values corresponding to both metals. The total capacity obtained in bimetallic systems is only slightly below the theoretical value, while mercury uptake does not differ and cadmium uptake was only slightly reduced in comparison to single metal system. The strong affinity and selectivity of P3 sample for mercury was so confirmed.

q (Hg)	q (Cd)	q (Hg+Cd)	q (Hg)	q (Cd)	q (Hg+Cd)
[mmol Hg g^{-1}]	[mmol Cd g^{-1}]	[mmol (Me) g^{-1}]	[mmol Hg g^{-1}]	[mmol Cd g^{-1}]	[mmol (Me) g^{-1}]
1.50	0.35	1.85	1.50	0.30	1.80
single metal system	single metal system	theoretic values obtained by summing single metal sorption capacities	bimetallic system at 100 mg Cd L^{-1}	bimetallic system at 200 mg Hg L^{-1}	bimetallic system

Table 44 Inhibition effect in mercury-cadmium system using P3 sorbent

On the other hand, a significant reduction in mercury sorption capacity was found when T sorbent was used. In this case two soft acids (Cd and Hg) competed for a hard base sorption site (carboxyl group), while the expected binding mechanism was ion exchange on carboxyl group. Mercury uptake seemed to be inhibited more than cadmium uptake, which was surprising, as firstly in single metals system T sorbent exhibited higher sorption capacities for mercury and secondly experimental pH was not the optimum pH for cadmium. The total uptake capacity of T sorbent was significantly reduced (Table 45).

q (Hg)	q (Cd)	q (Hg+Cd)	q (Hg)	q (Cd)	q (Hg+Cd)
[mmol Hg g^{-1}]	[mmol Cd g^{-1}]	[mmol (Me) g^{-1}]	[mmol Hg g^{-1}]	[mmol Pb g^{-1}]	[mmol (Me) g^{-1}]
0.8	0.4	1.2	0.6	0.3	0.9
single metal system	single metal system	theoretic values obtained by summing single metal sorption capacities	bimetallic system at 100 mg Cd L^{-1}	bimetallic system at 100 mg Hg L^{-1}	bimetallic system

Table 45 Inhibition effect in mercury-cadmium system using T sorbent

Contrary to our results, Herrero et al.[112] did not observe the competition effect between cadmium and mercury when using algal biomass of *C. baccata,* where the same sorption mechanism (ion exchange on carboxyl groups) as in the present study was expected.

Fiqueira et al.[231] investigated sorption behaviour in the cadmium-iron system (*Sargassum* biomass as biosorbent) and found that at 1.5 mmol Cd L^{-1} (C_f) presence of iron (1.5mmol L^{-1}) suppressed cadmium uptake to 75% of the original value. For 50% cadmium uptake reduction, a very high equilibrium iron presence was required. On the other hand the presence of cadmium affected very strongly the uptake of iron.

Mohapatra and Gupta[232] reported the competition among zinc(II), copper(II) and cobalt(II) during the biosorption by immobilized cyanobacteria (*Oscillatoria augustissima*). The sorption capacities for single metal decreased in order zinc > cobalt > copper. In binary systems copper inhibited both zinc and cobalt sorption, but the extent of inhibition of the former metal was greater that the latter. Zinc and cobalt were equally antagonistic to each other sorption. In contrast copper sorption remained almost unaffected at concentrations of competing metals.

4.5.9 Conclusion

The influence of cadmium and lead on mercury sorption was investigated in this part of work. This characteristic is essential for practical application of the biosorption processes. Wastewaters often contain more than one type of metal ion, which may interfere in the removal and/or recovery of the metal of interest. The presence of other cation can affect the sorption of metal ions (primary cation) and hence influence its removal efficiency. The

interactions between metals can be of very different characters (synergistic, antagonistic or none) and there is no way to predict such behaviour on the basis of single metal studies.

Both P3 and T biosorbents were tested for the sorption from mercury-lead and mercury-cadmium systems. The selectivity of P3 sorbent for mercury was confirmed. In most cases, the presence of competing ions slightly influenced metal sorption, but the impact of competing ion was not proportional to the metal concentration. The only exception concerns mercury sorption by T biosorbent in presence of cadmium. In this case the decreasing impact was proportional to concentration of competing ions.

4.6 Column experiments

In batch adsorption studies powdered biomass was used. The small particle size, low density and strength may cause difficulties in column applications (i.e. clogging, blockage and head loss).

The different behaviours of tested materials in contact with water were described in chapter 4.4. While the particles of T sorbent dispersed instantaneously in the solution, the particles of P3 biosorbent tended to aggregate and form lumps. This may cause important clogging problems, especially in column systems. To overcome this problem, biosorbents can be immobilized in a solid matrix, which is a process traditionally recommended in literature.[233] Even though this treatment operation improves remarkably the hydrodynamic properties of biosorbent, it is rather costly and usually lead to a certain drop in sorption capacities (based on volumetric sorption capacities), thus more sorption material is then necessary. The use of P3 sorbent in column process was not tested.

Tolypocladium biomass was supplied in forms of beads and could have been used directly in column. As described in chapter 3 the granules were produced within the filtration process on an infusorial earth layer. The macroscopic aspect revealed rather spherical shape of particles (Figure 24, page 95), while the microscopic aspect shows that the small particles are rather oval (Figure 135).
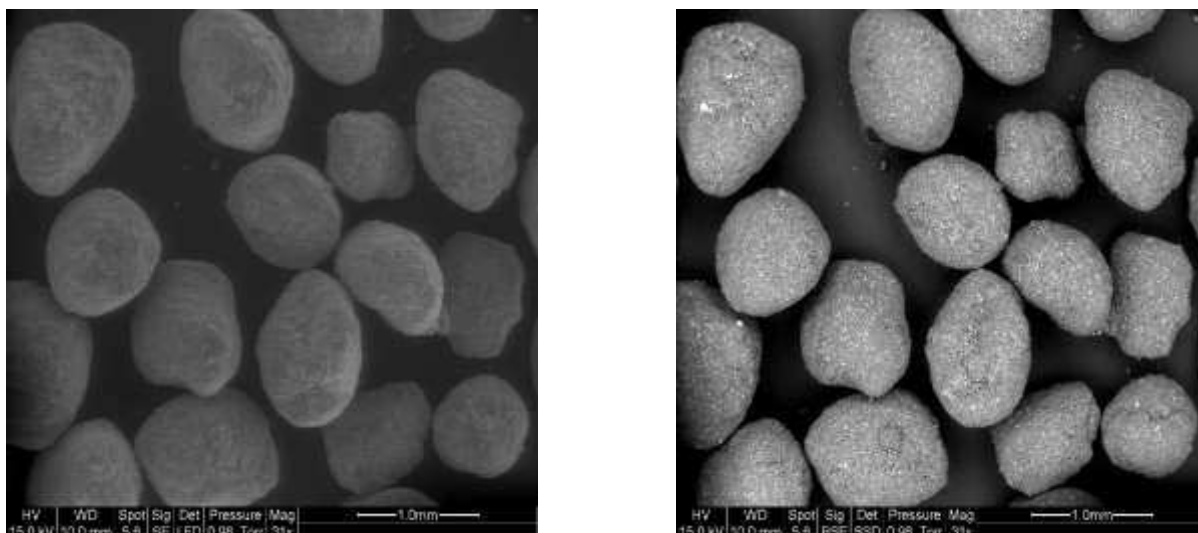
Figure 135 SEM micrograph of B2 particles (31 magnification), left – secondary electron mode, right – backscattered electron mode

SEM analysis was used to elucidate the structure of the immobilized sorbent and to identify the mode of interaction of biomass with the support. At first a hypothesis was formulated that the centre of granules was formed by the diatom shells, which was fold round by biomass. But as the particles were hard in dry state and became soft in wet state and disintegrated when used in mixed reactor (becoming so unsuitable for the use in such reactors), the hypothesis was reformulated. The idea that diatom shell residues are stuck mechanically (forming so a "grid") and the biomass is enwrapped in this "grid" somehow was proposed. This is visible in Figure 136 (left), where the diatom shells are well distinguishable (white shells), while black material corresponds to the biomass. No disintegration of the bead particles was observed during column experiments, after being re-dried, the particles became again hard.
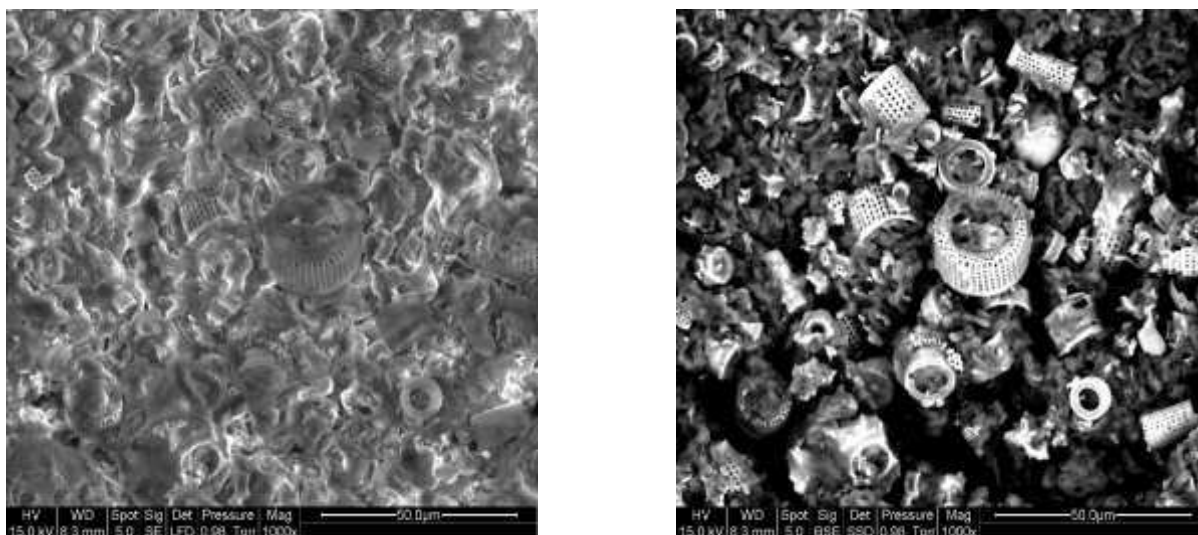
Figure 136 SEM micrograph of B2 particles (1000 magnification), left –secondary electron mode, right – backscattered electron mode

To test the sorption behaviour in batch mode, the mercury and hexavalent chromium sorption isotherms were determined for all beads fraction sizes (B1 – B8). These isotherms are summarized in Appendix F, where Figure 201 represents mercury sorption isotherms and Figure 215 corresponds to hexavalent chromium sorption isotherms, while Figure 216 shows total chromium sorption isotherms. Results of the modelling with Langmuir and Freundlich equations are presented in Table 63 for mercury and in Table 65 for hexavalent chromium. The experimental procedure is equally presented in Appendix F (page 311). In the case of both studied metals, an important drop in sorption capacities was observed (about 70% for both metals). This drop was partially related to the content of inert material in the beads (approx. 30%) and may be also related to inaccessibility of some sorption sites inside the bead particles.

4.6.1 Mercury

The experimental procedure for sorption in dynamic mode was described in chapter 3.4.5. The behaviour of *Tolypocladium* beads in a fixed bed column was studied to determine the breakthrough point - a crucial parameter for potential large scale applications. Accumulation of metals in the column is dependent on bed height (Z) (quantity of adsorbent inside the column), flow rate of solution (Q), inlet concentration (C_{in}) and size of adsorbent particles (d_p).

In the present study the bed height and flow rate (120 mL h^{-1}) were kept constant and the influence of inlet concentration (i.e. 100, 250 and 1000 mg Hg L^{-1}) and the influence of particles diameter on service time of the column and its breakthrough point were investigated. With regard to the inner column diameter (20 mm), only beads of diameter inferior to 2.5 mm were used (B1 – B3 size fraction). The ratio of inner column diameter and particle diameter should be superior to 10 in order to prevent creation of flow shortcuts and other irregularities.

The experiments were performed at ambient temperature. The working pH was that of the solution (pH 7) and was not controlled during the process. However, the pH of effluent was regularly checked. Effluent samples were analyzed in order to detect the breakthrough point. The breakthrough point (the time at which mercury concentration in the effluent reached 5% of the inlet concentration) was used to evaluate the breakthrough curves.

The breakthrough curves are presented by plotting the increase of normalized concentration (defined as the ratio of effluent to inlet concentration) versus volume of effluent. The individual breakthrough curves are listed in Appendix F, the evolution of effluent pH is superimposed in the Figures 185 – 192. Interestingly, the value of effluent/inlet concentration ratio never reached one, while it usually levelled off at a lower but stable value. The same behaviour was described by Huang C.-P. et al.[234] for dynamic sorption of copper(II) by *Saccharomyces cerevisiae* immobilized on sand and by Kapoor and Viraraghavan[137] for cadmium, copper, lead and nickel fixed bed column sorption by immobilized *Aspergillus niger*.

Another interesting observation was done throughout the experiments. A brown colouring of the effluent, probably due to a biomass leaching, appeared within the first hours of experiments. The intensity and time of this leaching seemed to be related to mercury concentration. The intensity of colour increased with increasing metal concentration, whereas the time of colouring decreased. Nevertheless, it seemed that there was no relation between this leaching and biosorption, as the breakthrough point appeared long time after disappearance of the colouring.

Figure 137 shows the influence of inlet concentration using B1 size of beads. The change in the concentration affected significantly the breakthrough curve. The driving force for biosorption is the concentration difference between the solute in the biosorbent and the solute in the solution. A high concentration difference provides a high driving force, which favours biosorption. Much sharper breakthrough curves were observed for higher mercury concentrations, while the service time shortened. The breakthrough was attained after 5 hours for 1000 mg Hg L^{-1}, while it corresponded to 12 and 68 hours for 250 and 100 mg Hg L^{-1},

respectively. This finding appears logic as the decreased inlet concentration caused a slower transport between liquid and solid due to the decreased concentration gradient. It resulted also in enlarged mass transfer zone, which led to more flat breakthrough curve (100 mg Hg L^{-1}). The breakthrough time decreased logarithmically with the increase of inlet concentration. Similar behaviour was observed for the two other size fraction used (Figure 211– B2 and Figure 212 – B3 size fraction, Appendix F).
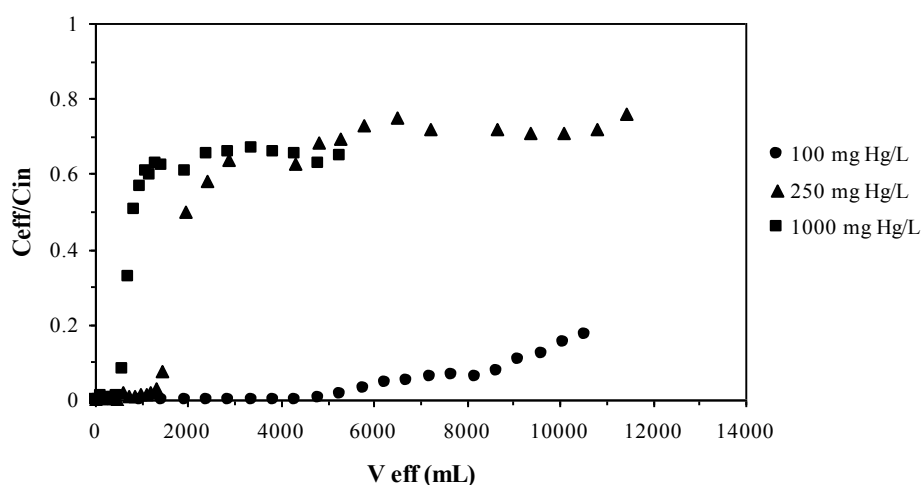
Figure 137 Influence of inlet concentration on mercury breakthrough curve using B1 size fraction

In the case of B3 size fraction (Figure 212), the breakthrough point appeared soon after the beginning of experiments for all tested concentration levels. The height of adsorption zone increases with increasing inlet concentration and especially with increasing size of biosorbents particles. It seemed that the transfer zone was larger than the bed height (short bed column) and that unfavourable operational conditions were chosen.

Figure 138 presents the influence of particle size on breakthrough curves at inlet concentration 100 mg Hg L^{-1}. Increasing particle diameter led to a decrease of column service time. Fluctuation of B3 experimental points in Figure 138 could be due to irregularities in inlet concentration.
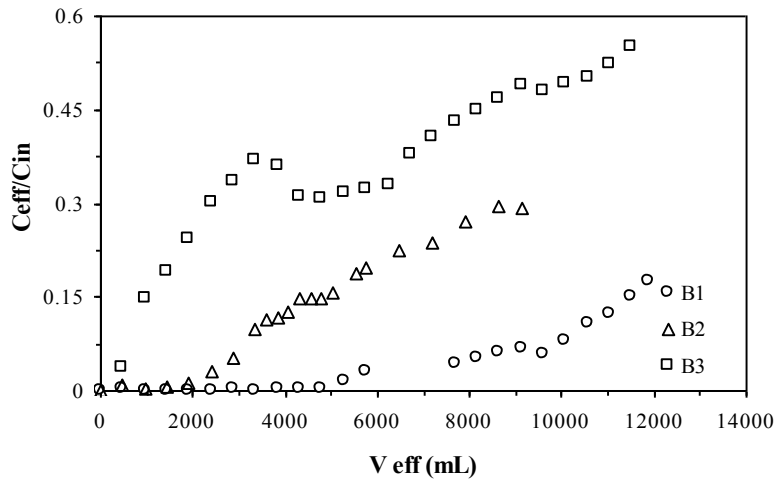
Figure 138 Influence of particle size on mercury breakthrough curve (C_{in} = 100 mg Hg L^{-1})

Similar trends were observed for the two other inlet concentrations tested (Figure 213, Figure 214, corresponding to 250 and 1000 mg Hg L^{-1}, respectively).

The main characteristics of obtained curves are summarized in Table 46. The total adsorbed contaminant quantity (q_{total}) – maximum column capacity - was calculated according to Eq. 43, whereas the area under the breakthrough curve (A) was obtained by integrating the adsorbed concentration (C_{ad}, [mg L^{-1}]) versus t plot using the rectangle method.

$$q_{total} = \frac{QA}{1000} = \frac{Q}{1000} \int_{t=0}^{t=t_{total}} C_{ad} dt$$

Eq. 43

Where:

A	is the area under the breakthrough curve, [mg h L^{-1}]
C_{ad}	is the adsorbed concentration, [mg L^{-1}]
q_{total}	maximum column sorption capacity, [mg]
Q	is the volumetric flow rate, [mL h^{-1}]

The total mercury amount injected to the column (m_{total}) was calculated according as follows:

$$\mathbf{m_{total}} = \frac{\mathbf{C_{in}Qt_{total}}}{1000}$$

Where:

m_{total} is the total amount of contaminant injected to column, [mg]

C_{in} is the inlet concentration, [mg L^{-1}]

Q is the volumetric flow rate, [mL h^{-1}]

t_{total} is the total flow time, [h]

The column performance is described as the total removal percentage of contaminant with the respect to flow volume and can be found from the ratio of total adsorbed quantity to the total amount of contaminant injected to the column. The equilibrium contaminant uptake in the column is defined as the total amount of contaminant sorbed per gram of sorbent at the end of total flow time:

$$\mathbf{q_{eq}} = \frac{\mathbf{q_{total}}}{\mathbf{X}}$$

Where:

X corresponds to mass of the sorbent in the column, [g],

q_{eq} is the equilibrium uptake, [mg g^{-1}].

The unadsorbed contaminant concentration at equilibrium in the column can be defined as:

$$\mathbf{C_{eq}} = \frac{\mathbf{m_{total} - q_{total}}}{\mathbf{V_{eff}}} \times 1000$$

The breakthrough time corresponds to the time when the effluent concentration reached 5% of inlet concentration.

Total adsorbed mercury quantity (q_{total}), removal percentage and equilibrium uptake (q_{eq}) increased with increasing mercury inlet concentration from 100 to 1000 mg Hg L^{-1}. Aksu and Gonen[185] observed that the values of q_{total} and q_{eq} for phenol uptake by activated sludge biomass increased with increasing inlet concentration, but the removal percentage showed an opposite character.

Sorbent size	C_{in} [mg L^{-1}]	q_{total} [mg]	m_{total} [mg]	% removal	q_{eq} [mg g^{-1}]	C_{eq} [mg L^{-1}]	t_{br} h
	100	440	1256	35	26	69	68
B1	250	336	895	38	19	129	12
	1000	1799	3623	50	102	543	5
	100	130	922	14	7	87	24
B2	250	253	729	35	14	165	5
	1000	488	1102	44	28	522	2.45
	100	412	1167	35	23	66	8
B3	250	285	806	35	17	167	3
	1000	1208	1865	65	69	342	1

Table 46 The effects of initial mercury concentration and particle size on the total adsorbed quantity (q_total), equilibrium uptake (q_eq) and total removal percentage for adsorption of Hg on *Tolypocladium* beads

A successful design of a column sorption process requires prediction of the concentration-time profile (breakthrough curve) for the effluent. Various mathematical models can be used to describe fixed bed systems. In our study, the dynamic behaviour of the column was described with Adams Bohart (Eq. 31, page 75), Thomas (Eq. 38, page 78) and Yoon and Nelson (Eq. 40, page 79) models.

The Adams Bohart model was used for the description of the initial part of the breakthrough curve. It is based on the surface reaction theory and assumes that equilibrium is not instantaneous. Therefore, the rate of the sorption is proportional to the fraction of sorption capacity still remaining on the sorbent. The model is characterized by two constants k_{AB} (mass transfer coefficient) and N_0 (saturation concentration). They may be obtained by linear regression when plotting $ln\ C_{eff}/C_{in}$ versus time. The linearization is performed only for the first part of breakthrough curve (corresponding to $C_{eff} = 0.15\ C_{in}$). Model parameters are summarized in Table 47. The model was not applicable on the breakthrough curve at

1000 mg Hg L^{-1} using B3 size fraction as the effluent concentration exceeded immediately the range of tested concentrations.

sorbent size	C_i	N_0	k_{AB}	R^2
	[mg L^{-1}]	[10^3 mg L^{-1}]	[10^{-3} L mg^{-1} h^{-1}]	-
B1	100	45	0.76	0.852
	250	18	1.32	0.809
	1000	42	0.59	0.702
B2	100	21	1.05	0.909
	250	9	2.76	0.817
	1000	15	1.43	1
B3	100	7	2.02	0.861
	250	-	-	-
	1000	8	1.85	0.963

Table 47 Adams Bohart model parameters

Aksu and Gonen[185] reported that for phenol sorption on activated sludge biomass both parameters were influenced by increasing inlet concentration and flow rate. The values of k_{AB} decreased, while N_0 increased. Aksu and Gonen concluded that overall system kinetics is dominated by external mass transfer in the initial part of dynamic biosorption. However, similar dependence of experimental data was not found in this case.

The fit of the model is illustrated in Figure 139, where the influence of inlet concentration is shown for B2 fraction size. The model predicted well the breakthrough time, especially at higher inlet concentrations.
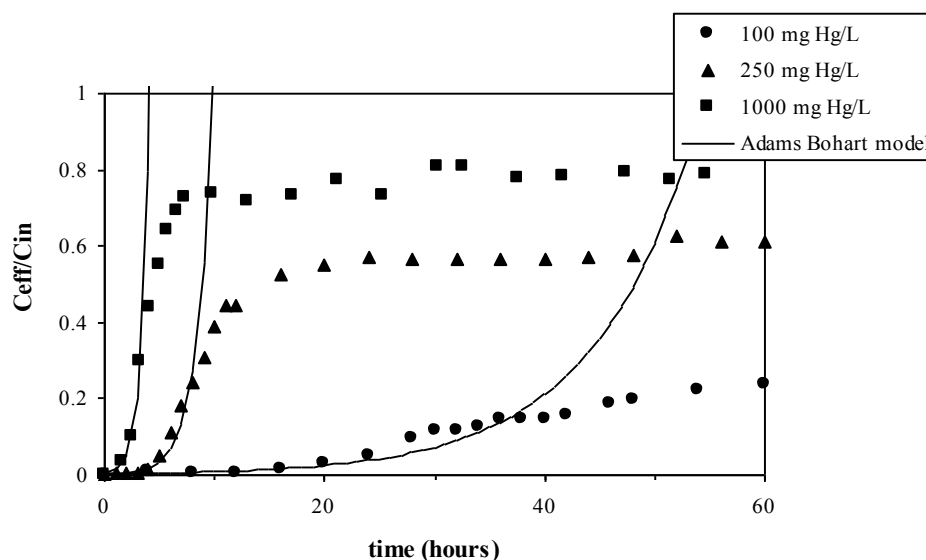
Figure 139 Fit of the Adams Bohart model at different inlet mercury concentrations using B2 size fraction

The Thomas model is one of the most widely used methods to describe biosorption column data. The model assumes Langmuir kinetics of sorption-desorption and no axial dispersion. It was derived for sorption process where the driving force obeyed second-order reversible kinetics. In the present study the column data were fitted by Thomas model to determine the Thomas rate constant (k_{Th}) and maximum solid phase concentration (q_0). The parameters were obtained by linear regression when plotting $ln\ (C_{in}/C_{eff}-1)$ as a function of time. Model parameters are summarized in Table 48.

sorbent size	C_i	k_{Th}	q_0	R^2
	[mg L^{-1}]	[10^{-5} L h^{-1} mg^{-1}]	[mg g^{-1}]	-
	100	73.9	83	0.873
B1	250	108.6	36	0.862
	1000	20.3	115	0.503
	100	63	52	0.788
B2	250	110.8	28	0.691
	1000	55.8	37	0.768
	100	21.3	54	0.688
B3	250	494.1	3	0.786
	1000	16.9	68	0.832

Table 48 Thomas model parameters

Vijayaraghavan and Prabu[235] reported that the values of kinetic constant decreased with increasing inlet concentration and increasing bed height, while it increased with the increase in flow rate values when *Sargassum wightii* biomass was used for copper(II) uptake. Similar behaviour was described by Han et al.[186] for lead and copper biosorption by chaff and by Aksu and Gonen[185] for phenol sorption using activated sludge.

In the present study a poor fit of this model to experimental data was found (see R^2 values in Table 48) and thus the trend observed by other authors could not have been confirmed. As illustrated in Figure 140 the model largely over-predicted the breakthrough point for initial concentration 250 mg Hg L^{-1}, while it followed the experimental data only approximately in case of 100 mg Hg L^{-1}. Only in the case of high inlet concentration the experimental data conformed to the model. Aksu and Gonen stated that the model is suitable for adsorption processes where the external and internal diffusions are not the limiting step, which is probably not the case in our study.
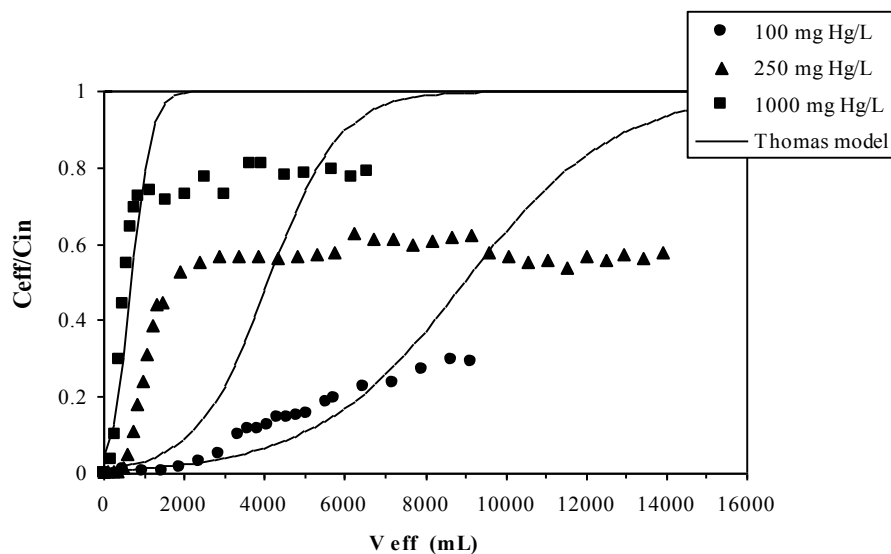
Figure 140 Fit of the Thomas model at different inlet mercury concentrations using B2 size fraction

The Yoon and Nelson model was developed to describe and predict adsorption and breakthrough of adsorbate vapours or gasses on activated charcoal. It is characterized by two parameters k_{YN} (rate constant) and τ (time required for 50% breakthrough). These constants are easily obtained by linear regression when plotting $ln(C_{eff}/(C_{in}-C_{eff}))$ as a function of time. The model parameters are summarized in Table 49.

sorbent size	Ci	k_{YN}	τ	R^2
	[mg L^{-1}]	[h^{-1}]	[h]	-
	100	0.08	112	0.873
B1	250	0.22	26	0.557
	1000	0.22	11	0.503
	100	0.06	74	0.788
B2	250	0.28	16	0.691
	1000	1.01	6	0.549
	100	0.02	80	0.688
B3	250	0.12	20	0.786
	1000	0.16	4	0.832

Table 49 Yoon and Nelson model parameters

Even in this case the model performed a poor fit to experimental data, but nevertheless the model breakthrough curve followed approximately the experimental data (Figure 141).

Vijayaraghavan and Prabu[235] reported that the values of k_{YN} followed the same trend (increasing) as k_{Th} parameter and found that τ parameter corresponded well to experimental data. The same conclusions were drawn by Aksu and Gonen.[185] Hamdaoui[236] found also good agreement between experimental data and model prediction for dynamic sorption of methylene blue by cedar sawdust and bricks.
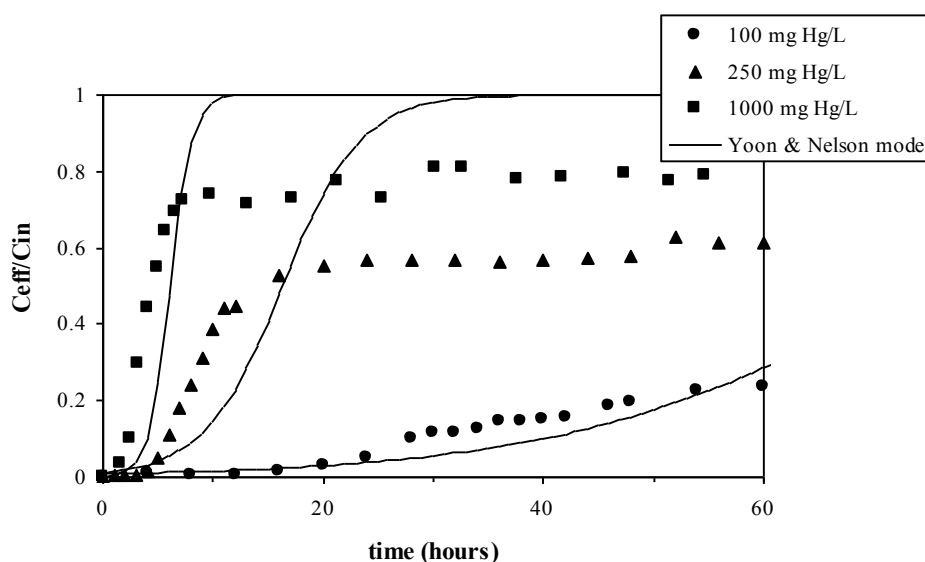
Figure 141   Fit of the Yoon & Nelson model at different inlet mercury concentrations using B2 size fraction

4.6.2 Hexavalent chromium

The experimental procedure for sorption in dynamic system was similar to that used for mercury. The bed height (Z) and flow rate (Q) were kept constant and the influence of inlet concentration and the influence of particles diameter on service time of the column and its breakthrough point were investigated. Size fraction B2 and B3 were used and only two concentration levels were tested (namely 100 and 1000 mg Cr(VI) L^{-1}). The experiments were performed at ambient temperature. The working pH was that of the solution (pH 2) and was not controlled during the process. However, the pH of effluent was regularly checked. Effluent samples were analyzed for both hexavalent and total chromium amount in order to detect the breakthrough point. The breakthrough point was used to evaluate the breakthrough curves.

A typical S-shaped breakthrough curve is displayed in Figure 142 (corresponding to inlet concentration 100 mg Cr(VI) L^{-1}, B2 sorbent size). The effluent/inlet ratio attained stable value 0.8 after 4500 mL of solution were pumped through the column, which corresponds approximately to 55 hours of experiments. It is interesting to observe that the value of this fraction never reached one (Figure 143 corresponding to the same inlet concentration, B3 size fraction), where five more litres of solution have passed without any change of this value, as already observed for mercury.

The dynamic experiments performed with hexavalent chromium were done before the experiments performed with mercury. At first, piston pumps were used to dose the solution, but as several pumps broke down during the experiments, causing so a total failure of the experiment, peristaltic pumps were obtained instead. Such a problem is illustrated in Figure 143, where certain problems with flow of solution are visible. In fact, the pump got out of order and the solution level lowered for a certain time and the column resembled to a batch reactor for certain period of time. When the pump was changed and the experiment continued, a decrease of normalized effluent concentration was observed. This finding signifies, according to Helfferich[237], that the process was governed by intraparticle diffusion. Helfferich proposed a simple experimental method to distinguish between external and intraparticle diffusion control called "interruption test". The beads are removed from the solution for a brief of period of time and are then re-immersed. The pause gives time for the concentration gradients in the beads to level out. Thus, with particle diffusion control, the rate immediately after re-immersion is greater than prior to the interruption. With film diffusion control, no

concentration gradients in the beads exist, and the rate depends on the concentration difference across the film. The interruption does not affect this difference and, hence, has no effect on the rate. The same behaviour may be observed when stopping column feed (like in this case).

The differences between hexavalent and total chromium amounts were only negligible compared to the batch mode. The reason could be that in batch systems the ions released by the biosorbent are maintained in solutions, but in continuous systems, these ions are continually removed from system. If consequently the reduction is some kind of secondary process appearing after certain equilibrium is established, this process may not be observed in column sorption.

Another interesting fact was observed during the first stage of the column experiment; a brown-pink colouring of effluent probably due to leaching of biomass appeared within the first 15 hours of experiment. This observation may be related to a slight discrepancy between both forms of chromium obtained in the first stage of the process.

The selection of the second concentration level 1000 mg L^{-1} did not reveal to be appropriate as the breakthrough point appeared very early after the beginning of the experiment (see Appendix F - Figure 221 corresponding to B2 size fraction and Figure 222 corresponding to B3 size fraction). The influence of increasing inlet concentration is illustrated in Figure 223 for B2 size fraction.
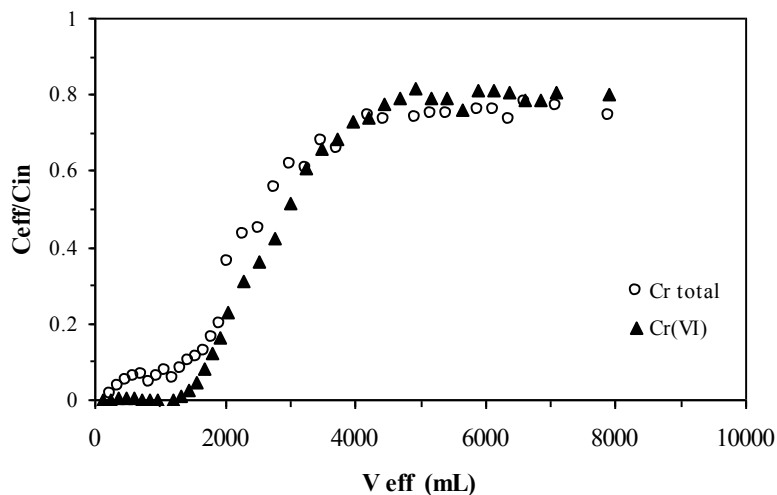
Figure 142 Chromium breakthrough curve (B2, C$_{in}$ = 100 mg Cr L^{-1})
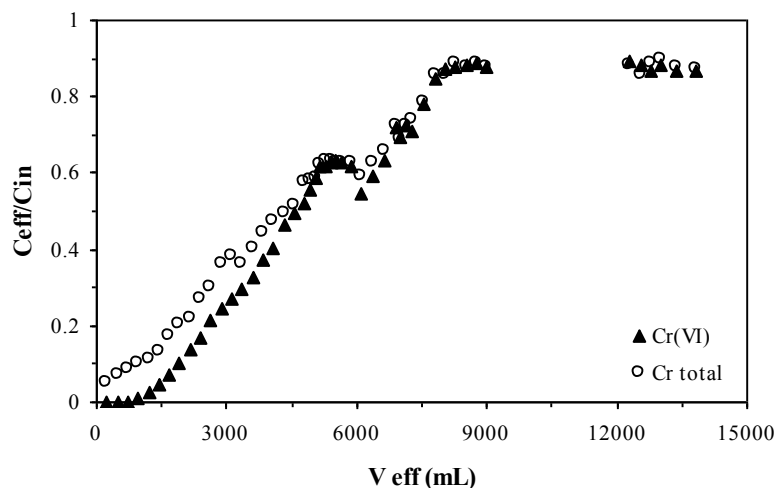
Figure 143 Chromium breakthrough curve (B3, C_{in} = 100 mg Cr L^{-1})

The main characteristics of obtained curves are summarized in Table 50. Total adsorbed mercury quantity (q_{total}), removal percentage and equilibrium mercury uptake (q_{eq}) increased with increasing chromium inlet concentration from 100 to 1000 mg Cr(VI) L^{-1}. Malkoc et al.[217] observed that the values of q_{total} and q_{eq} for hexavalent chromium uptake by olive pomace (olive oil industry waste) increased with increasing inlet concentration, but the removal percentage showed an opposite trend.

Sorbent size	C_{in}	q_{total}	m_{total}	% removal	q_{eq}	C_{eq}	t_{br}
	[mg L^{-1}]	[mg]	[mg]		[mg g^{-1}]	[mg L^{-1}]	h
B2	100	250	760	33	13	87	28
	1000	1568	2140	73	89	258	0.5
B3	100	425	863	49	22	49	14
	1000	1993	2603	77	116	224	0.5

Table 50 The effect of initial hexavalent chromium concentration and particle size on the total adsorbed quantity (q$_{total}$), equilibrium uptake (q$_{eq}$) and total removal percentage for adsorption of Hg on *Tolypocladium* beads

The Adams Bohart, the Thomas and the Yoon & Nelson models were used to describe experimental data. Generally, the data corresponding to inlet concentration 1000 mg Cr(VI) L^{-1} were not describable with these models. For the Adams Bohart model, the concentration range was immediately exceeded. For the Thomas model, negative values of kinetic constants

were obtained and the application of the Yoon and Nelson model resulted in negative values of 50% breakthrough time. The model parameters for 100 mg L^{-1} are summarized in following tables (Tables 50 - 52).

sorbent size	C_i	N_0	k_{AB}	R^2
	[mg L^{-1}]	[10^3 mg L^{-1}]	[10^{-3} L mg^{-1} h^{-1}]	-
B2	100	16	2.2	0.559
B3	100	7	5.63	0.836

Table 51 Adams Bohart model parameters

sorbent size	C_i	k_{Th}	q_0	R^2
	[mg L^{-1}]	[10^{-5} L h^{-1} mg^{-1}]	[mg g^{-1}]	-
B2	100	198	28	0.853
B3	100	129	27	0.715

Table 52 Thomas model parameters

sorbent size	C_i	k_{YN}	τ	R^2
	[mg L^{-1}]	[h^{-1}]	[h]	-
B2	100	0.19	46	0.853
B3	100	0.12	45	0.715

Table 53 Yoon and Nelson model parameters

The fit of the models is illustrated in following figures. Figure 144 shows that Adams Bohart model fitted reasonably well the experimental data and predicted well the breakthrough point. Yoon and Nelson model fitted the experimental data only approximately (see Figure 144). On the opposite hand, the Thomas model largely over-predicted the breakthrough and did not fit the experimental data at all as displayed in Figure 145.
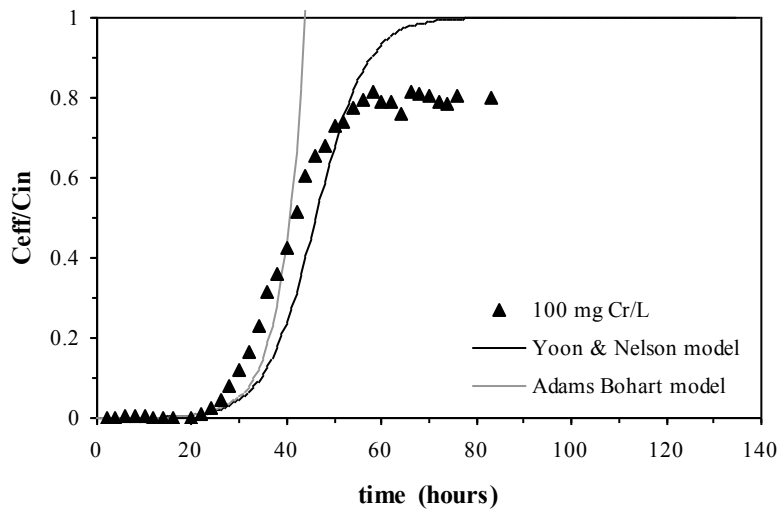
Figure 144 Fits of the Adams Bohart and the Yoon & Nelson models at 100 mg Cr(VI) L^{-1} using B2 size fraction
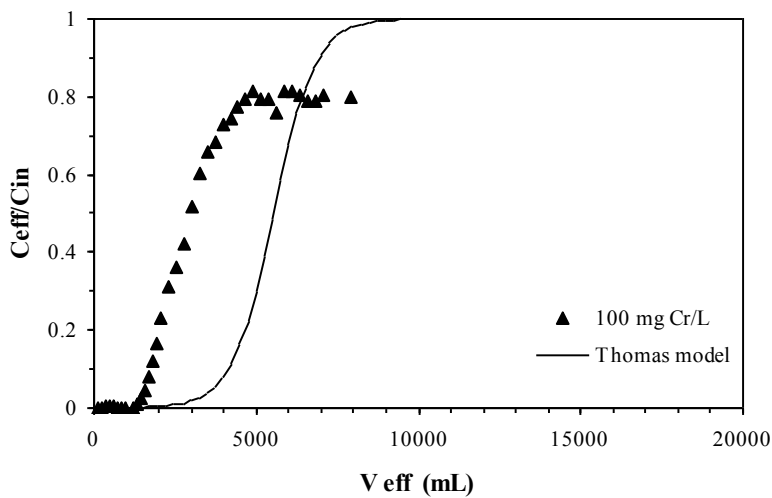
Figure 145 Fit of the Thomas model at 100 mg Cr(VI) L^{-1} using B2 size fraction

4.6.3 Conclusion

It was demonstrated that the *Tolypocladium* beads (biomass immobilized with infusorial earth) could be used in biosorption fixed bed column for mercury and hexavalent chromium uptake. Two parameters were tested. The influence of inlet concentration was

evaluated and the influence of particles diameter was investigated, while the bed height and flow rate were kept constant.

Increasing the inlet concentration led to decrease of column service time, while it caused the shortening of adsorption zone and therefore the breakthrough curves became sharper.

Two unusual observations were done within the experiments. The effluent/inlet concentration ratio did not reach one and levelled off at a lower but stable value. This is not inconvenient for the sorption process as it does not influence the apparition of the breakthrough point. A brown colouring of effluent appeared within the first hours of experiments, but it did not seem to be directly related to the sorption process as the breakthrough point arrived much later after the colouring disappeared.

Three models were used to describe experimental data. The breakthrough time was well predicted by Adams Bohart model for both metals. Thomas model reveals inappropriate as it largely over-predicted experimental data. The Yoon and Nelson model followed approximately the experimental data and could be used for rough approximation.

5 Conclusions

The objective of this study was to investigate the sorption properties of two industrial waste biomass samples – *Tolypocladium* sp. and *Penicillium oxalicum var. Armeniaca* - supplied by Czech industrial partners.

The bibliographic study has shown that biosorption is a promising technique; nevertheless its application has so far been constrained. The nature of interactions between metals and biological materials is extremely complex. Several mechanisms were proposed (chelation, ion exchange and electrostatic interaction), while these mechanisms may sometimes overlap. The bibliographic study also revealed the importance of pH of the sorption system on both metal speciation and biosorption mechanisms.

The experimental part confirmed good biosorption properties of both tested materials. While *Tolypocladium* biomass (referred as T sample) was ready to be used as supplied by the producer, *Penicillium* had to be submitted to several treatment procedures prior to being used as biosorbent. Biosorbent prepared by drastic treatment with NaOH (10M) – referred as P3 sample - revealed more efficient than the samples treated with less concentrated alkali. The analogy with chitin deacetylation procedure has been considered and may explain that the conversion of the biomass with alkaline treatment was efficient for deacetylation of chitin present in the cell wall of fungi.

Both materials have been successfully tested for biosorption of mercury, hexavalent chromium, cadmium and lead. The best sorption of cationic species was observed at pH close to neutrality, while hexavalent chromium was better removed from acid solutions.

Regarding maximum sorption capacities the biosorbent P3 clearly shows higher capacity for each individual metal (Hg, Cr, Cd and Pb) than biosorbent T. Comparing the maximum uptake capacity (derived from Langmuir model) in mass units the following order is obtained for P3 sorbent: Hg>>Cr>Pb>Cd, based on molar units the order changes significantly to: Hg$\cong$Cr>Cd>Pb. The same comparison for sorbent T is as follows: Hg>>Cr$_{total}$>Pb>Cd in mass units and Hg> Cr$_{total}$>Pb>Cd in molar units. Partial reduction of hexavalent chromium was observed in the case of T sorbent.

The sorption capacities of both tested materials towards mercury and chromium were on the upper boundary of the range reported in the literature, while the sorption capacities obtained for cadmium and lead were only mediocre.

When sorption mechanisms were investigated, the chelation of cations on nitrogen containing groups was proposed for P3 sample due to its content of chitin and chitosan (identified by FTIR spectroscopy), while for hexavalent chromium the electrostatic mechanism took place.

In the case of T sample, presence of carboxyl groups was confirmed on its surface. Furthermore, a significacnt decrease of pH was observed in this case indicating that a possible release of protons took place in the sorption process. Thus an ion exchange mechanism was proposed for cationic species. In the case of hexavalent chromium, a combined process of sorption and reduction was observed.

The use of instrumental analyses enabled to confirm the formulated hypotheses. FTIR analysis of metal saturated samples confirmed, that in the case of P3 sample, the adsorption bands corresponding to amine or amide groups were modified. A decrease in their intensity, their shifts and even disappearance were observed in the presence of the target metals confirming so the hypothesis of metal chelation on nitrogen containing groups.

For T sample, the changes in the FTIR spectra were less evident. Only the relative intensity of the band corresponding to a carbonyl of a carboxyl group decreased. Thus the ion exchange on carboxyl group was not excluded as the biosorption mechanism in the case of T sample. FTIR spectrum of chromium saturated T sample did not help to clarify the possible mechanism of the combined sorption/reduction mechanism, though the carboxyl group may probably participate in this process.

The target metals were found on the surface of each tested biosorbent sample by scanning electron microscope. It was possible to quantify their amount on SEM images visually and this amount appeared to be proportional to the sorption capacities reported earlier. According to the best sorption performance towards mercury, this metal was found in abundance on the surface of both biosorbents. While in the case of the T sample the formation of spherical microstructures was observed (consistently with information appearing in the literature), in the case of P3 sample numerous spots of much smaller size were observed together with chlorine. The visual identification of chromium and cadmium was more difficult due to their lower atomic numbers; nevertheless their presence was confirmed by EDX microanalysis. Concerning lead, well distinct white zones (islands-like) were found on the surface of P3 sample, supporting so the hypothesis of microprecipitation phenomenon. However, distinct small spots of lead were found on the surface of T sample.

Kinetics studies enabled to discuss the influence of several parameters on the rate of the process. The process followed pseudo-second order reaction kinetics and the Ho's

equation fitted well the experimental data. It was observed that the rate of biosorption decreased with increasing metal concentration and increasing particle diameter, while the influence of sorbent dosage was not clear. Unsatisfactory results were obtained for cadmium and lead. While cadmium biosorption efficiency was too low under selected experimental conditions, several irregularities were observed during lead biosorption.

Mercury biosorption seemed to be controlled by film diffusion as its rate decreased with increasing concentration and increasing sorbent size. In the case of hexavalent chromium, the influence was not clear. Very low correlation coefficients were obtained for T sorbent. This may indicate that artificial separation of film and intraparticle diffusion into separate models was not appropriate or that diffusion was not the rate limiting process. Hexavalent chromium biosorption was not sensitive to change in sorbent size in both cases, which may signify that the process took place in the entire particle and was not limited to its surface.

The influence of a second metal (cadmium and lead) on mercury sorption was also investigated. This characteristic is essential for practical application of the biosorption processes. The presence of other cations can affect the sorption of metal ions (primary cation) and hence influence its removal efficiency. Both P3 and T biosorbents were tested for the sorption from mercury-lead and mercury-cadmium systems. The selectivity of P3 sorbent for mercury was confirmed. In most cases, the presence of competitor ions influenced only slightly metal sorption, but the impact of competitor ion was not proportional to metal concentration. The only exception concerns mercury sorption by T biosorbent in the presence of cadmium; in this case the decreasing impact was proportional to concentration of competing ions.

Finally, it was demonstrated that *Tolypocladium* beads (biomass immobilized with infusorial earth) could be used in fixed-bed column for mercury and hexavalent chromium uptake. Two parameters were tested. The influence of inlet concentration was evaluated and the influence of particle diameter was investigated, while the bed height and flow rate were kept constant.

Increasing the inlet concentration led to a decrease of the column service time, while it caused the shortening of adsorption zone and therefore the breakthrough curves became sharper. Two unusual observations were done within the experiments. The effluent/inlet concentration ratio did not reach one and levelled off at a lower but stable value. This is not a drawback for the sorption process as it does not influence the appearance of the breakthrough

point, but it means that the saturation of the column is difficult to reach. A brown colouring of effluent appeared within the first hours of experiments, but it did not seem to be directly related to the sorption process as the breakthrough point arrived much later after the colouring disappeared. The breakthrough time was well predicted by Adams Bohart model for both metals.

Even though that P3 sample in its powdered form performed higher sorption capacities during batch experiments, its hydrophobicity made it difficult to use in a column mode due to possible clogging of the column. Therefore this material was not tested in a dynamic system. Additionally, the very low yield obtained during the preparation of P3 sorbent together with the important production of alkaline waste waters makes it less advantageous as a biosorbent. Actually, in an industrial scale, the significant production of alkaline filtrate would necessitate a neutralization treatment.

The feasibility of a desorption process was not investigated within this study due to very low acquisition costs of the materials. However, it should be kept in mind that the saturated material becomes a dangerous waste and as so it should be treated. Regarding high sorption capacities of biosorbents, low volumes of saturated materials would be eventually produced. Immobilization in solid matrixes and their disposal or incineration may be proposed as treatment techniques. Incineration (not suitable for volatile metals) leads to an important reduction of volume. These ashes could be then immobilized or leached out to recover the metals.

Nevertheless, the metals can be desorbed directly from the biomass. Numerous studies have illustrated that employing alkaline, acidic or complexing agents lead to successful elution. The priority of an elution process is to concentrate maximum of metal in minimal volume of the eluant. Good results were reported for cationic species, while hexavalent chromium elution revealed less advantageous as desorption proceeded via reduction. These problems were not taken into account in the present study, but the perspectives of this work may be found in this area.

6 Résumé en français

6.1 Biosorption

La contamination de l'environnement est due, entre autres, à l'activité industrielle humaine. Les activités industrielles ont perturbé les cycles naturels des métaux de façon importante. En raison de graves accidents d'intoxication de la population, les lois pour la protection de l'environnement se sont multipliées, signe d'une sensibilisation générale.

Différentes méthodes chimiques de traitement des effluents industriels métallifères ont été développées. Ces méthodes largement utilisées ont plusieurs inconvénients, comme la production de boues par précipitation et les coûts élevés dans le cas de techniques échangeuses d'ions et de méthodes électrochimiques. Dans ces conditions, l'utilisation de biomatériaux peut se révéler intéressante. Les procédés de biosorption ont fait l'objet d'une attention soutenue au cours des dernières années.

La biosorption est un procédé très étudié depuis près d'une trentaine d'années. Il s'agit de l'adsorption des métaux sur des matériaux d'origine biologique. Il existe deux mécanismes d'interaction entre le matériel biologique et le métal. Le premier mécanisme est dit « actif », lorsque l'interaction se fait entre le métal et le microorganisme vivant et que des procédés métaboliques sont mis en jeu. Le second mécanisme, « passif », dit physico-chimique, est basé sur l'interaction des groupements fonctionnels de la biomasse avec le métal. Si le microorganisme est vivant, il s'agit généralement d'un processus combiné. Le phénomène passif au contraire ne nécessite pas une activité biologique du microorganisme ; la biomasse peut être inactivée. Les matériaux dits morts sont dans ce cas davantage utilisés, car l'utilisation de biomasses non vivantes permet de remédier aux problèmes de toxicité et d'éliminer les contraintes, notamment économiques, que constituent la culture et l'approvisionnement de la biomasse vivante. Différents matériaux inactivés ont été testés pour étudier leurs capacités d'accumulation. Parmi eux, différentes algues, levures, champignons filamenteux et leurs dérivés (alginate, chitosane) ont fait l'objet de la plus grande attention. Ce sont surtout les champignons filamenteux (*Aspergillus niger, Rhizopus arrhizus, Penicillium* sp. etc.) qui présentent l'avantage de provenir généralement de sous-produits

d'autres industries: agro-alimentaire, synthèse d'enzymes, souvent peu ou mal valorisés. En tant que déchets, ces matériaux sont très peu coûteux.

La nature exacte des différentes interactions intervenant dans le procédé de biosorption est très peu connue. Une grande variété de mécanismes chimiques et physiques peut être impliquée : parmi eux, l'adsorption, la précipitation, la complexation et les phénomènes de transport. La récupération d'ions métalliques en solution aqueuse par ce procédé a fait l'objet d'un grand nombre de publications. Les biosorbants utilisés présentent des compositions chimiques diverses, qui dépendent principalement de leur origine mais aussi de leur mode de préparation. Les groupes aminés (-NH$_2$), carboxyliques (-COOH), phosphates (-PO$_4^{3-}$) et sulfates (-SO$_4^{2-}$) constituent les principaux groupes fonctionnels qui vont intervenir au niveau de la fixation des espèces métalliques. L'affinité et la spécificité des agents biosorbants vis-à-vis des métaux vont dépendre des propriétés chimiques des sites actifs.

L'étude bibliographique a démontré l'existence de deux groupes principaux de biosorbants – notamment les biosorbants issus d'algues et de leurs dérivés et les biosorbants fongiques et leurs dérivés.

Les biosorbants fongiques sont en général constitués de chitine ou de son dérivé (le chitosane), composés très actifs dans la biosorption. Leurs structures sont données sur les figures suivantes (Figures 1 – 2).
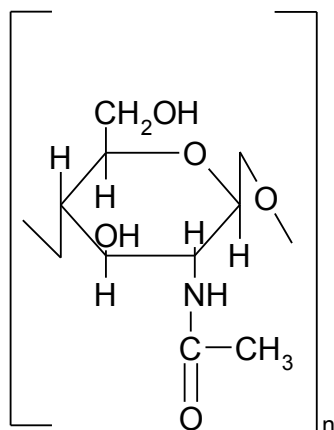
Figure 146 Unité monomère de la chitine
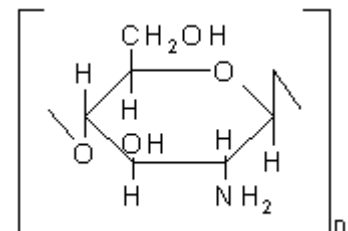
Figure 147 Unité monomère du chitosane

Le doublet électronique libre de l'azote (des groupes aminés ou amides) est susceptible de se lier aux cations métalliques à des pH proches de la neutralité (ou à faible acidité) par des mécanismes de chélation. D'autre part, la protonation des groupes aminés dans des solutions acides confère à la biomasse un caractère cationique, et par conséquent un fort potentiel d'attraction électrostatique des composés anioniques.

Néanmoins les groupes carboxyliques, ainsi que les groupes phosphatés éventuellement situés dans la paroi cellulaire peuvent également participer au processus de biosorption.

Mais ce sont surtout les biosorbants issus d'algues, qui sont en majorité constitués de matériaux présentant davantage de groupes carboxyliques. Ainsi le mécanisme d'échange d'ions a été identifié comme le mécanisme principal de biosorption par ces matériaux.

De nombreuses études ont été publiées sur la biosorption des métaux étudiés. Les études les plus importantes ont été résumées dans la partie bibliographique de la présente thèse. Le rôle primordial du pH initial a été montré. Pour les espèces cationiques, le pH optimal se trouve proche du pH neutre, alors que le pH acide favorise la biosorption des espèces anioniques (telles que les ions chromate). Dans le cas du chrome hexavalent (sous sa forme anionique) plusieurs mécanismes ont été décrits – notamment l'attraction électrostatique[55,54], la réduction[120,121] et les phénomènes combinés d'adsorption et de réduction[37,122].

Du point du vue de la description du procédé de biosorption en termes mathématiques, la biosorption est considérée comme une adsorption et est décrite par les mêmes modèles et équations.

6.2 Objectif

L'objectif de la présente thèse était d'étudier les possibilités de valorisation des déchets de biomasse issus de procédés de fermentation (produits en République Tchèque) en tant que biosorbants métalliques. Quatre métaux parmi les plus toxiques ont été choisis pour notre étude. Il s'agit du plomb, du cadmium, du mercure (formes cationiques) et du chrome hexavalent (forme anionique).

Dans le cadre de cette thèse, deux échantillons de déchets de biomasse on été obtenus. *Penicillium oxalicum var. Armeniaca* (CCM 8242) est un champignon filamenteux utilisé par l'entreprise Ascolor Biotec (République Tchèque) pour produire un colorant alimentaire rouge (Arpink Red™) par un procédé de fermentation par submersion. L'autre échantillon, *Tolypocladium* sp. − *Mycellium sterilae* MS 2929 (dérivé du microorganisme CCM 8184) est un champignon filamenteux employé dans la production d'antibiotiques de type cyclosporine par l'entreprise IVAX Pharmaceuticals (République Tchèque).

Les deux biomasses on été utilisées dans leur forme inactivée. *Tolypocladium* sp., nous a été livré sous sa forme inactive, l'inactivation ayant lieu lors du procédé de séparation du produit pharmaceutique. L'antibiotique est produit par la biomasse elle-même pendant le processus de fermentation par submersion puis séparé de la biomasse par une extraction méthanolique. La biomasse est ensuite filtrée, traitée par vapeur d'eau et séchée. La biomasse a l'aspect d'une poudre gris noir, très facile à manipuler (Figure 148).

Figure 148 Biomasse de *Tolypocladium* sp.

Figure 149 Biomasse de *Penicillium oxalicum* var. Armeniaca

Au contraire, *Penicillium* a été livré dans sa forme brute (boue), contaminée par le colorant (Figure 149), et a dû être inactivé par traitement alcalin (détails dans le Tableau 1). Les différents traitements ont été choisis d'après la solubilité du colorant. Bien que le colorant soit soluble dans l'eau et l'alcool, le rinçage par ces solvants n'a pas permis de l'éliminer.

Echantillon	Traitement de préparation	Effet
P1	rinçage par l'eau déminéralisée	couleur persistante
P2	rinçage par l'éthanol et l'eau déminéralisée	couleur persistante
P3	NaOH (10 M, point d'ébullition, 3 heures), rincé à l'eau jusqu'à pH neutre, filtré et séché (séchoir à lit fluidisé)	couleur éliminée
P4	NaOH (1 M, point d'ébullition, 3 heures), rincé à l'eau jusqu'à pH neutre, filtré et séché (séchoir à lit fluidisé)	couleur éliminée
P4FD	NaOH (1 M, point d'ébullition, 3 heures), rincé à l'eau jusqu'à pH neutre, filtré et séché (lyophilisé)	couleur éliminée

Tableau 1 Détails sur les traitements employés pour la préparation de la biomasse de *Penicillium oxalicum*

Seul le traitement alcalin a été efficace. Ce traitement est souvent envisagé dans la littérature pour la préparation de biosorbants efficaces à partir de biomasses fongiques.[135] De plus, ce traitement est connu pour ses effets sur la composition chimique des matériaux organiques. Il entraîne la désacétylation des constituants chitineux des parois cellulaires des champignons, et favorise la dissolution des protéines (composants inactifs ou peu actifs dans la biosorption) et des glucanes ainsi que l'hydrolyse des lipides.[200,203]

Les deux traitements alcalins ont bien conduit à l'élimination complète du colorant, mais un lavage intensif a été nécessaire ensuite pour enlever les traces des résidus alcalins. Ce traitement, même s'il mène à la production d'un biosorbant efficace, réduit significativement la masse (le rendement du procédé de traitement en matière sèche est de 20 – 30%). En considérant que la biomasse vivante contient un taux élevé d'eau (83%), la réduction de masse de la biomasse d'origine est donc très forte. Le traitement mène également à la création de volumes importants d'effluents alcalins, ce qui peut constituer un inconvénient en vue

d'une application industrielle éventuelle. Seuls les échantillons ne présentant pas de traces de colorant ont été utilisés par la suite.

Les deux matériaux ont été utilisés sous la forme d'une poudre sèche, après broyage et criblage. Les échantillons de granulométrie suivante ont été préparés : G1 < 125 μm < G2 < 250 μm < G3 < 355 μm < G4 < 510 μm < G5 < 750 μm.

6.3 Résultats

Le travail s'est organisé autour de 4 tâches :

- Caractérisations physique et chimique des biosorbants
- Etude de la biosorption à partir de solutions synthétiques monométalliques
- Etude de la biosorption à partir de solutions mixtes
- Etude de la biosorption en réacteur dynamique (colonne à lit fixé).

6.3.1 Caractérisation

Premièrement, une analyse élémentaire a été effectuée sur les biosorbants préparés (Tableau 2). Les taux de carbone, d'azote et d'hydrogène ont été déterminés, la méthode employée n'a pas permis la détermination directe du taux d'oxygène. Cette analyse a montré que les matériaux sont composés majoritairement de carbone, mais un taux important d'azote a également été identifié. Le rapport molaire C/N a significativement augmenté pour les échantillons P traités par la soude, ce qui est lié à la solubilisation des glucanes et des protéines, ainsi qu'à la désacétylation des fractions chitineuses.

La composition de la biomasse T est significativement différente par rapport aux échantillons dérivés du *Penicillium*.

Biosorbant	C(%)	H(%)	N(%)	rapport molaire C/N
P1	48,1	7,6	4,4	13
P2	43,4	7,1	5,1	10
P3	43,0	7,8	3,3	15
P4	44,8	7,3	3,1	17
T	51,9	8,0	6,5	9

Tableau 2 Analyse élémentaire des biosorbants

La surface spécifique, la densité et la porosité ont été mesurées. Les densités et les valeurs de surface spécifique sont comparables à celles d'autres biosorbants cités dans la littérature[58]. Il faut noter que la surface spécifique est beaucoup plus faible que celle de matériaux poreux, tel que le charbon actif.

Echantillon	Densité	Surface spécifique BET	Volume des pores	Taille des pores
	$[g.cm^{-3}]$	$[m^2\ g^{-1}]$	$[cm^3\ g^{-1}]$	[nm]
P3	1,34	1,19	-	-
T	1,32	1,23	0,0018	17

Tableau 3 Caractérisation physique des biosorbants P3 et T

La caractérisation chimique a été effectuée par spectroscopie infrarouge (FTIR). L'analyse par spectroscopie infrarouge a montré que le traitement de *Penicillium* par la solution de soude concentrée à température élevée a contribué à la désacétylation des fractions chitineuses de la structure des parois cellulaires de ce champignon. Le spectre du produit final – biomasse P3 – est proche de celui du chitosane, ce qui indique la présence de groupes aminés dans cet échantillon (Figure 19).

Au contraire, le spectre infrarouge de biomasse T est caractérisé par la présence de groupes carboxyliques, matérialisée par un pic significatif à 1745 cm^{-1} (Figure 19).
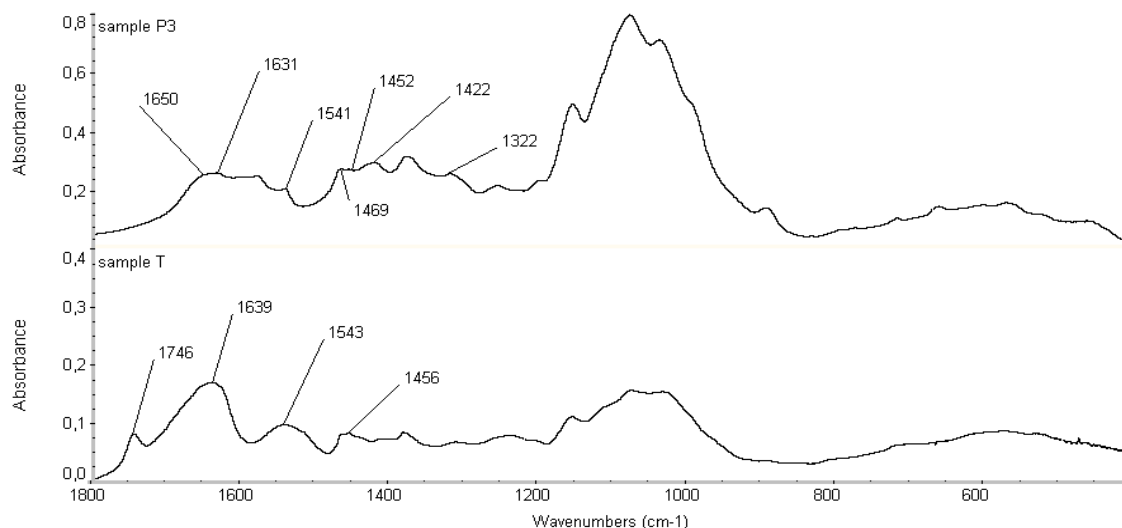
Figure 150 Comparaison des spectres FT-IR des échantillons P3 and T – détail 1800-400 cm⁻¹

6.3.2 Etude des équilibres de biosorption

L'étude de l'équilibre de biosorption constitue l'étape principale de chaque expérimentation. Il faut tout d'abord déterminer les conditions optimales d'expérimentation. L'étude bibliographique a montré que le pH de la solution joue un rôle primordial dans les procédés de biosorption. Nous avons donc déterminé en premier lieu le pH optimal. Cette étude nous a permis de choisir les biosorbants les plus performants parmi les 5 échantillons préparés, ainsi que de juger le traitement le plus efficace.

Le Tableau 4 récapitule les résultats obtenus. Le pH initial optimal pour les espèces cationiques est proche du pH neutre, alors que celui de l'espèce anionique est inférieur à 4 (milieu acide), indiquant l'existence de différents mécanismes mis en jeu. La biomasse P3 et la biomasse T ont été considérées d'après les premiers résultats comme les biosorbants les plus prometteurs et les expérimentations ont été poursuivies sur ces deux biosorbants.

Ces biomasses, employées lors de la fixation des ions métalliques, ont montré des propriétés d'échange protonique conduisant à des variations significatives du pH. Pour l'échantillon P3 (traité par la soude concentrée), une augmentation du pH a été observée, alors que dans le cas de la biomasse T, une forte baisse du pH vers une valeur d'équilibre égale à 4,5 a été notée. Ces changements de pH se sont révélés favorables pour la biosorption : lorsque le pH a été maintenu à sa valeur initiale, l'efficacité du procédé a fortement diminué.

Biosorbant	pH initial optimal			
	Hg	Cd	Pb	Cr(VI)
T	7	5	5	2*
P3	5	5	5	3*

Tableau 4 Les pH expérimentaux optimaux (*étant donné que Cr(VI) est susceptible de réduction à pH acide en présence de matière organique, la possibilité de la réduction a été testé)

Les courbes d'isotherme d'adsorption ont été obtenues en traçant la capacité de fixation en fonction de la concentration résiduelle du métal en solution. Ces courbes ont été modélisées par les équations de Langmuir et de Freundlich (Figure 151). Les résultats obtenus sont très différents selon les métaux. Dans le cas du mercure, des capacités de fixation très significatives pour les deux matériaux ont été observées. Les coefficients q_{max} caractérisant la capacité maximale de fixation ont atteint les valeurs de 270 mg g^{-1} (1,34 mmol g^{-1}) pour la biomasse P3 et de 160 mg g^{-1} (0,8 mmol g^{-1}) pour la biomasse T.
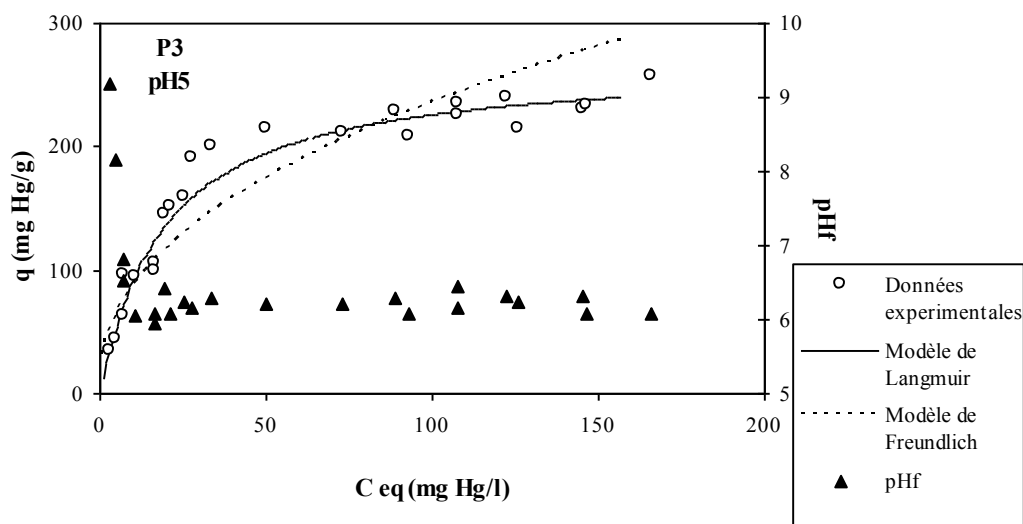
Figure 151   Isotherme d'adsorption de mercure (biomasse P3, pH$_i$=5)

De bons résultats ont également été obtenus dans le cas du chrome hexavalent. Le chrome hexavalent est un agent d'oxydation fort ; sa réduction étant fortement favorisée en milieu acide en présence de matière organique, il a été nécessaire de vérifier la concentration en chrome total ainsi qu'en chrome hexavalent. La différence entre les deux valeurs correspond à la fraction de chrome trivalent dans le système en équilibre. Dans le cas de la

biomasse P3, la présence de chrome trivalent n'a pas été observée. Au contraire, dans le cas de la biomasse T, la présence de chrome trivalent a été notée (Figure 152). Cette différence de comportement vis-à-vis du mécanisme d'oxydo-réduction pour les adsorbants P3 et T confirme la contribution de mécanismes distincts et la participation de groupes fonctionnels différents pour la fixation des ions métalliques pour ces deux matériaux.
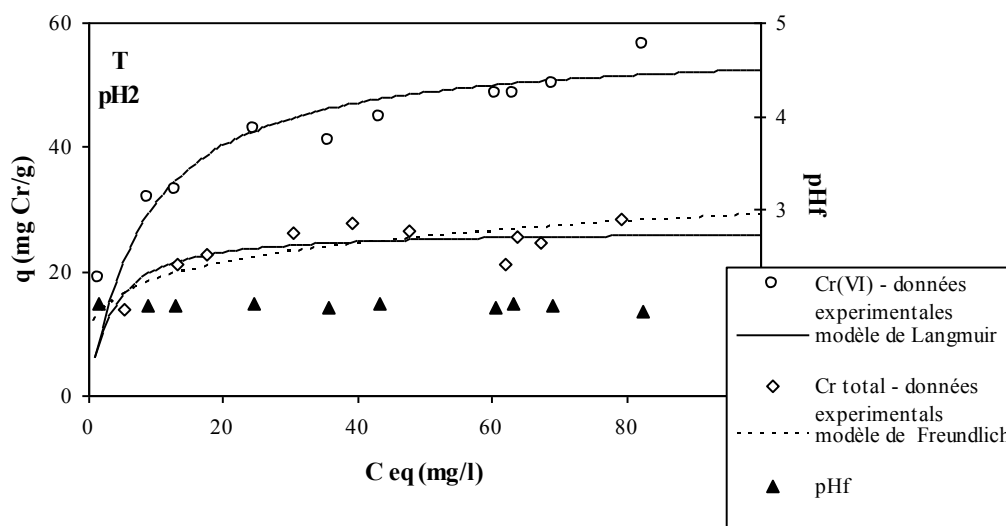
Figure 152 Isotherme d'adsorption du chrome (biomasse T, pH$_i$=2)

Une capacité de fixation très faible a été observée dans le cas du cadmium. Les résultats obtenus pour la fixation du plomb ne peuvent pas vraiment être comparés avec les résultats précédents, parce que les expérimentations ont été menées à une concentration plus faible pour prévenir le phénomène de précipitation de l'hydroxyde de plomb, qui aurait pu perturber la biosorption.

Le Tableau 5 résume les résultats obtenus dans le cadre de la détermination des isothermes d'adsorption.

Biosorbant	Métal	pH initial	Langmuir			Freundlich		
			q_{max}	b	R^2	k	n	R^2
			[mg g⁻¹]	[L.mg⁻¹]	-	[L g⁻¹]	-	-
			[mmol g⁻¹]	*[L mmol⁻¹]*	-			
P3	Hg	5	269 *1,34*	0,07 *14,04*	0,988	32	2,3	0,868
	Cd	5	36 *0,32*	0,05 *5,62*	0,929	6,0	2,8	0,895
	Pb	5	47,4 *0,23*	1,01 *209,3*	0,976	18,2	1,94	0,800
	Cr(VI)	3	71 *1,36*	0,39 *20,3*	0,990	27	4,1	0,810
T	Hg	7	161 *0,80*	0,50 *80,5*	0,973	59	3,9	0,730
	Cd	5	12 *0,11*	1,03 *115,8*	0,894	6,0	5,8	0,372
	Pb	5	28,4 *0,14*	0,61 *126,4*	0,945	10,3	2,58	0,68
	Cr (VI)	2	57 *1,09*	0,12 *6,2*	0,980	17,7	4,0	0,981
	Cr_{total}	2	27 *0,52*	0,31 *16,1*	0,955	11,9	5,1	0,650

Tableau 5 Isothermes de sorption pour les biosorbants P3 et T dans le cas de Hg, Cd, Pb et Cr(VI) – Paramètres des modèles, *les chiffres en italiques correspondent aux unités molaires*

6.3.3 Mécanisme d'élimination

Différentes méthodes d'analyse instrumentale ont été utilisées pour déterminer la nature des interactions entre les métaux et la biomasse. Le mécanisme de chélation des métaux sur les groupes aminés a été proposé pour la biomasse P3, alors que l'échange d'ions sur les groupes carboxyliques s'est révélé plus probable pour la biomasse T.

La diminution d'intensité des bandes d'adsorption correspondant aux groupes aminés a été observée dans le spectre infrarouge de la biomasse P3 saturée par le mercure.

Concernant les autres espèces cationiques, les mêmes effets ont été observés, mais en raison de leurs capacités d'adsorption plus faibles, la nature de ces effets est apparue moins évidente (Figure 47).
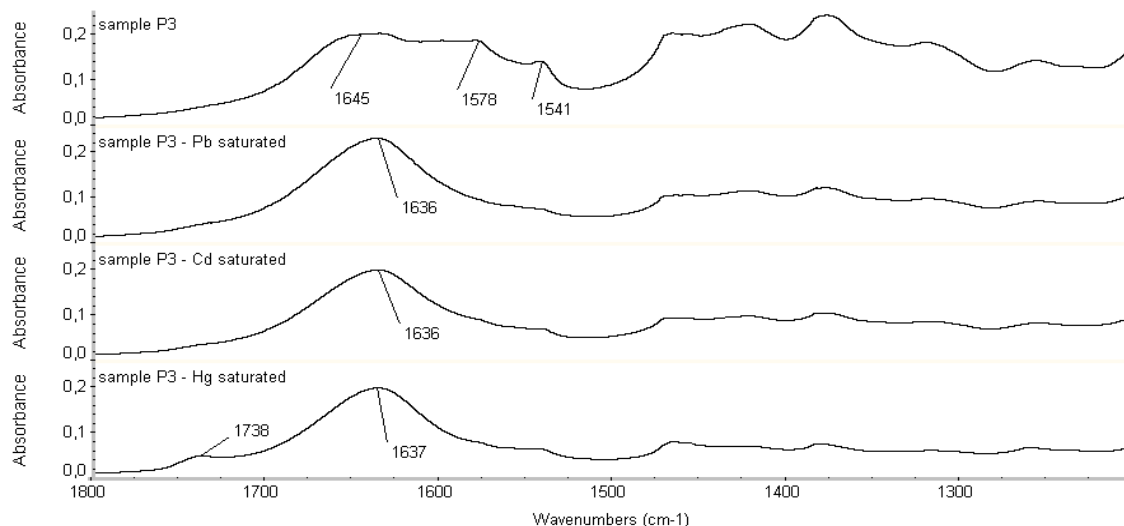
Figure 153 Spectres FTIR des échantillons P3 saturés par les métaux

Quant à l'adsorption des espèces anioniques, les échantillons de biomasse P3 protonée et saturée par le chrome ont également été étudiés. La participation des groupes aminés dans l'élimination du chrome a été confirmée. Néanmoins différents mécanismes sont impliqués– attraction électrostatique entre les groupes aminés protonés et le chrome dans sa forme anionique.

Concernant la biomasse T, les spectres infrarouges n'ont pas présenté de modification aussi évidente. La comparaison des spectres avant et après la saturation a mis en évidence la diminution d'intensité de la bande correspondant à la vibration d'étirement du carbonyl d'un groupe carboxylique. Ainsi, le mécanisme d'échange d'ions n'est pas exclu.

Les spectres de biomasse T protonée et en contact avec du chrome n'ont pas permis de confirmer le mécanisme combiné d'adsorption/réduction.

Les observations en microscopie électronique à balayage ont confirmé la présence des métaux étudiés à la surface des échantillons saturés. La quantité relative des métaux est proportionnelle aux capacités d'adsorption mesurées par l'étude des isothermes.

6.3.4 Cinétique et mécanismes diffusionnels

L'objet de cette partie de l'étude a consisté à déterminer le mode de transfert qui contrôle la cinétique de biosorption des métaux étudiés, en mettant en évidence l'intervention plus ou moins importante des mécanismes diffusionnels par l'utilisation de modèles simples.

La biosorption d'un soluté en phase liquide sur un support solide est contrôlée par différentes étapes incluant des phénomènes de diffusion et des phases de fixation proprement dite.

Il existe quatre étapes limitantes de la cinétique (Figure 8) :

1) le transport du soluté de la solution vers la couche limite entourant la particule
2) le transfert du soluté du film vers la surface adsorbante – diffusion de film ou externe
3) la diffusion du soluté de la surface vers les sites internes – diffusion intraparticulaire
4) la fixation du soluté sur les sites adsorbants
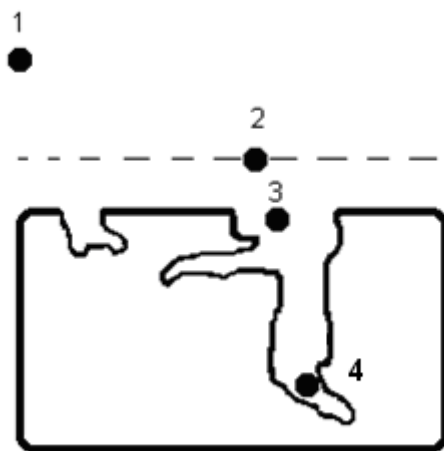
Figure 154 Phénomènes de transport en cinétique de biosorption[159]

La vitesse finale du procédé dépend de l'étape la plus lente car toutes les phases s'effectuent en série. L'étape 1) de diffusion de la solution vers la couche limite est fonction des conditions opératoires, notamment de la vitesse d'agitation du système. En effet, une vitesse insuffisante peut provoquer des gradients de concentration au sein de la solution mais, en supposant le réacteur parfaitement agité, on peut estimer que cette phase n'est pas limitante.

La phase de biosorption (4) proprement dite, est une phase quasi-instantanée en système isotherme, qui ne limite donc pas la cinétique globale de fixation, mais cette phase peut toutefois contrôler la vitesse globale si des phénomènes complémentaires tels que la précipitation interviennent.

On peut donc estimer que la phase de transfert au sein de la solution n'est pas limitante dans un réacteur parfaitement agité et que la biosorption est contrôlée par la diffusion externe ou par la diffusion intraparticulaire.

Les mécanismes diffusionnels ont fait l'objet de nombreuses études. Parmi les modèles proposés dans la littérature, une approche simplifiée a été choisie qui quantifie séparément la diffusion externe et la diffusion intraparticulaire. Ces modèles sont discutés en détail dans le manuscrit de la présente thèse.

Alors qu'un seul modèle a été utilisé pour l'évaluation de la contribution de la diffusion externe à la vitesse globale du procédé, deux modèles concernant la diffusion intraparticulaire ont été utilisés, le modèle de Weber et Morris et le modèle de Urano et Tachikawa.

L'étude de la cinétique a permis d'évaluer successivement l'effet de paramètres tels que la concentration en ions métalliques, la dose de biosorbant et la taille des particules de ce biosorbant.

En premier lieu, l'influence de la concentration initiale a été étudiée. L'application des différentes équations pour déterminer l'ordre de la réaction a montré que la cinétique de biosorption du mercure est du second ordre. La relation entre la vitesse d'élimination, l'efficacité du procédé et la concentration initiale est claire. Il a été notamment possible d'observer que l'efficacité du procédé (en matière de transfert) est favorisée par une concentration élevée du soluté ; le gradient de concentration peut favoriser la diffusion des ions métalliques au travers de la couche limite et/ou vers les sites intérieurs accessibles. Le temps nécessaire pour atteindre l'équilibre augmente aussi avec la concentration.

Les figures 10 et 11 illustrent l'effet de la concentration en mercure sur les mécanismes diffusionnels.
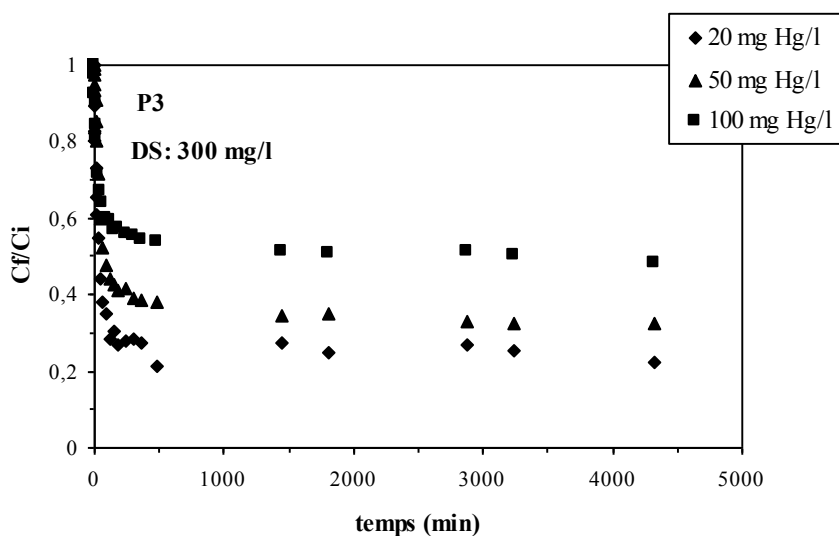
Figure 155 Effet de la concentration initiale sur la cinétique de biosorption (pH$_i$=5, biomasse P3, 300 mg adsorbant l^{-1})
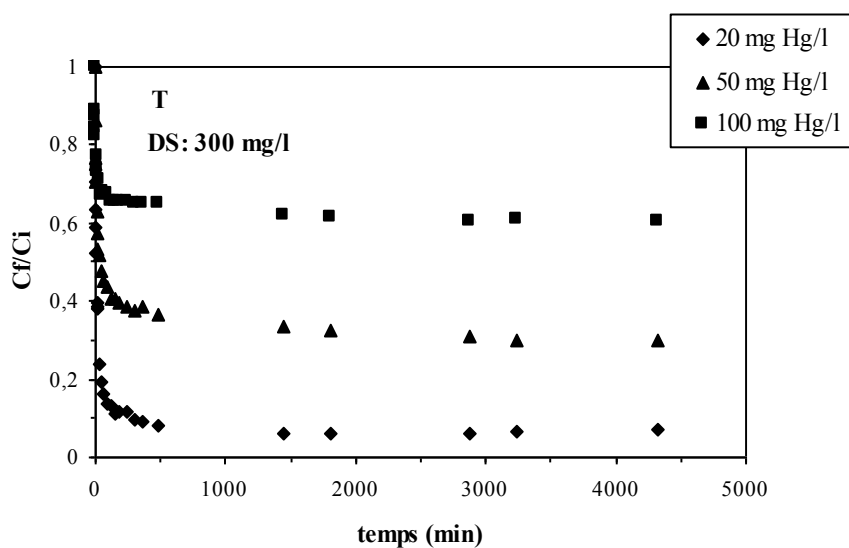
Figure 156 Effet de la concentration initiale sur la cinétique de biosorption (pH$_i$=7, biomasse T, 300 mg adsorbant l^{-1})

Accroître la concentration initiale en métal provoque un abaissement du coefficient de transfert externe et une amélioration, au début de la cinétique, du coefficient de diffusion intraparticulaire (selon le modèle de Morris et Weber). Les figures montrent que le procédé peut être divisé en deux phases. Une première phase de biosorption très rapide a lieu en quelques heures, qui peut correspondre à l'adsorption des cations métalliques à la surface des

particules. En effet, une chute importante de la concentration dans la couche limite entourant la particule est observée lors du contact entre la solution et les particules de biosorbant. En conséquence, le gradient de concentration est réduit, ce qui provoque une baisse du flux entre le cœur de la particule et la solution. Pour une concentration faible (20 mg Hg l^{-1}), cette première phase constitue l'essentiel de l'adsorption du procédé car la cinétique est ensuite limitée par un faible gradient de concentration. Pour les concentrations plus importantes, le gradient de concentration reste toutefois assez élevé après la saturation de surface pour forcer les ions métalliques à pénétrer dans les pores des particules. On peut donc conclure que ces deux phases varient en fonction du gradient de concentration.

L'augmentation de dosage du biosorbant a permis d'augmenter l'efficacité du procédé. Néanmoins, l'existence d'un seuil au-dessus duquel l'efficacité n'augmente plus a été observée. L'influence directe du dosage sur les procédés diffusionnels n'a pas été constatée.

Quant à l'effet de la taille de particules, l'allure des courbes indique une diminution de la vitesse d'adsorption avec une augmentation de diamètres des particules. Le temps nécessaire pour atteindre l'équilibre est du même ordre de grandeur, quelle que soit la taille des particules alors que la concentration à l'équilibre diminue avec le diamètre. Cela indique que la taille du biosorbant ne modifie pas la vitesse globale du procédé mais les capacités d'adsorption. Le phénomène se produit donc essentiellement en surface de la particule et non dans l'ensemble de la particule.

Dans le cas du chrome, une efficacité globale plus faible a été en général observée. Les mêmes tendances que dans le cas du mercure ont été obtenues : l'efficacité diminue avec l'augmentation de la concentration initiale et avec la diminution du dosage. La cinétique de biosorption du chrome est également de second ordre.

La réduction du chrome en présence de la biomasse T ayant été observée pendant la détermination des isothermes, nous avons souhaité étudier l'évolution de ce phénomène en fonction du temps. Il a été observé qu'une faible proportion de chrome et une forte dose de biomasse favorisent la réduction. Le fait que la réduction se soit produite surtout dans la deuxième phase de biosorption est plutôt surprenant (Figure 157).
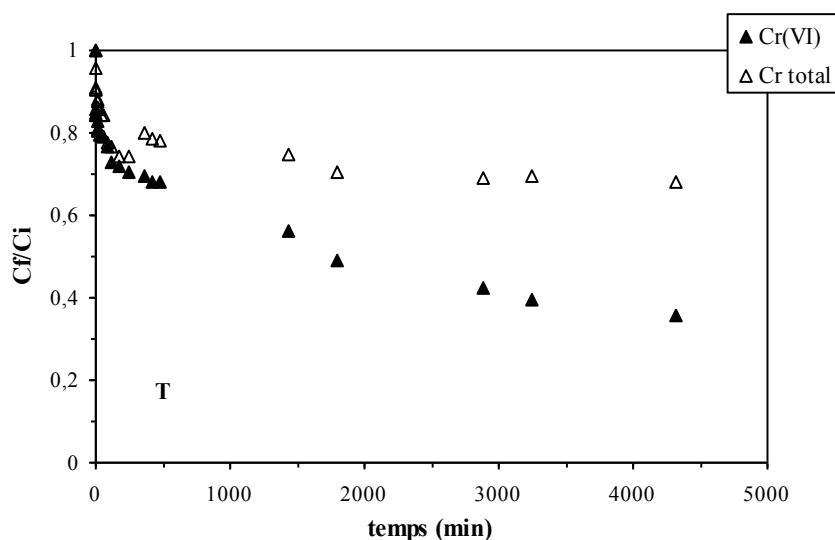
Figure 157 Comparaison de l'efficacité de l'élimination du Cr(VI) et Cr$_{total}$ (pH$_i$=2, 50 mg Cr(VI) l^{-1}, 500 mg adsorbant l^{-1})

L'application de modèles de diffusion pour la biomasse T s'est révélée difficile, les données expérimentales ne suivant pas une tendance linéaire. Cela signifie que la séparation artificielle des deux phénomènes n'est pas justifiée ou que le procédé n'est pas contrôlé par la diffusion.

Dans le cas de la biomasse P3, la réduction du chrome n'a pas été observée. L'idée d'un mécanisme d'attraction électrostatique entre les groupes aminés et le chrome (HCrO$_4^-$) parait donc plus appropriée pour décrire le phénomène de fixation. Ni l'effet de la concentration initiale ni l'effet du dosage ne se sont révélés significatifs sur les coefficients de diffusion. Par ailleurs, aucune influence significative de la taille des particules sur la vitesse de l'élimination et sur l'efficacité n'a été réellement observée. Ce fait signifie que la biosorption a eu lieu dans l'ensemble des particules et que le procédé n'est pas sensible à la surface spécifique des particules.

Une efficacité de fixation très faible a été observée dans le cas du cadmium. Les expérimentations n'ont donc pas été poursuivies. Dans le cas du plomb, une fluctuation assez forte des données expérimentales a été régulièrement observée. Des indications indirectes qu'il s'agit d'un mécanisme de microprécipitation ont été obtenues. La cinétique n'a suivi ni une équation du premier ordre ni une équation du second ordre et les modèles de diffusion ne sont pas applicables, car une diminution rapide de la concentration a été notée dans les

premières minutes des expérimentations, ce qui aboutit à une dépendance non linéaire de ces données.

6.3.5 Expérimentations menées en solution mixte

Les effluents industriels contiennent souvent plusieurs métaux, en plus des sels et de la matière organique, ainsi que des particules solides. Les différents composés peuvent souvent interagir entre eux en formant de nouvelles espèces. Il apparaît donc important pour d'éventuelles applications industrielles d'étudier la biosorption à partir de solutions mixtes. L'interaction des métaux en solution et des changements d'état (formation de complexes de différentes charges) peuvent réduire l'efficacité du procédé. De plus, il peut y avoir compétition entre les métaux pour le même site de fixation. Des effets synergétiques ne peuvent pas être exclus non plus. Ces effets dépendent du nombre de métaux présents en solution, de leurs combinaisons et de leurs concentrations, mais surtout du mécanisme de fixation.

Comme il a été montré dans les paragraphes précédents, les meilleurs résultats en termes de capacité de biosorption ont été obtenus dans les cas du mercure et du chrome hexavalent. Comme le pH optimal de biosorption du chrome est acide et comme la biosorption des cations métalliques est insignifiante dans cette zone de pH (cela a été montré dans la littérature et confirmé par nos expérimentations), les expérimentations en solution mixte n'ont pu être menées que dans le cas du mercure. L'influence de la présence du cadmium et du plomb sur l'efficacité de la biosorption du mercure a été étudiée en détail. Les expérimentations ont été menées au pH optimal des deux métaux. Dans le cas où le pH optimal des deux métaux était différent, les expérimentations ont été faites au pH optimal du mercure.

Dans le cas de la biomasse P3, la capacité de biosorption du mercure en présence de plomb n'a été influencée que faiblement, tandis que la capacité de fixation du plomb a fortement chuté. Aucune corrélation entre cette chute et la concentration de mercure n'a pu être observée. La spéciation des deux métaux en solution mixte, étudiée au moyen du logiciel Visual MINTEQ ver. 2.5[213], n'a pas permis de mettre en évidence des interactions entre ces deux métaux. L'étude par spectroscopie infrarouge des biomasses saturées a confirmé que ce

sont les groupes aminés qui interviennent dans l'élimination des deux métaux étudiés. Une compétition entre les deux métaux pour le même site de biosorption était attendue, mais n'a pas été confirmée. La modélisation a révélé également que les deux métaux n'existent pas sous la même forme. Alors que le plomb est présent dans la solution sous sa forme cationique (Pb^{2+}), le mercure existe au contraire sous forme non ionique ($HgCl_2$). Il est donc possible, que, même si la fixation s'effectue sur le même groupe fonctionnel, la nature des forces de fixation soit différente. La capacité de biosorption totale (obtenue comme la somme des capacités des métaux individuels en unité molaire) n'a pas diminué quand les métaux étaient présents en solution mixte. Cela signifie que la réduction de la capacité de fixation du plomb a été compensée par une faible augmentation de celle du mercure. La sélectivité de la biomasse P3 pour le mercure a donc été confirmée.

Dans le cas du cadmium, des concentrations en cet élément équivalentes à celles du mercure ont pu être utilisées, ce qui a permis de mieux percevoir d'éventuels effets de compétition.

Pour la biomasse P3, une inhibition faible de la capacité de fixation du mercure a été observée à concentration faible en mercure (de l'ordre de 30%), alors que pour une concentration en mercure plus élevée, cette inhibition a disparu et une augmentation a été observée. D'un autre côté, une faible diminution de la capacité de fixation du cadmium en présence de mercure a été également observée. La capacité totale de fixation a très peu diminué par rapport à la capacité totale théorique calculée sur la base de résultats correspondant aux systèmes monométalliques. La compétition entre les deux métaux en solution est faible.

Le seul cas dans lequel une corrélation entre un effet d'inhibition et la concentration du deuxième métal a été notée correspond à la biosorption par biomasse T du mercure en présence de cadmium (Figure 158). L'inhibition de la fixation du mercure a été plus évidente à des concentrations d'équilibre plus élevées.
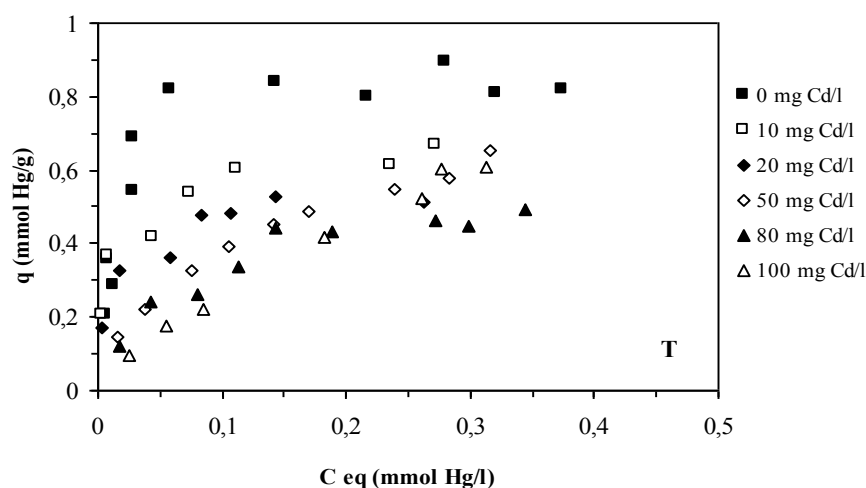
Figure 158   Isothermes d'adsorption du mercure pour la biomasse T à pH initial 7 et pour des concentrations en cadmium entre 0 et 100 mg Cd L^{-1}

L'inhibition de la biosorption du cadmium a été également observée. A faible concentration du métal, l'ion compétiteur a peu d'influence sur la capacité de fixation. L'effet de la présence des ions compétiteurs est plus marquée en s'approchant de la saturation de l'adsorbant. Une importante baisse de la capacité totale de fixation a été également notée, indiquant l'existence de l'effet de compétition.

La modélisation de spéciation a montré qu'à pH final (le même pour les deux matériaux), la majorité du mercure existe sous la forme HgCl$_2$ et la majorité du cadmium sous forme Cd^{2+}. La modélisation de spéciation des deux métaux en solution n'a pas permis de mettre en évidence des interactions entre ces métaux. L'étude des spectres infrarouges a montré la présence de groupes carboxyliques en surface de la biomasse T. De fortes indications ont également été obtenues indiquant que ces groupes interagissent avec les métaux. Néanmoins, la participation des groupes aminés n'a pas pu être exclue. La théorie de l'échange d'ions sur les groupes carboxyliques paraît la plus adaptée. Il n'a pas été possible d'établir avec certitude le mécanisme de compétition.

6.3.6 Expérimentations en colonne

Après l'étude des mécanismes d'adsorption en régime statique, qui a permis notamment de caractériser les conditions opératoires optimales, de définir les mécanismes mis en jeu et d'évaluer les possibles effets réciproques de compétition, l'intérêt a été porté sur les performances de biosorption en régime dynamique. L'expérimentation en colonne est un outil indispensable pour comprendre et modéliser le transport et les interactions des solutés en milieu poreux et également en vue d'une mise en œuvre sur un site industriel. Au cours de son passage dans le matériau poreux, la concentration du métal diminue progressivement. La variation de la concentration en sortie au cours du temps dépend des processus physico-chimiques à l'intérieur de la colonne (mécanisme de biosorption, phénomènes diffusionnels).

L'utilisation de matériaux sous forme de poudre comme dans les réacteurs statiques se révèle défavorable en raison de leurs faibles propriétés hydrodynamiques. La petite taille et la faible densité peuvent provoquer des difficultés telles que le colmatage et le blocage de la colonne.

Le comportement des deux biomasses au contact de l'eau diffère, comme nous l'avons observé au cours des expérimentations cinétiques. La biomasse T a été dispersée immédiatement après son addition dans le système. La biomasse P3 a montré, lors de son ajout dans le système sous forme pulvérulente, des tendances à s'agréger en formant des grumeaux vraisemblablement en raison de son hydrophobicité. Ce comportement aurait pu causer de graves perturbations de fonctionnement en colonne.

Pour prévenir les difficultés mentionnées ci-dessus, la littérature recommande l'immobilisation des poudres sur un support solide. Bien que cette opération améliore le comportement hydrodynamique, elle occasionne une augmentation des coûts et souvent une baisse de la capacité de fixation ramenée au poids total de l'adsorbant conditionné.

Dans la présente étude, les expérimentations avec la biomasse P3 n'ont pas été poursuivies, tandis que la biomasse T a été utilisée sous la forme de billes. Le producteur de la biomasse *Tolypocladium* nous a livré la biomasse sous forme de billes provenant du procédé de séparation de la biomasse par filtration sur un lit de diatomées. En se mélangeant avec les

enveloppes des diatomées, des billes ont été produites. Les billes étaient de tailles variables (entre une poudre et de grosses billes de quelques millimètres). A l'état sec, les billes sont dures et cohésives. A l'état mouillé, elles se délitent plus facilement.

Avant l'utilisation en colonne à lit fixe, les billes ont été tamisées (0<B1<0,5mm<B2<1mm<B3<2,5mm<B4<3,15mm<B5<5,0mm<B6<5,6mm<B7<8mm), caractérisées par différentes analyses et testées dans les réacteurs statiques afin de comparer leurs capacités de fixation avec des poudres, dans le cas du mercure et du chrome hexavalent. Il a été prouvé que les billes contiennent approximativement 30% de matière inorganique, en majorité composée de SiO_2 (résidus de diatomées). Une chute importante de la capacité de fixation a été observée dans le cas du mercure ainsi que dans le cas du chrome hexavalent. La réduction est de l'ordre de 70% dans les deux cas. La réduction est due au contenu en matière inorganique (approximativement 30%), mais peut aussi être liée à l'inaccessibilité de certains sites dans la particule.

Le montage expérimental est montré sur la Figure 159. Une colonne en verre a été utilisée. Le diamètre intérieur de la colonne est de 2 cm et sa hauteur est de 15 cm. Une hauteur de lit de billes à l'état sec de 8 cm a été choisie, les billes ayant tendance à augmenter de volume en s'hydratant. La hauteur réelle du lit atteinte dans la colonne est de l'ordre de 11 cm. Seules les billes B1 – B3 ont été utilisées. Deux types de flux ont été testés (flux ascendant et flux percolant). Le flux ascendant se révèle plus approprié pour minimiser la formation de chemins préférentiels.

Figure 159 Montage expérimental de la colonne de biosorption

Les solutions monométalliques aux pH optimaux ont été distribuées par une pompe péristaltique en entrée de colonne. Les échantillons en sortie de colonne ont été collectés régulièrement à l'aide d'un collecteur de fractions et ensuite analysés. Le débit de la solution (120 ml h^{-1}) et la hauteur de lit ont été maintenus stables, alors que les concentrations et la taille des billes utilisées ont varié. La courbe et le temps de percée ont été les deux paramètres cruciaux à étudier.

La Figure 160 montre que l'augmentation de la concentration en entrée modifie significativement l'allure de la courbe de percée. La biosorption dans un système dynamique est due à la différence de concentration du soluté dans le biosorbant et dans la solution. Plus le gradient de concentration est élevé, plus la biosorption est importante. Des courbes de percée plus aiguës ont été observées pour des concentrations plus élevées, indiquant un transfert de masse plus efficace à l'intérieur de la colonne en raison d'un gradient de concentration plus élevé entre la solution et le solide. L'augmentation de la concentration initiale conduit à une réduction du temps de percée. Ces observations apparaissent logiques puisqu'une concentration faible provoque un transport plus lent entre le liquide et le solide en raison d'un gradient de concentration moins élevé. En conséquence, la zone de transport s'élargit et la courbe de percée est plus plate. Le temps de percée diminue logarithmiquement avec

l'augmentation de la concentration. Un comportement similaire a été obtenu avec les deux autres tailles de billes utilisées.
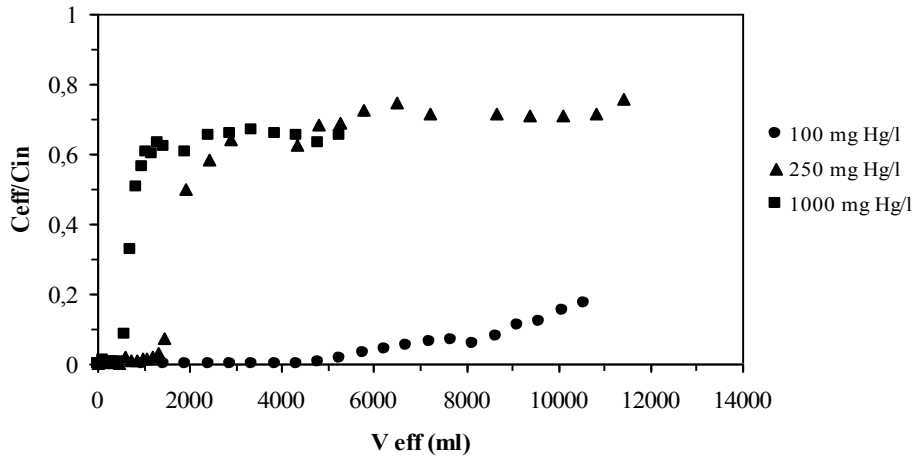
Figure 160 Effet de la concentration initiale sur les courbes de percée (taille des particules: B1)

La Figure 161 montre l'influence de la taille des particules. L'augmentation de la taille des particules a provoqué une réduction du temps de service des colonnes.
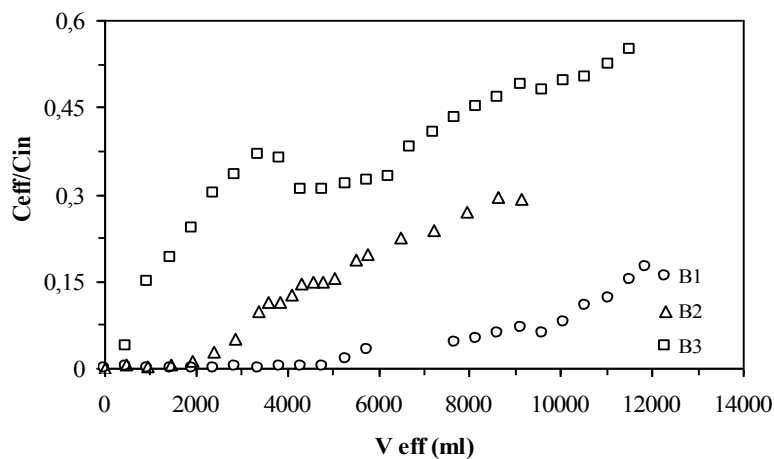
Figure 161 Influence de la taille des particules sur les courbes de percées (C_{in}: 100 mg Hg l^{-1})

A part l'augmentation du volume du lit biosorbant, deux autres faits intéressants ont été observés. Le rapport C_{eff}/C_{in} n'a jamais atteint la valeur 1. Ce fait, observé par d'autres

auteurs, n'a pas pu être expliqué. Cette observation n'est cependant pas vraiment importante pour une éventuelle application industrielle, car, une fois le point de percée atteint, la colonne est mise hors service. La coloration de l'effluent en début d'expérimentation a aussi été observée et expliquée par la macération de certains composés de la biomasse, mais aucune relation entre le temps de percée et le temps de coloration n'a été observée. Néanmoins, ce phénomène peut se révéler gênant pour l'application industrielle.

Dans le cas du chrome hexavalent, nous avons mené moins d'expérimentations. Les concentrations en chrome hexavalent et chrome total ont été déterminées sur les échantillons en sortie de colonne.

L'arrêt accidentel de la pompe a permis de mettre en évidence le mécanisme de contrôle. En arrêtant l'alimentation de la colonne, le système s'est trouvé en régime statique, ce qui a permis de caractériser la contribution de la diffusion intraparticulaire (Figure 162). D'après Helfferich[237], cette observation confirme que le système est contrôlé par la diffusion intraparticulaire.
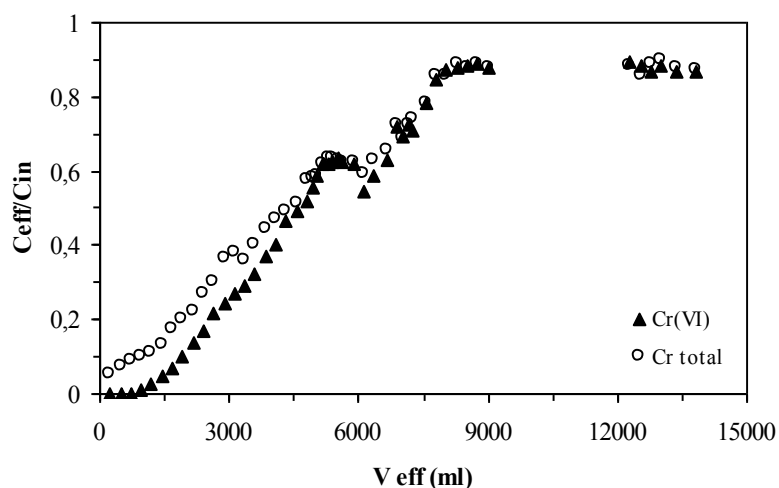
Figure 162 Courbe de percée du chrome (granulométrie B3, C_{in}: 100 mg Cr l^{-1})

Une méthode très simple – nommée *interrruption test* - pour distinguer entre le contrôle par diffusion externe et le contrôle par diffusion intraparticulaire a été proposée par Helfferich. Les billes sont enlevées du système pour une courte période de temps et ensuite

replongées dans la solution métallique. La pause permet au gradient de concentration dans les billes de s'égaliser. Ainsi, pour les systèmes contrôlés par diffusion intraparticulaire, la vitesse du procédé augmente immédiatement après le renouvellement du contact (le cas présent). Pour les systèmes contrôlés par diffusion externe, aucun gradient n'existe au sein des particules, parce que la vitesse globale du procédé dépend du gradient de concentration à travers la couche limite et donc, dans ce cas, aucun effet sur la vitesse ne peut être observé. On peut alors conclure que le procédé est contrôlé par la diffusion intraparticulaire.

De matière surprenante, les différences entre la concentration en chrome total et la concentration en chrome hexavalent ont été négligeables par rapport au système statique (Figure 163).
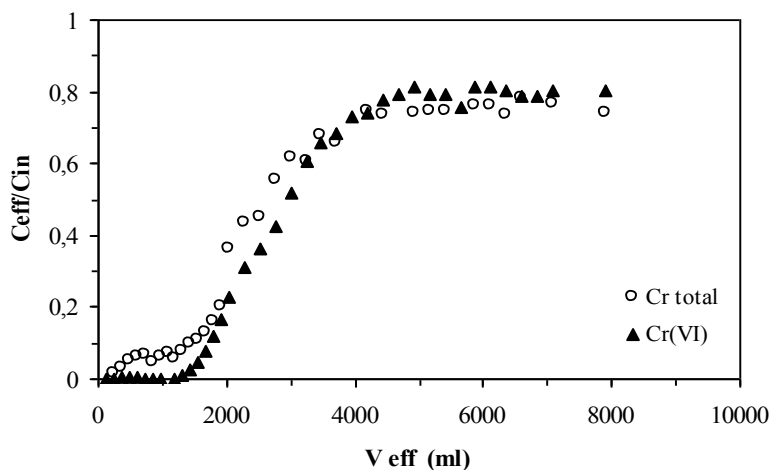
Figure 163 Courbe de percée du chrome (granulométrie B2, C_{in}: 100 mg Cr l^{-1})

Mais ce fait peut être toutefois relié aux résultats précédents. La réduction a été observée en régime statique pour les poudres et également pour les billes. Au cours des expérimentations cinétiques, il a été montré que la réduction est un phénomène secondaire qui se produit durant la deuxième phase. La différence principale entre les régimes statique et dynamique est que, en régime statique, le système reste intact pendant toute l'expérimentation, alors que, en régime dynamique, la solution est continuellement enlevée du système. En supposant que la réduction est un effet « secondaire », elle ne peut donc pas se produire en système dynamique.

De plus, dans le cas du chrome, il a été observé que l'augmentation de la concentration et de la taille des particules réduit le temps de service de la colonne.

Trois modèles (Adams-Bohart, Thomas et Yoon & Nelson) basés sur différentes hypothèses ont été utilisés pour la description du comportement des billes en régime dynamique. En général, c'est seulement le modèle d'Adams et Bohart qui correspond bien aux données expérimentales et à l'allure des courbes de percée et qui prédit exactement le temps de percée.

6.4 Conclusions

La possibilité de la valorisation des biomasses de déchets *Penicillium oxalicum var. Armeniaca* et *Tolypocladium* sp. a été confirmée. La biosorption de quatre métaux toxiques – mercure, chrome hexavalent, cadmium et plomb – a été étudiée.

Alors que la biomasse de *Tolypocladium* a été utilisée en l'-état, la biomasse de *Penicillium* a dû subir un traitement alcalin.

Cette étude a permis d'estimer les performances globales de la biosorption du mercure, chrome hexavalent, cadmium et plomb par les deux biosorbants sous forme de poudre en régime statique et du mercure et chrome hexavalent par la biomasse de *Tolypocladium* sous forme de billes (mélange avec des diatomées) en régime dynamique.

Les capacités maximales de fixation peuvent atteindre, dans des conditions opératoires optimales, 270 mg Hg g^{-1} biomasse P3 (à pH 5), 160 mg Hg g^{-1} biomasse T (à pH 7), 70 mg Cr(VI) g^{-1} biomasse P3 (à pH 3) et 55 mg Cr(VI) g^{-1} biomasse T (à pH 2). Ces valeurs figurent parmi les valeurs les plus élevées citées dans la littérature. Au contraire pour le plomb et le cadmium les performances sont décevantes.

Concernant les isothermes d'adsorption, l'exploitation des résultats a permis d'appréhender les mécanismes mis en jeu lors de la fixation de ces ions métalliques. L'étude par spectroscopie infrarouge a permis de montrer les points communs entre la biomasse P3 et le chitosane et donc de proposer un mécanisme de fixation identique. Il s'agit de la chelation sur les groupes aminés à pH proche de la neutralité et d'attraction électrostatique entre les groupes aminés protonés et les ions chromates à pH acide. Alors que les groupes carboxyliques ont été identifiés sur la biomasse T, un mécanisme d'échanges d'ions proche de celui souvent cité pour les algues a été proposé. Un phénomène combiné d'adsorption et de réduction a été observé pendant la biosorption du chrome hexavalent par la biomasse T.

Le pH, par son effet sur la spéciation des espèces métalliques en solution et sur la charge portée par les groupes fonctionnels présents sur la biomasse, influence notablement les performances de fixation. Bien que pour les espèces cationiques à pH acide, une forte compétition entre les protons et les métaux réduise les performances de biosorption, pour le

chrome hexavalent (espèce anionique), la biosorption est fortement favorisée en milieu acide (adsorption par attraction électrostatique sur les composés protonés des parois cellulaires).

Ces différentes considérations, en ce qui concerne le mécanisme global de fixation, sont en concordance avec les résultats enregistrés dans les études cinétiques. Ces études ont permis de cerner les étapes limitantes. Les mécanismes diffusionnels semblent particulièrement importants.

Dans le cas du mercure, l'augmentation de la concentration métallique initiale entraîne principalement une diminution de la contribution de la diffusion externe au niveau du contrôle cinétique et une augmentation des coefficients de la diffusion intraparticulaire. De plus, la biosorption du mercure s'est révélée sensible à la variation du diamètre des particules, ce qui signifie que le procédé est de nature plutôt surfacique.

Dans le cas du chrome hexavalent, le procédé s'est effectué plutôt dans le volume des particules et ne montre donc pas de sensibilité à la taille des particules. L'influence des paramètres étudiés sur la vitesse globale n'a pas été établie, il est donc possible que la vitesse du procédé soit contrôlée par les deux phénomènes et que le phénomène prédominant dépende des conditions opératoires. Dans le cas de la biomasse T, les résultats obtenus n'ont pas pu être modélisés par les modèles choisis. Cela peut signifier que la description du procédé global par deux modèles indépendants n'est pas justifiée ou que le procédé n'est pas contrôlé par la diffusion.

Les expérimentations menées en régime dynamique ont démontré la faisabilité de la biosorption en utilisant la biomasse de *Tolypocladium*, immobilisée sur la terre de diatomées, conditionnée sous forme de billes, pour les effluents dilués contenant soit du chrome hexavalent soit du mercure. Les courbes de percée sont contrôlées par plusieurs paramètres tels que la concentration initiale et le diamètre des particules. Le procédé est sans doute contrôlé par diffusion intraparticulaire, comme illustré dans le cas de chrome, et comme indiqué par les pentes moins raides des courbes de percée. Lorsque l'on augmente la taille des particules, la hauteur de la zone de transfert augmente.

Bien que la biomasse P3 ait montré de meilleures capacités de fixation sous forme de poudre en régime statique, son comportement hydrophobe ne la rend pas appropriée pour une telle utilisation en régime dynamique. De plus, le faible rendement pendant sa préparation ainsi que la production importante d'effluents alcalins, la rendent moins favorable pour son utilisation en tant que biosorbant.

La faisabilité de la désorption n'a pas fait l'objet du présent travail en raison du coût réduit des biosorbants. Néanmoins, la biomasse saturée devient un déchet dangereux. Elle peut être soit incinérée, concentrant alors les métaux dans les cendres (ce que est inapproprié dans le cas des métaux volatils), soit immobilisé dans des matrices solides qui peuvent être ensuite mises en décharge. Mais dans le cas où il y a un intérêt à recycler les métaux fixés, le procédé de désorption peut devenir intéressant. Dans le cas du recyclage, il est nécessaire de récupérer les métaux fixés dans un volume d'éluant le plus faible possible. De nombreuses études ont montré que l'utilisation de différents éluants (acides, alcalins, agents complexants) permet un taux important de récupération des métaux fixés. De bons résultats ont été obtenus particulièrement pour les espèces cationiques. La récupération du chrome s'effectue principalement par réduction, ce qui rend le procédé moins avantageux dans l'optique d'une possible application industrielle.

Ce dernier point n'a pas été abordé dans cette thèse, il représente toutefois une clé du procédé pour une approche économique compétitive.

List of symbols

C_i	initial metal concentration in solution [mg L^{-1}, mmol L^{-1}]
$C_{f,eq}$	final (equilibrium) metal concentration in solution [mg L^{-1}, mmol L^{-1}]
m	mass [g]
V	volume [L]
q	amount of adsorbed metal per unit weight of biosorbent [mg g^{-1}, mmol g^{-1}]
q_{max}	constant in Langmuir model corresponding to the maximum sorbate uptake under the given experimental conditions, [mg g^{-1}, mmol g^{-1}]
b	constant in Lagmuir model related to the affinity between the sorbent and sorbate, [L mg^{-1}, L mmol^{-1}].
k	constant in Freundlich equation related to the maximum binding capacity [L g^{-1}, L mol^{-1}]
n	constant in Freundlich equation related to the affinity or binding strength [dimensionless].
k_1	rate constant of pseudo-first-order reaction in Lagergren's model [min^{-1}]
q_{eq}, q_t	denote uptake at equilibrium and at time t, respectively, in Lagergren's and Ho's model [mg g^{-1}, mmol g^{-1}].
k_2	rate constant of pseudo-second-order reaction in Ho's model, [g (mg min)$^{-1}$]
β_L	mass transfer coefficient in external mass transfer diffusion model, [m s^{-1}]
S	specific surface area, [m^{-1}]
m	concentration of solid in solution in external mass transfer diffusion model [mg L^{-1}]
d_p	particle diameter [m]
δ	particle density [kg m^{-3}]
ε	particle voidage [-].
K	intraparticle diffusion coefficient in W&M model [mmol g^{-1} s$^{1/2}$]
D	intraparticle diffusion coefficient in U&T model [m^2 s^{-1}]
Z	column depth [cm]
ε	void fraction in the bed [-]
U_0	superficial velocity [cm min^{-1}]
E	dispersion coefficient [cm^2 min^{-1}].

r	adsorption rate [mg L^{-1} min^{-1}]
k_{AB}	kinetic constant in Adams Bohart model [L mg^{-1} min^{-1}].
C_{eff}, C_{in}	effluent and inlet concentrations, respectively, [mg L^{-1}]
k_{Th}	rate constant in Thomas model [mL min^{-1} mg^{-1}]
q_0	maximum solid-phase concentration of the solute (column experiments) [mg g^{-1}]
X	amount of sorbent in the column [g].
k_{YN}	rate constant in Yoon and Nelson model [min^{-1}]
τ	time required for 50% adsorbate breakthrough in Y&N model [min]
t	breakthrough (sampling) time [min]
A	area under the breakthrough curve [mg h L^{-1}]
C_{ad}	adsorbed concentration [mg L^{-1}]
q_{total}	maximum column sorption capacity [mg]
Q	volumetric flow rate [mL h^{-1}]
m_{total}	total amount of contaminant injected to column [mg]
t_{total}	total flow time [h]
q_{eq}	equilibrium uptake [mg g^{-1}].

List of figures

270

273

List of Tables

Appendix A

mi micromeritics®

Sample: Biomasa ∅ P3
Operator: Lhotka
Submitter: UAT VSCHT Praha
File: C:\2020\DATA\000-187.SMP

Started: 22.11.2005 13:43:02odp.
Completed: 22.11.2005 19:54:52odp.
Report Time: 8.12.2005 10:32:58odp.
Sample Mass: 0.0981 g
Warm Free Space: 17.0482 cm³ Measured
Equilibration Interval: 10 s
Automatic Degas: Yes

Analysis Adsorptive: N2
Analysis Bath Temp.: -195.800 °C
Thermal Correction: No
Smoothed Pressures: No
Cold Free Space: 51.8543 cm³
Low Pressure Dose: None

Summary Report

Surface Area

Single point surface area at P/Po = 0.220406058: 1.1527 m²/g

BET Surface Area: 1.1874 m²/g

Langmuir Surface Area: 1.6343 m²/g

t-Plot Micropore Area: 1.3210 m²/g

t-Plot External Surface Area: -0.1336 m²/g

BJH Adsorption cumulative surface area of pores
between 1.7000 nm and 300.0000 nm diameter: 0.4928 m²/g

BJH Desorption cumulative surface area of pores
between 1.7000 nm and 300.0000 nm diameter: 0.8477 m²/g

Pore Volume

Single point adsorption total pore volume of pores
less than 143.07810 nm at P/Po = 0.986287449: 0.006158 cm³/g

t-Plot micropore volume: 0.000582 cm³/g

BJH Adsorption cumulative volume of pores
between 1.7000 nm and 300.0000 nm diameter: 0.008159 cm³/g

BJH Desorption cumulative volume of pores
between 1.7000 nm and 300.0000 nm diameter: 0.008258 cm³/g

Pore Size

Adsorption average pore width (4V/A by BET): 20.74272 nm

BJH Adsorption average pore diameter (4V/A): 66.2252 nm

BJH Desorption average pore diameter (4V/A): 38.9658 nm

Horvath-Kawazoe

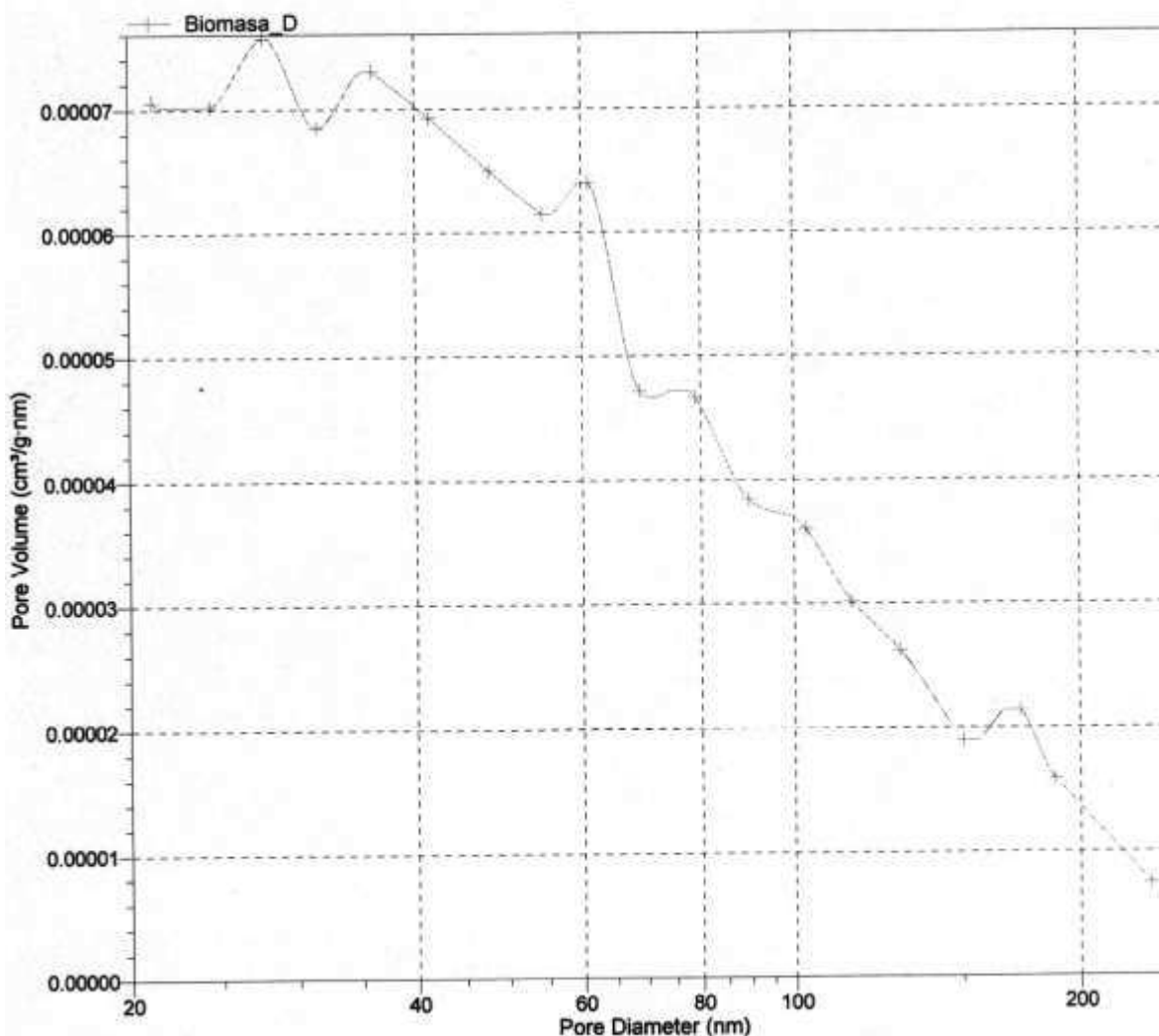Maximum pore volume at P/Po = 0.000000000: 0.000000 cm³/g

Median pore width: 0.00000 nm

BJH Adsorption dV/dD Pore Volume

Sample: Biomasa_T
Operator: Lhotka
Submitter: UAT VSCHT Praha
File: C:\2020\DATA\000-188.SMP

Started: 23.11.2005 9:37:46odp.
Completed: 23.11.2005 15:38:40odp.
Report Time: 8.12.2005 10:34:06odp.
Sample Mass: 0.2297 g
Warm Free Space: 16.8513 cm³ Measured
Equilibration Interval: 10 s
Automatic Degas: Yes

Analysis Adsorptive: N2
Analysis Bath Temp.: -195.800 °C
Thermal Correction: No
Smoothed Pressures: No
Cold Free Space: 50.4791 cm³
Low Pressure Dose: None

Summary Report

Surface Area

Single point surface area at P/Po = 0.200041024: 0.9088 m²/g

BET Surface Area: 1.2321 m²/g

Langmuir Surface Area: 2.1273 m²/g

t-Plot External Surface Area: 1.7856 m²/g

BJH Adsorption cumulative surface area of pores
between 1.7000 nm and 300.0000 nm diameter: 0.3283 m²/g

BJH Desorption cumulative surface area of pores
between 1.7000 nm and 300.0000 nm diameter: 1.0399 m²/g

Pore Volume

Single point adsorption total pore volume of pores
less than 497.02373 nm at P/Po = 0.996112592: 0.001805 cm³/g

t-Plot micropore volume: -0.000384 cm³/g

BJH Adsorption cumulative volume of pores
between 1.7000 nm and 300.0000 nm diameter: 0.001434 cm³/g

BJH Desorption cumulative volume of pores
between 1.7000 nm and 300.0000 nm diameter: 0.001160 cm³/g

Pore Size

Adsorption average pore width (4V/A by BET): 5.85881 nm

BJH Adsorption average pore diameter (4V/A): 17.4717 nm

BJH Desorption average pore diameter (4V/A): 4.4604 nm

Horvath-Kawazoe

Maximum pore volume at P/Po = 0.000000000: 0.000000 cm³/g

Median pore width: 0.00000 nm

ASAP 2020 V1.05 H   Unit 1   Serial #: 172   Page 1

Sample: Biomasa_T
Operator: Lhotka
Submitter: UAT VSCHT Praha
File: C:\2020\DATA\000-188.SMP

Started: 23.11.2005 9:37:46odp.
Completed: 23.11.2005 15:38:40odp.
Report Time: 8.12.2005 10:34:05odp.
Sample Mass: 0.2297 g
Warm Free Space: 16.8513 cm³ Measured
Equilibration Interval: 10 s
Automatic Degas: Yes

Analysis Adsorptive: N2
Analysis Bath Temp.: -195.800 °C
Thermal Correction: No
Smoothed Pressures: No
Cold Free Space: 50.4791 cm³
Low Pressure Dose: None
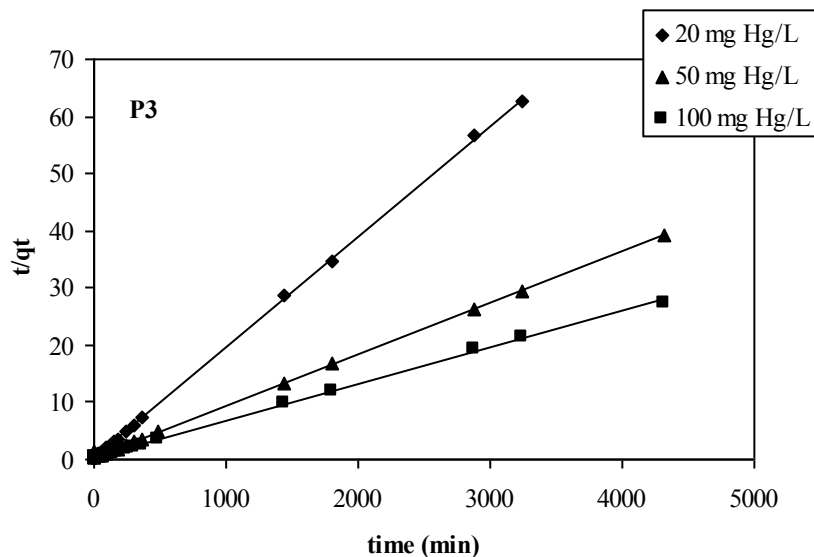

BJH Adsorption dV/dD Pore Volume
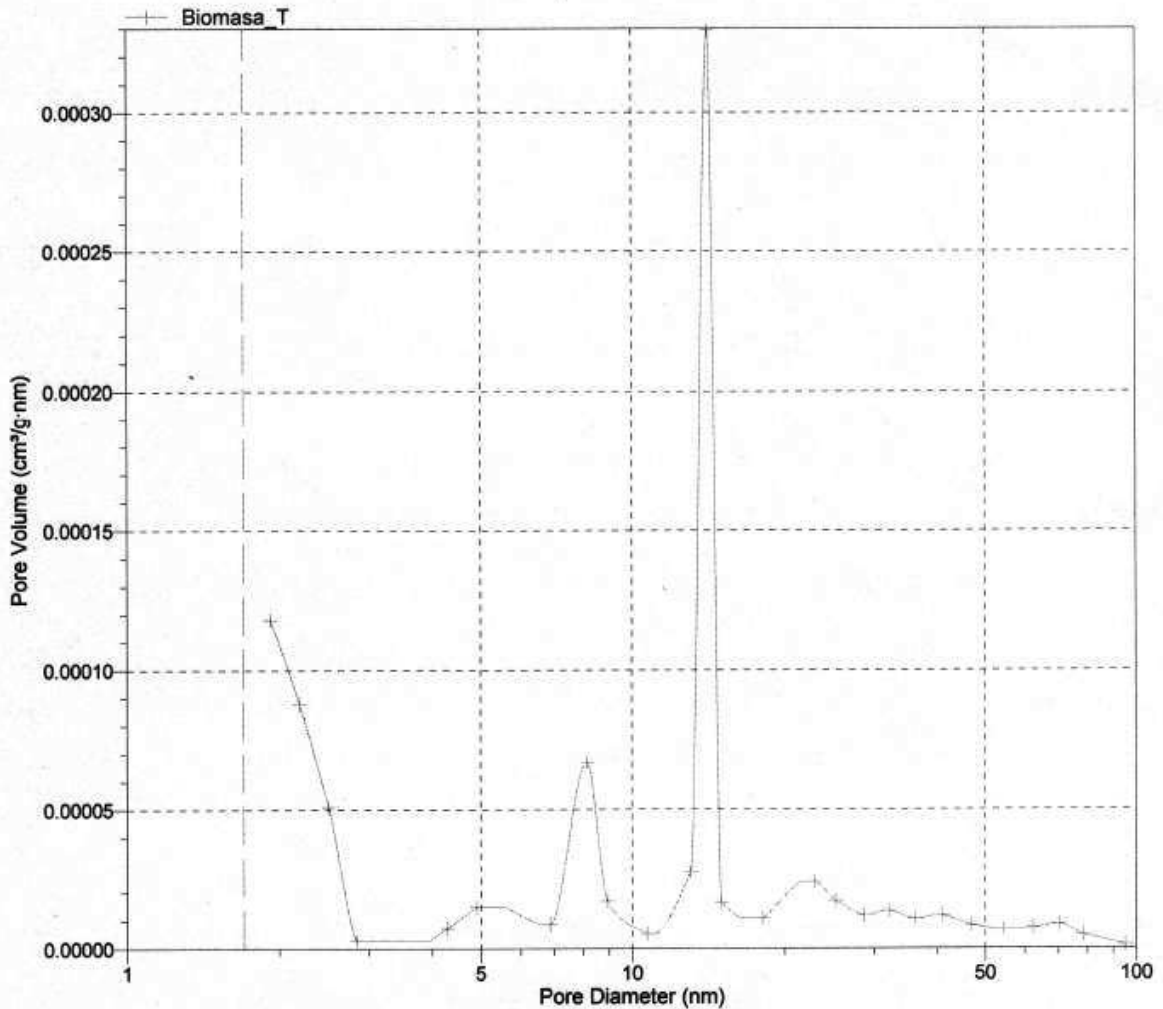
Appendix B

Figure 164 Influence of mercury concentration on sorption kinetics – linearization of Ho's equation (pH$_i$=5, P3 sample, 300 mg sorbent L^{-1}, lines in figure correspond to linear regression)

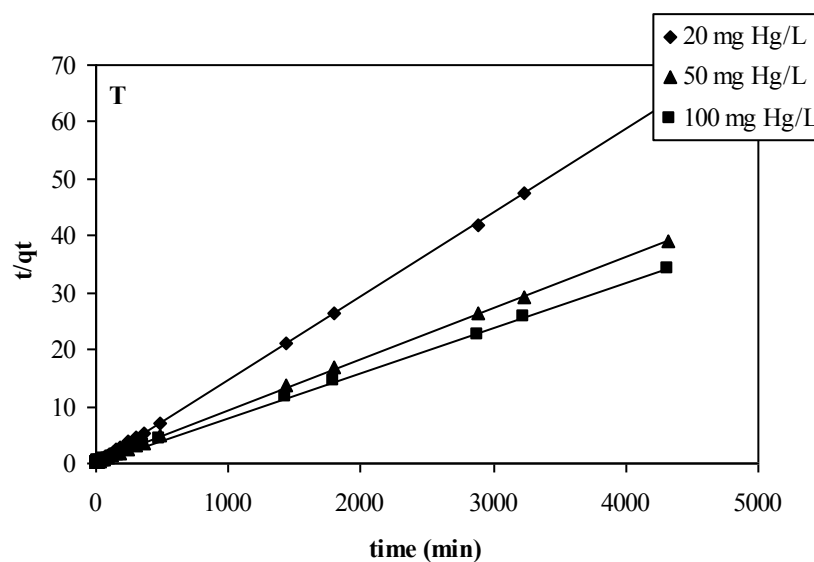**Figure 165 Influence of mercury concentration on sorption kinetics – linearization of Ho's equation (pH$_i$=7, T sample, 300 mg sorbent L^{-1}, lines in figure correspond to linear regression)**
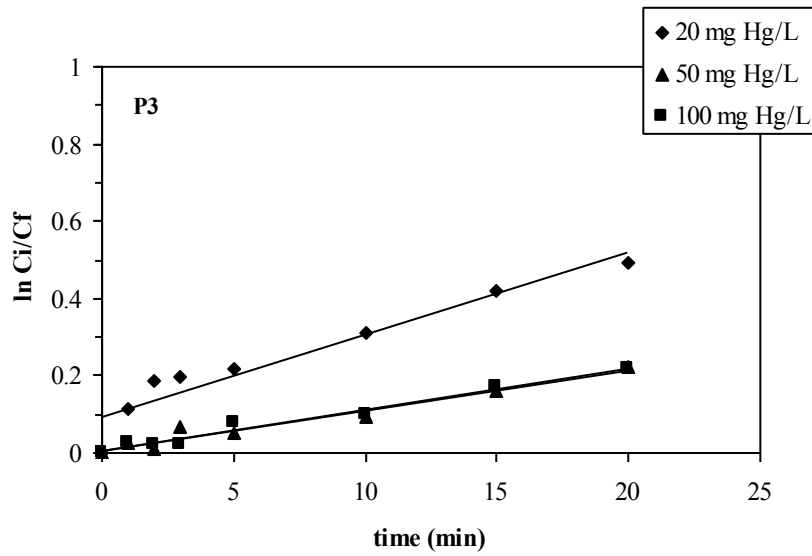
Figure 166 Influence of mercury concentration on sorption kinetics – External mass transfer model (pH$_i$=5, P3 sample, 300 mg sorbent L^{-1}, lines in figure correspond to linear regression)

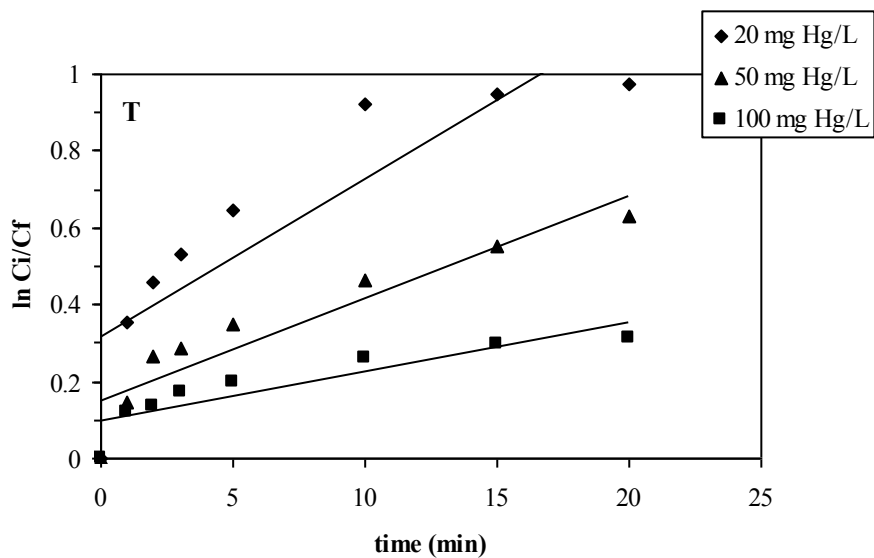**Figure 167 Influence of mercury concentration on sorption kinetics – External mass transfer model (pH$_i$=7, T sample, 300 mg sorbent L^{-1}, lines in figure correspond to linear regression)**

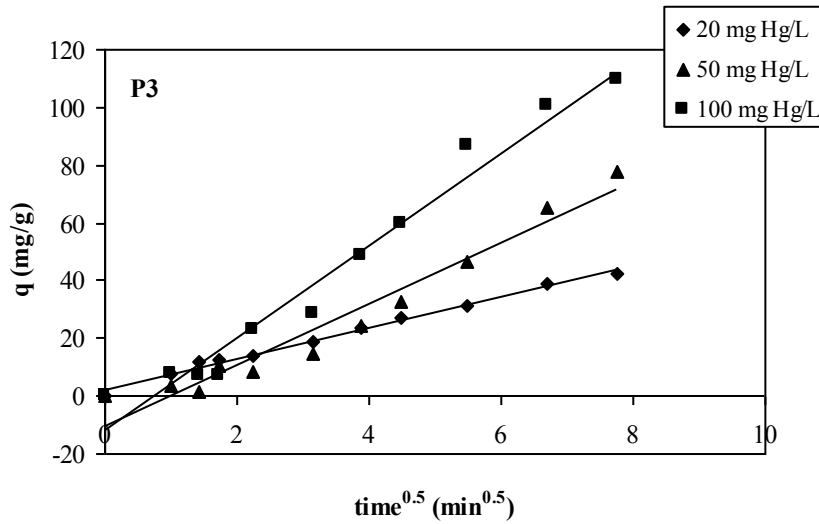**Figure 168 Influence of mercury concentration on sorption kinetics – W&M model (pH$_i$=5, P3 sample, 300 mg sorbent L^{-1}, lines in figure correspond to linear regression)**

Figure 169 Influence of mercury concentration on sorption kinetics – W&M model (pH$_i$=7, T sample, 300 mg sorbent L^{-1}, lines in figure correspond to linear regression)

Figure 170 Influence of mercury concentration on sorption kinetics – U&T model (pH$_i$=5, P3 sample, 300 mg sorbent L^{-1}, lines in figure correspond to linear regression)
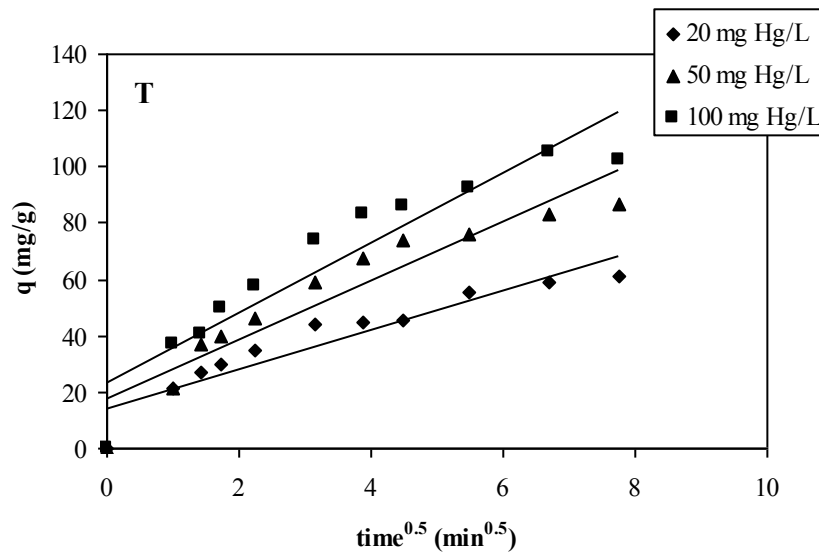

Figure 171 Influence of mercury concentration on sorption kinetics – U&T model (pH$_i$=7, T sample, 300 mg sorbent L^{-1}, lines in figure correspond to linear regression)
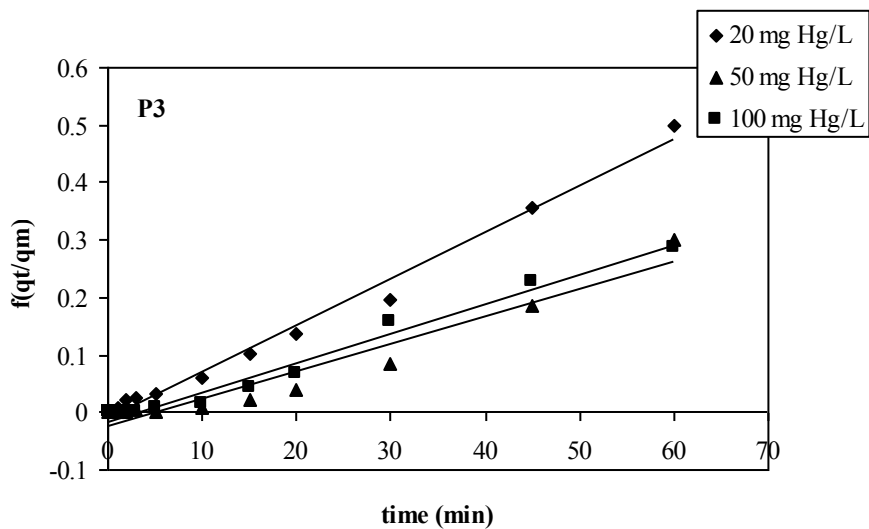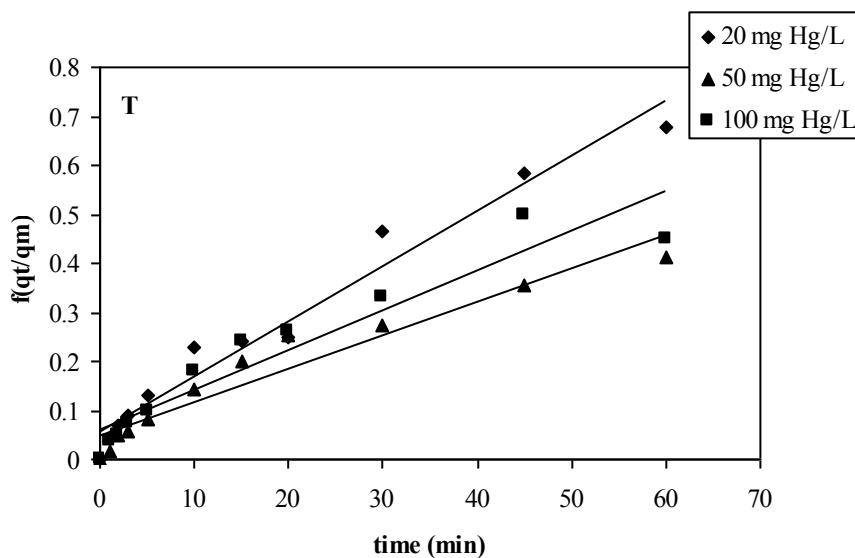
Biosorbent	C_i	k_2	g_e	R^2
	[mg L^{-1}]	[10^{-5} g mg^{-1} min^{-1}]	[mg g^{-1}]	-
	20	58.4	82.2	1
P3	50	17.6	104.0	0.999
	100	NS	125.2	0.994
	20	55.0	97.1	1
T	50	57.0	108.6	1
	100	142.4	106.2	0.999

Table 54 The effect of initial metal ion concentration on mercury biosorption kinetics at 100 sorbent L^{-1} – pseudo second-order reaction-rate fit (C_i: initial metal ion concentration, k_2: rate constant, g_e: metal ion removal capacity at equilibrium, R^2: correlation coefficient)

Biosorbent	SD	k_2	g_e	R^2
	[mg L^{-1}]	[10^{-5} g mg^{-1} min^{-1}]	[mg g^{-1}]	
	100	58.4	82.2	1
P3	300	164.0	51.5	1
	500	160.0	30.0	1
	100	55.0	97.1	1
T	300	232.1	68.3	1
	500	NS	34.9	1

Table 55 The effect of sorbent dosage on mercury biosorption kinetics at 20 mg Hg L^{-1} – pseudo second-order reaction-rate fit (C_i: initial metal ion concentration, k_2: rate constant, g_e: metal ion removal capacity at equilibrium, R^2: correlation coefficient, NS – not significant)

Biosorbent type	SD	k_2	g_e	R^2
	[mg L^{-1}]	[10^{-5} g mg^{-1} min^{-1}]	[mg g^{-1}]	-
	100	17.6	104.0	0.999
P3	300	19.3	111.4	1
	500	32.0	77.0	1
	100	57.0	108.6	1
T	300	39.0	110.9	1
	500	79.9	84.1	1

Table 56 The effect of sorbent dosage on mercury biosorption kinetics at 50 mg Hg L^{-1} – pseudo second-order reaction-rate fit (C_i: initial metal ion concentration, k_2: rate constant, g_e: metal ion removal capacity at equilibrium, R^2: correlation coefficient)

Biosorbent type	SD	k_2	g_e	R^2
	[mg L^{-1}]	[10^{-5} g mg^{-1} min^{-1}]	[mg g^{-1}]	-
	100	NS	125.2	0.994
P3	300	16.9	154.9	0.999
	500	17.3	144.2	1
	100	142.4	106.2	0.999
T	300	39.0	126.9	1
	500	51.01	119.3	1

Table 57 The effect of sorbent dosage on mercury biosorption kinetics at 100 mg Hg L^{-1} – pseudo second-order reaction-rate fit (C_i: initial metal ion concentration, k_2: rate constant, g_e: metal ion removal capacity at equilibrium, R^2: correlation coefficient, NS – non-significant value)

Biosorbent	Sorbent size	k_2 [10^{-5} g mg^{-1} min^{-1}]	g_e [mg g^{-1}]	R^2 -
	G1	19.3	111.4	1
	G2	21.4	92.8	0.999
P3	G3	9.3	96.6	0.998
	G4	5.2	112.4	0.997
	G5	2.6	125.0	0.860
	G1	39.0	110.9	1
	G2	27.6	80.2	0.999
T	G3	39.8	76.2	1
	G4	10.4	91.6	0.999
	G5	7.4	100.0	0.996

Table 58 The effect of sorbent particle size on mercury biosorption kinetics – pseudo second-order reaction-rate fit (C_i: initial metal ion concentration, k_2: rate constant, g_e: metal ion removal capacity at equilibrium, R^2: correlation coefficient)
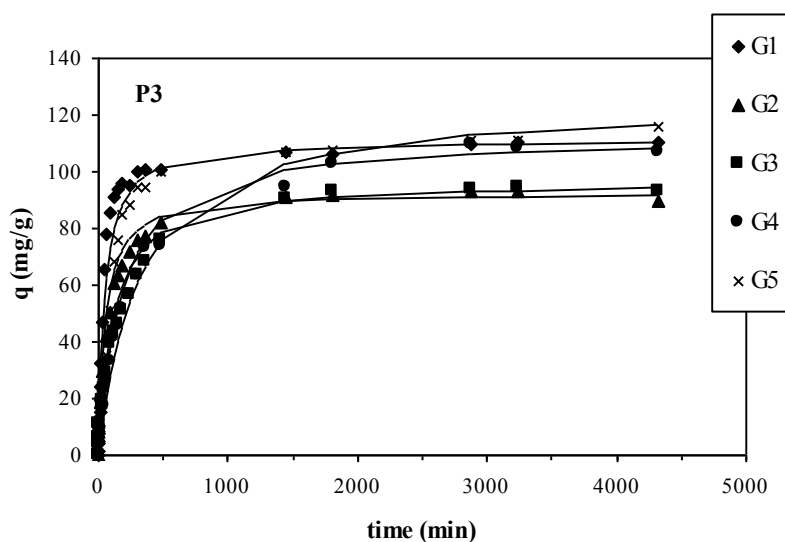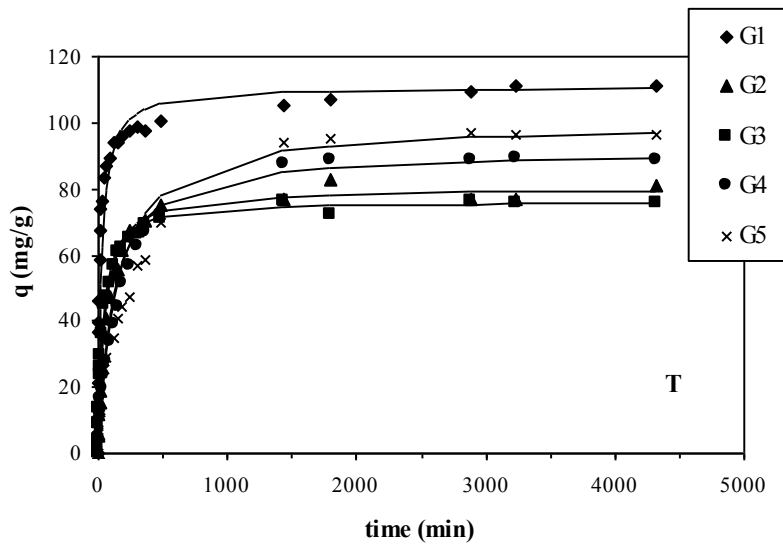

Figure 172 Influence of biosorbent particles size on sorption kinetics – pseudo second order rate equation fit (pH$_i$=5, P3 sample, 50 mg Hg L^{-1}, 300 mg sorbent L^{-1}, lines in figure correspond to model fit)

Figure 173 Influence of biosorbent particles size on sorption kinetics – pseudo second order rate equation fit (pH$_i$=7, T sample, 50 mg Hg L^{-1}, 300 mg sorbent L^{-1}, lines in figure correspond to model fit)
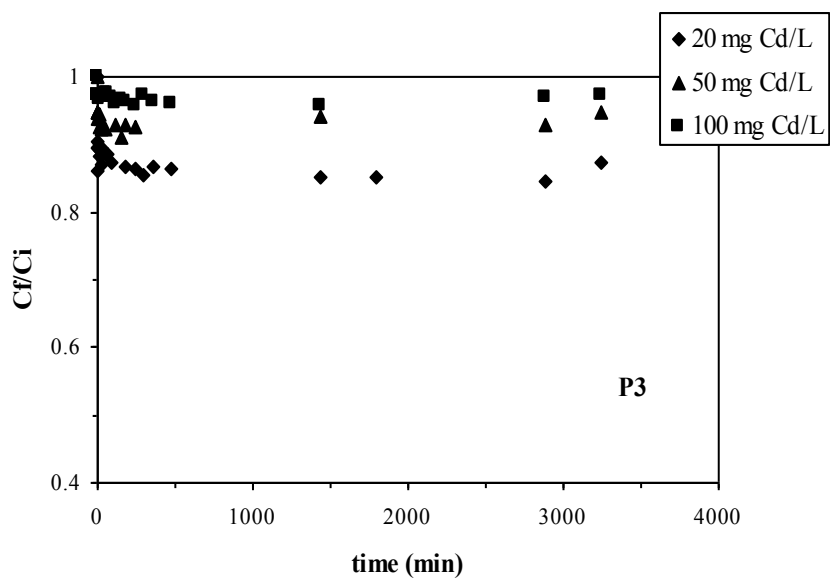
Appendix C

Figure 174 **Influence of cadmium concentration on sorption kinetics (pH$_i$=5, P3 sample, 300 mg sorbent L^{-1})**
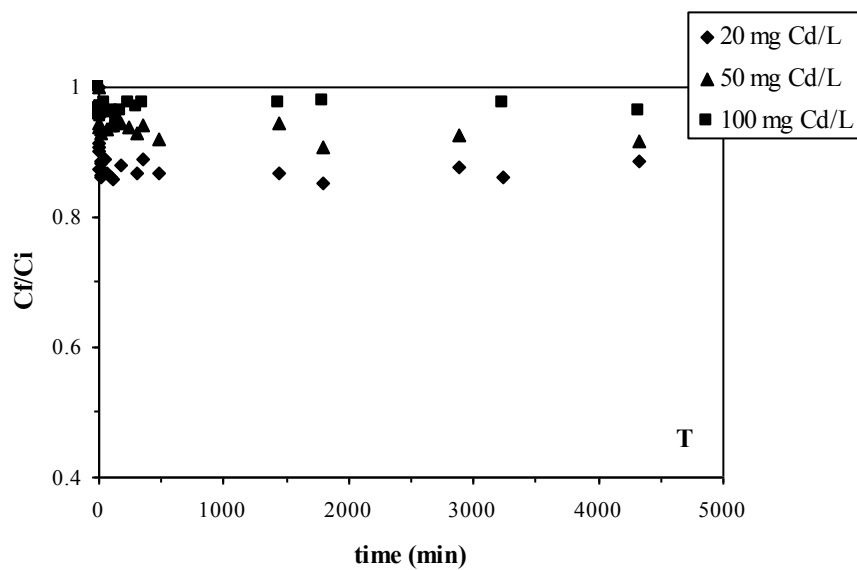

Figure 175 **Influence of cadmium concentration on sorption kinetics (pH$_i$=5, T sample, 300 mg sorbent L^{-1})**

Appendix D

Figure 176 Influence of hexavalent chromium concentration on sorption kinetics – pseudo second order rate equation fit (pH$_i$=3, P3 sample, 300 mg sorbent L^{-1}, lines in figure correspond to model fit)

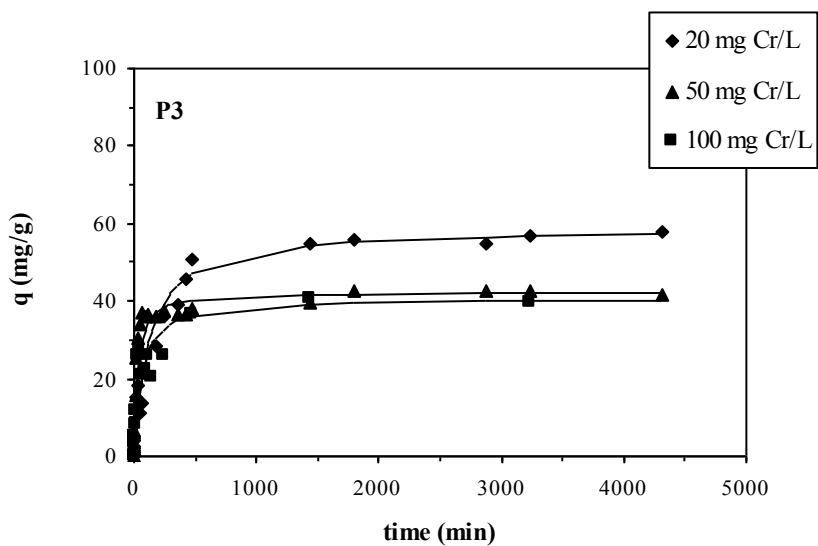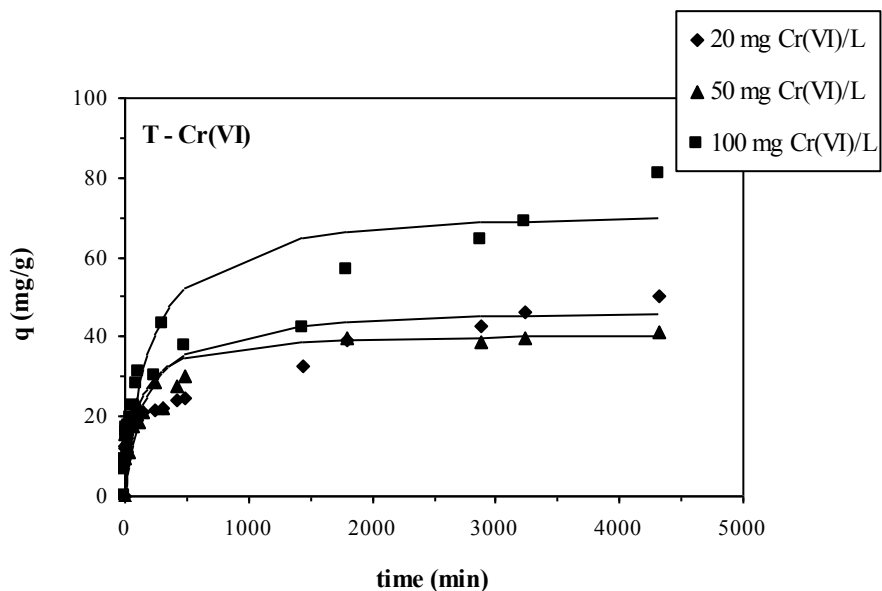**Figure 177 Influence of hexavalent chromium concentration on sorption kinetics – pseudo second order rate equation fit (pH$_i$=2, T sample, 300 mg sorbent L^{-1}, lines in figure correspond to model fit)**

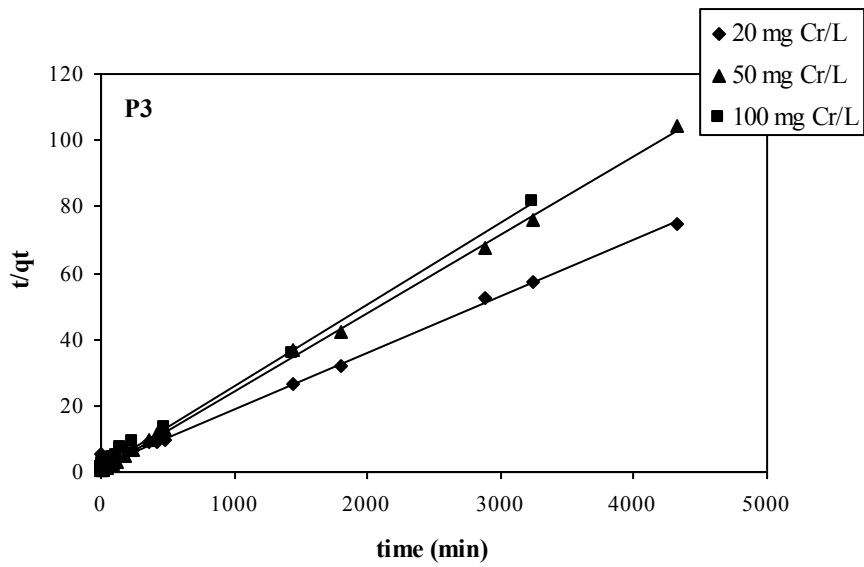**Figure 178 Influence of chromium concentration on sorption kinetics – linearization of Ho's equation (pH$_i$=3, P3 sample, 300 mg sorbent L^{-1}, lines in figure correspond to linear regression)**
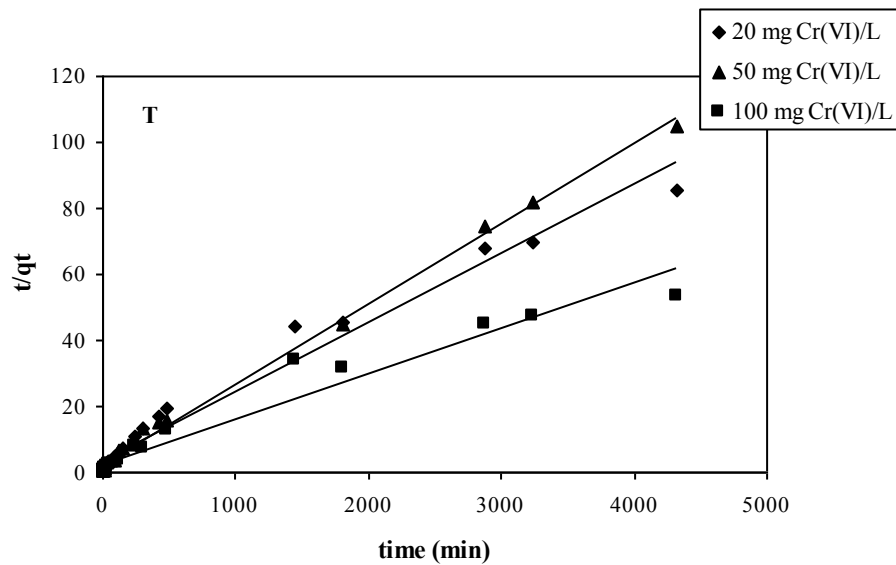

Figure 179 Influence of chromium concentration on sorption kinetics – linearization of Ho's equation (pH$_i$=2, T sample, 300 mg sorbent L^{-1}, lines in figure correspond to linear regression)

Biosorbent type		C_i	K_1	g_e	R^2
		[mg L^{-1}]	[10^{-5}min^{-1}]	[mg g^{-1}]	-
P3	*Cr(VI)*	20	125.15	38.93	0.857
		50	163.41	16.92	0.387
		100	105.49	23.92	0.784
T	*Cr(VI)*	20	61.24	36.08	0.954
		50	92.76	24.90	0.844
		100	48.87	63.23	0.916

Table 59 The effect of initial metal ion concentration on chromium biosorption kinetics at 300 sorbent L^{-1} – pseudo first-order reaction-rate fit (C_i: initial metal ion concentration, k_1: rate constant, g_e: metal ion removal capacity at equilibrium, R^2: correlation coefficient)

Figure 180 Influence of sorbent dosage on hexavalent chromium sorption kinetics – pseudo second order reaction rate equation fit (pH$_i$=3, P3 sample, 50 mg Cr(VI) L^{-1}, lines in figure correspond to model fit)
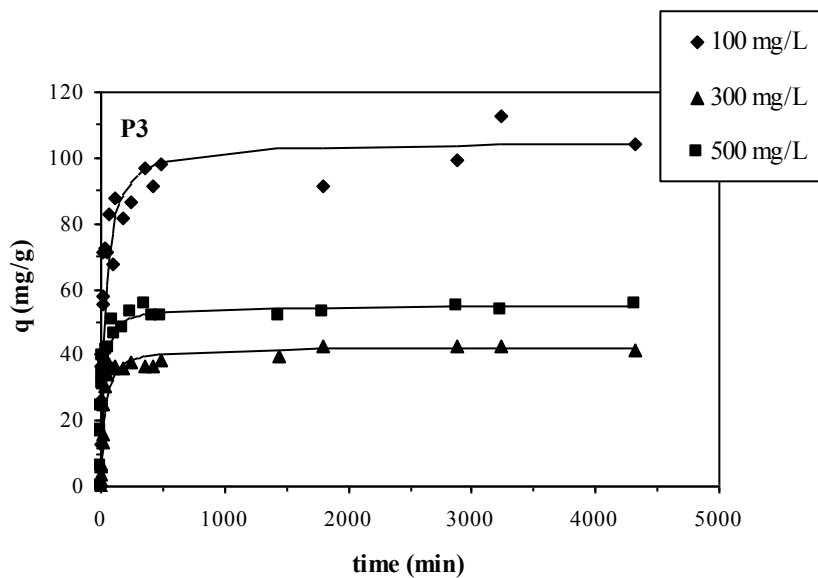
Figure 181 Influence of sorbent dosage on hexavalent chromium sorption kinetics – pseudo second order reaction rate equation fit (pH$_i$=2, T sample, 50 mg Cr(VI) L^{-1}, lines in figures correspond to model fit)
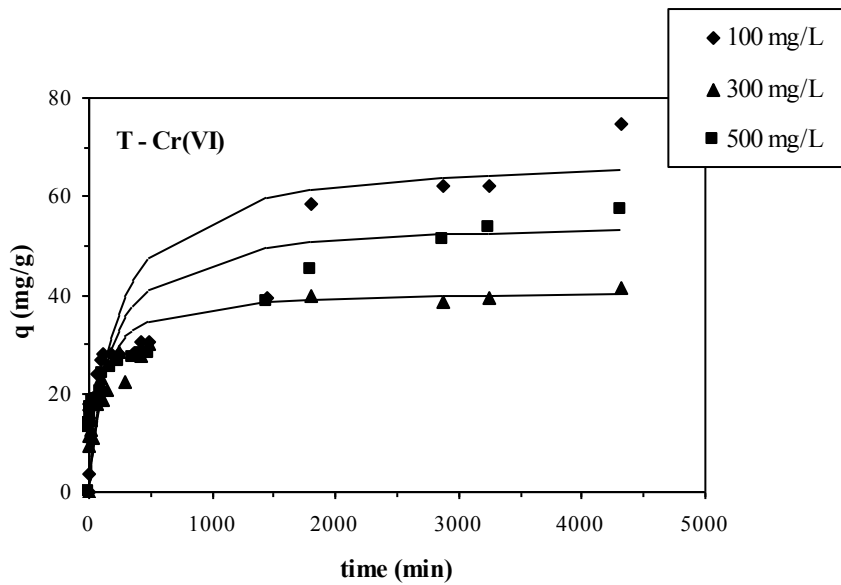

Figure 182 Influence of initial metal concentration on hexavalent chromium sorption kinetics – External mass transfer model (pH$_i$=3, P3 sample, 50 mg Cr(VI) L^{-1}, lines in figures correspond to linear regression)

Figure 183 Influence of initial metal concentration on hexavalent chromium sorption kinetics – External mass transfer model (pH$_i$=2, T sample, 50 mg Cr(VI) L^{-1}, lines in figures correspond to linear regression)

Figure 184 Influence of initial metal concentration on hexavalent chromium sorption kinetics – W&M model (pH$_i$=3, P3 sample, 50 mg Cr(VI) L^{-1}, lines in figures correspond to linear regression)
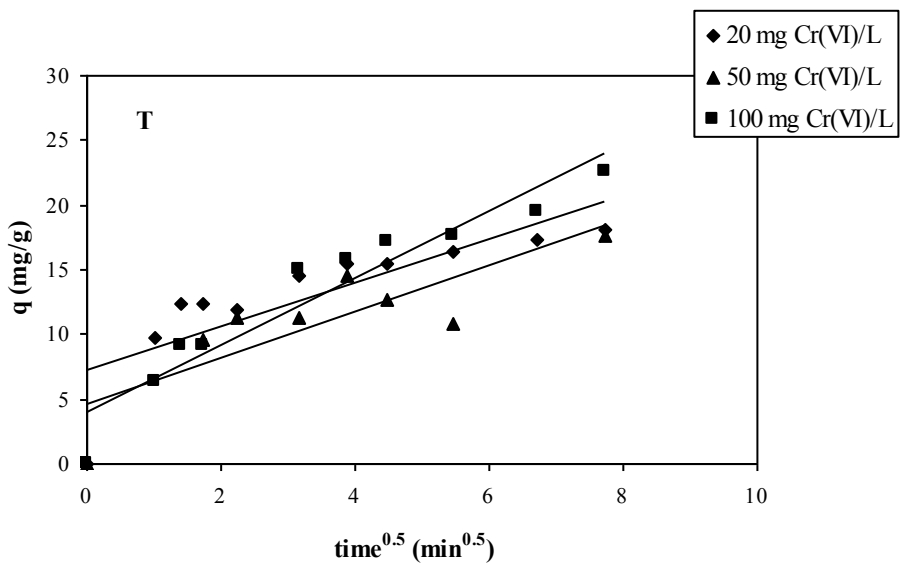
Figure 185 Influence of initial metal concentration on hexavalent chromium sorption kinetics – W&M model (pH$_i$=2, T sample, 50 mg Cr(VI) L^{-1}, lines in figures correspond to linear regression)
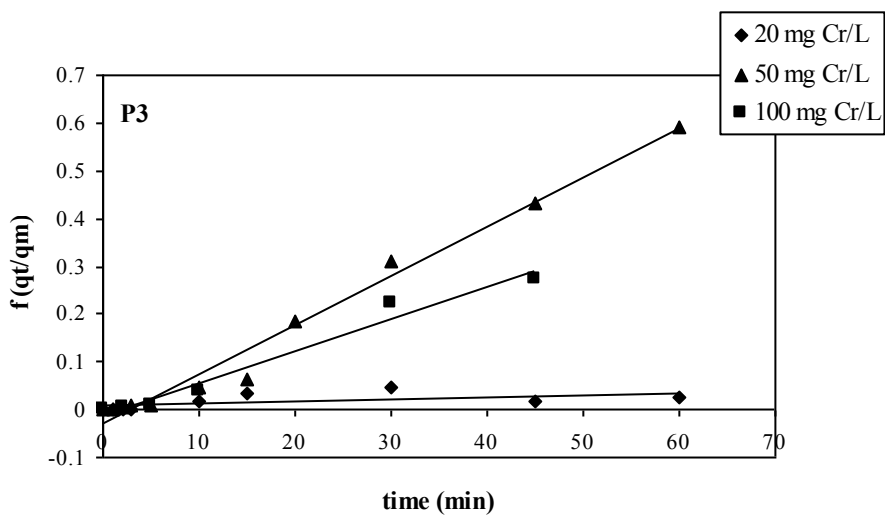
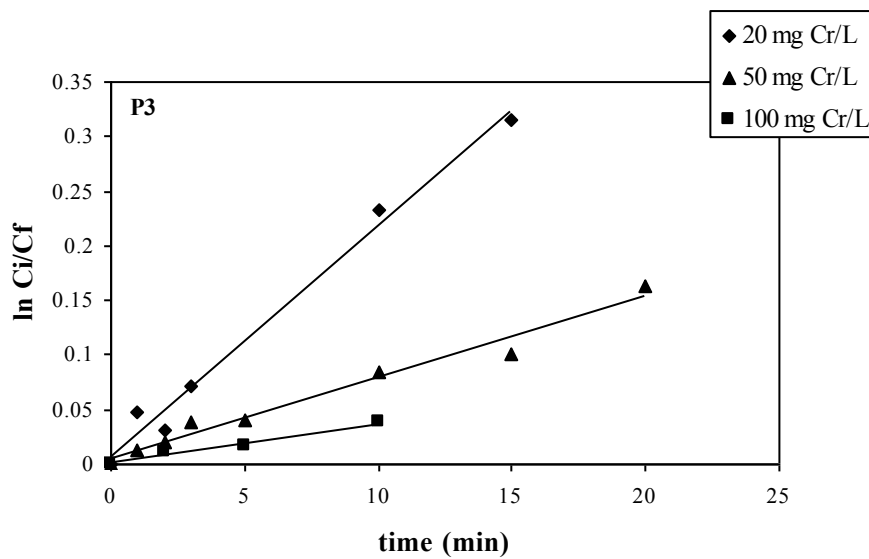**Figure 186 Influence of initial metal concentration on hexavalent chromium sorption kinetics – U&T model (pH$_i$=3, P3 sample, 50 mg Cr(VI) L^{-1}, lines in figures correspond to linear regression)**
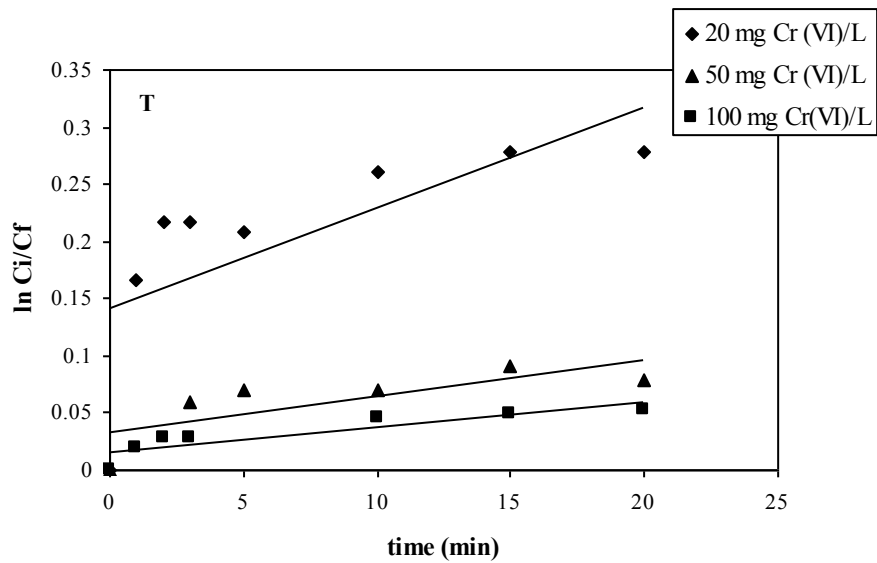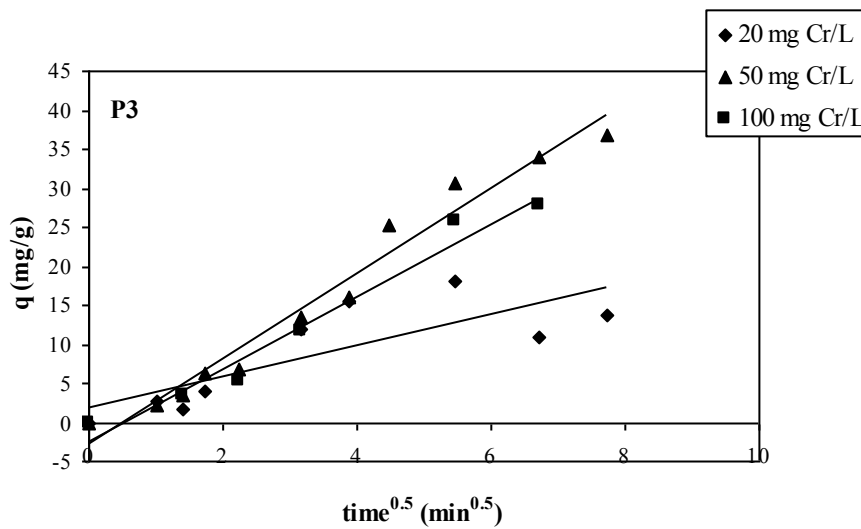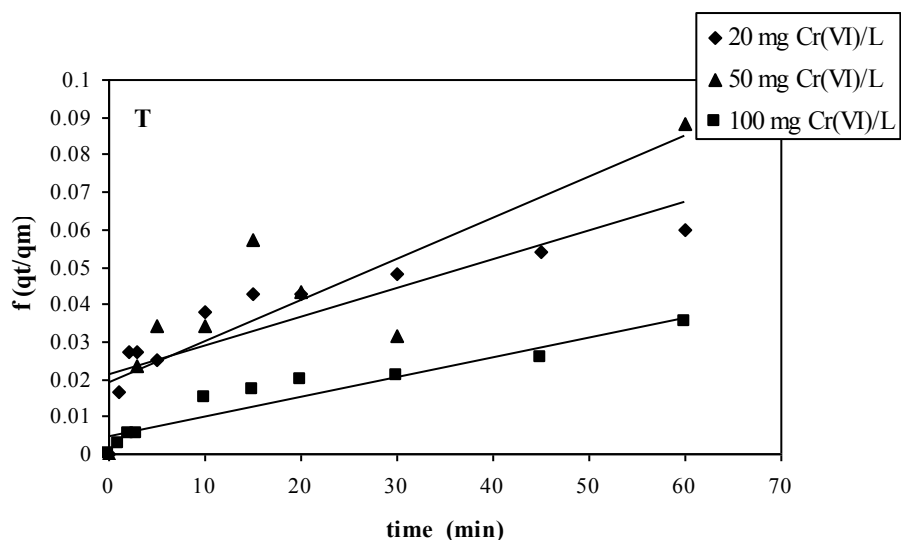
Figure 187 **Influence of initial metal concentration on hexavalent chromium sorption kinetics – U&T model (pH$_i$=2, T sample, 50 mg Cr(VI) L^{-1}, lines in figures correspond to linear regression)**

Biosorbent type		C$_i$	k$_2$	g$_e$	R^2
		[mg L^{-1}]	[10^{-5}g mg^{-1} min^{-1}]	[mg g^{-1}]	-
P3		100	30.1	104.9	0.995
		300	91.5	42.4	0.999
		500	105.1	54.9	0.999
T	*Cr(VI)*	100	6.8	68.6	0.948
		300	26.6	41.1	0.996
		500	11.1	55.2	0.978
	Cr$_{total}$	100	24.1	69.1	0.984
		300	36.5	34.2	0.979
		500	53.1	26.4	0.994

Table 60 The effect of sorbent dosage on chromium biosorption kinetics at 50 mg Cr(VI) L^{-1} – pseudo second-order reaction-rate fit (C$_i$: initial metal ion concentration, k$_2$: rate constant, g$_e$: metal ion removal capacity at equilibrium, R^2: correlation coefficient)

297

Biosorbent type	d_p	k_2	g_e	R^2
		$[10^5 \text{ g mg}^{-1} \text{ min}^{-1}]$	$[\text{mg g}^{-1}]$	-
	G1	91.5	42.4	0.999
	G2	155.5	25.6	0.998
P3	G3	30.5	36.9	0.972
	G4	128.4	44.4	0.999
	G5	27.1	37.6	0.974
	G1	26.6	41.1	0.996
	G2	21.5	39.0	0.959
T	G3	11.1	51.5	0.963
	G4	16.3	47.1	0.980
	G5	18.6	47.1	0.984

Table 61 The effect of sorbent particle size on hexavalent chromium biosorption kinetics – pseudo second-order reaction-rate fit (C_i: initial metal ion concentration, k_2: rate constant, g_e: metal ion removal capacity at equilibrium, R^2: correlation coefficient
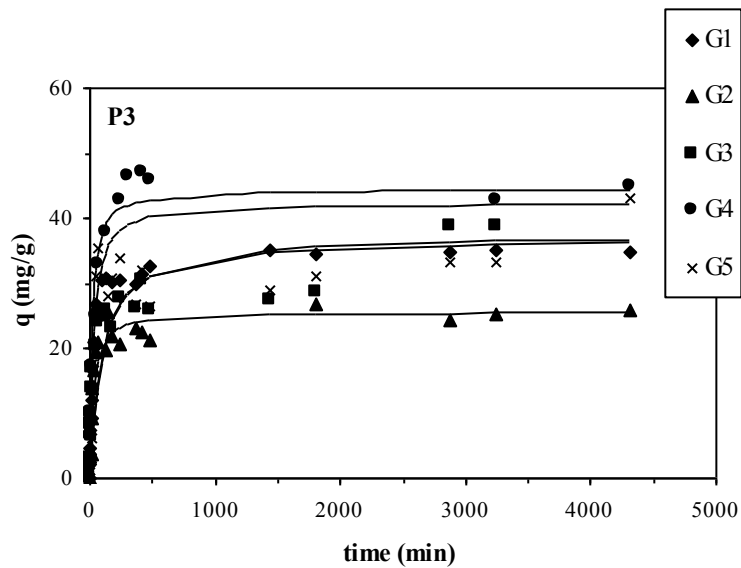
Figure 188 Influence of sorbent size on sorption kinetics – pseudo second order rate equation fit (pH$_i$=3, P3 sample, 50 mg Cr(VI) L^{-1}, 300 mg sorbent L^{-1}, lines in figures correspond to model fit)
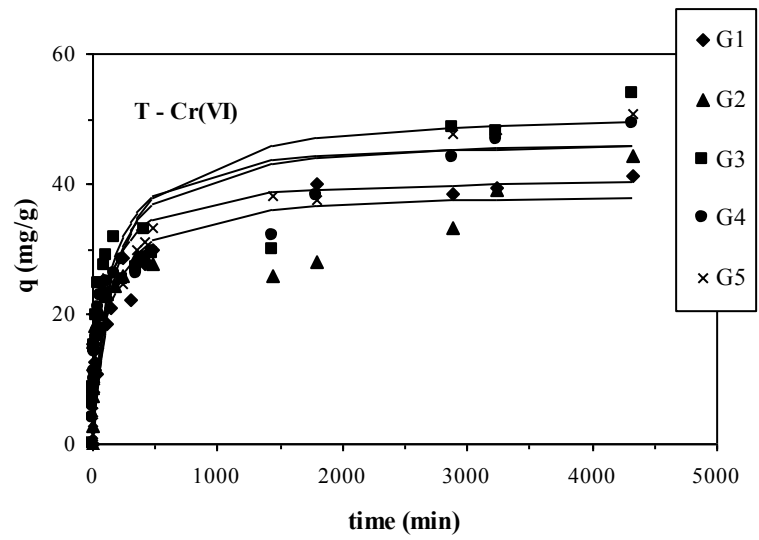
Figure 189 Influence of sorbent size on sorption kinetics – pseudo second order rate equation fit (pH$_i$=2, T sample, 50 mg Cr(VI) L^{-1}, 300 mg sorbent L^{-1}, lines in figure correspond to model fit)

Appendix E
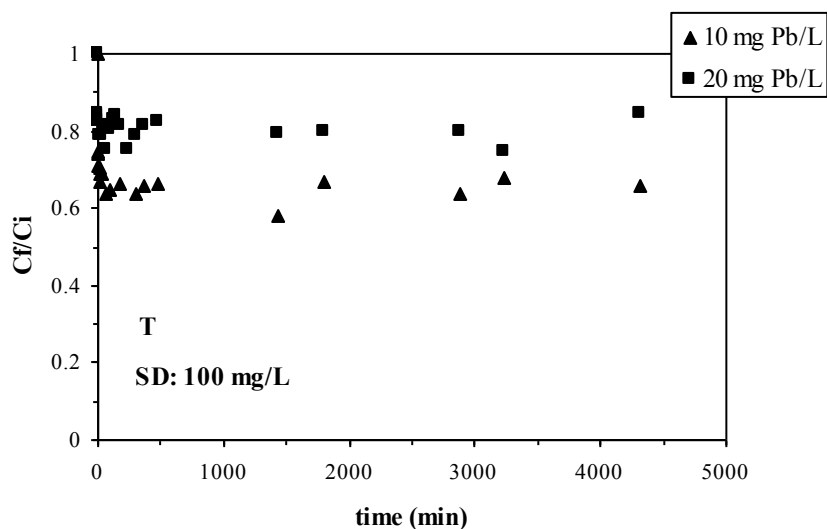
Figure 190 Influence of lead concentration on sorption kinetics (pH$_i$=5, T sample, 100 mg sorbent L^{-1})

Biosorbent	C$_i$	k$_2$	g$_e$	R^2
	[mg L^{-1}]	[10^{-5} g mg^{-1} min^{-1}]	[mg g^{-1}]	-
	5	209.53	13.32	0.999
P3	10	55.26	28.19	0.994
	20	18.25	50.41	0.984
	5	NS	NS	NS
T	10	1332.88	15.43	0.995
	20	130.74	19.04	0.993

Table 62 The effect of initial metal ion concentration on lead biosorption kinetics at 300 sorbent L^{-1} – pseudo second-order reaction-rate fit (C$_i$: initial metal ion concentration, k$_2$: rate constant, g$_e$: metal ion removal capacity at equilibrium, R^2: correlation coefficient, NS – non significant)
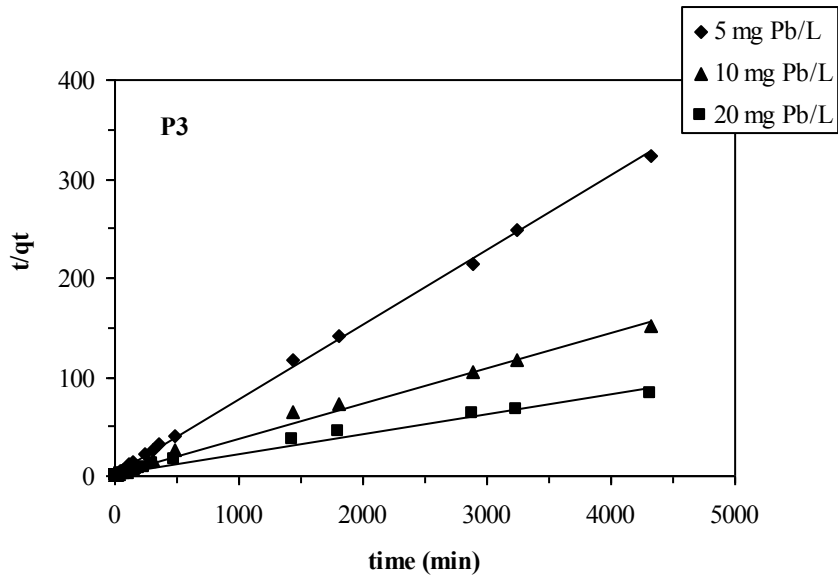
Figure 191 Influence initial lead concentration on sorption kinetics – linearization of Ho's equation (pH$_i$=5, P3 sample, 300 mg sorbent L^{-1}, lines in figure correspond to linear regression)
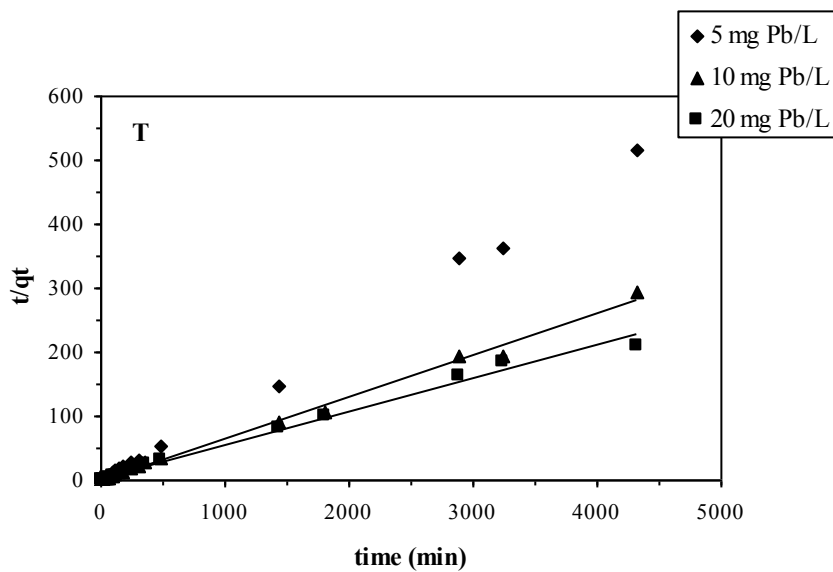
Figure 192 Influence of initial lead concentration on sorption kinetics – linearization of Ho's equation (pH$_i$=5, T sample, 300 mg sorbent L^{-1}, lines in figure correspond to linear regression)
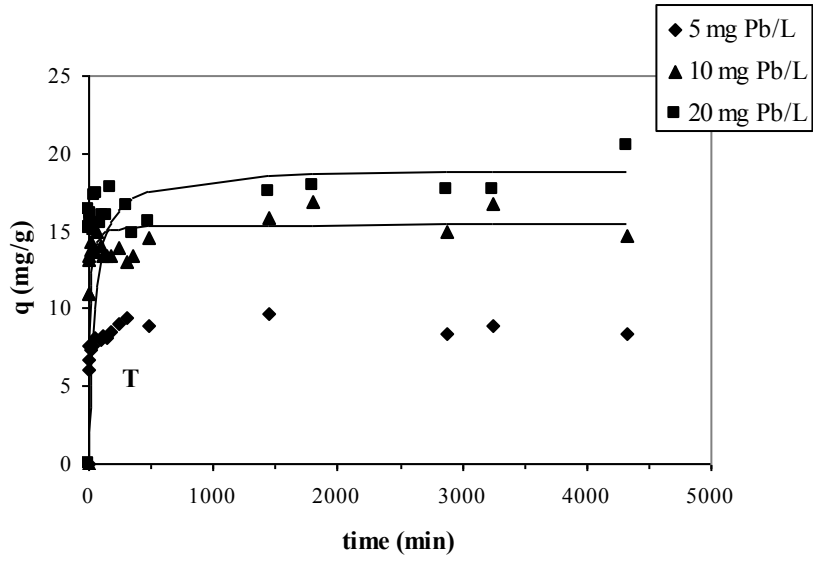
Figure 193 **Influence of initial lead concentration on sorption kinetics – pseudo second order rate equation fit (pH$_i$=5, T sample, 300 mg sorbent L^{-1})**
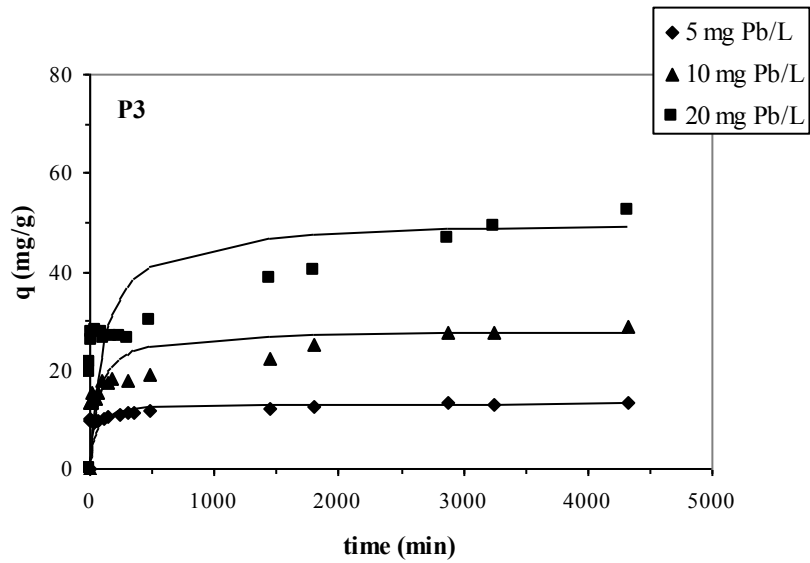
Figure 194 **Influence of initial lead concentration on sorption kinetics – pseudo second order rate equation fit (pH$_i$=5, P3 sample, 300 mg sorbent L^{-1})**
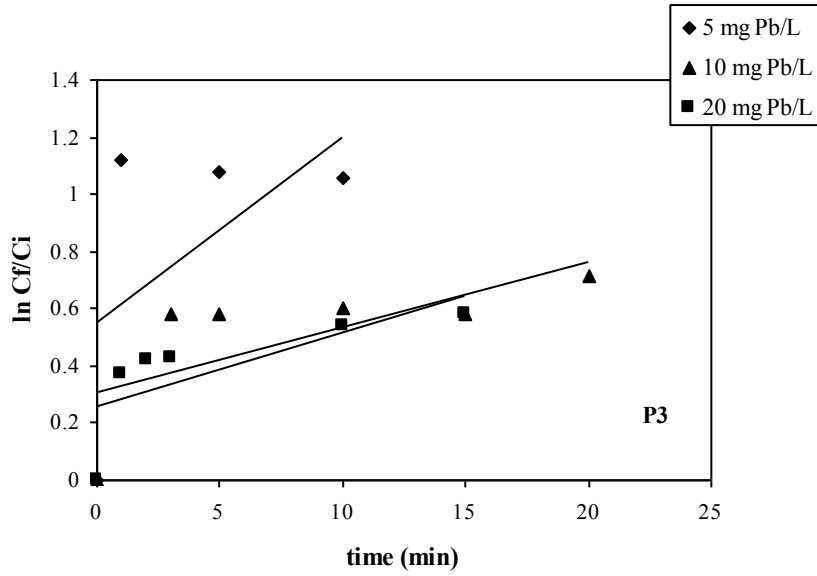
Figure 195 Influence of initial lead concentration on sorption kinetics – External mass transfer model (pH$_i$=5, P3 sample, 300 mg sorbent L^{-1}, lines in figure correspond to linear regression)
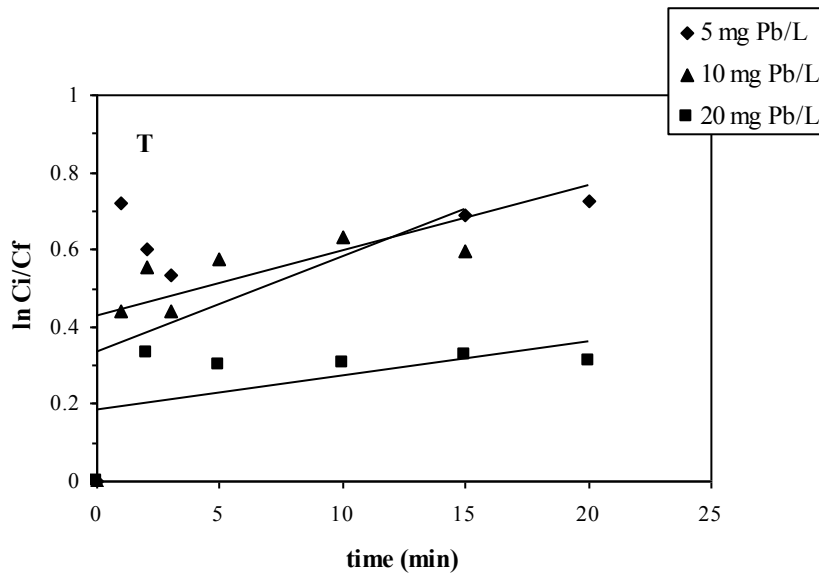
Figure 196 Influence of initial lead concentration on sorption kinetics – External mass transfer model (pH$_i$=5, T sample, 300 mg sorbent L^{-1}, lines in figure correspond to linear regression)

303
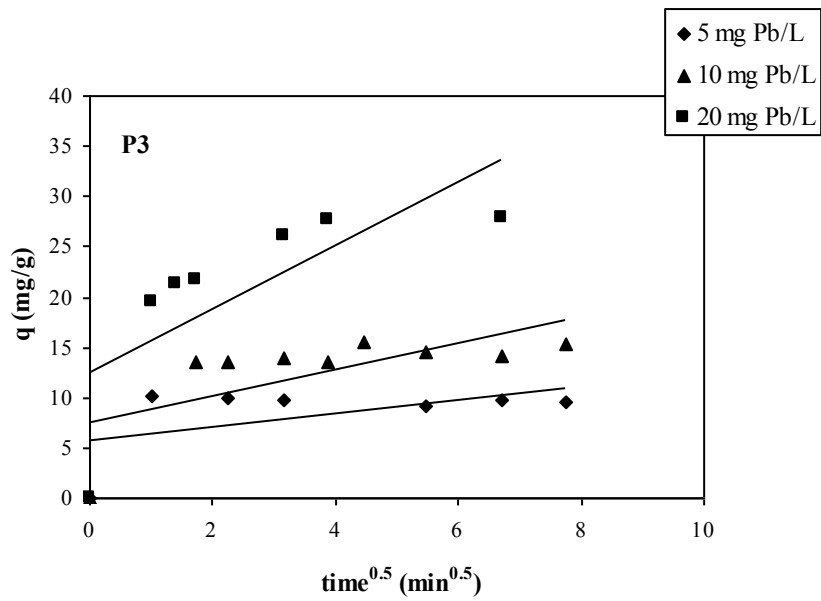
Figure 197 Influence of initial lead concentration on sorption kinetics – W&M model (pH$_i$=5, P3 sample, 300 mg sorbent L^{-1}, lines in figure correspond to linear regression)
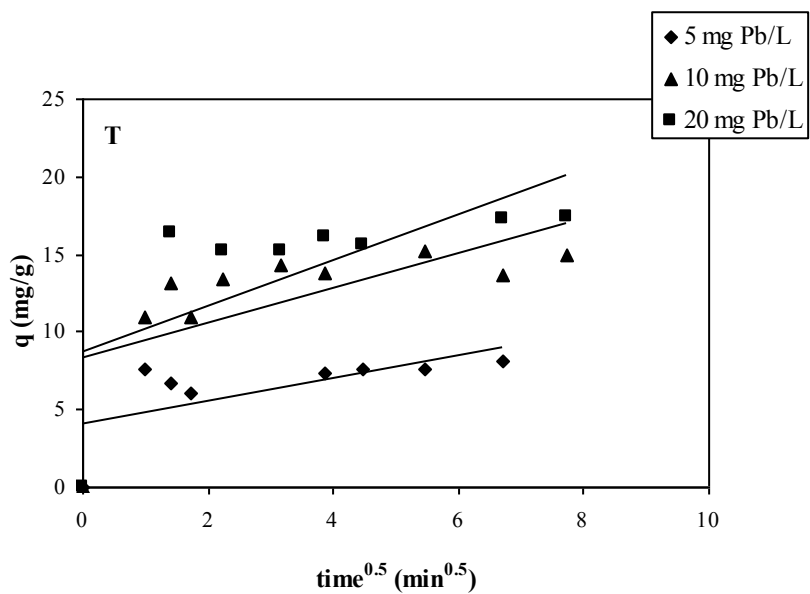
Figure 198 Influence of initial lead concentration on sorption kinetics – W&M model (pH$_i$=5, T sample, 300 mg sorbent L^{-1}, lines in figure correspond to linear regression)

304
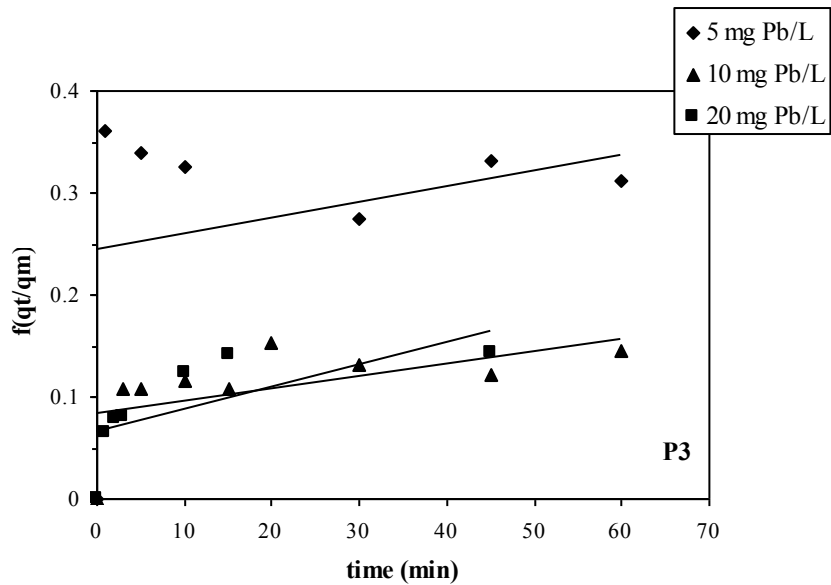
Figure 199 Influence of initial lead concentration on sorption kinetics – U&T model (pH$_i$=5, P3 sample, 300 mg sorbent L^{-1}, lines in figure correspond to linear regression)
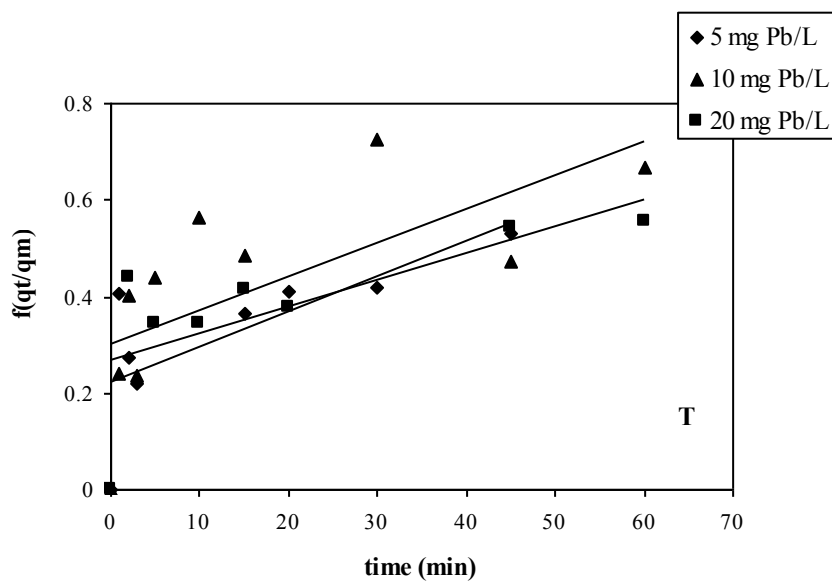
Figure 200 Influence of mercury concentration on sorption kinetics – U&T model (pH$_i$=5, T sample, 300 mg sorbent L^{-1}, lines in figure correspond to linear regression)

Appendix F

Sorption isotherms performed with *Tolypocladium* beads were carried out according to the experimental procedure described below. Given volumes of metal solutions (Ci: 10 - 100 mg Cr(VI) L^{-1} and 10 - 1000 mg Hg L^{-1}) were mixed with given amounts of sorbent samples (SD: 6 g sorbent L^{-1}). Lower sorbent dosage could not have been reached regarding the shape and weight of used particles. Thus the results are not comparable to the results obtain from batch experiments with non-immobilized *Tolypocladium* biomass due to much lower biosorbent dose in the latter case. The pH was not controlled during the experiments, but it was monitored before analysis (after 3 days of contact).
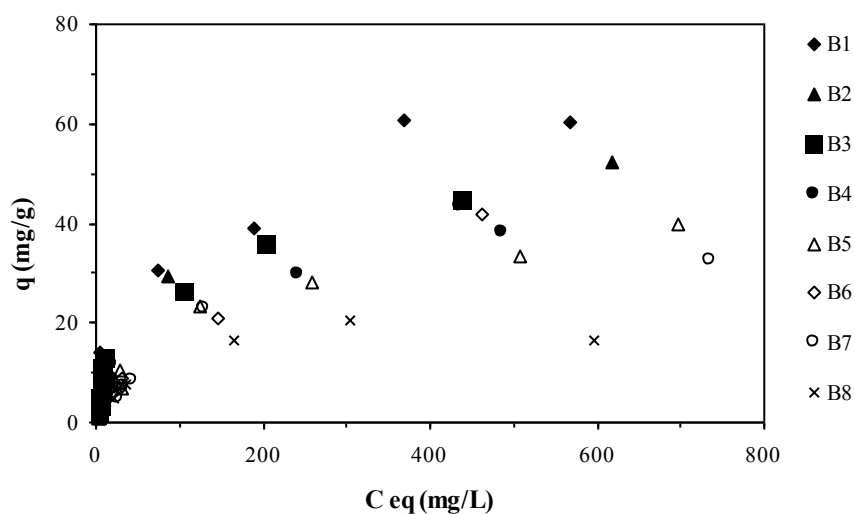
Figure 201 Mercury sorption isotherm using *Tolypocladium* beads at initial pH = 7

sorbent size	Langmuir			Freundlich		
	q_{max}	b	R^2	k	n	R^2
	[mg g^{-1}]	[L mg^{-1}]	-	[L g^{-1}]	-	-
B1	67.7	0.01	0.931	2.24	1.78	0.737
B2	54.8	0.02	0.96	2.13	1.85	0.721
B3	48.6	0.02	0.957	2.32	1.93	0.781
B4	41.6	0.02	0.981	1.67	1.82	0.865
B5	44.2	0.01	0.954	0.88	1.59	0.408
B6	52.4	0.01	0.919	0.92	1.56	0.919
B7	42.2	0.01	0.926	0.8	0.8	0.895
B8	19.3	0.02	0.947	0.69	1.69	0.754

Table 63 Mercury sorption isotherms – model parameters
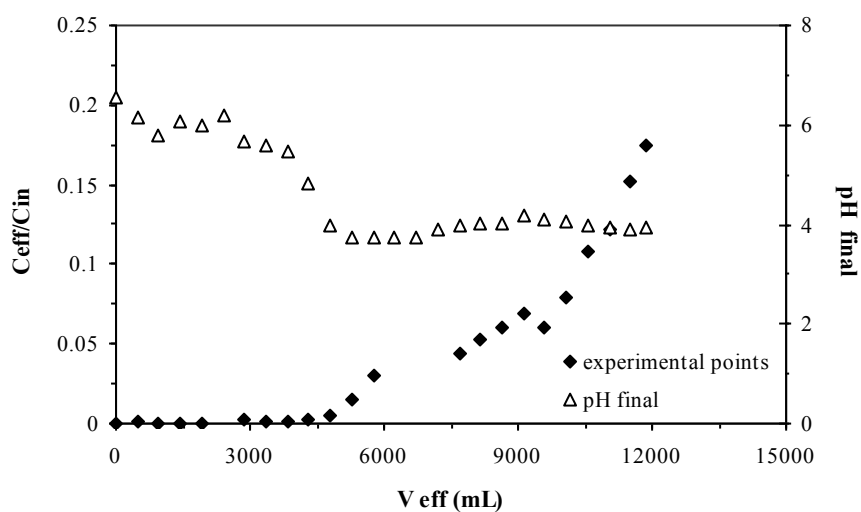
Figure 202 Mercury breakthrough curve (B1, Ci= 100 mg Hg L^{-1})
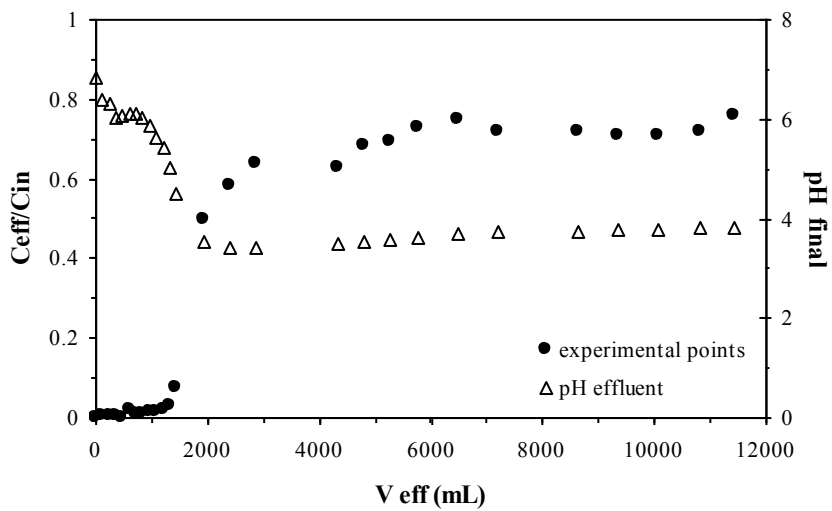
Figure 203 Mercury breakthrough curve (B1, Ci= 250 mg Hg L^{-1})
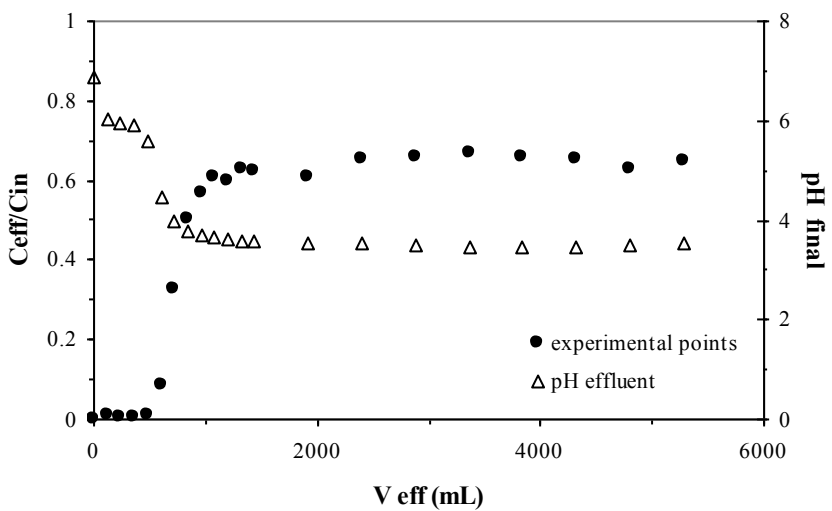
Figure 204 Mercury breakthrough curve (B1, Ci = 1000 mg Hg L^{-1})
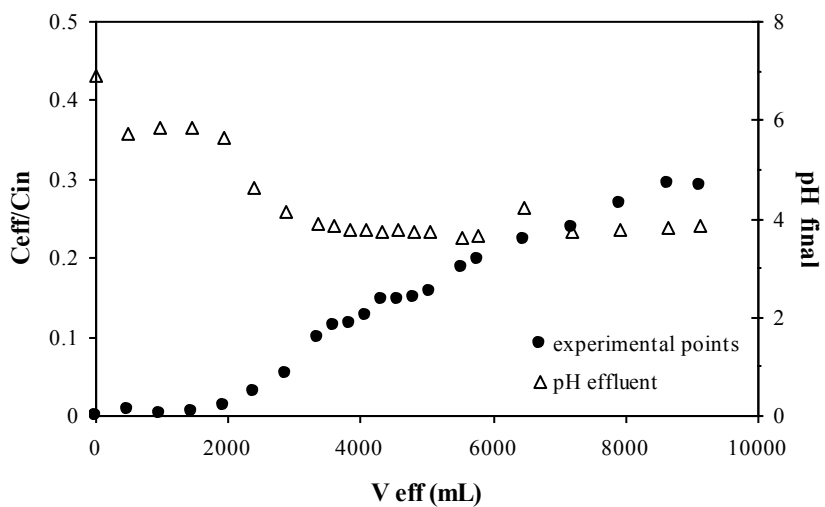
Figure 205 Mercury breakthrough curve (B2, Ci = 100 mg Hg L^{-1})
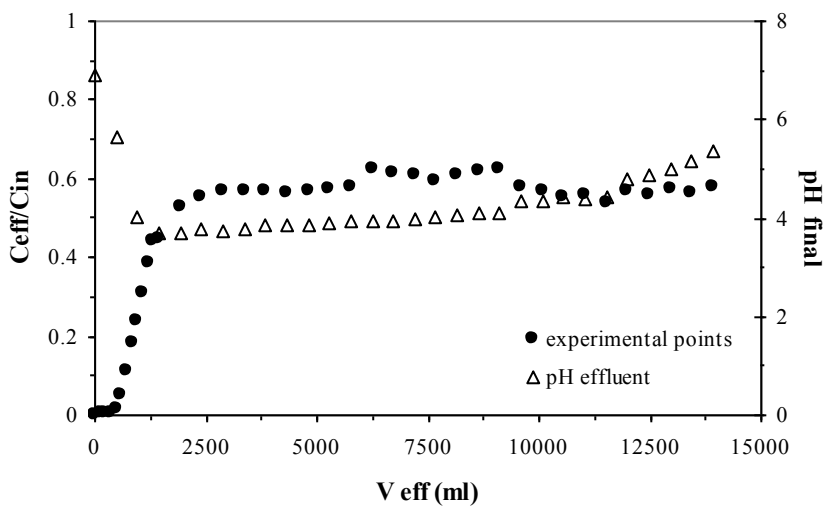
Figure 206 Mercury breakthrough curve (B2, Ci = 250 mg Hg L^{-1})
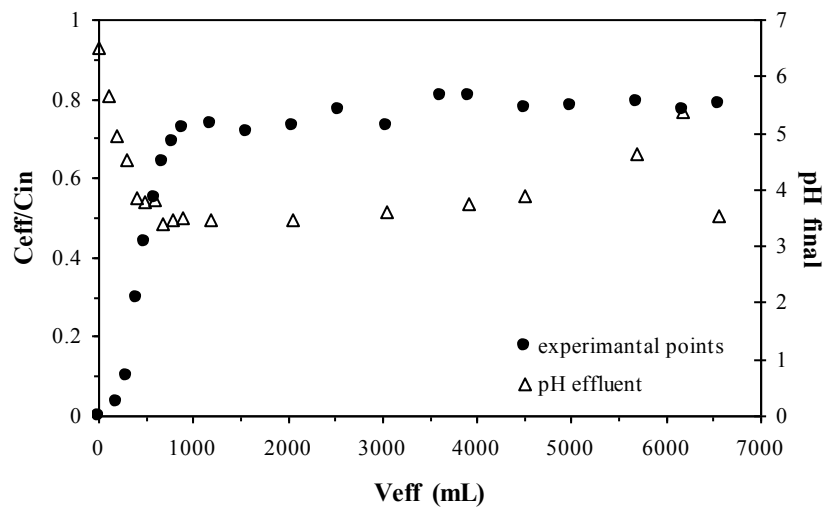
Figure 207 Mercury breakthrough curve (B2, Ci = 1000 mg Hg L^{-1})
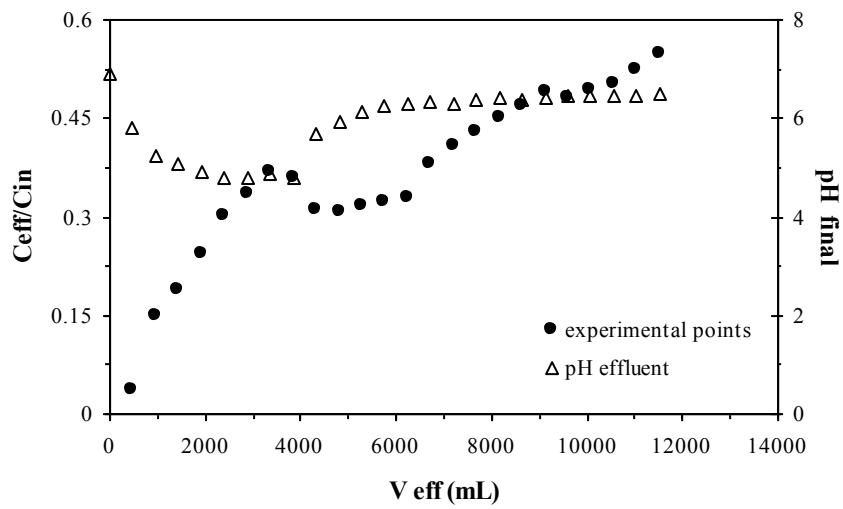
Figure 208 Mercury breakthrough curve (B3, Ci = 100 mg Hg L^{-1})
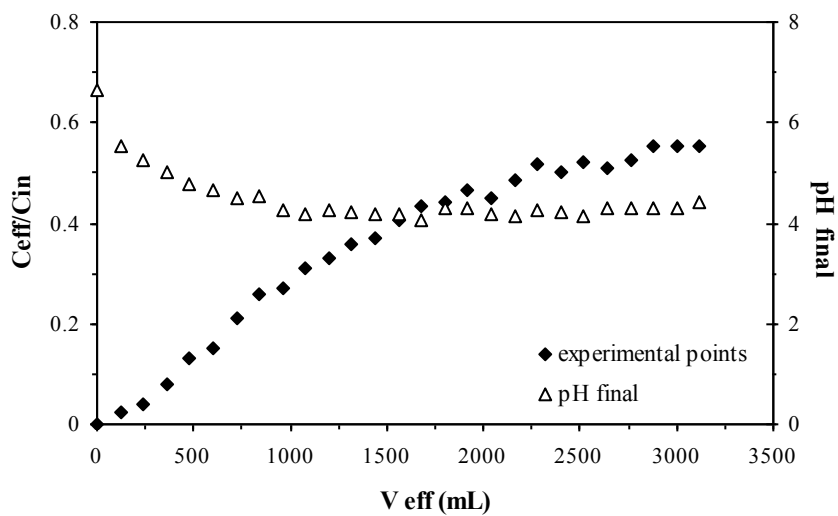
Figure 209 Mercury breakthrough curve (B3, Ci = 250 mg Hg L^{-1})
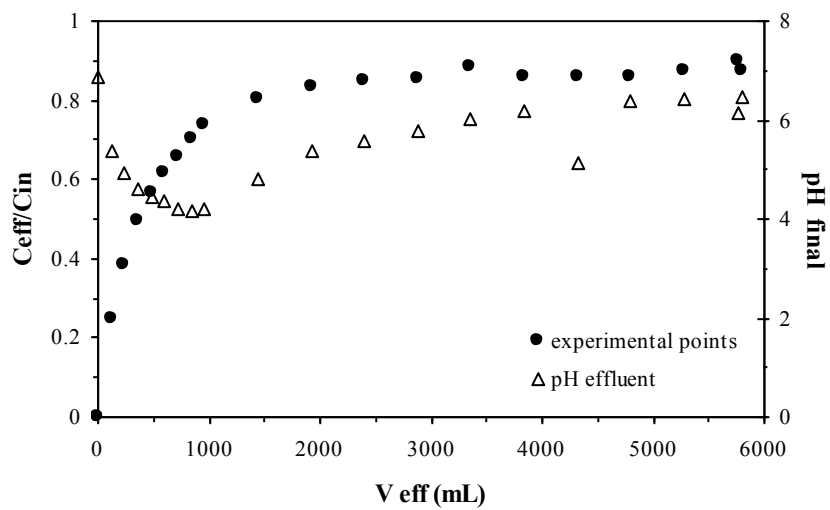
Figure 210 Mercury breakthrough curve (B3, Ci = 1000 mg Hg L^{-1})

311
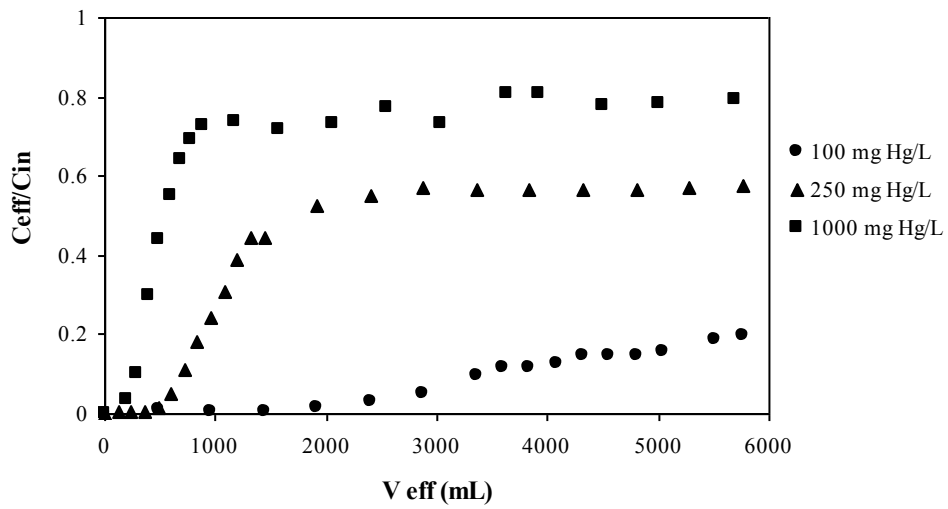
Figure 211 Influence of inlet concentration on mercury breakthrough curve using B2 size fraction
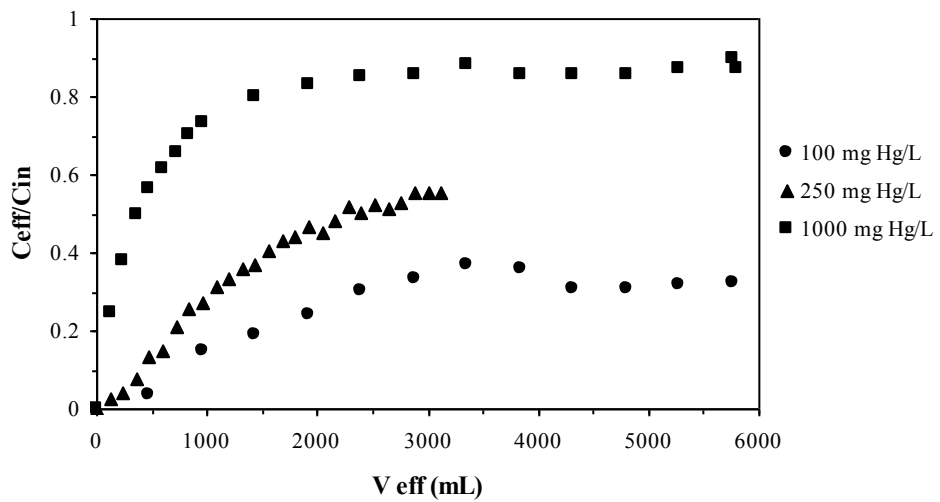
Figure 212 Influence of inlet concentration on mercury breakthrough curve using B3 size fraction
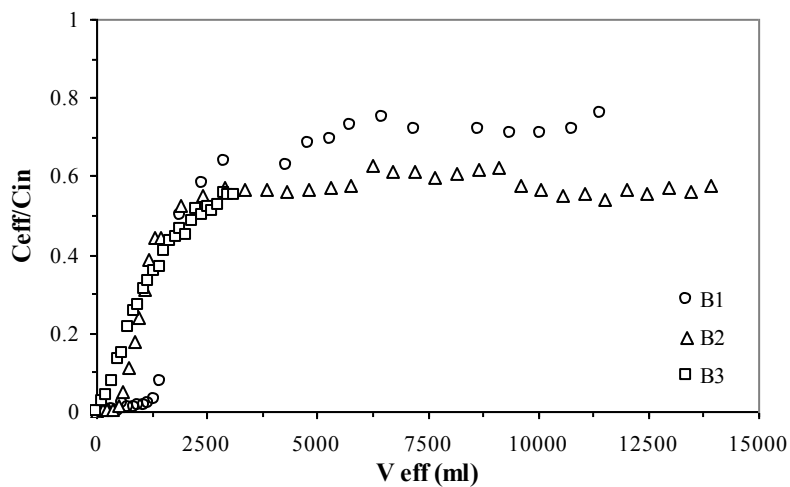
Figure 213 Influence of particle size on mercury breakthrough curve (Ci = 250 mg Hg L^{-1})
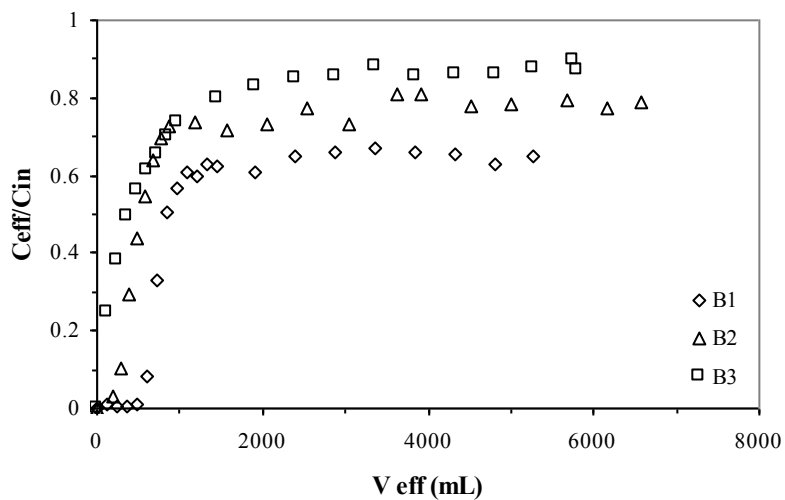
Figure 214 Influence of particle size on mercury breakthrough curve (Ci = 1000 mg Hg L^{-1})
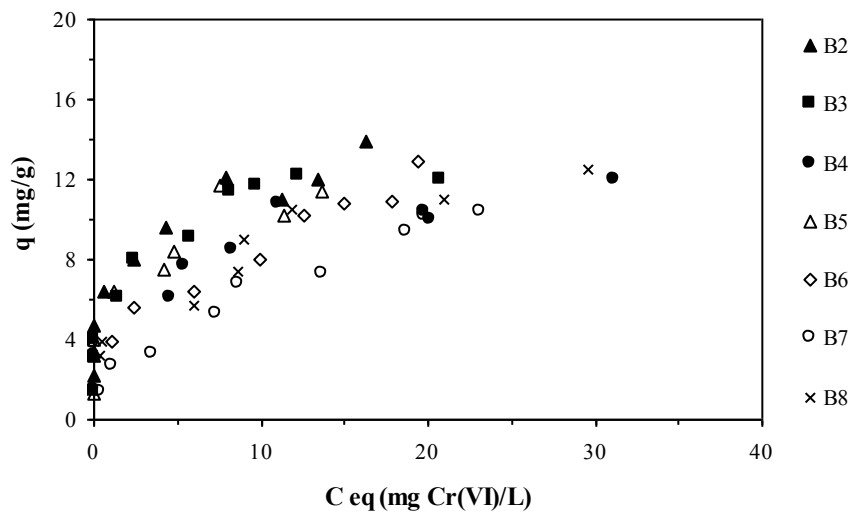
Figure 215 Hexavalent chromium sorption isotherm using *Tolypocladium* beads at initial pH = 2
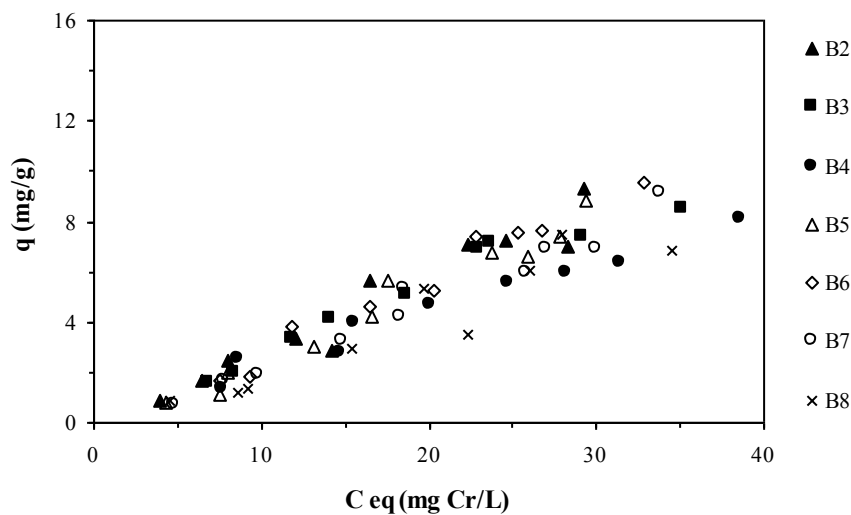
Figure 216 Total chromium sorption isotherm using *Tolypocladium* beads at initial pH = 2

314
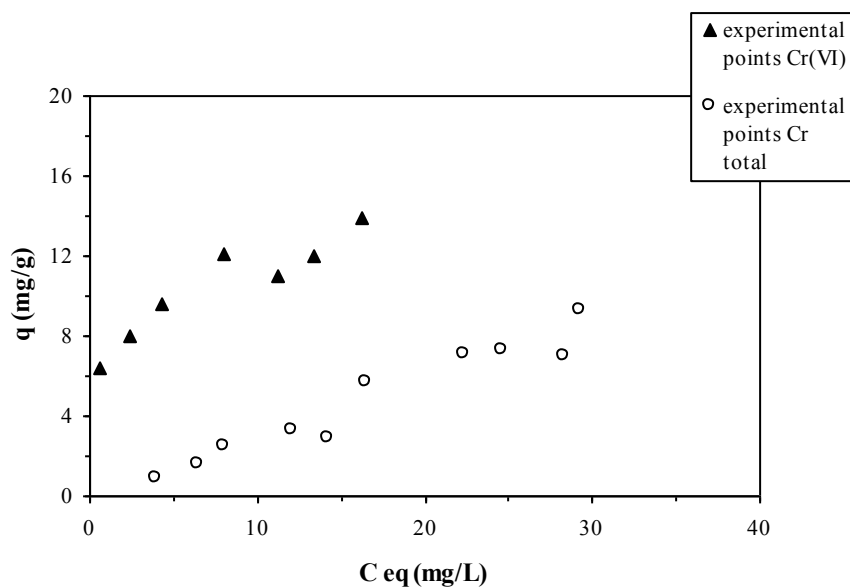
Figure 217 Chromium sorption isotherms using *Tolypocladium* beads (B2 size fraction, pHi = 2)

sorbent size	Langmuir			Freundlich		
	q_{max}	b	R^2	k	n	R^2
	mg g^{-1}	L mg^{-1}	-	L g^{-1}	-	-
B2	13	1.56	0.979	7.5	5.43	0.899
B3	12.3	1.48	0.99	6.73	4.82	0.863
B4	11.7	0.61	0.972	5.95	5.59	0.839
B5	11.3	1.66	0.972	6.4	4.87	0.814
B6	14.4	0.2	0.918	3.74	2.63	0.898
B7	11.5	0.21	0.897	4.14	5.46	0.453
B8	13.3	0.25	0.939	4.35	3.37	0.931

Table 64 Hexavalent chromium sorption isotherms – model parameters
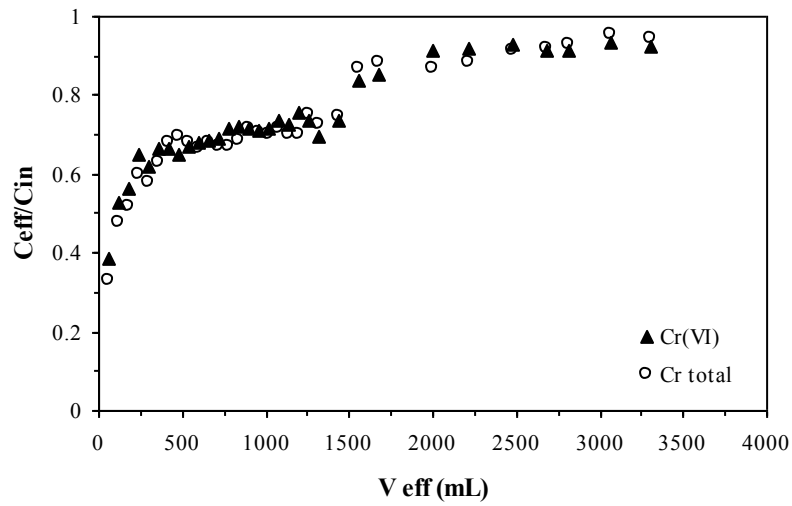
Figure 218 Chromium breakthrough curve (B2, Ci = 1000 mg Cr L^{-1})
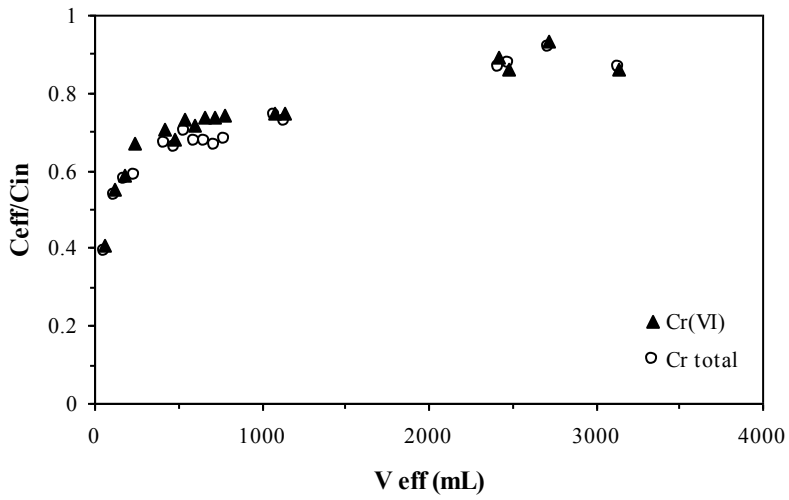
Figure 219 Chromium breakthrough curve (B3, Ci = 100 mg Cr L^{-1})
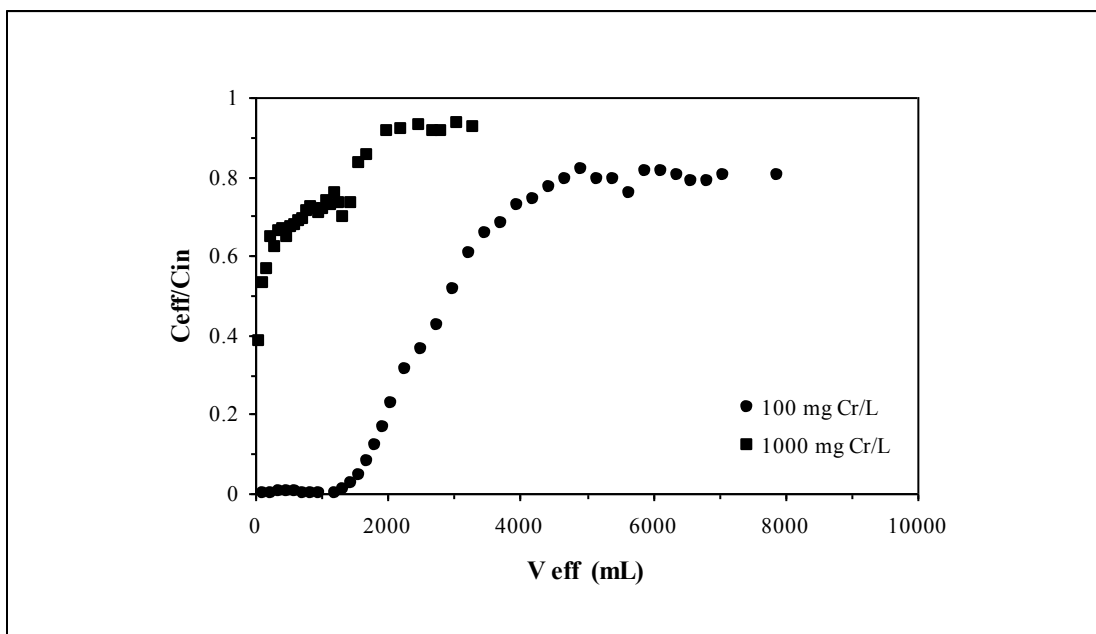
Figure 220 Influence of inlet concentration using B2 size fraction isotherms using *Tolypocladium* beads (B2 size fraction, pHi = 2)

sorbent size	Langmuir			Freundlich		
	q_{max}	b	R^2	k	n	R^2
	mg g^{-1}	L mg^{-1}	-	L g^{-1}	-	-
B2	13	1.56	0.979	7.5	5.43	0.899
B3	12.3	1.48	0.99	6.73	4.82	0.863
B4	11.7	0.61	0.972	5.95	5.59	0.839
B5	11.3	1.66	0.972	6.4	4.87	0.814
B6	14.4	0.2	0.918	3.74	2.63	0.898
B7	11.5	0.21	0.897	4.14	5.46	0.453
B8	13.3	0.25	0.939	4.35	3.37	0.931

Table 65 Hexavalent chromium sorption isotherms – model parameters
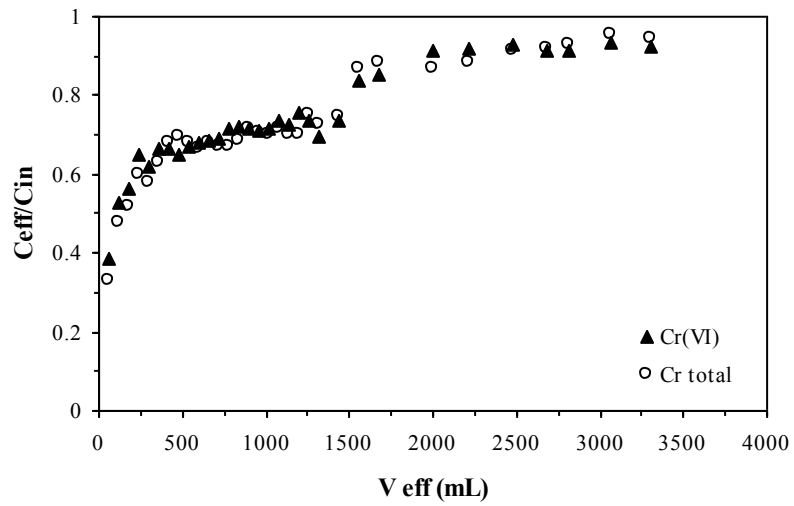
Figure 221 Chromium breakthrough curve (B2, Ci = 1000 mg Cr L^{-1})
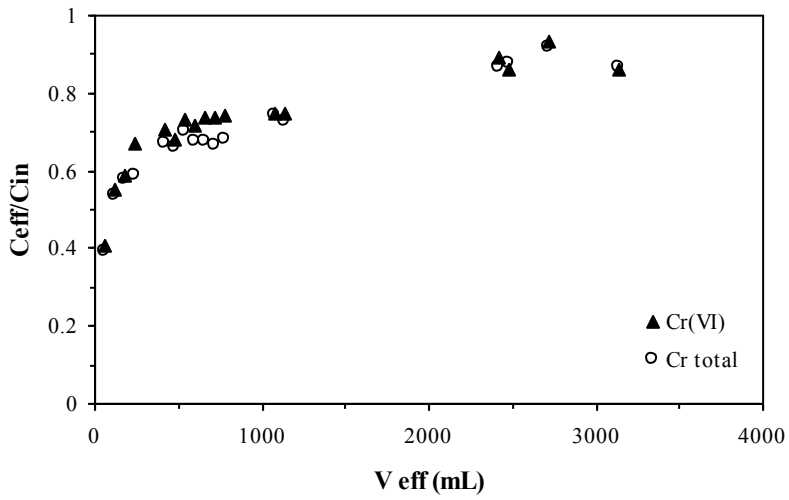
Figure 222 Chromium breakthrough curve (B3, Ci = 100 mg Cr L^{-1})
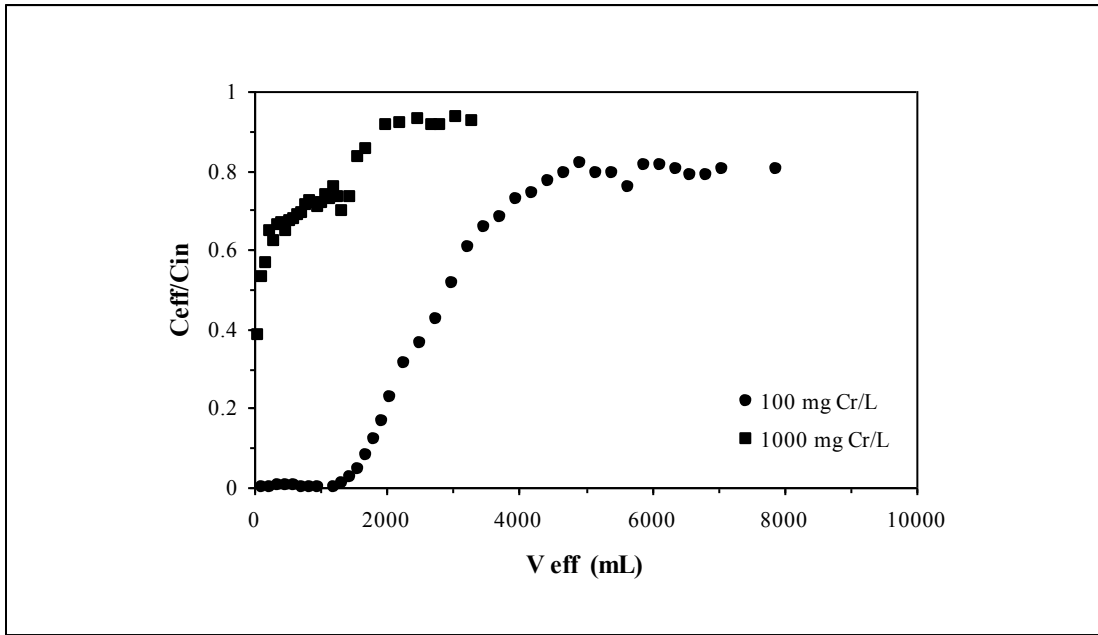
Figure 223 Influence of inlet concentration using B2 size fraction

Appendix G
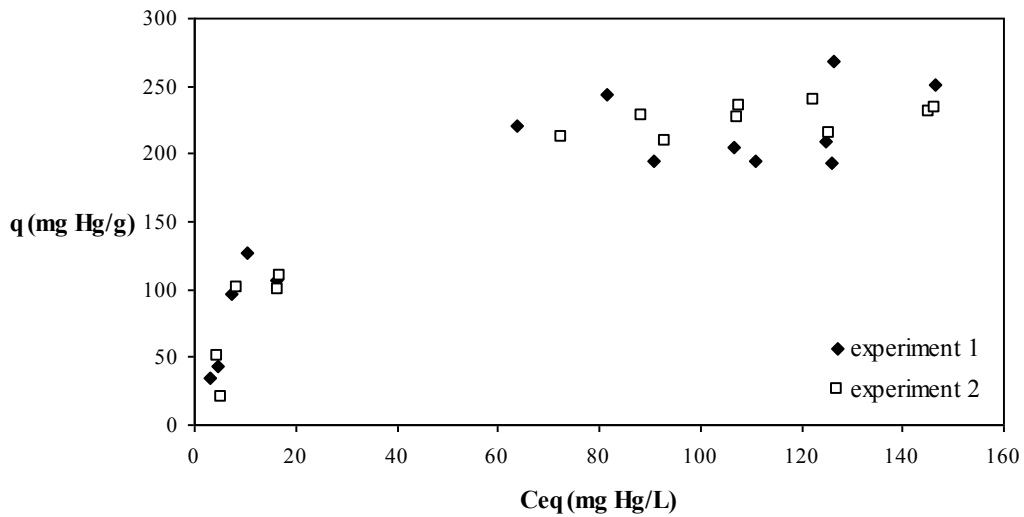
Figure 224 Comparison of Hg sorption isotherms for biosorbent P3 at initial pH5
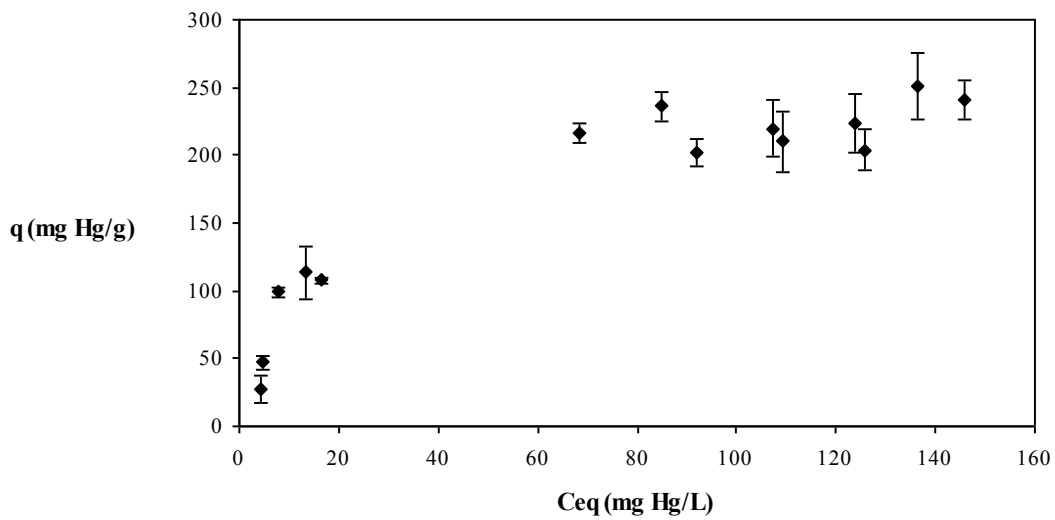
Figure 225 Repeatibility of Hg sorption isotherms for biosorbent P3 at initial pH5 -standard deviation included

References

[1] Harte J., Holleren C., Schneider R., Shirley Ch.: Toxics A to Z: Guide to everyday pollution hazards, University of California Press, 1991

[2] Embrick L. L., Porter K. M., Pendergrass A., Butcher D. J., Characterization of lead and arsenic contamination at Barber Orchard, Haywood County, NC, Microchemical Journal 81(2005)117-121

[3] De Meeus C., Eduljee G. H., Utton M., Assessment and management of risks arising from exposure to cadmium in fertilisers. I, Science of Total Environment 291(2002)167-187

[4] Larssen T., Vogt R. D., Seip H. M., Furuberg G., Liao B., Xiao J., Xiong J., Mechanisms for aluminum release in Chinese acid forest soils, Geoderma 91(1999)65-86

[5] Harada M., The global lessons of Minamata desease: An introduction to Minamata studies, Advances in Bioethics 8(2005)299-335

[6] Kudo A., Fujikawa Y., Miyahara S., Zheng J., Takigami H., Sugahara M., Muramatsu T., Lessons form Minamata mercury pollution, Japan – After a continuous 22 years of observation, Water Science and Technology, 38(1998)187-193

[7] Myers G. J., Davidson P. W., Cox C., Shamlaye C., Cernichiari E., Clarkson T. W., Twenty-seven years studying the human neurotoxicity of methyl mercury exposure, Environmental Research Section A 83(2000)275-285

[8] Dusek L., Svobodova Z., Janouskova D., Vykusova B., Jarkovsky J., Smid R., Pavlis P., Bioaccumulation of mercury in muscle tissue of fish in the Elbe Riber (Czech republic): multispecies monitoring study 1991-1996, Ecotoxicology and Environnmental Safety 61(2005)256-267

[9] Hrabik T. R., Watras C. J., Recent declines in mercury concentration in a freshwater fishery: isolating the effect of de-acidification and decreased atmospheric mercury deposition in Little Rock Lake, Science of the Total Environment 207(2002)229-237

[10] Wong C. S. C., Duzgoren-Aydin N. S., Aydin A., Wong M. H., Sources and trends of environmental mercury emissions in Asia, Science of the Total Environement (2005), in press

[11] Wise S. S., Holmes A. L., Ketter M. E., Hartsock W. J., Fomchenko E., Katsifis S., Thompson W. D., Wise J. P. Sr., Chromium is the proximate clastogenic species for lead chromate-induced clastogenicity in human bronchial cells, Mutation Research 560(2004)79-89

[12] Desjardin V., Bayard R., Huck N., Manceau A., Gourdon R., Effect of microbila activity on the mobility of chromium in soils, Waste Management 22(2002)195-200

[13] Fulladosa E., Desjardin V., Murat J.-C., Gourdon R., Villaescusa ., Cr(VI) reduction into Cr(III) as a mechanism to explain the low sensitivity of *Vibrio fischeri* bioassay to detect chromium pollution

[14] Chen J.-C., Wey M.-Y., The effect of operating conditions on the capture of metals with limestone during incineration, Environmental International 22(1996)743-752

[15] Chen J.-C., Wey M.-Y., Chiang B.-C., Hsieh S.-M., The simulation of hexavalent chromium formation under various incineration conditions, Chemosphere 36(1998)1553-1564

[16] Kazi F. K. M., Cooper P. A., Rapid-extraction oxidation process to recover and reuse copper, chromium and arsenic from industral wood preservative sludge, Waste Management 22(2002)293-301

[17] Saleh F., Parketon T. F., Lewis R. V., Huang J. H., Dickson K. L., Kinetics of chromium transformations in the environemnt, Science of the Total Environment, 86(1989)25-41

[18] Waalkes M. P., Cadmium carcinogenesis, Mutation Research 533(2003)107-120

[19] Ishihara T., Kobayashi E., Okubo Y., Suwazono Y., Kido T., Nishijyo M., Nakagawa H., Nogawa K., Association between cadmium concentration in rice and mortality in the Jinzu River basin, Japan, Toxicology 163(2001)23-28

[20] Vahter M., Berglund M., Akesson A., Liden C., Metals and women's health, Environmental Research Section A 88(2002)145-155

[21] Batariova A., Spevackova V., Benes B., Cejchanova M., Smid J., Cerna M., Blood and urine levels of Pb, Cd and Hg in the general population of the Czech Republic and proposed values, International Journal of Hygiene and Environmental Health 209(2006)359-366

[22] Osman K., Akesson A., Berglund M., Bremme K., Schutz A., Ask K., Vahter M., Toxic and essential elements in placentas of swedish women, Clinical Biochemistry 33(2000)131-138

[23] Hu C.-W., Chao M.-R., Wu K.-Y., Chang-Chien G.-P., Lee W.-J., Chang L. W., Lee W.-S., Characterization of multiple airborne particulate metals in the surrounding of a municipal waste incinerator in Taiwan, Atmospheric Environment 37(2003)2845-2852

[24] Tsadilas C. D., Karaivazoglou N. A., Tsotsolis N. C., Stamtiadis S., Samaras V., Cadmium uptake by tobacco as affected by liming, N form, and year of cultivation, Environmental Pollution 134(2005)239-246

[25] Ajmal M., Khan A., Nomani A. A., Ahmed S., Heavy metals: leaching from glazed surfaces of tea mugs, Science of Total Environment 207(1997)49-54

[26] Thomas V. M., Socolow R. H., Fanelli J. J., Siro T. G., Effects of reducing lead in gasoline: An analysis of the international experience, Environmental Science and Technology 33(1999)3942-3948

[27] Vahter M., Counter S. A., Laurell G., Buchanan L. H. Ortega F., Schutz A., Skerfving S., Extensive lead exposure in children in an area with production of lead-glazed tiles in the Eucodorian Andes, International Archives of Occupational and Environmental Health 70(1997)282-286

[28] Pitter P., Hydrochemie (in Czech), 3rd edition, Vydavatelstvi VSCHT, Praha, 1999, ISBN 80-7080-340-1

[29] Volesky B., Detoxification of metal-bearing effluents: biosorption for the next century, Hydrometallurgy 59(2001)203-216

[30] Gonzalez-Munoz M. J., Rodriguez M. A., Luque S., Alvarez J. R., Recovery of heavy metals from metal industry waste waters by chemical precipitation and nanofiltration, Desalination 200(2006)742-744

[31] Macchi G., Marani D., Pagano M., Bagnuolo G., A bench study on lead removal from battery manufacturing wastewaters by carbonate precipitation, Water Research 30(1996)3032-3036

[32] Andrus M. E., A review of metal precipitation chemicals for metal-finishing applications, Metal Finishing 98(2000)20-21

[33] Henke K. R., Robertson D., Krepps M. K., Atwood D. A., Chemistry and stability of precipitates from aqueous solutions of 2,4,6-trimercaptotriazine, trisodium salt, nonahydrate (TMT-55) and mercury (II) chloride, Water Research 34(2000)3005-3013

[34] Matlock M. M., Henke R. K., Atwood D. A., Robertson D., Aqueous leaching properties and environmental implications of cadmium, lead and zinc trimercatotriazine (TMT) compounds, Water Research 35(2001)3649-3655

[35] Matlock M. M., Henke K. R., Atwood D. A., Effectiveness of commercial reagents for heavy metal removal from water with new insights for future chelate designs, Journal of Hazardous Materials B92(2002)129-142

[36] Tassel F., Rubio J., Misra M., Jena B. C., Removal of mercury from gold cyanide solution by dissolved air flotation, Minerals Engineering 10(1997)803-811

[37] Kratochvil D., Pimentel P., Volesky P., Removal of trivalent and hexavalent chromium by seaweed biosorbent, Environmental Science and Technology 32(1998)2693-2698

[38] Sakalis A., Fytianos K., Nickel U., Voulgaropoulos A., A comparative study of platinised titanium and niobe/synthetic diamond as anodes in the electrochemical treatment of textile wastewaters, Chemical Engineering Journal 119(2006)127-133

[39] Hunsom M., Pruksathorn K., Damronglerd S., Vergnes H., Duverneuil P., Electrochemical treatment of heavy metals (Cu^{2+}, Cr^{6+}, Ni^{2+}) from industrial effluent and modeling of copper reduction, Water Research 39(2005)610-616

[40] Atkison S., World's largest desalinaton plant begins operating in Israel, Membrane Technology 12(2005)9-10

[41] Gholani M. M., Mokhtari M. A., Aameri A., Fard M. R. A., Application of reverse osmosis technology for arsenic removal from drinking water, Desalination 200(2006)725-727

[42] Slesarenko V. V., Electrodialysis and reverse osmosis membrane plants at power stations

[43] Eom T.-H., Lee C.-H., Kim J.-H., Lee C.-H., Development of an ion exchange system for plating wastewater treatment, Desalinaton 180(2005)163-172

[44] Curkovic L., Cerjan-Stefanovic S., Filipan T., Metal ion exchange by natural and modified zeolites, Water Research, 31(1997)1379-1382

[45] Dobrevsky I., Dimova-Todorova M., Panayotova T., Electroplating rinse waste water treatment by ion exchange, Desalination 108(1996)277-280

[46] McKay G. (Editor), Use of adsorbents for the removal of polutants from wastewaters, 1996, CRC Press, Boca Raton, ISBN 0-8493-6920-7, p. 2-3

[47] Frenzel I., Stamatialis D. F., Wessling M. Water recycling from mixed chromic acid waste effluents by membrane technology, Separation and Purification Technology 49(2006)76-83

[48] Salzman S. A., Allison G., Stagnatti F., Coates M., Hill R. J., Performance of constructed evaporation ponds for disposal of smelter waste water: a case study at Portland Aluminium, Victoria, Australia, Water Research 35(2001)2121-2128

[49] Johnson D. B., Biohydrometallurgy and the environment: Intimate and important interplay, Hydrometallurgy 83(2006)153-166

[50] Brierley C. L., Bioremediation of metal-contaminated surface and groundwaters, Geomicrobiology Journal 8(1990)201-223

[51] Volesky B., Sorption and Biosorption, 2003, BV Sorbex, Montreal, ISBN 0973298308, p.97-100

[52] Holan Z. R., Volesky B., Accumulation of cadium, lead and nickel by fungal and wood biosorbents, Applied Microbiology and Biotechnology 53(1995)133-146

[53] Fourest E., Roux J.-C., Heavy metal biosorption by fungal mycelial by-products: mechanism and influence of pH, Applied Microbiolology and Biotechnology 37(1992)399-403

[54] Prakasham R. S., Sheno Merrie J., Sheela R., Saswathi N., Ramakrishna S.V., Biosorption of chromium VI by free and immobilized *Rhizopus arrhizus*, Environmental Pollution 104(1999)421-427

[55] Sudha Bai R., Abraham T. E., Biosorption of Cr(VI) from aqueous solution by *Rhizopus nigricans*, Bioresource Technology 79(2001)73-81

[56] Chandra Sekhar K., Subramanian S., Modak J. M., Natarajan K. A., Removal of metal ions using an industrial biomass with the reference to environmental control, International Journal of Mineral Processing 53(1998)107-120

[57] Park D., Yun Y.-S., Jo J. H., Park J. M., Mechanism of hexavalent chromium removal by dead fungal biomass of *Aspergillus niger*, Water Research 39(2005)533-540

[58] Bayramoglu G., Celik G., Yalcim E., Yilmaz M., Arica M., Y., Modification of surface properties of *Lentinus sajor-caju* mycelia by physical and chemical methods: Evaluation of their Cr^{6+} removal efficiencies from aqueous medium, Journal of Hazardous Materials B119(2005)219-229

[59] Yan G., Viraraghavan T., Heavy-metal removal from aqueous solution by fungus *Mucor rouxii,* Water Research 37(2003)4486-4496

[60] Fourest E., Canal C., Roux J.-C., Improvement of heavy metal biosorption by mycelial dead biomasses (*Rhizopus arrhizus, Mucor miehei and Penicillium chrysogenum*) : pH control and cationic activation, FEMS Microbiology Reviews 14(1994)325-332

[61] Saglam N., Say R., Denizli A., Patir S., Arica M., Y., Biosorption of inorganic mercury and alkylmercury on to *Phanerochaete chrysosporium* mycelium, Process Biochemistry 34(1999)725-730

[62] Saglam A., Yalcinkaya Y., Denizli A., Arica M. Y., Genc O., Bektas S., Biosorption of mercury by carboxymethylcelllulose and immobilized *Phanerochaete chrysosporium*, Microchemical Journal 71(2002)73-81

[63] Kapoor A., Viraraghavan T., Cullimore D., R., Removal of heavy metals using the fungus *Aspergillus niger*, Bioresource technology 70(1999)95-104

[64] Niu H., Xu X. S., Wang J. H., Removal of lead from aqueous solution by *Penicillium* biomass, Biotechnology and Bioengineering, 42(1993)785-787

[65] Huang C., Huang C. P., Application of *Aspergillus oryzae* and *Rhizopus oryzae* fro Cu(II) removal, Water Research 30(1996)1985-1990

[66] Mcafee B., Gould D. W., Nadeau J. C., da Costa A. C. A.: Biosorption of metal ions using chitosan, chitin, and biomass of *Rhizopus oryzae*, Separation Science and technology, 36(2001), 3207-3222

[67] Puranik P R., Paknikar K. M., Bisorption of lead and zinc from solutions using *Streptoverticillum cinnamoneum* waste biomass, Journal of Biotechnology, 55(1997)113-124

[68] O'Mahony T., Guibal E., Tobin J.M., Reactive dye biosorption by *Rhizopus arrhizus* biomass, Enzyme and Microbial Technology 31(2002)456-463

[69] Yuzhu F., Viraraghavan T., Removal of Congo Red from an aqueous solution by fungus *Aspergillus niger*, Advances in Environmental Research 7(2002)239-247

[70] Rao J. R., Viraraghavan T., Biosorption of phenol from an aqueous solution by *Aspergillus biomass*, Bioresource Technology 85(2002)165-179

[71] Yakubu N. A., Dudeney A. W. L., Biosorption of uranium with *Aspergillus niger*, In: H. Eccles and S. Hunt (editors), Immobilisation of ions by bio-sorption, Elis Horwood Ltd., Chichester, 1986, 184-200

[72] Guibal E., Roulph C., Le Cloirec P., Uranium biosorption by a filamentous fungus *Mucor miehei*, Water Research 26(1992)1139-1145

[73] Tsezos M., Volesky B., Biosorption of uranium and thorium, Biotechnology and Bioengineering, 23(1981)583-604

[74] Volesky B., Sorption and Biosorption, 2003, BV Sorbex, Montreal, ISBN 0973298308, p.88-95

[75] Huang R. Y. M., Pal R., Moon G. Y., Characteristics of sodium alginate membranes for the pervaporation dehydration of ethanol-water and isopropanol-water mitures, Journal of Membrane Science 160(1999)101-113

[76] Martins B. L., Cruz C. V. V., Luna A. S., Henriques C. A., Sorption and desorption of Pb^{2+} by dead *Sargassum* sp. biomass, Biochemical Engineering Jounal 27(2006)310-314

[77] Yang J., Volesky B., Biosorption of uranium on *Sargassum* biomass, Water Research 33(1999)3357-3363

[78] Kratochvil D., Volesky B., Advances in the biosorption of heavy metals, Tibtech July 16(1998)291-300

[79] Luo F., Liu Y., Li X., Xuan Z., Ma J., Biosorption of lead ion by chemically-modified biomass of marine brown algae *Laminaria japonica*, Chemosphere (2006), in press

[80] Yu Q., Matheickal J. T., Yin P., Kaewsarn P., Heavy metal uptake capacities of common marine macro algal biomass, Water Research 33(1999)1534-1537

[81] Hashim M. A., Chu K. H., Biosorption of cadmium by brown, green, and red seaweeds, Chemical Engineering Journal 97(2004)249-255

[82] Nourbakhsh M., Sag Y., Ozer D., Aksu Z., Kutsal T., Caglar A., A comparative study of various biosorbents for removal of chromium(VI) ions from industrial waste waters, Process Biochemistry 29(1994)1-5

[83] McLean R. J. C., Beveridge T. J., Metal-binding capacity of bacterial surfaces and their ability to form mineralized aggregates, in Microbial Mineral Recovery, Ehrilch H. L., Brierly C. L. (eds.), McGraw-Hill Publishing Co., New York, 185-222

[84] Brierly J. A., Brierly C. L., Goyak G. M. , AMT-BIOCLAIM: A new wastewater treatment and metal recovery technology, In: Fundamental and Applied Biohydrometallurgy, Lawrence R. W., Branion R. M. R. and Ebner H. G. (eds.), 1986, Elsevier, Amsterdam, The Netherlands, p. 291-304

[85] Brierly J. A., Production and application of a *Bacillus*-based product for use in metals biosorption, in: Biosorption of heavy metals, Volesky B. (eds.), CRC Press, Boca Raton, USA, p. 305-312

[86] Jansson-Charrier M., Biosorption d'ions metallliques (uranium et vanadium) sur chitosan, Ph.D. thesis, Université Montpellier II, 1996

[87] Dzul Erosa M. S., Saucedo Medina T. I., Navarro Mendoza R., Avila Rodriquez M., Guibal E., Cadmium sorption on chitosan sorbents: kinetic and equilibrium studies, Hydrometallurgy 61(2001)157-167

[88] Chassary P., Vincent T., Marcano J. S., Macaskie L. E., Guibal E., Palladium and platinum recovery from bicomponent mixtures using chitosan derivates , Hydrometallurgy 76(2005)131-147

[89] Guzman J., Saucedo I., Revilla J., Navarro R., Guibal E., Copper sorption by chitosan in the presence of citrate ions: influence of metal speciation on sorption mechanism and uptake capacitieis, International Journal of Biological Macromolecules, 33(2003)57-65

[90] Ly Arrascue M., Maldonado Garcia H., Horna O., Guibal E., Gold sorption on chitosan derivates, Hydrometallurgy 71(2003)191-200

[91] Dambies L., Vincent T., Guibal E., Treatment of arsenic-containing solutions using chitosan derivatives: uptake mechanism and sorption performances, Water Research, 36(2002)3699-3710

[92] Gibbs G., Tobin J. M., Guibal E., Influence of chitosan pre-protonation on Reactive Black 5 sorption isotherms and kinetics, Industrial and Engineering Chemistry Research. 43(2004)1-11

[93] Sharma D., C., Forster C. F., Removal of hexavalent chromium using sphagnum moss peat, Water Research 27(1993)1201 - 1208

[94] Dean S., A., Tobin J. M., Uptake of chromium cations and anions by milled peat, Resources, Conservation and Recycling 27(1999)151-156

[95] Ucun H., Bayha Y., K., Kaya Y., Cakici A., Algur O., F., Biosorption of chromium (VI) from aqueous solution by cone biomass of *Pinus sylvestris*, Bioresource Technology 85(2002)155-158

[96] Ucun H., Bayan Y. K., Kaya Y., Cakici ., Algur O. F., Biosorption of lead(II) from aqueous solution by cone biomass of *Pinus sylvestris*, Desalination 154(2003)233-238

[97] Dakiky M., Khamis M., Manassra A. Mereb M., Selective adsorption of chromium (VI) in industrial wastewater using low-cost abundantly available adsorbents, Advances in Environmental Research 6(2002)533-540

[98] Lister S. K., Line M. A., Potential utilisation of sewage sludge and paper mill waste for biosorption of metals from pollluted waterways, Bioresource Technology 79(2001)35-39

[99] Villanueva-Espinosa J.F., Hernandez-Esparza M., Ruiz-Trevino F. A., Adsorptive properties of fish scales of Oreochromis Niloticus (Mojarra Tilapia) for metallic ion removal from waste water, Industrial and Engineering Chemistry Research 40(2001)3563-3569

[100] Conrad K., Bruun Hansen H. C., Sorption of zinc and lead on coir, Bioresource Technology (2006), in press

[101] Fiol N., Villaescusa I., Martinez M., Miralles N., Poch J., Serarols J., Sorption of Pb(II), Ni(II), Cu(II) and Cd(II) from aqueous solution by olive stone waste, Separation and Purification Technology (2006), in press

[102] Zeroual Y., Moutaouakkil A., Dzairi F. D., Talbi M., Chung P. C., Lee K., Blaghen M., Biosorption of mercury from aqueous solution by *Ulva lactuca* biomass, Bioresource Technology 90(2003)349-351

[103] Fourest E., Roux J.-C., Heavy metal biosorption by fungal mycelial by-products: mechanisms and influence of pH, Applied Microbiology and Biotechnology 37(1997)399-403

[104] Spanelova M., Svecova L., Guibal E., Influence of the treatment of fungal biomass on sorption properties for lead and mercury uptakne, in: Tzezos M., Hatzikioseyian A., Remoundaki E. (Eds.), Biohydrometallurgy: A sustainable technology in evolution, Part II, National Technical Univeristy of Athens, Athens, Greece, 2004, p. 899-909

[105] Dostalek P., Patzak M., Matejka P., Influence of specific growth limitation on biosorption of heavy metals by *Saccharomyces cerevisiae*, Intenational Biodeterioration and Biodegradation, 54(2004)203-207

[106] Atkinson B. W., Bux F., Kasan H. C., Considerations for application of biosorption technology to remediate metal-contaminated industrial effluents, Water SA 24(1998)129-135

[107] Gupta R., Ahuja P., Khan S., Sexena R. K., Mohapatra H., Microbial biosorbents: Meeting challenges of heavy metal pollution in aqueous solutions, Current Science 78(2000)967-973

[108] Davis T. A., Volesky B., Mucci A., A review of the biochemistry of heavy metal biosorption by brown algae, Water Research 37(2003)4311-4330

[109] Volesky B., Sorption and Biosorption, 2003, BV Sorbex, Montreal, ISBN 0973298308, p.41-46

[110] Green-Ruiz C., Mercury(II) removal from aqueous solutions by nonviable *Bacillus* sp. from a tropical estuary, Bioresource Technology (2005), in press

[111] Chen J.-Z., Tao X.-C., Xu J., Zhang T., Liu Z.-L., Biosorption of lead, cadmium and mercury by immobilized *Microcystis aeruginosa* in a column, Process Biochemistry 40(2005)3675-3679

[112] Herrero R., Lodeiro P., Rey-Castro C., Vilarino T., Sastre de Vicente M. E., Removal of inorganic mercury from aqueous solutions by biomass of the marine macroalga *Cystoseira baccata,* Water Research 39(2005)3199-3210

[113] Bajpai J., Shrivastava R., Bajpai A. K., Dynamic and equilibrium studies on adsorption of Cr(VI) ions onto binary bio-polymeric beads of cross linked alginate and gelatine, Colloids and Surfaces A- Physicochemical and Engineering Aspects 236(2004)81-90

[114] Gupta V. K., Shrivastava A. K., Jain N., Biosorption of chromium (VI) from aqueous solutions by green algae *Spirogyra* species, Water Research 35(2001)4079-4085

[115] Arica M. Y., Tuzun I., Yalcin E., Ince O., Bayramoglu G., Utilization of native, heat and acid-treated microalgae *Chlamydomonas reinhardtii* preparations for biosorption of Cr(VI) ions, Process Biochemistry 40(2005)2351-2358

[116] Zouboulis A. I., Loukidou M. X., Matis K. A ., Biosorption of toxic metals from aqueous solutions by bacteria strains isolated from metal-polluted soils, Process Biochemistry 39 (2004)909-916

[117] Aoyama M., Letter to editor – Comment on „ Biosorption of chromium(VI) from aqueous solution by cone biomass of *Pinus sylvestris*, Bioresource Technology 89(2003)317-318

[118] Sudha Bai R., Abraham T. E., Studies on enhancement of Cr(VI) biosorption by chemically modified biomass of *Rhizopus nigricans*, Water Research 36(2002)1224-1236

[119] Sudha Bai R., Abraham T. E., Studies on chromium(VI) adsorption-desorption using immobilized fungal biomass, Bioresource Technology 87(2003)17-26

[120] Park D., Yun Y.-S., Park J. M., Reduction of hexavalent chromium with the brown seaweed *Ecklonia* biomass, Environmental Science and Technology 38(2004)4860-4864

[121] Park D., Yun Y.-S., Park J. M., Studies on hexavalent chromium biosorption by chemically treated biomass of *Ecklonia* sp., Chemosphere 30(2005)1356-1364

[122] Cabatingan L. K., Agapay R. C., Rakels J. L. L., Ottens M., Van der Wielen L. A. M., Potential of biosorption for the recovery of chromate in industrial wastewaters, Industrial and Engineering Chemistry Research 40(2001)2302-2309

[123] Wei Ma, Tobin J. M., Determination and modelling of effects of pH on peat biosorption of chromium , copper and cadmium, Biochemical Engineering Journal 18(2004)33-40

[124] Martins R. J. E ., Pardo R., Bonaventura R. A. R., Cadmium(II) and zinc(II) adsorption by the aquatic moss *Fontalis antipyretica*: Effect of temperature, pH and water hardness, Water Research 38(2004)693-699

[125] Cruz C. V. C., da Costa A. C. A., Henriques C. A., Luna A. S., Kinetic modelling and equilibrium studies during cadmium biosorption by dead *Sargassum s*p. biomass, Biosource Technology 91(2004)249-257

[126] Goksungur Y., Uren S., Guvenc U., Biosorption of cadmium and lead ions by ethanol treated waste baker's yeast biomass, Biosource Technology 96(2004)103-109

[127] Rangsayatorn N., Pokethitiyook P., Upathem E. S., Lanza G. R., Cadmium biosorption by celss of *Spirulina platensis* TISTR 8217 immobilized in alginate and silica gel, Environement International 30(2004)57-63

[128] Marseaut S., Debourg A., Dostalek P., Votruba J., Kuncova G., Tobin J. M, A silica matrix biosorbent of cadmium, International Biodeterioration and Biodegradation, 54(2004)209-214

[129] Tsezos M., The role of chitin in uranium adsorption by *R. Arrhizus*, Biotechnology and Bioengineering XXV(1983)2025-2040

[130] Matheickal J. T., Yu Q., Biosorption of lead(II) from aqueous solutions by *Phellinus badius*, Minerals Engineering, 10(1997)947-957

[131] Selatinia A., Boukazoula A., Kechid N., Bakhti M. Z., Chergui A., Kerchich, Biosorption of lead (II) from aqueous solution by a bacterial dead *Streptomyces rimosus* biomass, Biochemical Engineering Journal 19(2004)127-135

[132] Matheickal J. T., Yu Q., Biosorption of lead(II) and copper(II) form aqueous solutions by pre-treated biomass of australian marine algae, Bioresource Technology 69(1999)223-229

[133] Dursun A. Y., A comparative study on determination of the equilibrium, kinetic and thermodynamic parameters of biosorption of copper(II) and lead(II) ions onoto pretreated *Aspergillus niger*, Biochemical Engineering Journal 28(2006)187-195

[134] Chang J.-S., Law R., Chang C.-C., Biosorption of lead, copper and cadmium by biomass of *Pseudomonas aeruginosa* PU21, Water Research 31(1997)1651-1658

[135] Kapoor A., Viraraghavan T., Biosorption of heavy metals on *Aspergillus niger* : effect of pre-treatment, Bioresource Technology 63(1998)109-113

[136] Kapoor A., Viraraghavan T., Heavy metal biosorption sites in *Aspergillus niger*, Bioresource Technolgy 61(1997), 221-227

[137] Kapoor A., Viraraghavan T., Removal of heavy metals from aqueous solutions using immobilized fungal biomass in continuous mode, Water Research 32(1998)1968-1977

[138] Lodeiro P., Barriada J. L., Herrero R., Sastre de Vicente M. E., The marine macroalga *Cystoserira baccata* as biosorbent for cadmium(II) and lead(II) removal: Kinetic and equilibrium studies, Environmental Pollution 142(2006)264-273

[139] Sarret G., Manceau A., Spadini L., Roux J.-C., Hazemann J.-L., Soldo Y., Eybert-Berard L., Menthonnex J., -J., Structural determination of Zn and Pb binding sites in *Penicillium chrysogenum* cell walls by EXAFS spectroscopy, Environmental Science and Technology 32(1998)1648-1655

[140] Naja G., Mustin C., Volesky B., Berthelin J., Stabilization of the initial electrochemical potential for a metal-based potentiometric titration study of a biosorption process, Chemosphere 62(2006)163-170

[141] Guibal E., Interactions of metal ions with chitosan-based sorbents: a review, Separation and Purification Technology 38(2004)43-74

[142] Langmuir I., The adsorption of gasse on plane surface of glass, mica and platinum, Journal of American Chemical Society 40(1918)1361-1403

[143] Volesky B., Sorption and Biosorption, 2003, BV Sorbex, Montreal, ISBN 0973298308, p.106

[144] Kratochvil D., Volesky B., Advances in the biosorption of heavy metals, Tibtech July 16(1998)291-300

[145] Freundlich H. M. F., Uber die adsorption losungen, Z.Phys.Chem. 57(1906)385-470

[146] Brunauer S., Emmet P. H., Teller E., Adsorption of gases in multimolecular layers, Journal of American Chemical Society 60(1938)309-319

[147] Dubinin M. M., Radushkevich L. V., Equation of the characteristic curve of activated charcoal, Chem.Zentr. 1(1947)875

[148] Radke C. J., Prausnitz J. M., Thermodynanamics of multi-solute addsorption from dilute liquid solutions, Journal of American Institute of Chemical Engineers 18(1972)761

[149] Jossens L., Prausnitz J.M., Fritz W., Schlunder U., Myers A. L., Thermodynamics of multisolute adsorption from dilute aquesou solutions, Chemical Engineering Science 33(1978)1097-1106

[150] Sips R., On the structure of a catalyst surface, Journal of Chemical Physics. 16(1948)490-495

[151] Sag Y., Aktay Y., Mass transfer and equilibrium studies for the sorption of chromium ions onto chitin, Process Biochemistry 36(2000)157-173

[152] Chu K. H., Removal of copper from aqueous solution by chitosan in prawn shell: adsorption equilibrium and kinetics, Journal of Hazardous Materials B90(2002)77-95

[153] Schiewer S., Volesky B., Ionic strength and electrostatic effects in biosorption of divalent metal ions and protons, Environmental Science and Technology 31(1997)2478-2485

[154] Lagergren S., Zur theorie der sogenannten adsorption geloster stoffe, Kungliga Svenska Vetenskapsakademiens, Handlingar 24(1898)1-39

[155] Azizian S., Kinetic models of sorption: a theoretical analysis, Journal of colloid and Interface Science 276(2004)47-52

[156] Ho Y. S., McKay G., The kinetics of sorption of divalent metal ions onto sphagnum moss peat, Water Research 34(2000)735-742

[157] Ho Y. S., Wase D. A. J., Forster C. F., Kinetic studies of competitive heavy metal adsorption by sphagnum moss peat, Environmental Technology 17(1997)71-77

[158] Ho Y. S., Ofomaja A. E., Pseudo-second-order model for lead ion sorption from aqueous oslutions onto palm kernel fiber, Journal of Hazardous Materials B129(2006)137-142

[159] Jurova E., diploma thesis, Institute of Chemical Technology, Prague, 2003

[160] Helfferich F., Ion Exchange, Dover Publications Inc., New York, 1962, ISBN 0-486-68784-8, p. 252

[161] Findon A., McKay G., Blair H. S., Transport studies for the sorption of copper ions by chitosan, Journal of Environmental Science and Health. Part A, Environmental Science and Engineering, A28(1993)173-185

[162] McKay G., Blair H. S., Findon A., Sorption of metal ions by chitosan, In: Immobilisation of ions by bio-sorption, Eccles H., Hunt S. (eds.), Ellis Horwood, 1986, p.59-69

[163] Weber W. J., Morris J. C., Advances in water pollution research: Removal of biologically-resistant pollutants from waste waters by adsorption. In: Proc.Int.Conf.on Water Pollution symp, Vol. 2, 1962, 231-266, Pergamon Press, Oxford

[164] McKay G., Poots V. J. P., Kinetics and diffusion processes in colour removal from effluent using wood as an adsorbent, Journal of Chemical Technology and Biotechnology 30(1980)279-292

[165] McKay G., Otterburn M. S., Sweeney A. G., The removal of colour from effluent using various adsorbents – III. Silica:rate processes, Water Research 14(1980)15-20

[166] Zhang X., Bai R., Mechanisms and kinetics of humic acid adsorption onto chitosan-coated granules, Journal of Colloid and Interface Science 264(2003)30-38

[167] Siqueira D. F., Reiter J., Breiner U., Stadler R., Stamm M., Competitive adsorption of functionalized polymers, Langmuir 12(1996)972-979

[168] Urano K., Tachikawa H., Process development for removal and recovery of phosphorus from wastewater by a new adsorbent. 2. Adsorption rates and breakthorugh curves, Industrial and Engineering Chemistry Research 30(1991)1897-1899

[169] Urano K., Yamamoto E., Tonegawa M., Fujie K., Adsorption of chlorinated organic compounds on activated carbon from water, Water Research 25(1991)1459-1464

[170] Kuyucak N., Volesky B., Accumulation of gold by algal biosorbent, Biorecovery 1(1989)189-204

[171] Volesky B., Holan Z. R., Biosorption of heavy metals, Biotechnology Progress 11(1995)235-250

[172] Volesky B., Sorption and Biosorption, 2003, BV Sorbex, Montreal, ISBN 0973298308, p.121-126

[173] Ma W., Tobin J. M., Development of multimetal binding model and application to binary metal biosorption onto peat biomass, Water Research 37(2003)3967-3977

[174] Sag Y., Kaya A., Kutsal T., The simultaneous biosorption of Cu(II) and Zn on *Rhizopus arrhizus*: application of the adsorption models, Hydrometallurgy 50(1998)297-314

[175] Pagnanelli F., Trifoni M., Beolchini F., Esposito A., Toro L., Veglio F., Equilibrium biosorption studies in single and multi-metal system, Process Biochemistry 37(2001)115-124.

[176] Ho Y. S., McKay G., Correlative biosorption equilibria model for a binary batch system, Chemical Engineering Science 55(2000)817-825

[177] Jeon C., Holl W. H., Application of the surface complexation model to heavy metal sorption equilibria onto aminated chitosan, Hydrometallurgy 71(2004)421-428

[178] Juang R.-S., Shao H.-J., A simplified equilibrium model for sorption of heavy metal ions from aqueous solutions on chitosan, Water Research 36(2002)2999-3008

[179] Tsezos M., Remoudaki E., Anglelatou V., A study of the effects of competing ions on the biosorption of metals, International Biodeterioration and Biodegradation (1996)19-29

[180] Bohart G., Adams E. Q., Some aspects of the behavior of charcoal with respect to chlorine, Journal of American Chemical Society 42(1920)523-544

[181] Wolborska A., Adsorption on activated carbon of p-nitrophenol from aqueous solution, Water Research 23(1989)85-91

[182] Thomas H. C., Heterogeneous ion exchange in a flowing system, Journal of American Chemical Society 66(1944)1664-1666

[183] Clark R. M., Evaluating the cost and performance of field-scale granular activated carbon systems, Environmental Science and Technology 21(1987)573-580

[184] Yoon Y. H., Nelson J. H., Application of gas adsorption kinetics. I. A theoretical model for respiratory cartridge service time, American Industrial Hygiene Association Journal 45(1984)509-516

[185] Aksu Z., Gonen F., Biosorption of phenol by immobilized activated sludge in a continuous packed bed: prediction of breakthrough curves, Process Biochemistry 39(2004)599-613

[186] Han R., Zhang J., Zou W., Xiao H., Shi J., Liu H., Biosorption of copper(II) and lead(II) from aqueous solution by chaff in a fixed-bed column, Journal of Hazardous Materials 133(2006)262-268

[187] Naja G., Volesky B., Multi-metal biosorption in a fixed-bed flow-through column, Colloids and Surfaces A: Physicochemical and Engineering Aspects 281(2000-)194-201

[188] Jegorov A., Matha V., Sedmera P., Havlicek V., Stuchlik J., Seidel P., Simek P., Cyclosporins from *Tolypocladium terricola*, Phytochemistry 38(1995)403-407

[189] Velkov T., Singaretnam L. G., Lawen A., An improved purification procedure for cyclosporin synthetase, Protein Expression and Purification 45(2006)275-287

[190] Windhofer F., Hauck K., Catcheside D. E. A., Kuck U., Kempken F., Ds-like restless deletion derivatives occur in *Tolypocladium inflatum* and two foreing hosis, *Neurospora crassa* and *Penicillium chrysogenum*, Fungal Genetics and Biology 35(2002)171-182

[191] Kempken F., Schreiner C., Schorgendorfer K., Kuck U., A unique repeated DNA sequence in the cyclosporine-producing strain of *Tolypocladium inflatum* (ATCC 34921), Experimental Mycology 19(1995)305-313

[192] Ramana Murthy M. V., Mohan E. V. S., Sadhukhan A. K., Cyclosporin-A production by *Tolypocladium inflatum* using solid state fermentor, Process Biochemistry 34(1999)269-280

[193] Dufossé L., Galaup P., Yaron A., Arad S. M., Blanc P., Chidambara Murthy K. N., Ravishankar G. A., Microorganism and microalgae as source of pigments for food use : a scientific oddity or an industrial reality ?, Trends in Food Science and Technology 16(2005)389-406

[194] Uzlova P., Rezanka T., Martinkova L., Kren V., Long-chain fatty acids from *Monascus purpureus*, Phytochemistry 43(1996)151-153

[195] Ogihara J., Kato J., Oishi K., Fujimoto Y., Eguchi T;, Production and structural analysis of PP-V, a homologue of monascorubramine, produced by a new isolate of *Penicillium sp.*, Journal of Bioscience and Bioengineering, 90(2000), 549-554

[196] Ogihara J., Kato J., Oishi K., Fujimoto Y., PP-R, 7-(2-hydroxyethyl)-monascorubramine, a red pigment produced in the mycelia of *Penicillium s*p. AZ, Journal of Bioscience and Bioengineering, 91(2001)44-47

[197] Hashem A. M., Optimization of milk-clotting enzyme productivity by *Penicillium oxalicum*, Bioresource Technology 70(1999)203-207

[198] Hashem A. M., Purification and properties of a milk-clotting enzyme produced by *Penicillium oxalicum*, Bioresource Technology 75(2000)219-222

[199] Zhang S. J., Yang. M., Yang Q. X., Zhang Y., Xin B. P., Pan F., Biosorption of reactive dyes by the mycelium pellets of a new ioslate of *Penicillium oxalicum*, Biotechnology Letters 25(2003)1479-1482

[200] Muzzarelli R. A. A., Tanfani F., Scarpini G., Chelating, film-forming, and coagulating ability of the chitosan-glucan complex from *Aspergillus niger* industrial waste, Biotechnology and Bioengineering, XXII(1980), 885-896

[201] Synowiecki J., Al-Khateeb N., Mycelia of *Mucor rouxii* as a source of chitin and chitosan, Food Chemistry, 60(1997), 605-610

[202] Arcidiacono S., Kaplan D. L., Molecular weight distribution of chitosan isolated from *Mucor rouxii* under different culture and processing conditions, Biotechnology and Bioengineering, 39(1992), 281-286

[203] Rane K. D., Hoover D. G., An evaluation of alkali and acid treatments for chitasan extraction from fungi, Process Biochemistry 28(1993)115-118

[204] Spanelova M., Machovic M., Brezina M., Characterization and sorption properties of *Aspergillus niger* waste biomass, Central European Journal of Chemistry 1(2003)192-200

[205] Varma A. J., Deshpande S. V., Kennedy J. F., Metal complexation by chitosan an dits derivatives : a review, Carbohydrate Polymers 55(2004)77-93

[206] Eltekova N. A., Razdyakonova G. I., Eltekov Y. A., Fractals in geometry of carbon black, Pure and Applied Chemistry 65(1993)2217-2221

[207] Ganan J., Gonzalez J. F., Gonzalez-Garcia C. M., Ramiro A., Sabio E., Roman S., Air-activated carbons from almond tree pruning: Preparation and characterization, Applied Surface Science 252(2006)5988-5992

[208] Schmitt J., Flemming H.-C., FT-IR spectroscopy in microbial and material analysis, International Biodeterioration and Biodegradation 41(1998)1-11

[209] Yee N., Benning L. G., Phoenix V. R., Ferris F. G., Characterization of metal-cyanobacteria sorption reactions: A combined macroscopic and infrared spectroscopic investigations, Environmental Science and Technology 38(2004)775-782

[210] Brugnerotto J., Lizardi J., Goycoolea F. M., Argulles-Monal W., Desbrieres J., Rinaudo M., An infrared investigation in relation with chitin and chitosan characterization, Polymer 42(2001)3569-3580

[211] Jansson-Charrier M., Saucedo I., Guibal E., Le Cloirec P., Approach of uranium sorption mechanisms on chitosan and glutamate glucan by IR and 13C-NMR analysis, Reactive and Functional Polymers 27(1995)209-221

[212] Baton D. A., Glescer L. S., Greenberg A. E., Standard methods for examination of water and waste water, 10th edition, 1995, APHA, AWWA, WEF

[213] www.lwr.kth.se/English/OurSoftware/vminteq

[214] Lin-Vien D., Colthup N. B., Fateley W. G., Grasselli J. G., The Handbook of infrared and Raman characteristic frequencies of organic molecules, 1991, Academic Press, San Diego, USA

[215] Ashkenazy R., Gottlieb L., Yannai S., Characterization of acetone-washed yeast biomass furnctional groups involved in lead biosorption, Biotechnology and Bioengineering, 55(1997)1-10

[216] Volesky B., Sorption and Biosorption, 2003, BV Sorbex, Montreal, ISBN 0973298308, p.52-53

[217] Malkoc E., Nuhoglu Y., Dundar M., Adsorption of chromium(VI) on pomace – An olive oil industry waste: Batch and column studies, Journal of Hazardous Materials (2006), in press

[218] Kumaresan R., Moorthy Babu S. , Ramasamy P., Morphological studies on electrodeposited mercury cadmium telluride thin films, Materials Chemistry and Physics 59(1999), 107-113

[219] Moreno T., Higueras P., Jones T., McDonald I., Gibbons W., Size fractionation in mercury-bearing airborne particles ($HgPM_{10}$) at Almadén, Spain: Implications fro inhalation hazards around old mines, Atmospheric Environement 39(2005)6409-6419

[220] Patil R. S., Lokhande C. D., Mane R. S., Pathan H. M., Joo O.-S., Han S.-H., Successive ionic layer adsorption and reaction (SILAR) trend for nanocrystalline mercury sulfide thin films growth, Materials Science and Engineering B 129(2006)59-63

[221] Eiden C. A., Jewell C. A., Wightman J. P., Interaction of lead and chromium with chitin and chitosan, Journal of Applied Polymer Science, 25(1980)1587-1599

[222] Tunali S., Cabuk A., Akar T., Removal of lead and copper ions from aqueous solutions by bacterial strain isolated from soil, Chemical Engineering Journal, 115(2006)203-211

[223] Krishnan K. A., Anirudhan T. S., Removal of mercury(II) from aqueous solutions and chlor-alkali industry effluent by steam activated and sulphurised activated carbons prepared from bagasse pith: kinetics and equilibrium studies, Journal of Hazardous Materials, 92(2002)161-183

[224] Aksu Z., Tezer S., Equilibrium and kinetic modelling of biosorption of Remazol Black B by *Rhizopus arrhizus* in a batch system: effect of temperature, Process Biochemistry 36(2000)431-439

[225] Jansson-Charrier M., Guibal E., Roussy J., Delanghe B., Le Cloirec P., Vanadium (IV) sorption by chitosan : kinetics and equilibrium, Water Research 30(1996)465-475

[226] Guibal E., Saucedo I., Roussy J., Roulph Ch., Le Cloirec P., Uranium sorption by glutamate glucan: A modified chitosan Part II: Kinetic studies, Water SA 19(1993)119-126

[227] Helfferich F., Ion Exchange, Dover Publications Inc., New York, 1962, ISBN 0-486-68784-8, p. 285

[228] Guibal E., Milot C., Tobin J. M., Metal-anion sorption by chitosan beads: Equilibrium and kinetic studies, Industrial and Engineering Chemical Research 37(1998)1454-1463

[229] Puranik P. R., Paknikar K. M., Influence of co-cations on biosorption of lead and zinc – a comparative evaluation in binary and multimetal systems, Bioresource Technology 70(1999)269-276

[230] Chassary P., Adsorption de métaux precieux (palladium, platine) sur chitosane, Ph.D thesis, Université Montpellier II, 2004

[231] Figueira M. M., Volesky B., Ciminelli V. S. T., Assessment of interference in biosorption of heavy metals, Biotechnology and Bioengineering, 54(1997)344-350

[232] Mohapatra H., Gupta R., concurrent sorption of Zn(II), Cu(II) and Co(II) by *Oscillatoria angustissima* as a function of pH in bimary and ternary metal solutions, Bioresource Technology 96(2005)1387-1398

[233] Volesky B., Sorption and Biosorption, 2003, BV Sorbex, Montreal, ISBN 0973298308, p.31-32

[234] Huang C.-P., Huang C.-P., Morehart A. L., The removal of Cu(II) from dilute aqueous solutions by *Saccharomyces cerevisiae*, Water Research, 24(1990)433-439

[235] Vijayaraghavan K., Prabu D., Potential of *Sargassum wightii* biomass for copper(II) removal from aqueous solutions: Application of different mathematical models to batch and continuous biosorption data, Journal of Hazardous Material (2006), in press

[236] Hamdaoui O., Dynamic sorption of methylene blue by cedar sawdust and crushed brick in fixed bed columns, Journal of Hazardous Materials (2006), in press

[237] Helfferich F., Ion Exchange, Dover Publications Inc., New York, USA, 1962, p.256

Publications and communications

International conferences:

- Svecova L., Spanelova M., Kubal M., Guibal E. : "Waste fungal biomass from fermentation industry for the sorption of Cd, Pb, Cr and Hg", 16th International Biohydrometallurgy Symposium, 25th – 29th September 2005, Cape Town, South Africa

- Spanelova M., Svecova L., Anderle J., Kubal M.: "A study of metal ions uptake by waste fungal biomass", SETAC Europe 14th Annual Meeting in Prague, 18th – 22th April 2004, Prague, Czech Republic (poster)

- Spanelova M., Svecova L., Guibal E.: "Influence of the treatment of fungal biomass on sorption properties for lead and mercury uptake", 15th International Biohydrometallurgy Symposium, 14th – 18th September 2003, Athens, Greece

- Spanelova M., Guibal E., Svecova L.: "Recovery of mercury ions by *Aspergillus niger* waste biomass", 11th European Congress on Biotechnology, 24th – 29th August 2003, Basel, Switzerland, (poster

National conferences:

- Švecová L., Španělová M., Guibal E.:"Valorization of waste biomass of *Aspergillus niger* for the uptake of lead from its solutions" (in Czech), Průmyslové technologie a ŽP, 18th June 2003, Ostrava, Czech Republic, followed by proceedings: S.Bartůšek (Edit.), p.87-95, ISBN 80-248-0328-3.

- Španělová M., Březina M., Švecová L.: „Characterization and adsorption properties of waste biomass of *Aspergillus niger*" (in Czech), Sanační technologie VI., 28th – 29th May 2003, Nové Město na Moravě, Czech Republic, (poster), followed by proceedings: J.Burkhard, M.Kubal (Edit.), p.121, ISBN 80-903203-5-X.

Publications :

- Svecova L., Spanelova M., Kubal M., Guibal E.: "Cadmium, lead and mercury biosorption on waste fungal biomass issued from fermentation industry. I. Equilibrium studies", <u>Separation and Purification Technology 52(2006)142-153, in press</u>

- Švecová L., Španělová M, Kubal M., Guibal E.: "Valorization of waste biomasses issued from Czech fermentation industry as metal biosorbents" (in Czech), <u>Odpadové fórum 2005(1), 36-38</u>

- Svecova L., Spanelova M., Kubal M., Guibal E.: "Waste fungal biomass from fermentation industry for the sorption of Cd, Pb, Cr and Hg", <u>Proceedings of the 16th Intenational Biohydrometalurgy Symposium, Editors: Harrison S. T. L., Rawlings D. E; Petersen J., ISBN 1-920051-171, p. 581 - 590</u>

- Spanelova M., Svecova L., Guibal E.: „Influence of the treatment of fungal biomass on sorption properties for lead and mercury uptake", <u>Biohydrometallurgy, Sustainable technology in evolution, Part II, Tsezos M., Hatzikioseyian A., Remoundaki E. (Editors), 15th Inter. Biohydrometal. Symp., 14 - 18 September 2003, Athens, Greece, ISBN 960-88415-2-6, p. 899-909</u>

Within the scope of my Ph.D. thesis and under my responsibility I had the pleasure to manage the final engineering project of Lenka Česaková. The final report of this project was successfully defended in June 2006 and led to obtention of engineering diploma.

Lenka Švecová

Study of adsorption properties of fungal biomass – Application in metallic wastewaters treatment

Spécialité : **Environmental Science**

Mots clefs :

> biosorption, waste biomass, *Penicillium oxalicum* var. Armeniaca, *Tolypocladium* sp., mercury, hexavalent chromium, cadmium, lead

Résumé

The objective of the present work was to study biosorption of mercury, cadmium, lead and hexavalent chromium by waste fungal materials *(Penicillium oxalicum* var. Armeniaca, *Tolypocladium* sp.) produced by Czech fermentation industry. Strong alkaline treatment of *Penicillium* biomass gave an efficient sorbent (called P3 sample), while biomass of *Tolypocladium* (referred as T sample) was used as supplied.

At first, their sorption properties have been checked for metal recovery from monometallic synthetic solutions. The best sorption of cationic species was observed at pH close to neutrality, while chromium was better removed from acidic solutions (pH 2-3). Regarding maximum sorption capacities (derived from sorption isotherms) biosorbent P3 clearly showed higher capacity than biosorbent T for each individual metal. The maximum sorption capacities at optimum experimental conditions may reach 270 mg Hg g^{-1} sample P3 (pH 5), 160 mg Hg g^{-1} sample T (pH 7), 70 mg Cr(VI) g^{-1} sample P3 (pH 3) and 55 mg Cr(VI) g^{-1} sample T (pH 2). These values are on the upper boundary of the ranger reported in the literature. On the contrary the sorption capacities obtained for cadmium and lead were less favourable. The process followed second-order reaction kinetics and the influence of diffusion phenomena on the transport rates in suspensions was discussed.

It was proved that nitrogen containing groups played an important role in biosorption mechanisms of P3 sorbent. Cations were removed by chelation at pH close to neutrality, while hexavalent chromium was sequestered by the electrostatic attraction to the protonated groups at acidic pH. In the case of T sample, the participation of carboxyl groups in the removal was observed and ion exchange mechanism was suggested. Concerning hexavalent chromium a combined process of sorption/reduction was reported, but the exact mechanism was not found.

Sorption from synthetic bimetallic solutions was tested further, while the selectivity of P3 sorbent for mercury was confirmed. The competitive behaviour was only observed in case Hg-Cd system using T sample.

Finally, the dynamic sorption in a fixed bed column system was studied using *Tolypocladium* beads (immobilized on infusorial earth). The column sorption was controlled by intraparticular diffusion. Influence of two parameters was tested; increasing inlet concentration and particle size led to a decrease of the column service time.

Lenka Švecová

Titre de la thèse : Etude des propriétés adsorbantes de biomasses fongiques – Application au traitement d'effluents métallifères

Spécialité : Sciences et Génie de l'Environnement

Mots clefs

biosorption; déchet de biomasse, *Penicillium oxalicum* var. Armeniaca, *Tolypocladium* sp., mercure, chrome hexavalent, cadmium, plomb

Résumé

L'objectif de la présente thèse a été d'étudier les possibilités de valorisation des déchets de biomasse (*Penicillium oxalicum* var. Armeniaca, *Tolypocladium* sp.) issus de procédés de fermentation en tant que biosorbants du plomb, du cadmium, du mercure et du chrome hexavalent. Alors que la biomasse de *Tolypocladium* (biomasse T) a été utilisée en l'état, la biomasse de *Penicillium* a dû subir un traitement alcalin (biomasse P3).

Dans un premier temps, la biosorption a été étudiée à partir de solutions synthétiques monométalliques. Le pH initial optimal pour les espèces cationiques est proche du pH neutre, alors que celui de l'espèce anionique est inférieur à 3 (milieu acide). Le biosorbant P3 a montré des capacités de fixation plus importantes pour tous les métaux étudiés par rapport au biosorbant T. Les capacités maximales de fixation peuvent atteindre, dans des conditions opératoires optimales, 270 mg Hg g^{-1} biomasse P3 (à pH 5), 160 mg Hg g^{-1} biomasse T (à pH 7), 70 mg Cr(VI) g^{-1} biomasse P3 (à pH 3) et 55 mg Cr(VI) g^{-1} biomasse T (à pH 2). Ces valeurs figurent parmi les valeurs les plus élevées citées dans la littérature. Au contraire pour le plomb et le cadmium les performances sont décevantes. La cinétique de biosorption du mercure et du chrome est du second ordre. L'influence des phénomènes de diffusion sur la vitesse globale du procédé a été largement discutée.

Pour les espèces cationiques, le mécanisme de chélation des métaux sur les groupes aminés a été proposé pour la biomasse P3, alors que l'échange d'ions sur les groupes carboxyliques s'est révélé plus probable pour la biomasse T. Pour ce qui concerne les espèces anioniques (ions chromates) la fixation procède par attraction electrostatique sur les groupes aminés protonés. Concernant la biomasse T, le mécanisme combiné d'adsorption/réduction observé pendant les expérimentations en régime statique n'a pas été clarifié.

La biosorption à partir de solutions mixtes a été également étudiée. La sélectivité de la biomasse P3 pour le mercure a été confirmée. Aucun mécanisme de compétition n'a été identifié.

Le travail expérimental s'est conclu par des expérimentations en régime dynamique (colonne à lit fixé) en utilisant la biomasse de *Tolypocladium,* immobilisée sur une terre des diatomées. Le procédé est contrôlé par diffusion intraparticulaire. Les courbes de percée dépendent de plusieurs paramètres tels que la concentration initiale et le diamètre des particules.